Experimental and Theoretical investigation of New Grubbs-type Catalysts for the Metathesis of Alkenes

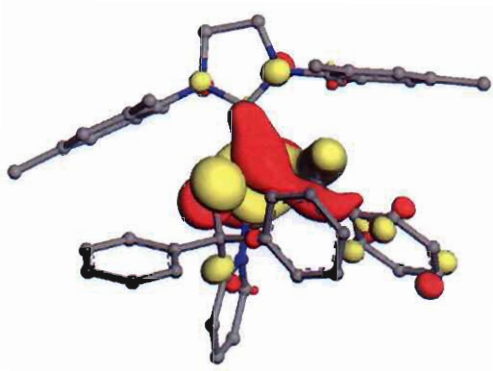

Margaritha Jordaan

Experimental and Theoretical investigation of New Grubbs-type Catalysts for the Metathesis of Alkenes

Margaritha Jordaan
B.Sc, Hons. B.Sc, M.Sc (PU for CHE)

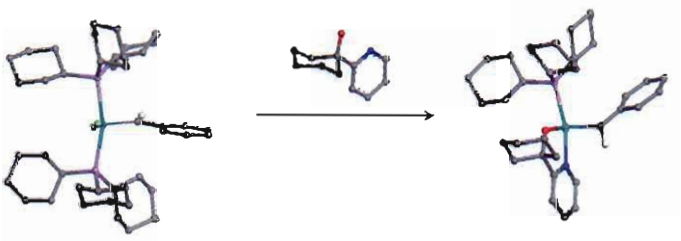

Thesis submitted in fulfilment of the requirements for the degree

PHILOSOPHIAE DOCTOR

in

CHEMISTRY

of the North-West University (Potchefstroom Campus).

Promoter: Prof. HCM Vosloo

Potchefstroom
2007

This thesis is dedicated to

Johan and all the people I love

Table of Contents

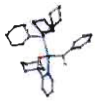

List of Abbreviations & Catalysts

GENERAL

$C_{\#}$	:	# indicates the carbon chain length e.g. C_7 is heptene, C_9 is nonene, etc.
=CRR'	:	alkylidene; carbene moiety where R, R' = H, alkyl or aryl groups
DFT	:	density functional theory
ΔE	:	change in electronic energy
$\Delta E_o^{\ddagger}$	:	activation energy
E_{d2}	:	formation energy
ΔG	:	change in Gibbs free energy
ΔH	:	change in enthalpy
H_α	:	carbene α-proton
HSAB	:	hard and soft acid-base
IP	:	isomerisation products
k_{init}	:	initiation rate
L_n	:	ligands coordinated to a metal
M	:	transition metal atom
M-H	:	metal hydride
M-C	:	metal carbon
M-Cl	:	metal chloride
NHC	:	N-heterocyclic carbene
O^Y	:	bidentate ligand coordinated to a metal at O and Y where Y = O, N, S, P, etc.
PES	:	potential energy surface
PMP	:	primary metathesis products
RCM	:	ring-closing metathesis
ROMP	:	ring-opening metathesis polymerisation
RT	:	room temperature
Ru=C	:	ruthenium carbene moiety
SHOP	:	Shell higher olefins process
SMP	:	secondary metathesis products
TS or TS's	:	transition state or transition states
TLC	:	thin layer chromatography

CHEMICALS AND LIGANDS

Ad	:	adamantyl
Cy	:	cyclohexyl
H_2IMes	:	1,3-bis-(2,4,6-trimethylphenyl)-2-imadazolidinylidene
Hx	:	hexyl
Hoqu	:	8-quinolinol anion
Me	:	methyl
Mes	:	1,3-bis-(2,4,6-trimethylphenyl)
Pico	:	picolinic acid
^{i}Pr	:	isopropyl
Py	:	pyridine
PCy_3	:	tricyclohexylphosphine
pyca	:	picolinic acid anion
Ph	:	phenyl
Quino	:	quinoline
THF	:	tetrahydrofuran
Ts	:	tosyl

CATALYSTS: (List of catalyst abbreviations together with structure and name)

Benzylidene-dichloro(bis(tricyclohexylphosphine))ruthenium

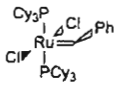

Gr1

Benzylidene-dichloro(tricyclohexylphosphine)(1,3-bis-(2,4,6-trimethylphenyl)-2-imadazolidinylidene)-ruthenium

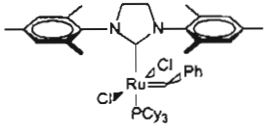

Gr2

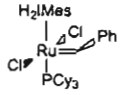

Benzylidene-dichloro(tricyclohexylphosphine)bis(pyridine)ruthenium

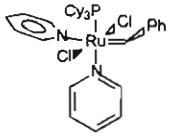

Gr1-Py

Benzylidene-dichloro(1,3-bis-(2,4,6-trimethylphenyl)-2-imadazolidinylidene)bis(pyridine)ruthenium

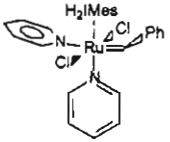

Gr2-Py

Benzylidene-dichloro(tricyclohexylphosphine)-[1-(2'-pyridinyl)cyclohexan-1-olato]ruthenium

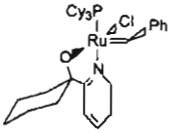

Gr1Cy

Benzylidene-chloro(tricyclohexylphosphine)-[1-(2'-pyridinyl)-1,1-diphenyl-methanolato]ruthenium

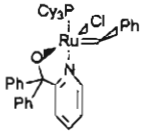

Gr1Ph

Benzylidene-chloro(tricyclohexylphosphine)-[1-(2'-pyridinyl)propan-2-olato]ruthenium

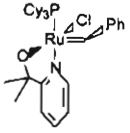

Gr1Me

Benzylidene-chloro(tricyclohexylphosphine)-[1-(2'-pyridinyl)-2,4-dimethylpentan-3-olato]ruthenium

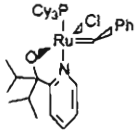

Gr1^{i}Pr

Benzylidene-chloro(tricyclohexylphosphine)-[8-quinolinolato]ruthenium

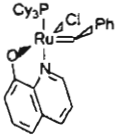

Gr1Quino

Benzylidene-chloro(1,3-bis-(2,4,6-trimethylphenyl)-2-imidazolidinylidene)-[1-(2'-pyridinyl)cyclohexan-1-olato]ruthenium

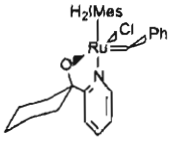

Gr2Cy

Benzylidene-chloro(1,3-bis-(2,4,6-trimethylphenyl)-2-imidazolidinylidene)-[1-(2'-pyridinyl)-1,1-diphenyl-methanolato]ruthenium

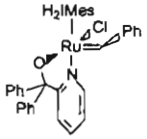

Gr2Ph

Benzylidene-chloro(1,3-bis-(2,4,6-trimethylphenyl)-2-imidazolidinylidene)-[1-(2'-pyridinyl)propan-2-olato]ruthenium

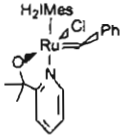

Gr2Me

Benzylidene-chloro(1,3-bis-(2,4,6-trimethylphenyl)-2-imidazolidinylidene)-[1-(2'-pyridinyl)-2,4-dimethylpentan-3-olato]ruthenium

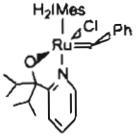

Gr2^{i}Pr

Benzylidene-chloro(1,3-bis-(2,4,6-trimethylphenyl)-2-imidazolidinylidene)-[8-quinolinolate]ruthenium

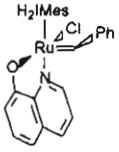

Gr2Quino

Benzylidene-chloro(tricyclohexylphosphine)pyridine-[pyridine-2-carboxylato]ruthenium

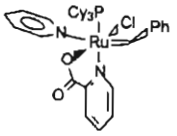

Gr1Pico-Py

Benzylidene-chloro(tricyclohexylphosphine)pyridine-[1-(2'-pyridinyl)cyclohexan-1-olato]ruthenium

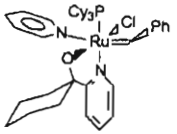

Gr1Cy-Py

Summary

Experimental and theoretical investigation of new Grubbs-type catalysts for the metathesis of alkenes

Despite the high selectivity of the first generation Grubbs precatalyst (**Gr1**) during the metathesis of terminal alkenes, it tends to have a limited lifetime at elevated temperatures. The development of the second generation Grubbs precatalyst (**Gr2**) has dealt with this problem to some extent. The replacement of one PCy_3 ligand with a N-heterocyclic carbene provided a system with improved activity and lifetime. However, **Gr2** shows low selectivity at elevated temperatures, due to the formation of secondary metathesis products during the metathesis reactions.

In this study, experimental and theoretical studies were combined to gain insight into the mechanism of the metathesis reaction and to predict structural and reactivity trends of the catalytic systems. A number of O,O- O,N-, O,S- and O,P-bidentate ligands were identified as possible hemilabile ligands for incorporation into **Gr1** and **Gr2**. The steric and electronic environment of the ligands was varied to determine the influence of these parameters on the 1-octene metathesis activity of the precatalysts. This investigation was motivated by the fact[12,13] that hemilabile ligands can release a free coordination site "on demand" of an incoming nucleophilic substrate while occupying it otherwise. This is believed to increase the thermal stability and activity of the catalytic systems and therefore prevent decomposition via free coordination sites. This was recently shown to be true for a number of Grubbs carbenes in ring-opening metathesis (ROMP) and ring-closing metathesis (RCM) reactions at elevated temperatures. Molecular modelling was used as a tool to design new Grubbs-type precatalysts, which were then synthesised and evaluated for 1-octene metathesis activity. Unfortunately, a number of the ligands could not be successfully incorporated into the Grubbs carbenes, for which possible reasons are discussed in the thesis. It was generally found that the O,O-, O,S- and carboxylic O,P-ligands resulted in the decomposition of the Grubbs carbenes. The yields of these complexes generally ranged from 0 – 10%, which made the purification and analysis process difficult. The incorporation of picolinic acid, a O,N-carboxylic ligand, into **Gr1** and **Gr2** resulted in a mixture of carbenes which could not be isolated. However, the O,N-alcoholate ligands with different steric bulk could be successfully incorporated into **Gr1** and **Gr2** with a yield ranging between 40 – 90% with a 98 – 100% purity. The incorporation of the sterically hindered hemilabile O,N-ligands into **Gr1** and **Gr2** improved the thermal stability, activity, selectivity and lifetime of these complexes towards the metathesis of 1-octene. Compared to **Gr1**, a 10 – 30% increase in the primary metathesis products (PMP) formation, together with a 4% decrease in isomerisation products (IP) was observed for the first generation hemilabile Grubbs

precatalysts. However, although no significant increase in PMP was observed after 7 h for the second generation analogues in comparison to **Gr2**, a 4 – 10 % increase was visible after 20 h, with a 5 – 15% increase in secondary metathesis products (SMP). A decrease in the activity of **Gr1** and **Gr2** was additionally observed after incorporating a hemilabile O,N-ligand with two phenyl groups into the system, while increasing their lifetime.

The ^{1}H NMR investigation of a first and second generation system with a pyridinyl alcoholate ligand predicted that the **Gr2**-system would show hemilabile characteristics, but not the **Gr1**-system. This indicated that two different mechanisms might be involved during the metathesis of 1-octene in the presence of a first and second generation O,N-chelated complex.

Additionally, a conceptual mechanistic model for the alkene metathesis reaction in the presence of **Gr1** was postulated and applied to the hemilabile first and second generation Grubbs analogues. A deeper insight into the NMR results was also gained with the use of molecular modelling. The catalytically active species which preferentially forms during the 1-octene metathesis reactions with **Gr1** and **Gr2** was identified and verified experimentally and theoretically. However, the results for the hemilabile complexes are still inconclusive and more in-depth studies should be done with a combination of ^{1}H and ^{31}P NMR. This must be done to obtain information on the hemilability of the precatalysts as well as the influence of the alkene on releasing a free coordination site. A number of research possibilities were identified which should be investigated in order to gain more insight into the mechanism of 1-octene metathesis with a hemilabile complex.

Opsomming

Eksperimentele en teoretiese ondersoek van nuwe Grubbs-tipe katalisatore vir die metatese van alkene

Ondanks die hoë selektiwiteit van die eerstegenerasie Grubbs-prekatalisator (**Gr1**) gedurende die metatese van terminale alkene, het dit 'n kort leeftyd by verhoogde temperature. Die ontwikkeling van die tweedegenerasie Grubbs-prekatalisator (**Gr2**) het die probleem tot 'n mate opgelos. Die vervanging van een PCy_3 ligand met 'n N-heterosikliese karbeen het 'n sisteem met verbeterde aktiwiteit en stabiliteit gelewer. Nogtans toon **Gr2** lae selektiwiteit by verhoogde temperature weens die vorming van sekondêre metateseprodukte gedurende die metatese-reaksies.

Gedurende die studie is eksperimentele en teoretiese studies gekombineer om insig te kry in die meganisme van die metatesereaksie en om struktuur- en reaktiwiteitstendense van die katalitiese sisteme te voorspel. 'n Aantal O,O-, O,N-, O,S- and O,P-bidentate ligande is as moontlike hemilabiele ligande vir inkorporering in **Gr1** en **Gr2** geïdentifiseer. Die steriese en elektroniese omgewing van die ligande is gevarieer om die invloed van hierdie parameters op die 1-okteenmetateseaktiwiteit van die prekatalisatore te bepaal. Dié ondersoek is gemotiveer deur die feit dat hemilabiele ligande 'n vry koördinasieposisie "op aandrang" van 'n inkomende nukleofiele substraat kan beskikbaarstel terwyl dit andersins beset word. Daar word geglo dat dit die termiese stabiliteit en aktiwiteit van die katalitiese sisteme verhoog en dus ontbinding via die vry koördinasieposisie vermy. Dit is onlangs as waar vir 'n aantal Grubbs-karbene in ringopeningmetatesepolimerisasie- (ROMP) en ringsluitingsmetatesereaksies (RCM) by verhoogde temperature aangetoon. Molekuulmodellering is as hulpmiddel gebruik om die nuwe Grubbs-tipe prekatalisatore te ontwerp, wat dan gesintetiseer en vir 1-okteen-metateseaktiwiteit geëvalueer is. Ongelukkig kon 'n aantal van die ligande nie suksesvol in die Grubbs-karbene geïnkorporeer word nie, waarvoor moontlike redes in die proefskrif bespreek word. Dit is algemeen gevind dat die O,O-, O,S- en karboksiliese O,P-ligande tot die ontbinding van die Grubbs-karbene gelei het. Die opbrengs van hierdie komplekse het algemeen in die gebied van 0 – 10% geval, wat die suiwering en analiseproses bemoeilik het. Die inkorporering van pikoliensuur, 'n O,N-karboksiliese ligand, in **Gr1** en **Gr2** het 'n mengsel van karbene tot gevolg gehad wat nie geïsoleer kon word nie. Nogtans kon die O,N-alkoholaatligande met verskillende steriese volume suksesvol in **Gr1** en **Gr2** geïnkorporeer word met 'n opbrengs wat in die gebied van 40 – 80% geval het met 'n suiwerheid van 98 – 100%. Die inkorporering van die steries gehinderde O,N-ligande in **Gr1** en **Gr2** het die termiese stabiliteit, aktiwiteit, selektiwiteit en leeftyd van hierdie komplekse teenoor die metatese van 1-okteen verbeter. In vergelyking met **Gr1** is 'n 10 – 30% toename in die vorming van primêre

metateseprodukte (PMP) tesame met 'n 4% toename in isomerisasieprodukte (IP) vir die eerstegenerasie Grubbs-prekatalisatore waargeneem. Nietemin, alhoewel geen beduidende toename in PMP na 7 h waargeneem is vir die tweedegenerasie analoë in vergelyking met **Gr2** nie, is 'n 4 – 10% toename na 20 h waargeneem, tesame met 'n 5 – 15% toename in sekondêre metateseprodukte (SMP). 'n Afname in die aktiwiteit van **Gr1** en **Gr2** is addisioneel waargeneem nadat 'n hemilabiele O,N-ligand met twee fenielgroepe in die sisteem geïnkorporeer is, terwyl dit hul leeftyd verhoog het.

Die ^{1}H-KMR-ondersoek van 'n eerste- en tweedegenerasie sisteem met 'n piridinielalkoholaat-ligand het voorspel dat die **Gr2**-sisteem, maar nie die **Gr1**-sisteem nie, hemilabiele eienskappe vertoon. Dit het daarop gedui dat twee veskillende meganismes dalk betrokke mag wees gedurende die metatese van 1-okteen in die teenwoordigheid van 'n eerste- en tweedegenerasie O,N-gecheleerde kompleks.

Addisioneel is 'n konseptueel-meganistiese model vir die alkeenmetatesereaksie in die teenwoordigheid van **Gr1** gepostuleer en op die hemilabiele eerste- en tweedegenerasie Grubbs-analoë toegepas. 'n Dieper insig in die KMR-resultate is ook met behulp van molekuulmodellering verkry. Die katalities-aktiewe spesies wat by voorkeur tydens die 1-okteenmetatese met **Gr1** en **Gr2** vorm, is geïdentifiseer en eksperimenteel en teoreties geverifieer. Die resultate vir die hemilabiele komplekse is egter nog onbeslis en meer diepgaande studies behoort nog met 'n kombinasie van ^{1}H- en ^{31}P-KMR gedoen te word. Dit moet gedoen word om inligting oor die hemilabiliteit van die prekatalisatore sowel as die invloed van die alkeen op die vrystelling van 'n vry koördinasieposisie te verkry. 'n Aantal navorsingsmoontlikhede is ook geïdentifiseer wat verder ondersoek moet word om meer insig in die meganisme van 1-okteenmetatese met 'n hemilabiele kompleks te verkry.

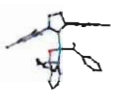

Publications

Parts of this study resulted in the following publications (see enclosed CD for copies):

1. Jordaan, M., van Helden, P., van Sittert, C.G.C.E., and Vosloo, H.C.M., "Experimental and DFT investigation of the 1-octene metathesis reaction mechanism with the Grubbs 1 precatalyst" *J. Mol. Catal. A: Chem.*, 2006, **254**, 145

2. Jordaan, M. and Vosloo, H.C.M., "Ruthenium catalyst with a chelating pyridinyl-alcoholato ligand for application in linear alkene metathesis" *Adv. Synth. Catal.*, 2007, **349**, 184

Introduction & Aim of study 1

1.1 INTRODUCTION

Research in coordination and organometallic chemistry, strongly supported in the last decade by theoretical studies,[1-13] has provided much insight into the mechanism of catalytic processes involving M-C or M-H bonds. Alkene metathesis is one example of a catalytic process involving M-C bonds that has been successfully applied in both academic and industrial environments with combined experimental and theoretical support.[8,10,14] The term *metathesis* is derived from the Greek words μετα (change) and τιθεημι (place), which refers to an interchange of atoms between molecules. It is an equilibrium-driven reaction where the total number of double bonds remains unchanged.[15] The alkene metathesis reaction, which is extensively used in catalysis and synthesis reactions, has opened up new routes to important petrochemicals, polymers and specialty chemicals.[15-19]

The largest application of the alkene metathesis reaction in, *inter alia* the field of petrochemicals, is the Shell higher olefins process (SHOP), which produces more than 10^5 tons of C_{10} and C_{20} alkenes annually.[20] In South Africa, Sasol Ltd. is using the Fisher-Tropsch process to make alkenes from synthesis gas, which can be obtained form coal or natural gas. With the use of existing process technologies such as the alkene metathesis reaction, the low value alkenes (1-heptene) are converted to high value alkenes (6-dodecene) which are used as detergent alcohol feedstock.[21]

A large number of catalytic systems are known to catalyse the ring-opening metathesis polymerisation (ROMP), ring-closing metathesis (RCM), etc. of alkenes, but only a limited number initiate the metathesis of terminal alkenes.[15,22,23] The main metals employed in these systems are ruthenium, molybdenum, rhenium or tungsten.[15] In this study, the well-defined ruthenium-based Grubbs systems, $RuCl_2(PCy_3)L(=CHPh)$ [L = PCy_3 (**Gr1**) or H_2IMes (**Gr2**)] are of interest due to their high metathesis activity and robustness to a wide range of substrates.[23-25] It is well known that **Gr1** is thermally unstable despite its high selectivity during the metathesis of alkenes.[22,23,26] The development of second generation Grubbs catalysts has improved the thermal stability, lifetime and activity of **Gr1** by replacing one PCy_3 group with a N-heterocyclic carbene (NHC) ligand.[27,28] The increasing interest in more stable and catalytically active systems for metathesis reactions, which was also a driving force for this study, has encouraged various researchers to modify **Gr1** and **Gr2** (see Chapter 2).[29-42]

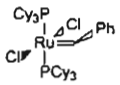

Gr1

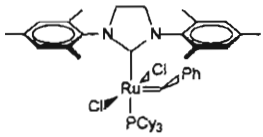

Gr2

Randl *et al.*[43] suggested that the activity in metathesis reactions is strongly dependent on the electronic properties of the Ru-carbene complex. He observed that 1 is extremely stable towards air and water during various alkene metathesis reactions, displaying a high selectivity towards cross-metathesis.[43] The use of bidentate ligands with a relatively rigid backbone might therefore be a way of increasing selectivity of catalytically active complexes. For example, the selectivity of the Rh-catalysts in the hydroformylation of styrene was improved by incorporating bidentate phosphite or phosphine ligands into the system.[44,45]

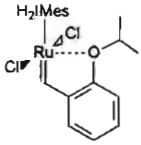

1

Hemilabile ligands, which are a class of bidentate ligands, have the ability to place two or more donor atoms with very different electronic properties close to the metal atom (Scheme **1.1**).[46,47]

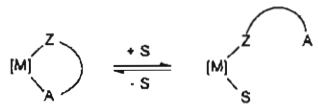

S = substrate
Z = tightly bound group
A = labile group

Scheme 1.1 Schematic representation of the concept of hemilability.[46,47]

The concept of hemilability of bidentate ligands predicts higher lifetime and stability by releasing a free coordination site "on demand" of *inter alia* an alkene (such as norbornene) and occupying it otherwise – thus preventing decomposition via free coordination sites.[30,48] Electronic properties, steric demands as well as ring size and rigidity of these bidentate ligands can influence the stability of the bidentate complexes[49] and therefore their catalytic performance.

It is generally accepted that alkene metathesis reactions catalysed by **Gr1** and **Gr2** proceed according to the simplified mechanism outlined in **Scheme 1.2**.[50-54]

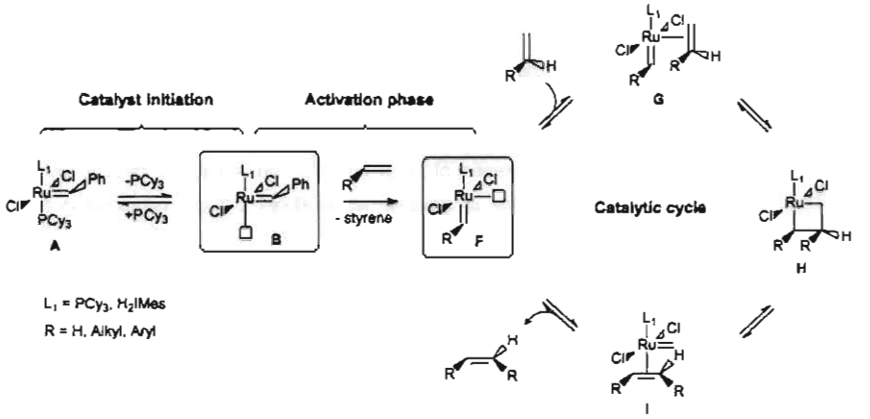

Scheme 1.2 Generally accepted mechanism for alkene metathesis catalysed by **Gr1** and **Gr2**.[50-54]

In both cases, the first step of the reaction involves dissociation of bound PCy_3 to form a 14-electron intermediate of the general form $RuCl_2L(=CHPh)$, **B**. This intermediate can be trapped by free PCy_3 to regenerate the starting alkylidene or can bind substrate to undergo metathesis. The steps following the initiation of the precatalyst consist of several successive formal [2+2] cycloadditions to form a ruthenacyclobutane (similar to H) and cycloreversions to form the respective catalytically active species.

Therefore, modification of the Grubbs carbenes to include ligands that could increase the electron density on the Ru-centre should be considered. This would lead to the stabilisation of the Ru^{IV} ruthenacyclobutane (**H**) and thereby increase the thermal stability of these systems as was observed for **Gr2**.[51,52,55]

1.2 AIM AND OBJECTIVES

For a catalyst to be successfully implemented in an industrial process, such as 1-alkene metathesis, certain prerequisites have to be fulfilled. The ideal catalyst has to combine high efficiency (i.e. effective use of starting materials, and minimal waste emission),[56] high selectivity (i.e. optimal conversion to the desired product),[57] and high total turnover (i.e. amount of product formed per given amount of catalyst) with durability (i.e. high stability and lifetime) and low overhead expenditure (i.e. cheap catalyst and little maintenance). Deckers[58] believes that understanding how catalyst structure and properties can affect these parameters, combined with chemical curiosity, can be the driving force for improvement and development of catalytic systems, which we strived to do in this study.

In an attempt to improve the thermal stability, activity and lifetime of **Gr1** and **Gr2** for the metathesis of linear alkenes, a number of first and second generation Grubbs-type precatalysts with hemilabile bidentate ligands were synthesised and evaluated for the metathesis of 1-octene. This was done due to the recent improvement of the activity of various ruthenium carbene (Ru=C) systems for ROMP and RCM reactions at elevated temperatures through incorporation of a hemilabile ligand into the system.[30,59]

To reach the aim of the study the following objectives are stated:

1. Systematically and extensively search the published literature on the metathesis of linear alkenes, with special emphasis on Ru=C catalytic systems, to gain a better understanding of the reaction and the reaction mechanism.

2. Use molecular modelling as a tool to design new Grubbs-type precatalysts with hemilabile bidentate ligands and to understand the mechanism of the reaction.

3. Synthesise and evaluate new Grubbs-type precatalysts with hemilabile bidentate ligands for 1-octene metathesis activity.

1.3 REFERENCES

1. Kawamura-Kuribayashi, H., Koga, N., and Morokuma, K., *J. Am. Chem. Soc.*, 1992, **114**, 2359

2. Ziegler, T., Folga, E., and Berces, A., *J. Am. Chem. Soc.*, 1993, **115**, 636

3. Sini, G., Macgregor, S.A., Eisenstein, O., and Teuben, J.H., *Organometallics*, 1994, **13**, 1049

4. Adlhart, C. and Chen, P., *Helv. Chim. Acta.*, 2003, **86**, 941

5. Adlhart, C. and Chen, P., *Angew. Chem. Int. Ed.*, 2002, **41**, 4484

6. Adlhart, C. and Chen, P., *J. Am. Chem. Soc.*, 2004, **126**, 3496

7. Cavallo, L., *J. Am. Chem. Soc.*, 2002, **124**, 8965

8. Jordaan, M., Van Helden, P., Van Sittert, C.G.C.E., and Vosloo, H.C.M., *J. Mol. Catal. A: Chem.*, 2006, **254**, 145

9. Vyboishchikov, S.F., Bühl, M., and Thiel, W., Prof., *Chem. Eur. J.*, 2002, **8**, 3962

10. Janse van Rensburg, W., Steynberg, P.J., Kirk, M.M., Meyer, W.H., and Forman, G.S., *J. Organomet. Chem.*, 2006, **691**, 5312

11. Janse van Rensburg, W., Steynberg, P.J., Meyer, W.H., Kirk, M.M., and Forman, G.S., *J. Am. Chem. Soc.*, 2004, **126**, 14332

12. Fomine, S., Vargas, S.M., and Tlenkopatchev, M.A., *Organometallics*, 2003, **22**, 93

13. Forman, G.S., McConnell, A.E., Tooze, R.P., Janse van Rensburg, W., Meyer, W.H., Kirk, M.M., Dwyer, C.L., and Serfontein, D.W., *Organometallics*, 2005, **24**, 4528

14. Adlhart, C., ***Intrinsic Reactivity of Ruthenium Carbenes: A Combined Gas Phase and Computational Study***, Ph.D thesis, Eidgenossische Technische Hochschule Zurich, 2003

15. Ivin, K.J. and Mol, J.C., ***Olefin Metathesis and Metathesis Polymerization***, Academic Press, San Diego, 1997

16. Dörwald, F.Z., ***Metal Carbenes in Organic Synthesis***, Wiley, 1999 p. 143

17. Rouhi, A.M., *Chem. Eng.*, 2002, 29

18. Wagner, P.H., *Chem. Ind.*, 1992, 330

19. Fürstner, A., Prof. Dr., *Angew. Chem. Int. Ed.*, 2000, **39**, 3012

20. Brugmaghim, J.L. and Girolami, G.S., *Organometallics*, 1999, **18**, 1923

21. Mol, J.C., *J. Mol. Catal. A: Chem.*, 2004, **213**, 39

22. Lehman, S.E., Jr., Schwendeman, J.E., O'Donnell, P.M., and Wagener, K.B., *Inorg. Chim. Acta.*, 2003, ***345***, 190

23. Dinger, M.B. and Mol, J.C., *Adv. Synth. Catal.*, 2002, **366**, 671

24. Grubbs, R.H., *J. Macromol. Sci. - Pure Appl. Chem.*, 1994, **A31**, 1829

25. Van Schalkwyk, C., Vosloo, H.C.M., and Du Plessis, J.A.K., *Adv. Synth. Catal.*, 2002, **344**, 781

26. Maechling, S., Zaja, M., and Blechert, S., *Adv. Synth. Catal.*, 2005, **347**, 1413

27. Huang, J., Schanz, H.-J., Stevens, E.D., and Nolan, S.P., *Organometallics*, 1999, **18**, 5375

28. Weskamp, T., Kohl, F.J., Hieringer, W., Gleich, D., and Herrmann, W.A., *Angew. Chem. Int. Ed.*, 1999, **38**, 2416

29. Van der Schaaf, P.A., Kolly, R., Kirner, H.-J., Rime, F., Mühlebach, A., and Hafner, A., *J. Organomet. Chem.*, 2000, **606**, 65

30. Denk, K., Fridgen, J., and Herrmann, W.A., *Adv. Synth. Catal.*, 2002, **344**, 666

31. Ung, T., Hejl, A., Grubbs, R.H., and Schrodi, Y., *Organometallics*, 2004, **23**, 5399

32. Chang, S., Jones II, L., Wang, C., Henling, L.M., and Grubbs, R.H., *Organometallics*, 1998, **17**, 3460

33. De Clercq, B. and Verpoort, F., *Tetrahedron Lett.*, 2002, **43**, 9101

34. Louie, J. and Grubbs, R.H., *Organometallics*, 2002, **21**, 2153

35. Garber, S.B., Kingsbury, J.S., Gray, B.L., and Hoveyda, A.H., *J. Am. Chem. Soc.*, 2000, **122**, 8168

36. Gessler, S., Randl, S., and Blechert, S., *Tetrahedron Lett.*, 2000, **41**, 9973

37. Kingsbury, J.S., Harrity, J.P.A., Bonitatebus, P.J., Jr., and Hoveyda, A.H., *J. Am. Chem. Soc.*, 1999, **121**, 791

38. Slugovc, C., Burtscher, D., Stelzer, F., and Mereiter, K., *Organometallics*, 2005, **24**, 2255

39. Hoveyda, A.H., Gillingham, D.G., Van Veldhuizen, J.J., Kataoka, O., Garber, S.B., Kingsbury, J.S., and Harrity, J.P.A., *Org. Biomol. Chem.*, 2004, **2**, 8

40. De Clercq, B. and Verpoort, F., *J. Mol. Catal. A: Chem.*, 2002, **180**, 67

41. De Clercq, B. and Verpoort, F., *Adv. Synth. Catal.*, 2002, **344**, 639

42. Van der Schaaf, P.A., Muhlbach, A., Hafner, A., and Kolly, R., 1999. Heterocyclyl ligand containing ruthenium and osmium catalysts. Patent: *WO 99/29701*

43. Randl, S., *Synth. Lett.*, 2001, **3**, 430

44. Kostas, I.D., *J. Organomet. Chem.*, 2001, **626**, 221

45. Le Gall, I., Laurent, P., Soulier, E., Salaün, J.-Y., and Des Abbayes, H., *J. Organomet. Chem.*, 1998, **567**, 13

46. Bielawski, C.W., ***Tailoring Polymer Synthesis with Designer Ruthenium Catalysts***, Ph.D thesis, California Institute of Technology, 2003

47. Slone, C.S., Weinberger, D.A., and Mirkin, C.A., *Progr. Inorg. Chem.*, 1999, **48**, 233

48. Meyer, W.H., Brull, R., Raubenheimer, H.G., Thompson, C., and Kruger, G.J., *J. Organomet. Chem.*, 1998, **553**, 83

49. Francis, J.A., Bott, S.G., and Barron, A.R., *J. Chem. Soc., Dalton Trans.*, 1998, 3305

50. Sanford, M.S. and Love, J.A. *in* ***Handbook of Metathesis***, Grubbs, R.H., Ed., *Mechanism of Ruthenium-Catalysed Olefin Metathesis Reactions*, Vol. 1, Wiley, 2003, p. 112

51. Sanford, M.S., Love, J.A., and Grubbs, R.H., *J. Am. Chem. Soc.*, 2001, **123**, 6543

52. Sanford, M.S., Ulman, M., and Grubbs, R.H., *J. Am. Chem. Soc.*, 2001, **123**, 749

53. Ulman, M. and Grubbs, R.H., *Organometallics*, 1998, **17**, 2484

54. Dias, E.L., Nguyen, S.T., and Grubbs, R.H., *J. Am. Chem. Soc.*, 1997, **119**, 3887

55. McGuinness, D.S., Cavell, K.J., Skeleton, B.W., and White, A.H., *Organometallics*, 1998, **18**, 1596

56. Trost, B.M., *Science*, 1991, **254**, 1471

57. Davis, M.E. and Scrib, S.L., ***Selectivity in Catalysis***, American Chemical Society, Washington, DC, 1993

58. Deckers, P.J.W., ***Non Flory-Schulz Ethene Oligomerization with Titanium-based Catalysts***, Proefschrift, Rijksuniversiteit Groningen, 2002

59. Wijkens, P., Jastrzebski, J.T.B.H., Van der Schaaf, P.A., Kolly, R., Hafner, A., and Van Koten, G., *Org. Lett.*, 2000, **2**, 1621

Literature Review: Alkene Metathesis 2

2.1 Introduction

Calderon[1] introduced the term alkene metathesis in 1967 to describe the disproportionation of alkenes. Alkene metathesis can be defined as a metal-catalysed carbon skeleton redistribution reaction in which all carbon-carbon double bonds are cut and rearranged in a statistical fashion (**Scheme 2.1**).[2,3]

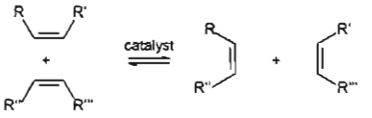

R, R', R'', R''' = H, alkyl, aryl

Scheme 2.1 Schematic representation of the alkene metathesis reaction.

Apart from the acyclic cross-metathesis reaction given in **Scheme 2.1**, a further four types of alkene metathesis reactions can be correlated with respect to each other as depicted in **Scheme 2.2**: ring-opening metathesis polymerisation (ROMP), ring-closing metathesis (RCM), ring-opening metathesis (ROM) and acyclic diene metathesis (ADMET).[4]

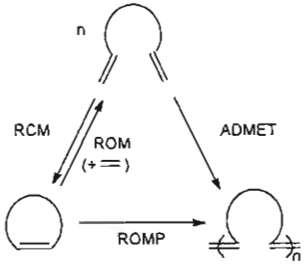

Scheme 2.2 Types of alkene metathesis reactions.[4]

In this study the focus will be on the metathesis of 1-alkenes with ruthenium alkylidene complexes, which can occur either through cross-metathesis or self-metathesis of the alkenes.[3] Cross-metathesis takes place between two different alkene substrates (**Scheme 2.1**), while self-metathesis occurs between the same alkene substrates, which may be either productive (**Scheme 2.3**) or unproductive (**Scheme 2.4**).[3]

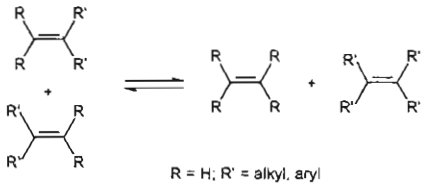

Scheme 2.3 Productive self-metathesis of an unsaturated, unsymmetrical alkene.

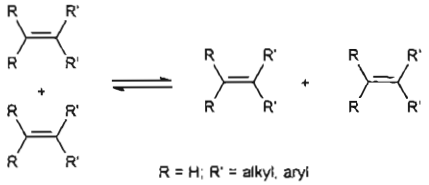

Scheme 2.4 Unproductive self-metathesis of an unsaturated, unsymmetrical alkene.

Although today the alkene metathesis reaction is a well-known reaction, it took several years for scientists to understand these reactions. In the last decade new insights into the mechanism of the alkene metathesis reaction were gained both through experimental and theoretical investigations. This is mainly due to fast technological development in computational chemistry as well as analytical techniques for identifying intermediate complexes forming during the reaction.

2.2 Historical Overview

In 1931, Schneider and Fröhlich[5] observed the pyrolytic combination of propene molecules to form ethene and butene, which was a non-catalytic metathesis reaction. Although it is generally thought that Banks and Bailey[6] discovered the metathesis reaction in 1964, Eleuterio[7,8] actually already patented it in 1957. He observed the formation of a propene-ethene copolymer from propene in the presence of a $MoO_3/Al_2O_3/LiAlH_4$ catalytic system. Banks and Bailey[6] applied the

process of Evering and Peters[9,10] for the transformation of propene into ethene and 2-butene on supported molybdenum oxide in 1964 in the Phillips Triolefin Process.[11] The first open publication on alkene metathesis, foreshadowed by the abovementioned patents, was a report by Truett et al.[12] in 1960 on the ROMP of norbornene. The reaction was initially known as alkene disproportionation until the term "alkene metathesis" was used in 1967 with the discovery of the first homogeneous WCl_6/EtOH/$EtAlCl_2$ catalytic system, which produced both metathesis and polymerisation products.[1] It was not until the discovery of heterogeneous and homogeneous catalysts, which could promote the reaction at lower temperatures and minimise side-reactions, that the potential of the metathesis reaction was realised.[2]

The time line of milestones in the field of alkene metathesis is displayed in **Figure 2.1** to show the important acceleration in catalyst precursor discoveries and the increasing use of ruthenium catalysts for metathesis.

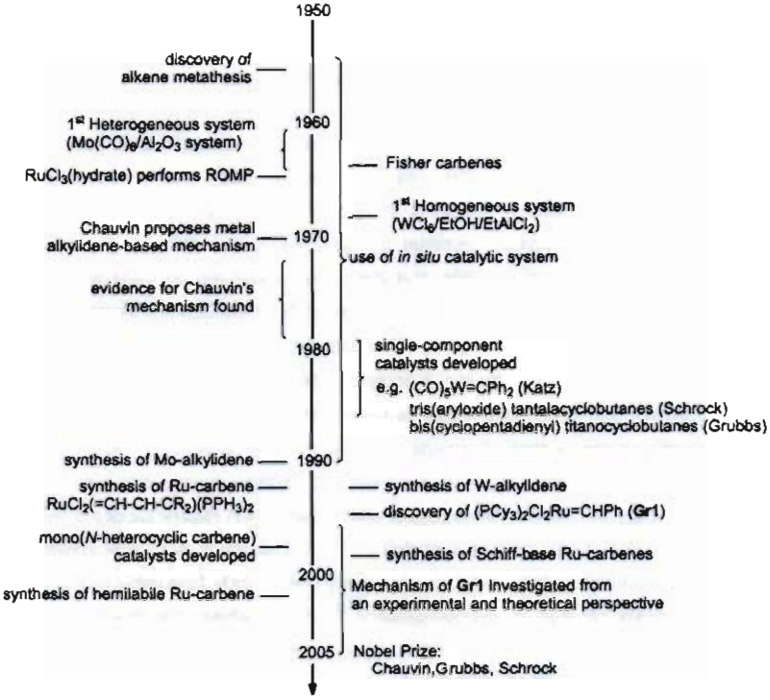

Figure 2.1 Time line of milestones in the development of alkene metathesis catalysts.[13,14]

2.3 Development of catalytic systems

From the late 1960's through the early 1980's, the majority of alkene metathesis reactions were carried out with ill-defined multicomponent heterogeneous and homogeneous systems. They consisted of transition metal salts deposited on solid supports or combined with main group alkylating agents. Some of the classic combinations included $WCl_6/SnBu_4$, $WOCl_4/EtAlCl_2$, MoO_3/Al_2O_3 and Re_2O_7/Al_2O_3, which were highly active for the metathesis of acyclic alkenes, but readily deactivated in the presence of air, water or polar functional groups.[3] The first single-component homogeneous catalysts for alkene metathesis were discovered during the late 1970's and early 1980's. These included bis(cyclopentadienyl) titanocyclobutanes,[15] tris(aryloxide) tantalacyclobutanes[16] and various dihalo-alkoxide-alkylidene complexes of tungsten,[17,18] which showed high activity towards ROMP of norbornene.

In the mid seventies, when the development of transition metal carbene complexes started, two different patterns of reactivity were discovered. At that time these complexes were divided into two classes, i.e., the Fischer- and Schrock-type carbenes, named after their discoverers.[19] Various other types of carbene complexes are also known today e.g. Casey carbene, Grubbs carbene etc., but they are all just variants of either the Fischer or Schrock carbene.

At this point it will be useful to define the term metal carbene complex, which refers to compounds of the general type $L_nM{=}CRR'$, where the carbene moiety, =CRR', is coordinated to a transition metal atom, M, and L_n represents the various other coordinated ligands. The first carbene complexes were evidently prepared in 1915, but it was not until the synthesis of $(OC)_5W{=}C(OMe)Ph$ by Fischer[20] in 1964, that they were recognised as carbene complexes.[21] Fischer carbenes are characterised by electrophilic reactivity of the carbene ligand containing π-donor substituents such as –OMe or $–NMe_2$. The carbene moiety is typically bound to electron-rich, low oxidation state metals, having π-acceptor ligands L_n.[22,23] Schrock carbenes have nucleophilic carbene ligands bound to higher oxidation state, early-transition metals, having non π-acceptor ligands and non σ-donor R groups.[22,24] The Grubbs carbenes can be related to the Schrock carbenes, in that they also have a nucleophilic carbene moiety, with the metal centre susceptible to nucleophilic attack. The molecular orbital diagrams in **Figure 2.2** depict the bonding in Fischer and Schrock metal carbene complexes.[22,25] Various forms of Fischer carbenes were shown to have metathesis activity, but they were rarely energetically favourable and the reaction with alkenes usually resulted in cyclopropanation.[23] Nonetheless, the research into these complexes was significant because it identified many of the basic organometallic processes that were intertwined with early mechanistic thinking.

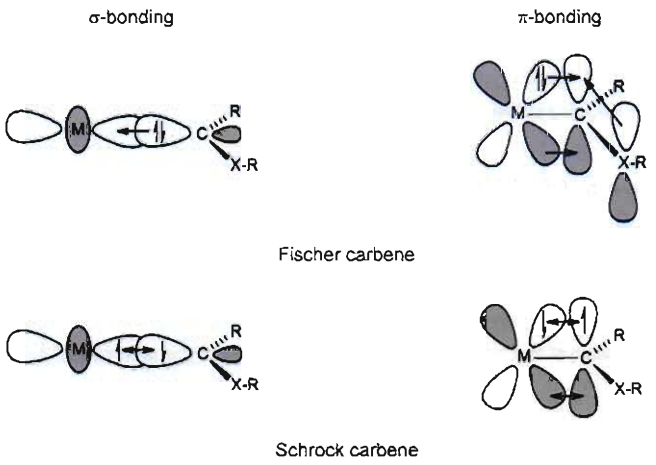

Figure 2.2 Molecular orbital diagrams depicting the bonding in Fischer and Schrock metal carbene complexes (X = O, N or S).[22,25]

In general, metal carbene complexes where the carbene substituents are exclusively composed of carbon and hydrogen or alkyl substituents, are referred to as either alkylidenes or (substituted) methylidenes.[26] Therefore, the term alkylidene(s) will be used hereafter to describe systems where the carbene moiety =CRR' contains no heteroatom substituents. For example, for R = H and R' = Ph the alkylidene is referred to as a benzylidene, while a methylidene contains R = R' = H. Therefore, the R' group determines the name of the alkylidene.

The molybdenum and tungsten alkylidenes of the general formula M(NAr)(OR')$_2$(=CHR) were the first Schrock-type carbenes to become widely used, particularly the alkoxy imido molybdenum complex **2**.[27-30] The high activity of **2** allowed it to react with both terminal and internal alkenes and to ROMP low-strain monomers, as well as to ring-close sterically demanding and electron-poor substrates.[27-31] However, this catalyst and others based on the early transition metals were limited by the high oxophilicity of the metal centres, which rendered them extremely sensitive to oxygen and moisture.[13]

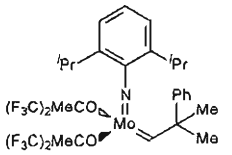

2

The prospect of solving the problems related to oxophilicity and functional group tolerance most likely inspired the continuous search for more stable and catalytically active complexes for the alkene metathesis reaction. In 1980, Tsuji et al.[32] summarised the challenge facing alkene metathesis in the following statement:

> "In order to exploit the metathesis reaction as a truly useful synthetic methodology, it is essential to discover a new catalyst system which can tolerate the presence of functional groups in olefin molecules."

Therefore, the key to improved functional group tolerance in alkene metathesis would be the development of a catalyst that reacts preferentially with alkenes in the presence of heteroatomic functionalities.

Grubbs[33] had been interested in the metathesis reaction early on, as indicated by his mechanistic proposal of a metallocyclopentane intermediate in the early 70's. After some exploration, which started in the mid eighties, of ill-defined catalysts that were prepared from late metal salts, Novak and Grubbs[34,35] found that ruthenium trichloride was active for the ROMP of strained cyclo-alkenes (such as norbornene) in organic solvents. This suggested that ruthenium might be the metal of choice for a potentially well-defined late transition metal alkene metathesis catalyst.[36] After applying the methodology for the synthesis of tungsten alkylidenes to the synthesis of a ruthenium catalyst, the first well-defined, metathesis-active ruthenium alkylidene complex was synthesised (**Scheme 2.5**).[37,38] The combination of *tris*-triphenylphosphine-ruthenium(II) chloride with 3,3-diphenylcyclopropene led to the isolation of **3** as a mixture of *cis*- and *trans*-bis(phosphine) isomers.[38,39] This catalyst (**3**) was active for the ROMP of highly strained cyclo-alkenes, but inactive for the metathesis of acyclic alkenes.[39] The activity of **3** was extended to the metathesis of less strained cyclic alkenes and acyclic alkenes with the replacement of the triphenylphosphine ligands with bulkier and more basic tricyclohexylphosphine (PCy_3) ligands (**4**).[40] The synthesis of these complexes remained difficult, due to the difficulty of synthesising diphenylcyclopropene, which limited the availability of these complexes.[41]

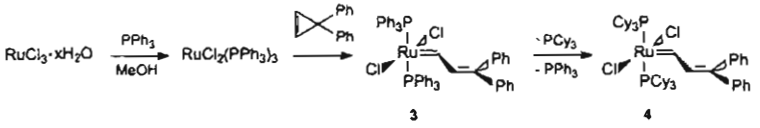

Scheme 2.5 Development of well-defined metathesis active ruthenium alkylidenes.[36,39]

Schwab et al.[41] developed an alternative route (**Scheme 2.6**) for the synthesis of ruthenium alkylidenes in the late 1990's, in which ruthenium(II) species were found to insert into α-diazoalkanes. The reaction of *tris*-triphenylphosphineruthenium(II) chloride with phenyldiazomethane and PCy_3 led to the development of a ruthenium(II) benzylidene (**Scheme 2.6**, **5a**) complex of wide academic and commercial utility, known as the first generation Grubbs catalyst (**Grl**).[36]

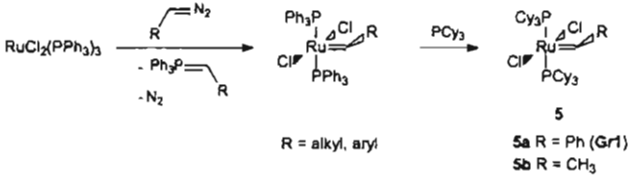

Scheme 2.6 Synthesis of ruthenium alkylidenes by insertion into α-diazoalkanes.[38,41]

However, the diazo route shown in **Scheme 2.6** was not ideal for large-scale reactions, due to the use of unstable reagents and large amounts of solvent.[13] For this reason, several groups developed new synthetic routes (eqs. 1-5) for the synthesis of ruthenium alkylidene complexes with the general formula $RuCl_2(PR'_3)_2(=CHR)$.[14,42,43] These Grubbs-type catalysts (benzylidene and vinylalkylidene) have been shown to be highly active for metathesis, moderately sensitive to air and moisture and significantly tolerant of functional groups.[38,40,41,44-47]

The development of single-component catalysts allowed the relationships between structure and reactivity to be more clearly defined. Grubbs and co-workers[48] noted that functional group tolerance and activity followed opposing periodic trends as the catalyst systems were varied from left to right and bottom to top on the periodic table. Therefore, these catalysts react more selectively with alkenes as the metal centres are varied in the abovementioned way.[48] This trend is illustrated for titanium, tungsten, molybdenum, and ruthenium in **Table 2.1**. The late transition metals showed higher reactivity towards alkenes than the early transition metals, which reacted readily with polar functional groups such as carbonyls.[49] This trend makes it possible to increase the functional group tolerance of an alkene metathesis catalyst by focusing on a later transition metal, such as ruthenium.

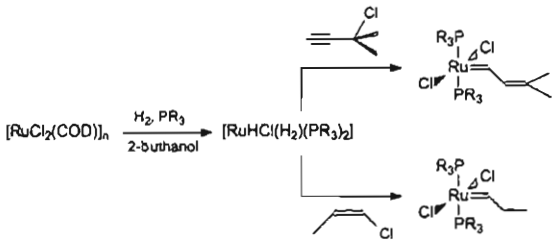

(1) [43]

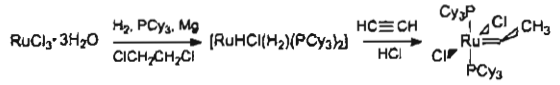

(2) [50]

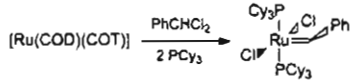

(3) [51]

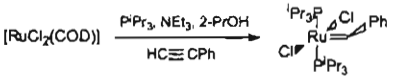

(4) [52]

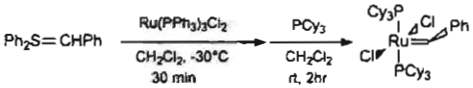

(5) [53]

An increasing interest in obtaining better reactivity and adapting the ruthenium carbene complexes to specific catalytic conditions, made the investigation of various modifications to **Gr1** feasible. With the variation of the ligand sphere around the ruthenium centre, a number of alkylidene complexes with higher substrate tolerance and increased reactivity were generated.[54] For the class of $RuX_2L_2(=CHR)$ complexes, the X- and L-type ancillary ligands were varied, as well as substituents on the functional alkylidene ligand. It has been found that changes in this ligand sphere can have profound and largely unpredictable effects on catalytic activity, stability and selectivity.[13,55] The alkylidene[39,41,44,45] and the phosphine[41,44,56] ligand as well as the exchange of the halogen,[45] have been investigated by several groups.

Table 2.1 Functional group tolerance of early and late transition metal alkene metathesis catalysts.[48]

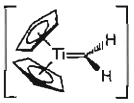

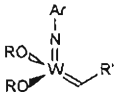

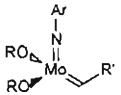

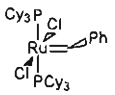

Titanium	Tungsten	Molybdenum	Ruthenium
Acids	Acids	Acids	**Alkenes**
Alcohols, Water	Alcohols, Water	Alcohols, Water	Acids
Aldehydes	Aldehydes	Aldehydes	Alcohols, Water
Ketones	Ketones	**Alkenes**	Aldehydes
Esters, Amides	**Alkenes**	Ketones	Ketones
Alkenes	Esters, Amides	Esters, Amides	Esters, Amides

Increasing reactivity

Increasing reactivity of metal-carbene complexes with alkenes in preference over other functional groups

Since phosphines suffer from significant P-C degradation at elevated temperatures,[57-59] the sterically demanding imidazolylidene ligands, which can mimic phosphine behaviour as well as show stability at higher temperatures,[60] were investigated. The replacement of both PCy_3 ligands in **Gr1** by N,N-disubstituted imidazolylidene moieties (**6**) gave a catalytic system that was too stable and hence did not demonstrate an improved activity profile.[61] This problem was overcome by the use of a mixed ligand system, through combining one kinetically inert, electron-donating N-heterocyclic carbene (NHC) ligand with a coordinatively labile ligand. These complexes were termed "second generation" catalysts due to the incorporation of an NHC-type ligand into **Gr1**. The more strongly electron-donating NHC ligand might therefore enhance the dissociation of the more labile *trans*-phosphine from the metal centre. Then, the steric bulk and electron-donating properties of the NHC ligand, should stabilise the electron-deficient intermediates and promote alkene metathesis.[62,63]

Three different research groups reported almost simultaneously on the preparation and catalytic properties of a variety of "second generation" ruthenium alkylidene complexes as illustrated by complexes **7-9**.[57,62-68] The replacement of the phosphine ligand in **Gr1** by a NHC[57,63,67] improved the lifetime and reactivity of **Gr1**.[64] This is due to the bulkiness and increased basicity of the NHC ligand compared to PCy_3. Various authors[69-72] have referred to both **7** and **8a** as the second generation Grubbs catalyst (Grubbs 2 or **Gr2**), which can be rather confusing, since these systems are structurally similar, differing only in the backbone of the NHC-ring (4,5-position).

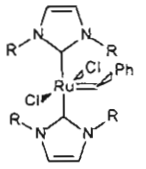

R = 2,4,6-trimethylphenyl
2,6-diisopropylphenyl

6

In **8a**, the 4,5-position is saturated, making the NHC ligand more electron-rich[73] and only this complex is commercially available as **Gr2**. Catalyst **8a** has also been reported to be more active than **7**,[63,74,75] particularly in the polymerisation of high strained alkenes such as DCPD.[36] In this thesis, **8a** will hereafter be referred to as **Gr2**.

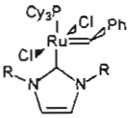

R = 2,4,6-trimethylphenyl

7

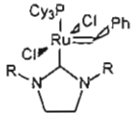

R = 2,4,6-trimethylphenyl (a)
2,6-diisopropylphenyl (b)

8

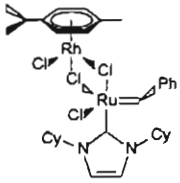

9

In 1998, Dias et al.[76] used an organometallic moiety as ligand to generate bimetallic carbene complexes **10a-c** from **Gr1**. These complexes showed higher activities towards ROMP of 1,5-cyclooctadiene than **Gr1**, which was dependant on the nature of the second metal, decreasing in the order Rh > Os > Ru.[76]

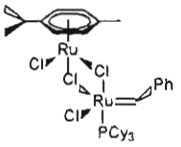

10a

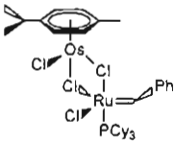

10b

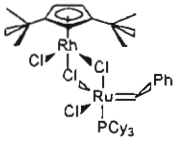

10c

In the last decade, several groups followed different design concepts (Figure 2.3) to obtain ruthenium carbene thermally switchable initiators for ROMP and/or RCM reactions.[46,77-88] This was in all probability motivated by the increasing interest in more stable and catalytically active systems for metathesis reactions.

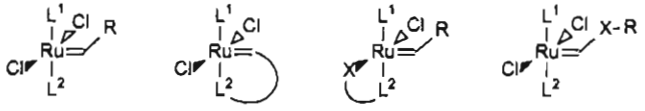

A B C D

L^1 = PCy_3, H_2IMes

Figure 2.3 Design concepts for thermally switchable initiators.[85]

The strategy behind the design concepts of these initiators were to slow down or even prevent the dissociation of L^2 at room temperature.[85] Up to now, this could not be applied to motif **A**, where an inert ligand L^2 in a position *trans* to L^1, which is mostly a phosphine such as PCy_3 or an NHC such as 1,3-bis(mesityl)-4,5-dihydroimidazol-2-ylidene (H_2IMes), was shown to be too labile at room temperature.[85] Several groups overcame this with the use of chelating ligands, where L^2 is either attached to the carbene (motif **B**, Hoveyda-type catalysts[46,83,84,88]) or via X (motif **C**,[78,80,81] where X is for example an oxygen) to the central ruthenium atom.

For motif **C**, Grubbs,[80] and later Verpoort,[87,88] introduced bidentate O,N-chelated Schiff-base ligands on **Gr1** to give complexes **11**. The development of these systems were motivated by the increasing interest into controlling *cis*/*trans* selectivity in alkene metathesis processes and maintaining high activity in polar protic solvents.[80,81,87] Their catalytic activity for RCM and ROMP increased with an increase in reaction temperature.[78,81,88]

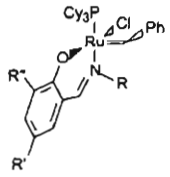

R', R" = H, R = 2,6-^{i}PrC$_6$H$_3$
R" = Me, R' = NO_2, R = 2,6-^{i}PrC$_6$H$_3$
R" = H, R' = NO_2, R = 2,6-^{i}PrC$_6$H$_3$
R" = H, R' = NO_2, R = 2,6-Me-4-MeOC$_6$H$_2$
R" = H, R' = NO_2, R = 2,6-Me-4-BrC$_6$H$_2$
R" = H, R' = NO_2, R = 2,6-Cl-4-CF_3C$_6$H$_2$
R" = H, R' = NO_2, R = 2,6-^{i}Pr-4-NO_2-C$_6$H$_3$
R" = H, R' = NO_2, R = CH_2-Ad

Ad = 

11

The significance of finding a well-defined alkene metathesis initiator possessing the ideal balance between activity and stability inspired Verpoort et al.[88] to develop a bimetallic ruthenium carbene system (**12**). The combination of the labile p-cymene with Schiff-base ligands produced catalytic systems that exhibited very high thermal stability and activity for both RCM and ROMP.

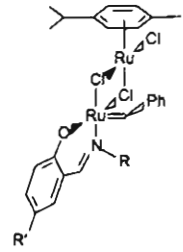

R' = H, R = Me
R' = NO_2, R = Me
R' = H, R = 2,6-Me-4-BrC$_6$H$_2$
R' = NO_2, R = 2,6-Me-4-BrC$_6$H$_2$
R' = H, R = 2,6-^{i}PrC$_6$H$_3$
R' = NO_2, R = 2,6-^{i}PrC$_6$H$_3$

12

The low reactivity of **11** at room temperature was mainly attributed to the additional stability of the chelating ligand. The thermal stability and activity of these complexes were increased through the combination of the Schiff-base ligand with a NHC ligand (**13**).[76,81,88] The presence of the bulky NHC ligand *trans* to the decoordinating part of the Schiff-base stabilised the reactive catalytic intermediate and/or prevented the decomposition of the carbene.[81]

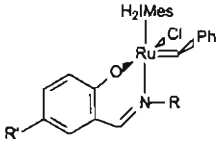

R' = H, R = Me
R' = NO_2, R = Me
R' = H, R = 2,6-Me-4-BrC_6H_2
R' = NO_2, R = 2,6-Me-4-BrC_6H_2
R' = H, R = 2,6-^{i}PrC_6H_3
R' = NO_2, R = 2,6-^{i}PrC_6H_3

13

Another example for motif **C** is the first and second generation ruthenium benzylidene complexes, synthesised by Herrmann and co-workers,[78] bearing a hemilabile pyridinyl alcoholate ligand (**14**). The NHC catalytic systems showed low activity for ROMP at room temperature due to their resting state stabilisation.[78] The catalytic activity of these systems increased with an increase in temperature, which was comparable to **Gr2**. However, the performance of the **Gr1**-type systems has not been tested for catalytic activity in any metathesis reaction. Hafner et al.[88] have patented another example, where the ruthenium alkylidene system is complexed by a tri-isopropylphosphine and pyridinyl alcoholate (**15**). Although no catalytic activity was reported for these systems, it has been claimed that these systems are active for ROMP and RCM reactions.[89]

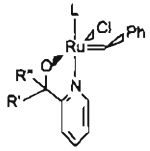

L = PCy_3, R'' = $(CH_2)_5$ **(14a)**

L = 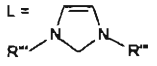

R' = R'' = Me; R''' = Cy **(14b)**
R' = R'' = Me; R''' = CH_2CH_2Ph **(14c)**
R'' = $(CH_2)_5$; R''' = CH_2CH_2Ph **(14d)**
R'' = $(CH_2)_5$; R''' = Cy **(14e)**

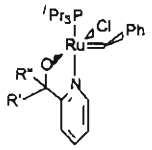

R' = R'' = Me **(15a)**
R' = R'' = Me **(15b)**
R'' = $(CH_2)_5$ **(15c)**
R'' = $(CH_2)_5$ **(15d)**

Hoveyda and co-workers[48] synthesised an active metathesis catalyst which contained an internal metal-oxygen chelate (motif **B**, **16**), which was readily obtained by the sequential treatment of $Cl_2Ru(PPh_3)_3$ with (2-isopropoxyphenyl)-diazomethane and PCy_3. They readily mediate the RCM of five-, six-, seven-, and eight-membered carbo- and heterocycles and are easily recovered chromatographically in high yield after the reaction is complete. This is mainly due to their excellent stability to air and moisture.

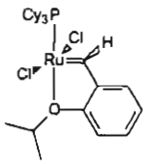

16

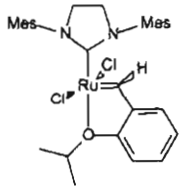

17

Blechert et al.[84] modified complex **16**, by introducing a NHC-ligand, to show that O-chelating benzylidene moieties can be used for the synthesis of ruthenium complexes with a non-phosphine leaving ligand (**17**) to obtain different selectivities and reactivities towards alkene metathesis reactions as compared to **Gr2**. For example, the ring closure of dienes such as **18** to form **19** is completed in less than 15 min at room temperature using **17**, whereas **Gr2** requires higher temperatures.[84] In contrast to **Gr2**, which proved to be an excellent catalyst for yne-ene CM,[80] analogous reactions with catalyst **17** yielded only traces of the desired products.

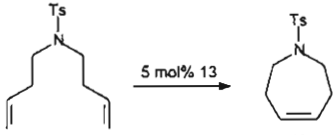

18 19

In D, Fischer-type carbenes (where X = O, N or S) (**20**, **21**) instead of Schrock carbenes were used to design a thermally switchable complex.[77,82] These catalytic systems have been mainly used for ROMP and/or RCM experiments at elevated temperatures.

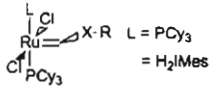

X-R = OCH2CH3
= SCH2CH3
= SPh
= N(carbazole)
= N(pyrrolidinone)

20

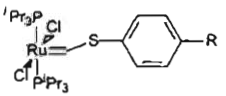

21

The various modifications to the Grubbs carbenes, as briefly outlined above, illustrate that the steric and electronic properties of the ligands coordinated to the ruthenium carbene (Ru=C) centre can improve the stability, activity and selectivity of **Gr1** and **Gr2**. During the last decade, new insights into the ruthenium-mediated alkene metathesis reaction have been gained through extensive synthetic,[41,42,44] mechanistic[45,91] and theoretical[92,93] investigations. Through progress in computer technology, computational chemistry has become a powerful tool to resolve the effect of ligand coordination and to gain deeper insights into the mechanism of catalytic reactions. For example, with the use of simple substrates and simplified ligands, a number of postulated mechanistic pathways have been investigated for the alkene metathesis reaction in order to resolve certain aspects of the reaction mechanism, which includes whether the metathesis reaction progresses according to an associative or dissociative mechanism (§ 2.6.2).[94-97]

In 2005 the Nobel prize was awarded to the pioneers in metathesis i.e. Chauvin, Schrock and Grubbs. The committee awarding the prize said:[98]

> "This represents a great step forward for 'green chemistry,' reducing potentially hazardous waste through smarter production. Metathesis is an example of how important basic science has been applied for the benefit of man, society and the environment."

This exemplifies the importance of the metathesis reaction for both academic and industrial use for the production of new molecules.

2.4 Properties of organometallic catalysts

The design of new transition metal complexes with enhanced activity and selectivity for application in alkene metathesis reactions is of great importance. In these complexes, the metal atom itself may have a number of roles, based on its coordination geometry, oxidation state and magnetic, electronic or photochemical behaviour. The properties of the complex can be tuned or completely altered by the ligands (molecules or ions) that are bonded to the metal. Therefore, various factors can influence the catalytic activity and selectivity of the transition metal complexes as summarised under the following headings:

1. Bonding ability of transition metals
2. Variability of the coordination number of the transition metal
3. Variability of the oxidation state of the transition metal
4. Choice of ligands
5. Ligand effects

2.4.1 Bonding ability of transition metals

A transition metal ion has nine valence shell orbitals, i.e. five *nd*-, one (n+1)*s*- and three (*n*+1)*p*-orbitals. The availability of these valence orbitals gives transition metals the ability to form both σ- and π-bonds with other moieties or ligands, which plays a major role in the catalytic activity of transition metals and their complexes. An example of this ability of transition metals can be seen in **Figure 2.4** for the bonding of ethene to a transition metal centre. The filled π-orbital of the ethene molecule overlaps with one of the empty metal orbitals to form a σ-bond. This metal-ethene σ-overlap is shown in **Figure 2.4** (a). A π-bond is formed through the interaction of the unoccupied antibonding π-orbitals on ethene with the filled *d*-orbitals of the metal. This metal-ethene π-overlap, which is known as metal-to-ligand back donation, is illustrated in **Figure 2.4** (b). The combined bonding is shown in **Figure 2.4** (c).[22,99-101] The bonding components illustrate a synergy, i.e. they reinforce and/or compliment each other. In the σ-component, the electron density flows from an ethene bonding orbital to the metal, while in the π-component, electron density is transferred from the metal to the ethene antibonding orbitals. A weakening or reduction in the bond order of the ethene carbon-carbon single bond results from these transferences.[101,102] The coordination of an alkene to a metal centre therefore alters the electron density in the carbon-carbon single bond and in many cases makes it more susceptible to a nucleophilic attack by OH^--, H^-- and R^--species.[98]

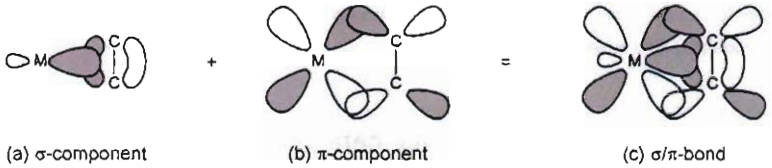

(a) σ-component (b) π-component (c) σ/π-bond

Figure 2.4 Molecular orbital representation of ethene bonded to a transition metal.[99]

Trivalent phosphorus compounds are important ligands in many transition metal catalyst systems. In principle, these ligands can bond to transition metals by making use of both σ- and π-orbitals in much the same way as C_2H_4 and carbonyl ligands. The σ-component is formed by donation of the phosphine lone pair to an empty σ-orbital on the metal. The π-component of the bonding is formed by back donation from a filled metal orbital to an empty orbital on the phosphine ligand. This empty phosphorous orbital has been described as being either a *d*-orbital or an antibonding σ-orbital (σ*), both of which have π-symmetry with respect to the metal ligand bond (**Figure 2.5**).[99,103]

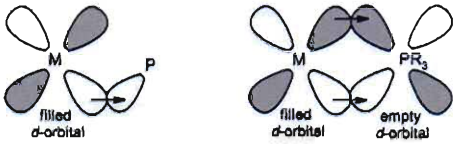

Figure 2.5 Molecular orbital representation of back donation from a filled metal orbital to an empty orbital on the phosphine ligand.[104]

As was the case for the alkene, the σ-component results in a transfer of electron density from the ligand to the metal and the π-component in metal-to-ligand back bonding. The σ-donating capacity of the phosphine ligand tends to decrease as electron-withdrawing (electronegative) groups are placed on the phosphorous atom. At the same time, the energy of the π-acceptor (σ*) on phosphorous is lowered in energy, providing an increase in back bonding ability. Therefore, phosphines can exhibit a range of σ-donor and π-acceptor capabilities, and the electronic properties of a metal centre can be tuned by the substitution of electronically different but isosteric phosphines.[103] Transition metal elements can therefore readily form strong bonds with compounds containing π-electron systems or which have orbitals of suitable symmetry/energy to form *d*π-bonds in order to change the catalytic activity of the catalysts.

2.4.2 Variability of the oxidation state of the transition metal

Theoretically, transition metals have access to a number of formal positive oxidation states, due to the available valence *d*- and *s*-electrons. This implies that transition metals can form an array of complexes with different oxidation states, but not all of these complexes are stable.[99]

However, the ability to readily interchange between oxidation states during the course of a reaction is perhaps more important than the number of oxidation states available for the transition metal. For example, rhodium undergoes a I → III → I oxidation/reduction cycle for every catalytic cycle during the hydrogenation of alkenes (**Figure 2.6**).[105] In a typical hydrogenation reaction at ambient conditions the rhodium must be capable of going through this sequence every minute.[105] The Group 8 transition metals have the ability to readily enter into redox cycles, which is one of the main factors that contribute to their wide range of catalytic activity.

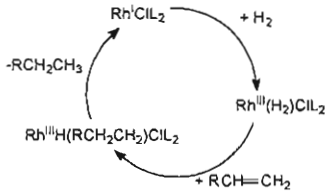

Figure 2.6 A catalytic cycle for the hydrogenation of alkenes in the presence of $RhClL_2$ complexes

2.4.3 Variability of the coordination number of the transition metal

The ability of a transition metal to accommodate different ligands in its coordination sphere is important if it contributes to the catalytic reaction between one or more substrates. Transition metal complexes containing as many as nine ligands in the coordination sphere are well established,[99] *inter alia* ReH_9^{2-} and $WH_6(PR)_3$. However, transition metal complexes with coordination numbers between four and six are more commonly encountered.

As in the case of oxidation state (§ 2.4.2), the ability to adopt different coordination numbers and consequently different stereochemistries as well as change between them, is of great importance to the catalytic activity of the transition metal complex.[89] For example, during the hydrogenation reaction catalysed by $RhCl(PPh_3)_3$ (**Figure 2.7**), the rhodium goes from a four coordinated square planar structure to a six coordinated octahedral structure, to a five coordinated square pyramidal structure, to a six coordinated octahedral structure, to a five coordinated square pyramidal structure, to a four coordinated trigonal structure and back to a four coordinated square planar structure during one catalytic cycle of the reaction.[105]

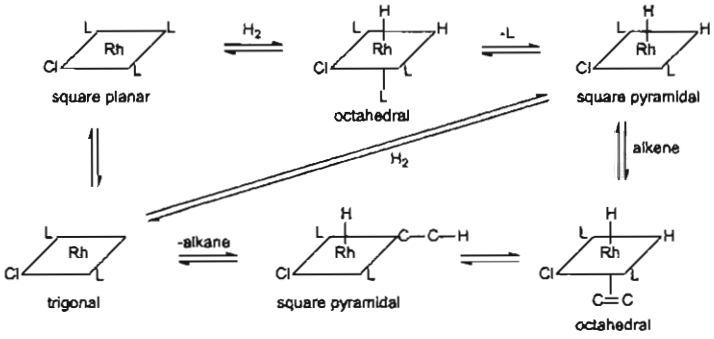

Figure 2.7 Stereochemical changes during the hydrogenation of alkenes catalysed by $RhClL_3$ (L = PPh_3).[105]

2.4.4 Choice of ligands

In the context of transition metal coordination chemistry a ligand can be defined[99] as any element or combination of elements, which forms chemical bonds with a transition element. This ligand can even be a transition metal. In order to coordinate to a metal, a ligand must have electron density that is available to donate to an empty metal orbital.[108] For many ligands, this electron density resides in a lone pair of electrons making these ligands nucleophilic, while the metal ion is electrophilic due to the available empty *d*-orbitals that can accept the lone pair electrons. Transition metals can form bonds with almost every element in the periodic table as well as with any organic molecule.[106] It is this property which results in the rich coordination chemistry of transition metals and leads to their role in catalysis.

Three different types of ligands can be identified, i.e. monodentate, bidentate and multidentate ligands. Monodentate ligands can form one coordinate bond with a central metal ion, while bidentate ligands (**Figure 2.8**) form two and multidentate (**Figure 2.9**) three/more coordinate bonds with a central metal ion.[107]

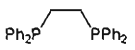

Bis(diphenylphosphino)ethane (=diphos or dppe)

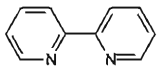

2,2'-bipiridine (bpy)

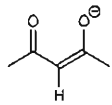

Acetylacetonate (acac)

Figure 2.8 Examples of bidentate ligands with two heteroatoms.

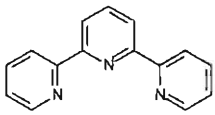

Terpyridine (trpy)

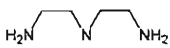

Diethylene triamine (dien)

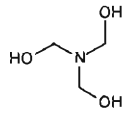

Tris(hydroxymethyl)amine (tris)

Figure 2.9 Examples of multidentate ligands with three/more heteroatoms.

Monodentate ligands can basically be divided into two groups:[99]

1. ligands with a formal ionic charge, e.g. Cl^-, H^-, OH^-, CN^-, $alkyl^-$, $aryl^-$ and $COCH_3^-$; and
2. neutral ligands, e.g. CO, alkene, alkyne, tertiary-, secondary- and primary-phosphine, -arsine or -phosphite, H_2O and amine.

The distinction between ionic and neutral ligands is useful in determining the oxidation state of the metal centre and in describing reactions. In most transition metal complexes, ionic ligands form covalent, rather than ionic bonds.[99] In most cases, the charge separation in the bond between the metal centre and neutral ligands is larger than in the bond between a metal centre and ionic ligands.[99] The majority of ligands are anions or neutral molecules which function as electron-pair donors.[108] Based on the nature of the donating electron pairs, ligands can be classified as lone pair, π-bonding and σ-bonding electron pair donors. Examples of ligands with donating electron pairs are illustrated in **Figure 2.10**.

(a) lone pair donors (b) π-bonding donors (c) σ-bonding donors

Figure 2.10 Examples of various ligands with donating electron pairs.

Ligands that donate electron pairs to form a M-L σ-bond are called σ-donors, but some of these ligands might behave like π-acceptors due to their orbitals having the appropriate π-symmetry as illustrated in **Figure 2.11**.[104]

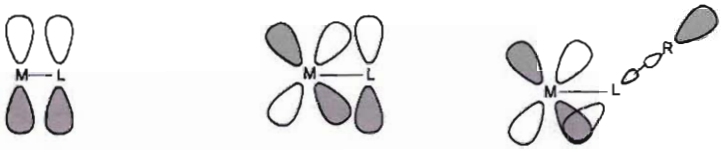

(a) pπ-pπ (b) dπ-pπ (c) dπ-σ*

Figure 2.11 Origins of π-bonding.[104]

It is important to make a further distinction between ligands, namely ligands that form part of the products (participative ligands) and those that do not form part of the products (non-participative ligands) during the catalytic cycle. Although the latter group of ligands does not physically contribute to the direct products of the catalysed reaction, they influence the activity and selectivity of the catalytic system.[99,109]

2.4.5 Ligand effects

The ability of transition metal complexes to accommodate both participative and non-participative ligands within their coordination sphere offers researchers the possibility of directing the course of a reaction between participating ligands. This is achieved by modifying the structural and electronic properties (σ-donating, π-donating or -accepting abilities) of the non-participating ligands.[99] Changing the donor atom of the ligand can modify its coordination ability and therefore the electronic properties of the ligand. Modifying the steric and electronic environment of the active position of the ligand, i.e. the position where the participative ligand combines with the metal centre, can influence the behaviour of a transition metal catalyst. The resulting effect is usually a combination of both electronic and steric parameters. For example, the solubility of a ligand, and hence that of the resultant complexes, can be affected by the substituents on the ligand *inter alia* functional groups can be added to a ligand in order to enhance solubility in a particular solvent.[105] Although no real theories exist regarding the contribution of the different parameters to the final influence of the ligands, a number of concepts can be used to determine the influence of the non-participative ligand, i.e. the *trans*-effect, the ligand electron donor/acceptor properties and the cone angle of, for example, phosphine ligands.[99]

As mentioned in § 2.4.4, monodentate as well as chelating ligands, i.e. bi- and multidentate ligands, can coordinate to the mental centre. In chelating ligands, the distance between, and the orientation of, the donor atoms are important as these influence the nature of the interactions between the ligands and the metal.[106] The term chelate effect refers to the generalisation that chelate ligands form more stable complexes than analogous monodentate ligands.[110] Relating this to ring structure, it is the enhanced stability of a complex system containing chelate rings as compared to the stability of a system that is similar but contains none or fewer rings coordinated to the metal.[102] The thermodynamic relationship of this entropically driven effect is:

$$\Delta G^\circ = -RT \ln \beta$$
$$\Delta G^\circ = \Delta H^\circ - T\Delta S^\circ$$

with ΔG° the standard Gibbs energy change, ΔH° the standard enthalpy change, ΔS° the standard entropy change, R the gas constant, T the temperature and β the stability constant.

This indicates that β increases as ΔG° becomes more negative, while a negative ΔG° can result from making ΔH° more negative or making ΔS° more positive.[102] The question still remains - what makes certain ligands coordinate to certain metal ions? This can be explained by the hard and soft acid-base (HSAB) principle, whereby hard (Lewis) acids tend to combine with hard (Lewis) bases, whilst soft acids prefer soft bases (**Table 2.2**).[111]

Table 2.2 The classification of Lewis acids and bases.[111]

	Hard	Borderline	Soft
Acids	H^+, Li^+, Na^+, K^+ Be^{2+}, Mg^{2+}, Ca^{2+} Mn^{2+}, Cr^{2+}, Cr^{3+}, Al^{3+} SO_3, BF_3	Fe^{2+}, Co^{2+}, Ni^{2+}, Cu^{2+}, Ru^{2+}, Zn^{2+}, Pb^{2+}, SO_2, BBr_3	Cu^+, Ag^+, Au^+, Tl^+, Hg^+ Pd^{2+}, Cd^{2+}, Pt^{2+}, Hg^{2+}, BH_3
Bases	F^-, OH^-, H_2O, NH_3 CO_3^{2-}, NO_3^-, O^{2-} SO_4^{2-}, PO_4^{3-}, ClO_4^-	$\underline{N}O^{2-}$, SO_3^{2-}, Br^- N^{3-}, N_2 C_6H_5N, $SC\underline{N}^-$	H^-, R^-, $\underline{C}N^-$, $\underline{C}O$, I^- $S\underline{C}N^-$, PR_3, C_6H_6 R_2S

*The underlined element is the site of attachment to which the classification refers

Pearson,[112] building on earlier work by Ahrland, Chatt and Davies,[113] developed the concept of hard and soft acids and bases in the 1960's. Essentially, small non-polarisable or hard donor atoms tend to form stable complexes with small, high charge density, or hard cations, whereas large polarisable or soft donors tend to form stable complexes with large, low charge density, or soft cations.[112] This indicates that, in general, high oxidation state metals, e.g. Cr^{3+} and Al^{3+}, which are low in electron density and require good σ-donor ligands, tend to bind with saturated ligands, e.g. NH_3, H_2O or F^-, known as hard bases.[114] By virtue of their reduced state, soft metals possess an excess electron density and therefore prefer ligands with which a covalent bond can be formed. These ligands must also have empty orbitals available into which some of the excess electron density can be donated, known as back bonding.[114] In general, ligands are nucleophilic because they have available electron lone pairs and metal ions are electrophilic because they have available empty *d*-orbitals to accept the lone pair electrons. Therefore, transition metal ions act as Lewis acids, which can bind to Lewis bases (ligands) to give a coordination complex ML_n.

2.5 Chelating ligands: hemilability

The chemistry of transition metal complexes with chelating ligands containing mixed functionalities is enjoying an increase in popularity, as the different features associated with each donor atom give unique reactivity to their metal complexes.[115-117] Hemilabile ligands, which are a class of chelating ligands, have the ability to place two or more donor atoms with very different electronic properties close to the metal atom. The relevance of these ligands is increasing in coordination and organometallic chemistry, since they can reversibly create and/or occupy a vacant coordination site at the metal, with consequent stabilisation of reactive intermediates or enhancement of reactivity in catalytic reactions.[118,119] Therefore, these ligands are ideal for

inducing changes in the properties of the metal centre.[118] Jeffrey et al.[120] first introduced the term "hemilabile" ligand in 1979 for phosphine-amine[121] and phosphine-ether[120,121] ligands that

> "would bind well enough to allow isolation but would readily dissociate the hard ligand component, thus generating a vacant site for substrate binding".[120]

These ligands possess both tightly bound (Z) and substitutionally labile (A) bonding groups, via combination of 'soft' and 'hard' donor atoms, to give systems in which the effective electron donation to the metal centre depends on the coordination mode of the labile group (A) (**Scheme 2.7**).[122-125] Therefore, in the presence of small molecule substrates, the labile portion of the ligand (A) will dissociate to allow formation of a metal-small molecule complex, while the tightly bound moiety (Z) keeps the ligand anchored to the metal centre (**Scheme 2.7**).[124,126] Upon chelation the hard donor atom will stabilise the higher oxidation state of the metal centre, while the soft donor atom will consequently stabilise the lower oxidation state of the metal centre.[127]

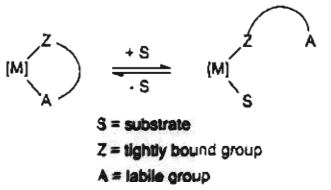

Scheme 2.7 Schematic representation of the concept of hemilability.[124,126]

Thus, the concept of hemilability of bidentate ligands predicts higher activity and stability by releasing a free coordination site "on demand" of *inter alia* an alkene and occupying it otherwise – thus preventing decomposition via free coordination sites.[119] The flexible coordination mode of hemilabile ligands has previously been exploited to maximise the stability of metal complexes while retaining their reactive possibilities, and has been implicated in a number of catalytic reactions.[128] The ether-phoshine ligand *o*-(diphenylphosphino)anisole (**22**) was the first to be termed hemilabile in a ruthenium(II) system (**23**) investigated by Jeffrey and Rauchfuss[120] in 1979 for carbonylation reactions.

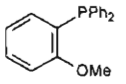

22

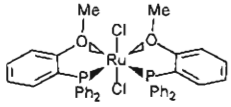

23

Much attention has been given to hemilabile phosphine ligands due to their ability of improving certain properties in transition metal complexes, through binding different functional groups to the phosphorous atom.[129-131] The electronic and steric properties of the ligands could therefore be altered and used to tune the catalytic activity of the catalytic system. The ability of the hemilabile ligand to furnish open coordination sites and stabilise reactive transition metal centres during the course of the reaction is an important property of these types of ligands.[124] The reversible protection of coordination sites can lead to improved stability and reactivity of the catalytic system. The steric and conformational factors of the ligand backbone dictate the capacity of the weakly coordinated atom to afford an empty coordination site.[124] Since that initial discovery in 1979, a number of hemilabile ligands have been reported and incorporated in the synthesis of transition metal complexes. Various transition metal complexes with hemilabile P,P-,[132-134] P,N-,[135,136] P,O-,[122,137] O,N-,[78,138,139] N,N-,[134,140] O,O-[141,142] and S,O-ligands[119,141,143] have been synthesised and a number of them applied to catalytic reactions (**Tables 2.3a-c** and **Appendix A**). For instance, the hemilabile ligand effects on catalyst selectivity have been observed for hydrogenation of alkenes[117,144] and ketones,[134] hydroformylation of epoxides[145] and alkenes,[146,147] alkyne dimerisation,[137] alkene codimerisation,[141] CO_2/butadiene coupling reactions,[148] ROMP[78,81], RCM[81] and catalytic isomerisation of allyl to vinyl ethers.[149] Some catalytic systems with ether-phosphine ligands (P,O) were not directly applied to catalytic reactions, but the hemilabile nature of these ligands was observed through insertion reactions with small molecules *inter alia* CO, SO_2, acetonitrile, phenylacetylene, ethene, etc.[150-152] In these ligands the strength of the metal-oxygen bond depends on the O-basicity, the donor strength of the phosphine, and the coordination abilities of the incoming substrates.[150] It was also shown that the oxygen donors in complexes with two or three hemilabile ether-phosphine ligands compete for one coordination site, revealing a fluxional behaviour in solution that was studied by variable-temperature ^{31}P NMR spectroscopy.[152]

In **Tables 2.3a-c**, various examples of transition metal complexes with hemilabile ligands are displayed with their application in catalytic reactions. A more extensive table is given in **Appendix A**. The complexes displayed in **Tables 2.3a-c** contributed to our choice of possible hemilabile ligands for use in the manipulation of the ruthenium carbene complexes for application in alkene metathesis.

Chelating Schiff-base ligands (**Table 2.3a**, **24**),[81,86] pyridinyl-alcoholate ligands (**Table 2.3a**, **25**)[78] and pyca (**Table 2.3b**, **26**) have been successfully incorporated into the **Gr1** and/or **Gr2** systems for ROMP and RCM reactions. The use of chelating ligands was most probably motivated by the general agreement[45,94,97,153,154] that the 14-electron complex coordinated with only one L-type ligand ($RuX_2L(=CHR)$) is the active metathesis species. This indicates that only one L-type ligand should remain coordinated (the "strong" donor ligand) and the other one should be labile (the "weak" donor ligand).

Table 2.3a Metathesis reactions

Catalytic system	M	L_1	R_1	R_2	Z^A	
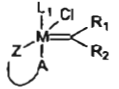	$Ru^{80,81,165}$	H_2IMes, PCy_3	Ph	H	O^N	= 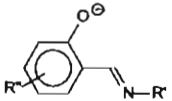 (24) Schiff-base

R'' = H, R' = 2,6-^{i}PrC$_6$H$_3$

R'' = 4-NO_2, R' = 2,6-^{i}PrC$_6$H$_3$

R'' = 4-NO_2, R' = 2,6-Me-4-MeOC$_6$H$_2$

R'' = 4-NO_2, R' = 2,6-Me-4-BrC$_6$H$_2$

R'' = 4-NO_2, R' = 2,6-Cl-4-CF_3C$_6$H$_2$

R'' = 6-Me-4-NO_2, R' = 2,6-^{i}PrC$_6$H$_3$

R'' = 4-NO_2, R' = 2,6-^{i}Pr-4-NO_2-C$_6$H$_3$

R'' = 4-NO_2 R' = 

	Ru^{78}		Ph	H	O^N	= 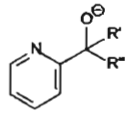 (25) Pyridinyl alcoholate	$R^{i,i}$ = $(CH_2)_5$ R' = R'' = Me

Table 2.3b Carbonylation

Catalytic system	M	L_1	L_2	Z^A		
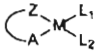	$Pd^{139,158,157}$	PPh_3 $PMePh_2$ $P(CH_2Ph)_3$ $P(C_6H_{11})_3$	Me	O^N	=	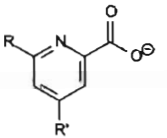 (26) pyridinecarboxylate (pyca)	R = H R' = H, NO_2
		PPh_3 $PMePh_2$ $P(C_6H_{11})_3$ PEt_3	Ph		=		R = H, Me R' = H, NO_2
	Pt^{156}	PPh_3	Me	O^N	=	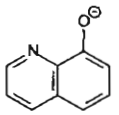 (27) quinolin-8-olate (hoqu)	

Table 2.3c Co-dimerisation of styrene with ethylene

Catalytic system	M	L_1	Z^A			
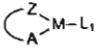	Pd^{141}	η^3-propene	N^(=O) =	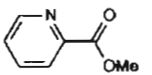 (28) methylpicolinate	N^O =	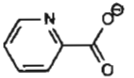 (26) pyridinecarboxylate (pyca)

Therefore, with the increase in donor strength of one ligand at the expense of the other, the activity of the catalyst could be increased.[36] The use of bidentate ligands with a relatively rigid backbone might be a way of increasing the selectivity and stability of the catalytically active complexes. One can mention the hydroformylation reaction with Rh-complexes bearing bidentate phosphite or phosphine ligands[146,147] and enantioselective hydrogenation using chiral bidentate ligands[158] as examples. Thus, the incorporation of bidentate hemilabile ligands, which can release a free coordination site "on demand" of an alkene, for example norbornene,[78] and occupying it otherwise, is another way of increasing the selectivity and stability of the catalytic systems. In general, the stability of the bidentate complexes as well as their catalytic performance is influenced by electronic properties, steric demand as well as ring size and rigidity of the chelating ligand.[159]

Verpoort et al.[88] suggested that the Schiff-base ligands act as hemilabile ligands, with the decoordination and coordination of the N-donor atom instead of the usual PCy_3 dissociation, during the metathesis reaction (**Scheme 2.8**). According to the proposed mechanism, the active intermediate (having a vacancy for alkene coordination) is stabilised or, respectively, destabilised when the steric and electronic parameters are altered. Diminishing the electron density on the nitrogen atom stimulates the decoordination of the N-donor atom, while an increase in the steric bulk of the ligand has an opposite influence on the RCM and ROMP activity of these initiators. In RCM reactions the introduction of more bulkiness in the Schiff-base ligand stabilises the reactive intermediate and thus stimulates the decoordination of the N-donor atom. In ROMP reactions, the growing polymer remains attached to the metal centre and therefore the incoming monomer will be hindered by the "polymer tail" when the Schiff-base is too bulky (**Figure 2.12**).[88]

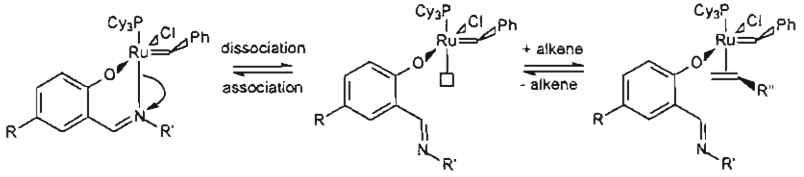

Scheme 2.8 Mechanism for metathesis with catalytic systems with Schiff-base ligands.[88]

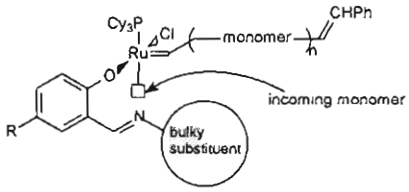

Figure 2.12 Illustration of the influence of steric Schiff-bases on ROMP activity.[88]

Denk et al.[78] synthesised a range of second generation systems with hemilabile pyridinyl alcoholate ligands (**14**) for the ROMP of norbornene and cyclooctene. These systems showed an increase in activity with an increase in temperature, due to the presence of the strongly binding NHC ligand. Hafner et al.[89] patented another example, but no activity data was available. The fact that these ligands are easily accessible through the reaction of 2-lithiopyridine with symmetric ketones[160] make them an ideal choice for further investigation.

Pyridinylcarboxylate (pyca, **26**) and quinolin-8-olate (hoqu, **27**) are derivatives of the pyridinyl alcoholate ligands with increased steric and/or electronic properties. It has been shown[139,156,157] that the nitrogen atom in these ligands undergoes partial dissociation from the metal centre during carbonylation reactions. In the catalytic systems containing both phosphine ligands and pyca, the lability of the nitrogen atom increased with an increase in the basicity of the phosphine ligands.[139] In contrast, during the codimerisation of styrene with ethene, little to no catalytic activity was observed for the palladium systems complexed with pyca (**26**) or methylpicolinate (**28**) and η^2-propene, indicating that these ligands displayed no hemilabile characteristics.[141] Therefore, the hemilability of these ligands might be influenced by the presence of an electron-donating ligand such as phosphines. Two pyca ligands have recently been complexed to **Gr2** for application in RCM. However, only after addition of the cocatalyst, HCl, did the system show any activity after 12 h at 40 °C to achieve 70% conversion. To my knowledge, no first or second generation hemilabile complexes have been previously investigated for linear alkene metathesis reactions, apart form our recent publication.[161] Therefore, in this study the hemilability of pyca, hoqu and other derivatives of pyridinyl alcoholate, coordinated to **Gr1** and **Gr2** systems, was investigated for application in 1-alkene metathesis.

A number of catalytic systems, with potentially hemilabile ligands, have also been synthesised and applied to various catalytic reactions, but no hemilabile behaviour was observed for them (**Tables 2.3d-g** and **Appendix B**).

Table 2.3d Epoxidation reactions

Catalytic system	M	L_1	L_2	Z_1^A_1	Z_2^A_2
	Mo^{160}	O	O	O^N = 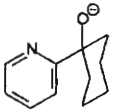 (29) (pyridinyl alcoholate)	O^N =  (28) (pyridinyl alcoholate)

Table 2.3e Alkene polymerisation

Catalytic system	M	L_1	L_2	Z^A	
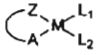	Ni^{162}	PPh_3 py $PPhMe_2$	Ph	O^P =	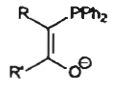 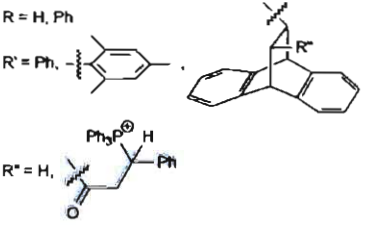 (30)

Table 2.3f Metathesis reactions

Catalytic system	M	L_1	R_1	R_2	Z^A	
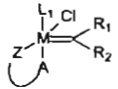	$Ru^{78,163-165}$	PCy_3	Ph	H	P^P =	 **31**
	$Ru^{71,166}$	Cl	H	$CH{=}CMe_2$	P^P =	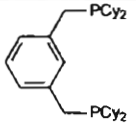 **32**

Table 2.3g Catalytic activity not tested

Catalytic system	M	L_1	L_2	Z^A			
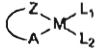	Al^{159}	^{t}Bu	^{t}Bu	O^N =	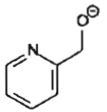 **33**	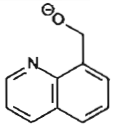 **34**	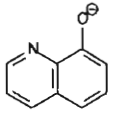 **27**

Catalytic system	M	L_1	L_2	Z_1^A_1		Z_2^A_2	
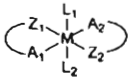	Ru, Os^{127}	Cl, Br	Cl, Br	O^N =	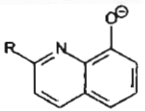 R = H, Me **27b**	O^N =	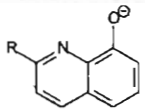 R = H, Me **27b**

For example, **29** has been complexed to Mo and subjected to epoxidation reactions, but no hemilabile behaviour was observed.[160] On the other hand, Hermann et al.[78] reported that **29**, which was complexed to **Gr2**, has displayed hemilability during ROMP. Although some systems (**Table 2.3g**) were not tested for catalytic activity and therefore no comment on their hemilability could be made, derivatives of these ligands were shown to display hemilabile behaviour (**Table 2.3a & 2.3b**). Therefore, these systems are also considered as possibilities for further investigation in this study. A more extensive table of chelating ligands displaying no hemilability is given in **Appendix B**.

2.6 Reaction mechanism of alkene metathesis

In the seventies, a variety of mechanisms were postulated for the alkene metathesis reaction based on experimental and theoretical studies.[3] The different mechanisms can be divided into two groups, namely pairwise and non-pairwise mechanisms.

2.6.1 Pairwise mechanisms

Initially it was thought that the alkene metathesis reaction mechanism involved the "pairwise" exchange between two alkenes in the coordination sphere of a metal via a weakly held cyclobutane-type complex.[3,167] The suggested mechanism led to many controversies which gave rise to a variety of proposed intermediates (**Figure 2.13**) being thought to take part in the alkene metathesis reaction e.g. quasi-cyclobutane- (6),[168] a tetramethylene metal- (7)[169] or a tetramethylene ring complex (8 and 9).[33,170]

Although the quasi-cyclobutane mechanism (6) indicated that the reaction involved the cleavage of the C-C double bonds and not the transfer of groups attached to the double bond,[167] minimal experimental support was received. Therefore Pettit et al.[169] proposed a tetramethylene complex (7), in which four methylene units are bonded to a central metal atom. In a further attempt to explain alkene metathesis, Grubbs proposed that the redistribution of groups around the double bonds was due to a rearranging metallacyclopentane intermediate (**Figure 2.13** (8)) and not a tetramethylene complex.[33] Later, he suggested that one mode of rearrangement could lead to formation of a cyclobutane complexed to a metal carbene (9) as illustrated in **Figure 2.13**.[170] Grubbs' reaction mechanism received support from studies of the metal catalysed [2+2] cycloaddition reaction e.g. valence isomerisation of cubane to syn-tricyclooctadiene,[171] cycloaddition reactions of norbornadiene[172] and rearrangements of exo-tricyclo[3.2.1.$0^{2,4}$]octene,[173] but was eventually discarded in favour of the non-pairwise metal carbene chain mechanism (abbreviated to carbene mechanism), in which the propagating species is a metal carbene complex formed from the catalyst/substrate system.

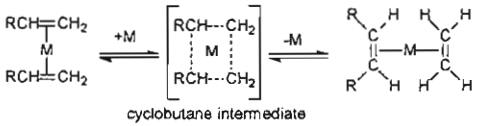

(6)

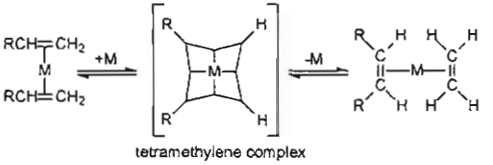

(7)

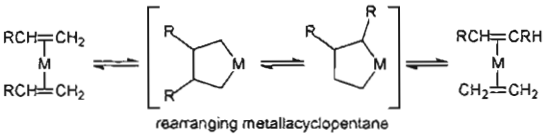

(8)

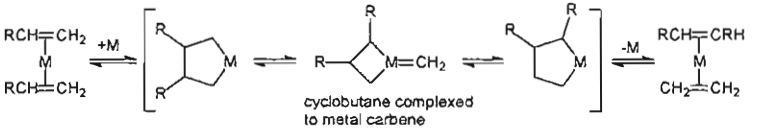

(9)

Figure 2.13 Unusual intermediates proposed initially for the alkene metathesis reaction.

2.6.2 Non-pairwise mechanism

In 1971, Herrisson and Chauvin[174] suggested that the alkene metathesis reaction is initiated by a metal carbene. The metal carbene, they proposed, reacts with an alkene to form a metallacyclobutane intermediate that breaks apart to form a new alkene and a new metal carbene, which propagates the reaction (**Scheme 2.9**).

Initially this proposal received little support, but by 1975 the evidence in its favour became so compelling that the pairwise mechanism was discarded.[3] For example, labelling experiments (**Scheme 2.10**) revealed that the kinetic product of the metathesis of 1,7-octadiene derivatives is a statistical distribution (1:2:1) of d_0-, d_2- and d_4-labelled ethene and not a non-statistical distribution (1:1.6:1) as predicted by the pairwise mechanism.[175-177]

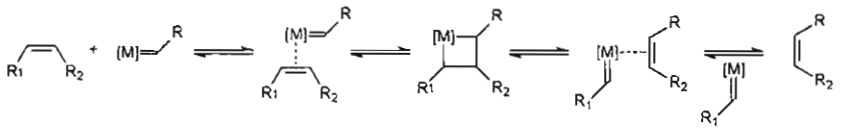

Scheme 2.9 Chauvin's metallacyclobutane mechanism.[174]

With the discovery of well-defined carbene complexes of Ta, Mo, W, Re and Ru, which would act as initiators without the need for activation by heat, light or cocatalyst, spectroscopic techniques could be used to detect the propagating metal-carbene and intermediate metallacyclobutane complexes in some of these systems.[3] This provided additional support for the Chauvin mechanism.

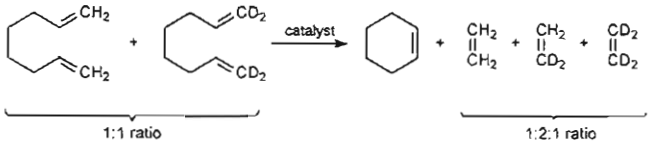

Scheme 2.10 Labelling experiment to confirm the Chauvin mechanism for the alkene metathesis reaction.

Mechanistic studies have played an important role in the development of ruthenium-based alkene metathesis catalysts. The performance of ruthenium carbene complexes has been improved by extensive synthetic,[41,42,44,49,68,178] mechanistic[45,91] and theoretical[92,93] investigations, which provided increased activity, improved functional group tolerance and higher thermal stability. Initial investigation of the alkene metathesis mechanism with ruthenium carbenes, which focused on the ring-closing metathesis of diethyl diallylmalonate (**Scheme 2.11**), established that the pathway involves substitution of an alkene for a phosphine.[45] Whether alkene binding preceded the loss of phosphine (associative pathway, **Scheme 2.12**) or phosphine dissociation preceded alkene binding (dissociative pathway, **Scheme 2.13**) was unclear.

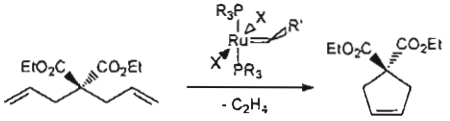

Scheme 2.11 Ring-closing metathesis of diethyl diallylmalonate.

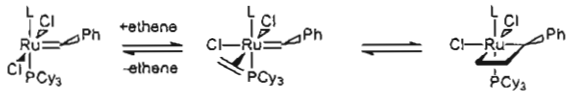

Scheme 2.12 Associative alkene metathesis mechanism.

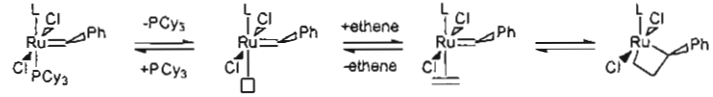

Scheme 2.13 Dissociative alkene metathesis mechanism.

Through subsequent kinetic and mechanistic studies, it was shown that the dissociative pathway is the operative mechanism.[153,154] In support of this mechanism, Chen et al.[91,93,179] have provided mass spectrometric evidence for the dissociative substitution of a phosphine ligand with an alkenic substrate during the ruthenium catalysed alkene metathesis reaction in the gas phase.

The currently accepted mechanism for alkene metathesis reactions, which is consistent with Chauvin's metallacyclobutane mechanism discovered in 1971,[174] involves:[180]

(i) the coordination of an alkene to the metal centre,

(ii) [2+2] cycloaddition between the metal carbene and the alkene to form a metallacyclobutane,

(iii) rupture of the metallacyclobutane to regenerate a carbene and an alkene, and

(iv) displacement of the coordinated alkene with a new alkene to begin the cycle again.

A simplified mechanistic pathway for the alkene metathesis reaction is illustrated in **Scheme 2.14**,[45,153] with the precursor complex **A** reacting with the supplied alkene to form either **E** or **H** (**E** is preferred). Species **F** and **I** can also undergo unproductive metathesis (not included in **Scheme 2.14**),[3] which are illustrated in **Scheme 2.15** for an alkylidene complex. In the unproductive case, the same methylidene complex is generated, while in the productive step, the alkylidene compound **F** (or analogues of it) is formed.

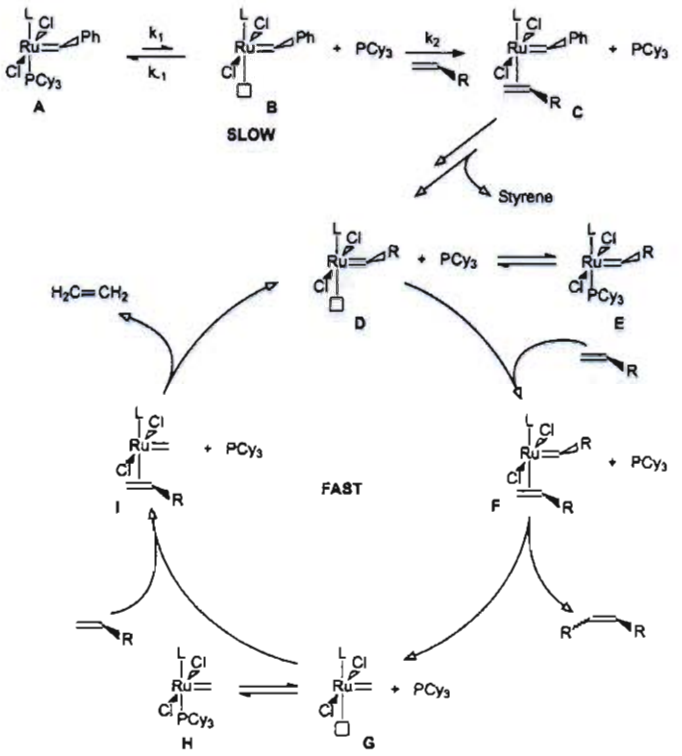

Scheme 2.14 A simplified mechanistic pathway for the alkene metathesis reaction.

Scheme 2.15 Productive vs. unproductive alkene metathesis reaction.

The catalytic activity of **A** is dictated by the relative rates of three processes:[153,154,181]

- phosphine dissociation (initiation) (k_1)
- phosphine recoordination (k_{-1})
- alkene binding (k_2)

High catalytic activity is expected when catalyst initiation is efficient (i.e. k_1 is large) and when the resulting 14-electron intermediate (**B**) reacts rapidly with the alkene substrate relative to free phosphine (i.e. k_{-1}/k_2 is small). Although neither k_{-1} nor k_2 have been measured directly for **Gr1** in solution, the ratio of rate constants for phosphine versus alkene binding (k_{-1}/k_2) have been determined experimentally[153] for the reaction of **Gr1** and **Gr2** with ethyl vinyl ether. This ratio can be a measure of the extent to which a catalyst prefers to remain in the catalytic cycle. Love et al.[181] determined the k_{-1}/k_2 ratio, according to eq. 10, under pseudo first-order conditions in the alkene by applying the steady state approximation to the proposed intermediate **B**, assuming all steps following alkene binding are fast.

$$\frac{1}{k_{obs}} = \frac{k_{-1}[PCy_3]}{k_1 k_2 [\text{alkene}]} + \frac{1}{k_1} \qquad (10)$$

Although the initiation of **Gr1** ($9.6 \pm 0.2\ s^{-1}$) is faster than that of **Gr2** ($0.13 \pm 0.01\ s^{-1}$), the k_{-1}/k_2 ratio of **Gr1** (1.53×10^4) is up to four orders of magnitude greater than **Gr2** (1.25), indicating that the rate of metathesis catalysed by **Gr2** can be up to twice that of **Gr1**.[153,154,181] The large k_{-1}/k_2 ratio for **Gr1** indicates that the unsaturated intermediate (**B**) must have a high affinity for binding free PCy_3, even in the presence of an excess of highly coordinating, electron-rich alkene substrates.[153] The activity of **Gr1** and **Gr2** is therefore related to the phosphine dissociation rate k_1, as well as the ratio of k_{-1} and k_2, which determines whether the catalyst binds alkene or returns to its resting state.

2.7 Molecular modelling in catalysis

The term *theoretical chemistry* may be defined as a mathematical description of chemistry, whereas *computational chemistry* is used when a mathematical method is developed to a point where it can be automated for implementation on a computer.[182] In theoretical chemistry, algorithms and computer programs are usually developed by chemists together with physicists to predict atomic and molecular properties and reaction paths for chemical reactions. Computational chemists, on the other hand, simply apply existing computer programs and methodologies to answer specific chemical questions.[182] *Molecular modelling* is a combination of theoretical methods and computational techniques to model or mimic the behaviour of molecules.[183]

Therefore, one of the main questions or aims of a computational study has to be the exploration of the mechanism of a given reaction, and in our case that of the alkene metathesis reaction. Molecular modelling can be used to investigate reactions in which the active species either has a very short lifetime, or is present in very low concentrations, so that it cannot be easily isolated. Through the construction of a potential energy surface (PES), viz. a plot of energy vs. reaction coordinate, a number of quantities which are of interest in molecular modelling, *inter alia* equilibrium and transition state (TS) geometries and energies, can be directly obtained.[184] An example of a PES is given in **Figure 2.14**.[185] Although it is possible to derive TS energies experimentally from kinetic data relative to reactants and/or products, only a qualitative idea of the TS structure can be obtained. This is mainly due to the fact that the techniques available for structure elucidation are either too slow or not sensitive enough.[186] Molecular modelling or theoretical methods can therefore be used to describe TS structures and can also be applied to the design of new catalytic systems.[187]

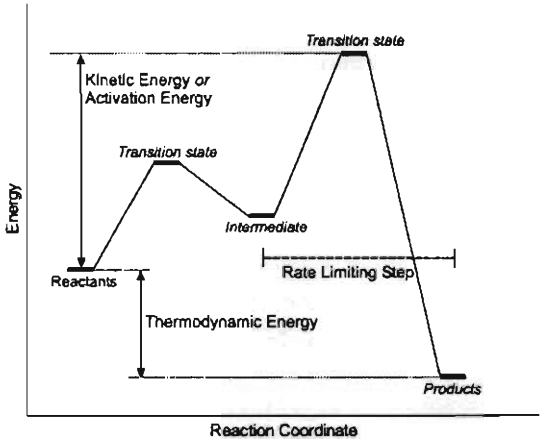

Figure 2.14 One-dimensional potential energy surface (PES).[185]

The energy minima and maxima points on the PES are usually referred to as stationary points. The energy minima, also referred to as local minima, correspond to stable molecules (reactants and products), while energy maxima correspond to transition states (TS's). An intermediate on the PES refers to species that may be too reactive during a reaction to allow easy isolation and characterisation. The term global minimum (not depicted in **Figure 2.14**) refers to the lowest energy minimum point on the PES.

The energy minima along the PES given in **Figure 2.14** correspond to equilibrium geometries with the relative energies relating to thermochemical stabilities. Therefore, the overall process in **Figure 2.14** is thermodynamically favoured (exothermic).[184] The position of TS's along the reaction coordinate usually corresponds to TS geometries and their energies to kinetic or activation energies, relative to the local minima. The reaction step that involves the highest energy TS is referred to as the rate-limiting step of the reaction.[188]

Studies of transition metal mediated reactions with molecular modelling have increased exponentially over the past decade, due to the improvement of computer hardware and theoretical methods.[187] Theoretical studies on hydroformylation of alkenes,[187,189-200] the Dötz reaction,[197,201-205] hydrogenation of CO_2,[206-219] CO,[197,220-239] and alkenes,[197,198,232,240-257] polymerisation,[258-278] oligomerisation,[274,275,277-282] trimerisation of ethene[283-286] and several other catalytic reactions have been covered in numerous publications and review articles. Since the inclusion of all these studies will be impractical and the primary focus of this study is alkene metathesis, only this reaction will be looked at in more detail.

2.7.1 Computational investigation of alkene metathesis

In the last few years, in all probability encouraged by the current available experimental data for mechanistic studies on ruthenium carbene complexes both in solution[45,153,154,287,288] and gas phase,[91,93,179,289,290] several computational studies have appeared.[67,92-96,267,291-301] Although substantial experimental evidence[91,93,153,154,179] exists that the dissociative pathway (**Scheme 2.13**) is favoured for the alkene metathesis reaction, the subsequent steps in the catalytic cycle has not yet been characterised experimentally.[154] Thus, it has been indicated that the tetracoordinated 14-electron complex $[RuX_2(PR_3)(=CHR')]$ or $[RuX_2(NHC)(=CHR')]$ is the reactive catalytic species that forms from the pentacoordinate $[RuX_2(PR_3)_2(=CHR')]$ or $[RuX_2(PR_3)(NHC)(=CHR')]$ precatalysts, respectively. However, it has remained unclear whether the incoming alkene will coordinate to the 14-electron intermediate complex in the *cis* or *trans* position relative to the ancillary ligand, and whether the metallacyclobutane is an intermediate or just a transition state.[154] With the use of quantum-chemical calculations (computational studies), some of these issues can be investigated.

Most of the computational studies considered only selected parts of the catalytic cycle, focusing either on the formation of the ruthenium carbene[92,294-296,299] or looking at some intermediates of the catalytic cycle.[93,291,301-303] Only a few studies have treated the complete mechanism (**Scheme 2.16** path 2/7) and/or alternative reaction pathways up to the cleavage of the metallacyclobutane.[54,94-97,267,293,297,298] A summarised overview of the possible reaction pathways investigated in these studies is given in **Scheme 2.16**.[97] In the majority of the computational studies a truncated model system (*inter alia* PH_3 instead of PCy_3) was investigated for the alkene

metathesis reaction. For example, Meier et al.[95,96] performed molecular dynamic studies at the DFT level on PH_3 **Gr1**-model systems for pathways 1/4 and 2/6. A higher reactivity for the 14-electron complex **B** was reported relative to the 16-electron complex **A**. Vyboishchikov et al.[94] investigated the associative path 1/4 as well as the *cis*- and *trans*-dissociative pathways 2/5 and 2/7 for the first and second generation truncated systems. A preference for the dissociative path 2/7 was found in the ΔG^0_{298} surface with *trans*-orientation of the incoming alkene,[94] since a high barrier for initial alkene coordination impeded the other possibilities.

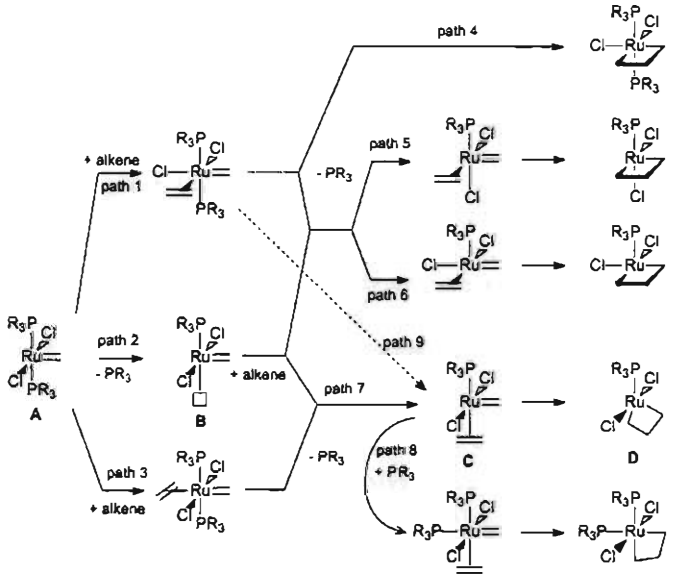

Scheme 2.16 Schematic representation of postulated mechanisms for alkene metathesis by Grubbs-type ruthenium carbene complexes.[97]

DFT calculations on a $RuCl_2(PMe_3)_2(=CH_2)$ system by Forman et al.[304] indicated that phenol might play a number of roles in the metathesis cycle. Although the initiation rate (k_1, **Scheme 2.15**) of **Gr1** is slowed and k_{-1} impeded, it is predicted that phenol enhances the electrophilic character of the alkylidene carbon, therefore enhancing the probability of reaction with an alkene substrate.[304] This was supported by experimental results, which indicated that the addition of phenol improved the activity and lifetime of **Gr1** in certain self-metathesis, cross-metathesis and ethenolysis reactions.[304] Grubbs et al.[154] noted a similar result for second generation ruthenium alkylidene systems, in which the initiation rate (k_1) was found to be roughly

generation ruthenium alkylidene systems, in which the initiation rate (k_1) was found to be roughly proportional to the dielectric constant of the reaction medium. Forman et al.[304] suggested that the phenol coordinates through a hemilabile interaction of the OH group with the metal centre to stabilise the 14-electron intermediate species (**Scheme 2.16, B**) as illustrated in **Scheme 2.17**.

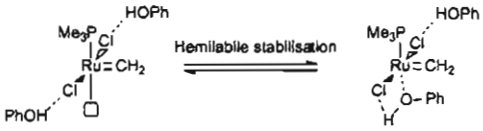

Scheme 2.17 Hemilabile stabilisation effect of phenol on Ru-alkylidene complexes.[304]

Although the use of truncated model systems have contributed a great deal to the clarification of the alkene metathesis mechanism, the steric and electronic influences of the real ligands and substrates are not taken into consideration during these computations. The size of the ligands (Tolman cone angles for PCy_3 and PH_3 are 170° and 87°, respectively), their electronic properties and conformational flexibility have a great influence on the catalyst stability – the 16-electron complex $(PH_3)_2Cl_2Ru{=}CH_2$ has never been isolated nor detected – as well as the catalytic reactivity of these systems.[305,306]

A few studies, incorporating the whole ligand system, have investigated either only path 2/7[93,291,293] or concluded it to be favoured over the associative pathway 1/4,[297] or even suggested a more favourable variant (path 2/7/8).[298] Cavallo et al.[291] focused on substituents, ligand and solvent effects, indicating that the role of the solvent is mainly to facilitate phosphine dissociation while not affecting alkene coordination. Adlhart et al.[54,97] recently extensively re-investigated all these pathways (**Scheme 2.16**) to determine the role of ligands (PCy_3 and H_2IMes) and substrates (norbornene, ethyl vinyl ether and styrene) on the activity of the ruthenium carbene complexes as compared to the truncated systems. Previous computations have been carried out with ethene as substrate, starting with the methylidene or benzylidene complex, or used the methylidene complex with propene as starting substrate. They indicated that the reaction strongly depends on the alkene substrate as well as the ancillary ligands. For example, the presence of electron-withdrawing phosphine ligands will destabilise the 14-electron metallacyclobutane intermediate (**D, Scheme 2.16**) relative to the 14-electron carbene species (**Scheme 2.16, B**), because electron deficiency in **B** is partly compensated by conjugation with the carbene, while in the metallacyclobutane the compensation for electron deficiency is interrupted. The metallacyclo-butane was also found to be an intermediate which is more stable than the alkene carbene

complex for the NHC-containing systems, but less stable for the phosphine systems.[94,291] Adlhart et al.[54] found this to be true during the degenerate alkene metathesis reaction of **Grl** with ethene, but experimentally concluded that the metallacyclobutane is a transition state rather than an intermediate. In contrast, Piers *et al.*[307] recently provided experimental evidence that the ruthenacyclobutane is an intermediate. With the use of 400 MHz ^{1}H-NMR, they directly observed the 14-electron ruthenacyclobutane intermediate (**35**), which is formed from the highly active 14-electron ruthenium alkene metathesis catalyst **36**.

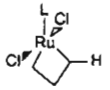

L = H_2IMes

35

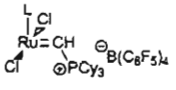

L = H_2IMes

36

The stabilisation of the Ru(IV) species through the strongly σ-donating NHC ligand made this observation possible. This has not yet been observed for **Grl**-systems and therefore the debate of whether the metallacyclobutane is a transition state or an intermediate will continue, but is beyond the scope of this study.

We[308] recently reported our theoretical and experimental results for the 1-octene metathesis reaction in the presence of **Grl**. Using DMol^3 DFT calculations, we described the 1-octene metathesis reaction by a dissociative mechanism. The formation of the catalytically active heptylidene species was found to be kinetically and thermodynamically favoured, with *trans*-tetradecene the more thermodynamically favoured product to form. The computational results were in agreement with the experimental results obtained with NMR and GC/MSD experiments.

In a recent communication by Janse van Rensburg et al.,[303] it was indicated through theoretical and experimental investigations that substrate-induced decomposition of Ru-alkylidene metathesis complexes is possible. It is proposed that the decomposition involves a β-hydride transfer from a ruthenacyclobutane intermediate to form a coordinatively unsaturated Ru-complex (**Scheme 2.18**), which should be inactive for metathesis.[303] Molecular modelling can therefore be of immense use in understanding catalytic reactions and to postulate the source of side reactions e.g. isomerisation, which is sometimes difficult to determine experimentally. It is proposed that the isomerisation of alkenes during the Ru-catalysed metathesis reaction arises from the substrate-induced decomposition of the catalyst.[303]

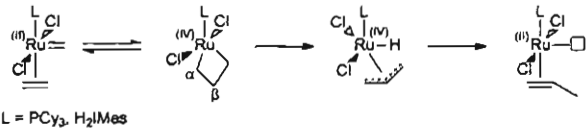

Scheme 2.18 Substrate-induced catalyst decomposition during ruthenium-catalysed alkene metathesis.[303]

Forman et al.[309] eliminated the competing isomerisation process that takes place during metathesis reactions by developing an improved, more active first generation ruthenium alkylidene system (37).

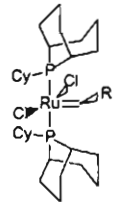

37

Fundamental insight into the reactivity and stability of **37** as compared to **Gr1** and **Gr2** was obtained through theoretical investigations of the metathesis mechanisms.[310] They believe that the higher conversions obtained for **37** are attributed to its similarity to **Gr2** instead of **Gr1**. This is likely due to the phoban-Cy ligand of **37** displaying two-fold symmetry similar to the NHC ligands, despite not having a formal two-fold symmetry as opposed to the three-fold symmetry of PCy_3.[310]

While the focus of a computational study is to reproduce experimental data, as well as verify previous computational investigations, the goal must also be to predict what will happen when new catalytic systems are used in the reaction scheme. To my knowledge, no computational investigation of ruthenium carbene complexes with chelating ligands has been reported. This study will look at possible hemilabile ruthenium carbene complexes for the alkene metathesis reaction as compared to the **Gr1** and **Gr2**.

2.8 References

1. Calderon, N., Chen, H.Y., and Scott, K.W., *Tetrahedron Lett.*, 1967, **8**, 3327

2. Haines, R.J. and Leigh, G.J., *Chem. Soc. Rev.*, 1975, **4**, 155

3. Ivin, K.J. and Mol, J.C., ***Olefin Metathesis and Metathesis Polymerization***, Academic Press, San Diego, 1997

4. Mol, J.C. *in* ***Applied Homogeneous Catalysis with Organometallic Compounds***, Cornils, B. and Herrmann, W.A., Eds., *Metathesis*, Vol. 2, VCH (Weinheim), 1996, p. 318

5. Schneider, V. and Frolich, P.K., *Ind. Eng. Chem.*, 1931, **23**, 1405

6. Banks, R.L. and Bailey, G.C., *Ind. Eng. Chem. Prod. Res. Dev.*, 1964, **3**, 170

7. Eleuterio, H.S., *J. Mol. Catal.*, 1991, **65**, 55

8. Eleuterio, H.S., 1963. Polymerization of cyclic olefins. Patent: *US 3 074 918*

9. Peters, E.F. and Evering, B.L., 1960. Olefin-polymerization catalysts. Patent: *US 2 936 291*

10. Peters, E.F. and Evering, B.L., 1960. Catalysts and their preparation. Patent: *US 2 963 447*

11. Wagner, P.H., *Chem. Ind.*, 1992, 330

12. Truett, W.L., Johnson, D.R., Robinson, I.M., and Montague, B.A., *J. Am. Chem. Soc.*, 1960, **82**, 2337

13. Trnka, T.M. and Grubbs, R.H., *Acc. Chem. Res.*, 2001, **34**, 18

14. Semeril, D. and Dixneuf, P.H. *in* ***Novel Metathesis Chemistry: Well-Defined Initiator Systems for Specialty Chemical Synthesis, Tailored Polymers and Advanced Material Applications***, Imamoglu, Y. and Bencze, L., Eds., *The Alkene Metathesis Ruthenium Catalyst Saga*, Vol. 122, Kluwer Academic, Dordrecht, 2003, p. 1

15. Grubbs, R.H. and Tumas, W., *Science*, 1989, **243**, 907

16. Wallace, K.C., Liu, A.H., Dewan, J.C., and Schrock, R.R., *J. Am. Chem. Soc.*, 1988, **110**, 4964

17. Kress, J., Osborn, J.A., Greene, R.M.E., Ivin, K.J., and Rooney, J.J., *J. Am. Chem. Soc.*, 1987, **109**, 899

18. Quignard, F., Leconte, M., and Basset, J.-M., *J. Chem. Soc., Chem. Commun.*, 1985, 1816

19. Dotz, K.H., *Angew. Chem. Int. Ed. Engl.*, 1984, **23**, 587

20. Fischer, E.O. and Maasbol, A.A., *Angew. Chem. Int. Ed. Engl.*, 1964, **3**, 580

21. Cardin, D.J., B. Cetinkaya, and Lappert, M.F., *Chem. Rev.*, 1972, **72**, 545

22. Mathey, F. and Sevin, A., ***Molecular Chemistry of the Transistion Elements - An Introductory Course***, Wiley, Chichester, 1996

23. Toreki, R., 2003. Fischer Carbene Complexes. [Web] http://www.ilpi.com/organomet/carbene.html [Date of access: 21/02/2006]

24. Unknown, 2005. Transition Metal Carbene Complex. [Web] http://en.wikipedia.org/wiki/Transition_metal_carbene_complex [Date of access: 21/02/2006]

25. Garrison, J.C. and Youngs, W.J., *Chem. Rev.*, 2005, **105**, 3978

26. Zaera, F., *Chem. Rev.*, 1995, **95**, 2651

27. Bazan, G.C., Oskam, J.H., Cho, H.N., Park, L.Y., and Schrock, R.R., *J. Am. Chem. Soc.*, 1991, **113**, 6899

28. Bazan, G.C., Khosravi, E., Schrock, R.R., Feast, W.J., Gibson, V.C., O'Regan, M.B., Thomas, J.K., and Davis, W.M., *J. Am. Chem. Soc.*, 1990, **112**, 8378

29. Schrock, R.R., Murdzek, J.S., Bazan, G.C., Robbins, J., DiMare, M., and O'Regan, M., *J. Am. Chem. Soc.*, 1990, **112**, 3875

30. Schrock, R.R., *Tetrahedron*, 1999, **55**, 8141

31. Kirkland, T.A. and Grubbs, R.H., *J. Org. Chem.*, 1997, **62**, 7310

32. Tsuji, J., *Tetrahedron Lett.*, 1980, **21**, 2955

33. Grubbs, R.H. and Brunck, T.K., *J. Am. Chem. Soc.*, 1972, **94**, 2538

34. Novak, B.M. and Grubbs, R.H., *J. Am. Chem. Soc.*, 1988, **110**, 960

35. Novak, B.M. and Grubbs, R.H., *J. Am. Chem. Soc.*, 1988, **110**, 7542

36. Morgan, J.P., ***Ruthenium-Based Olefin Metathesis Catalysts Coordinated with N-Heterocyclic Carbene Ligands: Synthesis and Applications***, Ph.D thesis, California Institute of Technology, 2002

37. Johnson, L.K., Grubbs, R.H., and Ziller, J.W., *J. Am. Chem. Soc.*, 1993, **115**, 8130

38. Nguyen, S.T., Johnson, L.K., and Grubbs, R.H., *J. Am. Chem. Soc.*, 1992, **114**, 3947

39. Wu, Z., Nguyen, S.T., Grubbs, R.H., and Ziller, J.W., *J. Am. Chem. Soc.*, 1995, **117**, 5503

40. Nguyen, S.T. and Grubbs, R.H., *J. Am. Chem. Soc.*, 1993, **115**, 9858

41. Schwab, P., Grubbs, R.H., and Ziller, J.W., *J. Am. Chem. Soc.*, 1996, **118**, 100

42. Wilhelm, T.E., Belderrain, T.R., Brown, S.N., and Grubbs, R.H., *Organometallics*, 1997, **16**, 3867

43. Nguyen, S.T. and Trnka, T.M. *in* ***Handbook of Metathesis***, Grubbs, R.H., Ed., *The Discovery and Development of Well-Defined, Ruthenium-Based Olefin Metathesis Catalysts*, Vol. 1, Wiley, 2003, p. 61

44. Schwab, P., France, M.B., Ziller, J.W., and Grubbs, R.H., *Angew. Chem. Int. Ed.*, 1995, **34**, 2039

45. Dias, E.L., Nguyen, S.T., and Grubbs, R.H., *J. Am. Chem. Soc.*, 1997, **119**, 3887

46. Kingsbury, J.S., Harrity, J.P.A., Bonitatebus, P.J., Jr., and Hoveyda, A.H., *J. Am. Chem. Soc.*, 1999, **121**, 791

47. Van Schalkwyk, C., Vosloo, H.C.M., and Du Plessis, J.A.K., *Adv. Synth. Catal.*, 2002, **344**, 781

48. Grubbs, R.H., *J. Macromol. Sci. - Pure Appl. Chem.*, 1994, **A31**, 1829

49. Pine, S.H., Zahler, R., Evans, D.A., and Grubbs, R.H., *J. Am. Chem. Soc.*, 1980, **102**, 3270

50. Wolf, J., Stüer, W., Grünwald, C., Werner, H., Schwab, P., and Schulz, M., *Angew. Chem. Int. Ed.*, 1998, **37**, 1124

51. Belderrain, T.R. and Grubbs, R.H., *Organometallics*, 1997, **16**, 4001

52. van der Schaaf, P.A., Kolly, R., and Hafner, A., *Chem. Commun.*, 2000, 1045

53. Gandelman, M., Rybtchinski, B., Ashkenazi, N., Gauvin, R.M., and Milstein, D., *J. Am. Chem. Soc.; (Communication)*, 2001, **123**, 5372

54. Adlhart, C., ***Intrinsic Reactivity of Ruthenium Carbenes: A Combined Gas Phase and Computational Study***, Ph.D thesis, Eidgenossische Technische Hochschule Zurich, 2003

55. Jafarapour, L. and Nolan, S.P., *J. Organomet. Chem.*, 2001, **617-618**, 17

56. Mohr, B., Lynn, D.M., and Grubbs, R.H., *Organometallics*, 1996, **15**, 4317

57. Huang, J., Stevens, E.D., Nolan, S.P., and Petersen, J.L., *J. Am. Chem. Soc.*, 1999, **121**, 2674

58. Huang, J., Schanz, H.-J., Stevens, E.D., and Nolan, S.P., *Organometallics*, 1999, **18**, 2370

59. Jafarapour, L., Schanz, H.-J., Stevens, E.D., and Nolan, S.P., *Organometallics*, 1999, **18**, 5416

60. Lappert, M.F., *J. Organomet. Chem.*, 1988, **358**, 185

61. Weskamp, T., Schattenmann, W.C., Spiegler, M., and Herrmann, W.A., *Angew. Chem. Int. Ed.*, 1998, **37**, 2490

62. Scholl, M., Trnka, T.M., Morgan, J.P., and Grubbs, R.H., *Tetrahedron Lett.*, 1999, **40**, 2247

63. Scholl, M., Ding, S., Lee, C.W., and Grubbs, R.H., *Org. Lett.*, 1999, **1**, 953

64. Huang, J., Schanz, H.-J., Stevens, E.D., and Nolan, S.P., *Organometallics*, 1999, **18**, 5375

65. Chatterjee, A.K., Morgan, J.P., Scholl, M., and Grubbs, R.H., *J. Am. Chem. Soc.*, 2000, **122**, 3783

66. Ackermann, L., Fürstner, A., Weskamp, T., Kohl, F.J., and Herrmann, W.A., *Tetrahedron Lett.*, 1999, **40**, 4787

67. Weskamp, T., Kohl, F.J., Hieringer, W., Gleich, D., and Herrmann, W.A., *Angew. Chem. Int. Ed.*, 1999, **38**, 2416

68. Weskamp, T., Kohl, F.J., and Herrmann, W.A., *J. Organomet. Chem.*, 1999, **582**, 362

69. P'Pool, J., 2005. Polar, Non-Coordinating Ionic Liquids As Solvents for Fundamental Organometallic Reactions. [Web] http://bama.ua.edu/~chem/seminars/student_seminars/fall05/papers-f05/ppool-sem.pdf [Date of access: 25/02/2006]

70. Jafarpour, L., Hillier, A.C., and Nolan, S.P., *Organometallics*, 2002, **21**, 442

71. Volland, M.A.O., Hansen, S.M., Rominger, F., and Hofmann, P., *Organometallics*, 2004, **23**, 800

72. Conrad, J.C. and Fogg, D.E., *Current Org. Chem.*, 2005, **10**, 185

73. Ku, R.-Z., Huang, J.-C., Cho, J.-Y., Kiang, F.-M., Reddy, K.R., Chen, Y.-C., Lee, K.-J., Lee, J.-H., Lee, G.-H., Peng, S.-M., and Liu, S.-T., *Organometallics*, 1999, **18**, 2145

74. Fürstner, A., Ackermann, L., Gabor, B., Goddard, R., Lehmann, C.W., Mynott, R., and Stelzer, F., *Chem. Eur. J.*, 2001, **7**, 3236

75. Trnka, T.M., Morgan, J.P., Sanford, M.S., Wilhelm, T.E., Scholl, M., Choi, T.L., Ding, S., Day, M.W., and Grubbs, R.H., *J. Am. Chem. Soc.*, 2003, **125**, 2546

76. Dias, E.L. and Grubbs, R.H., *Organometallics*, 1998, **17**, 2758

77. Van der Schaaf, P.A., Kolly, R., Kirner, H.-J., Rime, F., Mühlebach, A., and Hafner, A., *J. Organomet. Chem.*, 2000, **606**, 65

78. Denk, K., Fridgen, J., and Herrmann, W.A., *Adv. Synth. Catal.*, 2002, **344**, 666

79. Ung, T., Hejl, A., Grubbs, R.H., and Schrodi, Y., *Organometallics*, 2004, **23**, 5399

80. Chang, S., Jones II, L., Wang, C., Henling, L.M., and Grubbs, R.H., *Organometallics*, 1998, **17**, 3460

81. De Clercq, B. and Verpoort, F., *Tetrahedron Lett.*, 2002, **43**, 9101

82. Louie, J. and Grubbs, R.H., *Organometallics*, 2002, **21**, 2153

83. Garber, S.B., Kingsbury, J.S., Gray, B.L., and Hoveyda, A.H., *J. Am. Chem. Soc.*, 2000, **122**, 8168

84. Gessler, S., Randl, S., and Blechert, S., *Tetrahedron Lett.*, 2000, **41**, 9973

85. Slugovc, C., Burtscher, D., Stelzer, F., and Mereiter, K., *Organometallics*, 2005, **24**, 2255

86. Hoveyda, A.H., Gillingham, D.G., Van Veldhuizen, J.J., Kataoka, O., Garber, S.B., Kingsbury, J.S., and Harrity, J.P.A., *Org. Biomol. Chem.*, 2004, **2**, 8

87. De Clercq, B. and Verpoort, F., *J. Mol. Catal. A: Chem.*, 2002, **180**, 67

88. De Clercq, B. and Verpoort, F., *Adv. Synth. Catal.*, 2002, **344**, 639

89. Van der Schaaf, P.A., Muhlbach, A., Hafner, A., and Kolly, R., 1999. Heterocyclyl ligand containing ruthenium and osmium catalysts. Patent: *WO 99/29701*

90. Stragies, R., Voigtmann, U., and Blechert, S., *Tetrahedron Lett.*, 2000, **41**, 5465

91. Adlhart, C., Volland, M.A.O., Hofmann, P., and Chen, P., *Helv. Chim. Acta.*, 2000, **83**, 3306

92. Dölker, N. and Frenking, G., *J. Organomet. Chem.*, 2001, **617-618**, 225

93. Adlhart, C., Hinderling, C., Baumann, H., and Chen, P., *J. Am. Chem. Soc.*, 2000, **122**, 8204

94. Vyboishchikov, S.F., Bühl, M., and Thiel, W., Prof., *Chem. Eur. J.*, 2002, **8**, 3962

95. Meier, R.J., Aagaard, O.M., and Buda, F., *J. Mol. Catal. A: Chem.*, 2000, **160**, 189

96. Aagaard, O.M., Meier, R.J., and Buda, F., *J. Am. Chem. Soc.*, 1998, **120**, 7174

97. Adlhart, C. and Chen, P., *J. Am. Chem. Soc.*, 2004, **126**, 3496

98. Unknown, 2005. Trio wins Nobel Prize for 'green chemistry': Frenchman, 2 Americans develop environmentally friendly methods. [Web] http://www.msnbc.msn.com/id/9595718 [Date of access: 9 Dec 2005]

99. Masters, C., ***Homogeneous Transition-metal Catalysis - A Gentle Art***, Chapman and Hall, London, 1981

100. Van Sittert, C.G.C.E., ***Die Katalitiese Sintese van Oligomere van Fenielasetileen***, Ph.D thesis, Potchefstroomse Universiteit vir Christelike Hoër Onderwys, 1999

101. Chatt, J. and Duncanson, L.A., *J. Chem. Soc.*, 1953, 2939

102. Cotton, F.A. and Wilkinson, G., ***Advanced Inorganic Chemistry***, Fifth Edition, Wiley, New York, 1988

103. Toreki, R., 2004. Organometallic HyperTextBook - Phosphine Complexes. [Web] http://www.ilpi.com/organomet/phosphine.html [Date of access: 07-06-2005]

104. Hill, A.F., ***Organotransition Metal Chemistry***, Vol. 7, Royal Society of Chemistry, Chambridge, 2002

105. James, B.R., ***Homogeneous Hydrogenation***, Wiley, New York, 1973

106. Burrows, A., *Science Progress*, 2002, **85**, 199

107. Wikibooks, 2004. Transition metals (Inorganic Chemistry). [Web] http://en.wikibooks.org/wiki/Transition_metals_(Inorganic_Chemistry) [Date of access: 08-06-2005]

108. Fahrni, C.J., 2005. Coordination Compounds. [Web] http://web.chemistry.gatech.edu/class/1311/fahrni/set6.pdf [Date of access: 08-06-2005]

109. Van Schalkwyk, C., ***Die Katalitiese Sintese van Lineêre Alkene via 'n Metatesereaksie***, Ph.D thesis, Potchefstroomse Universiteit vir Christelike Hoër Onderwys, 2001

110. Wulfsberg, G., ***Principles of Descriptive Inorganic Chemistry***, University Science Books, California, 1991

111. Shriver, D.F. and Atkins, P.W., ***Inorganic Chemistry***, 3rd edition, Oxford University Press, New York, 1999

112. Pearson, R.G., *J. Am. Chem. Soc.*, 1963, **85**, 3533

113. Ahrland, S., Chatt, J., and Davies, N.R., *Quart. Rev.*, 1958, **12**, 265

114. Sargeson, A.M., *Pure Appl. Chem.*, 1984, **56**, 1603

115. Davies, J.A. and Hartley, F.R., *Chem. Rev.*, 1981, **81**, 79

116. Lindner, E., Haustein, M., Mayer, H.A., Gierling, K., Fawzi, R., and Steimann, M., *Organometallics*, 1995, **14**, 2246

117. Higgins, T.B. and A., M., *Inorg. Chim. Acta*, 1995, **240**, 347

118. Noack, C.L., ***Studies in Coordination Chemistry***, Ph.D thesis, Griffith University, 2003

119. Meyer, W.H., Brull, R., Raubenheimer, H.G., Thompson, C., and Kruger, G.J., *J. Organomet. Chem.*, 1998, **553**, 83

120. Jeffrey, J.C. and Rauchfuss, T.B., *Inorg. Chem.*, 1979, **18**, 2658

121. Rauchfuss, T.B., Patino, F.T., and Roundhill, M., *Inorg. Chem.*, 1975, **14**, 652

122. Bader, A. and Lindner, E., *Coord. Chem. Rev.*, 1991, **108**, 27

123. Lindner, E., *Coord. Chem. Rev.*, 1996, **155**, 145

124. Slone, C.S., Weinberger, D.A., and Mirkin, C.A., *Progr. Inorg. Chem.*, 1999, **48**, 233

125. Braunstein, P., and Naud, F., *Angew. Chem. Int. Ed. Engl.*, 2001, **40**, 680

126. Bielawski, C.W., ***Tailoring Polymer Synthesis with Designer Ruthenium Catalysts***, Ph.D thesis, California Institute of Technology, 2003

127. Lahiri, G.K., Bhattacharya, S., Ghosh, B.K., and Chakravorty, A., *Inorg. Chem.*, 1987, **26**, 4324

128. Drent, E. and Budzelaar, P.H.M., *Chem. Rev.*, 1996, **96**, 663

129. Valls, E., Suades, J., and Mathieu, R., *Organometallics*, 1999, **18**, 5475

130. Rogers, C.W. and Wolf, M.O., *Chem. Commun.*, 1999, 2297–2298

131. Lindner, E., Wald, J., Eichele, K., and Fawzi, R., *J. Organomet. Chem.*, 2000, **601**, 220

132. Pechmann, T., Brandt, C.D., and Werner, H., *Organometallics*, 2003, **22**, 3004

133. Hansen, S.M., Volland, M.A.O., Rominger, F., Eisenträger, F., and Hofmann, P., *Angew. Chem. Int. Ed.*, 1999, **38**, 1273

134. Baratta, W., Herdtweck, E., Siega, K., Toniutti, M., and Rigo, P., *Organometallics*, 2005, **24**, 1660

135. Rülke, R.E., Kaasjager, V.E., Wehman, P., Elsevier, C.J., Van Leeuwen, P.W.N.M., and Vrieze, K., *Organometallics*, 1996, **15**, 3022

136. Dekker, G.P.C.M., Buijs, A., Elsevier, C.J., and Vrieze, K., *Organometallics*, 1992, **11**, 1937

137. Pavlik, S., Gemel, C., Slugovc, C., Mereiter, K., Schmid, R., and Kirchner, K., *J. Organomet. Chem.*, 2001, **617**, 301

138. Desjardins, S.Y., Cavell, K.J., Jin, W., Skelton, B.W., and White, A.H., *J. Organomet. Chem.*, 1996, **515**, 233

139. Hoare, J.L., Cavell, K.J., Skelton, B.W., and White, A.H., *J. Chem. Soc., Dalton Trans.*, 1996, 2197

140. Jamieson, J.Y., Schrock, R.R., Davis, W.M., Bonitatebus, P.J., Zhu, S.S., and Hoveyda, A.H., *Organometallics*, 2000, **19**, 925

141. Britovsek, G.J.P., *J. Mol. Catal. A: Chem.*, 1996, **110**, 77

142. Schrock, R.R., Jamieson, J.Y., Dolman, S.J., Miller, S.A., Bonitatebus, P.J., Jr., and Hoveyda, A.H., *Organometallics*, 2002, **21**, 409

143. Esterhuysen, M.W., ***Homogeneous Catalysis with Palladium Complexes Exhibiting Hemilabile Characteristics***, M.Sc dissertation, University of Stellenbosh, 1998

144. Borns, S., Kadyrov, R., Heller, D., Baumann, W., Holz, J., and Borner, A., *Tetrahedron: Asymmetry*, 1999, **10**, 1425

145. Weber, R., Englert, U., Ganter, B., Keim, W., and Möthrath, M., *Chem. Commun.*, 2000, 1419

146. Kostas, I.D., *J. Organomet. Chem.*, 2001, **626**, 221

147. Le Gall, I., Laurent, P., Soulier, E., Salaün, J.-Y., and Des Abbayes, H., *J. Organomet. Chem.*, 1998, **567**, 13

148. Pitter, S. and Dinjus, E., *J. Mol. Catal. A: Chem.*, 1997, **125**, 39

149. Slone, C.S., Mirkin, C.A., Yap, G.P.A., Guzei, I.A., and Rheingold, A.L., *J. Am. Chem. Soc.*, 1997, **119**, 10743

150. Lindner, E., Geprags, M., Gierling, K., Fawzi, R., and Steimann, M., *Inorg. Chem.*, 1995, **34**, 6106

151. Lindner, E., Pautz, S., Fawzi, R., and Steimann, M., *J. Organomet. Chem.*, 1998, **555**, 247

152. Lindner, E., Haustein, M., Fawzi, R., Steimann, M., and Wegner, P., *Organometallics*, 1994, **13**, 5021

153. Sanford, M.S., Ulman, M., and Grubbs, R.H., *J. Am. Chem. Soc.*, 2001, **123**, 749

154. Sanford, M.S., Love, J.A., and Grubbs, R.H., *J. Am. Chem. Soc.*, 2001, **123**, 6543

155. De Clercq, B., Lefebvre, F., and Verpoort, F., *Appl. Catal. A: Genl.*, 2003, **247**, 345

156. Jin, H. and Cavell, K.J., *J. Chem. Soc., Dalton Trans.*, 1994, 415

157. Jin, H., Cavell, K.J., Skelton, B.W., and White, A.H., *J. Chem. Soc., Dalton Trans.*, 1995, 2159

158. Gergely, I., Hegedüs, C., Gulyás, H., Szöllosy, A., Monsees, A., Riermeier, T., and Bakos, J., *Tetrahedron Asym.*, 2003, **14**, 1087

159. Francis, J.A., Bott, S.G., and Barron, A.R., *J. Chem. Soc., Dalton Trans.*, 1998, 3305

160. Herrmann, W.A., Lobmaier, G.M., Priermeier, T., Mattner, M.R., and Scharbert, B., *J. Mol. Catal. A: Chem.*, 1997, **117**, 455

161. Jordaan, M. and Vosloo, H.C.M., *Adv. Synth. Catal.*, 2007, **349**, 184

162. Gibson, V.C., Tomov, A., White, A.J.P., and Williams, D.J., *Chem. Commun.*, 2001, 719

163. Volland, M.A.O., Straub, B.F., Gruber, I., Rominger, F., and Hofmann, P., *J. Organomet. Chem.*, 2001, **617-618**, 288

164. Trnka, T.M., Dias, E.L., Day, M.W., and Grubbs, R.H., *Arkivoc*, 2002, **xiii**, 28

165. Nieczypor, P., Van Leeuwen, P.W.N.M., Mol, J.C., Lutz, M., and Spek, A.L., *J. Organomet. Chem.*, 2001, **625**, 58

166. Amoroso, D., Snelgrove, J.L., Conrad, J.C., Drouin, S.D., Yap, G.P.A., and Fogg, D.E., *Adv. Synth. Catal.*, 2002, **344**, 757

167. Calderon, N., Ofstead, E.A., Ward, J.P., Judy, W.A., and Scott, K.W., *J. Am. Chem. Soc.*, 1968, **90**, 4133

168. Bradshaw, P., Howman, E.J., and Turner, L., *J. Catal.*, 1967, **7**, 269

169. Lewandos, G.S. and Pettit, R., *J. Am. Chem. Soc.*, 1971, **93**, 7087

170. Biefeld, C.G., Eick, H.A., and Grubbs, R.H., *Inorg. Chem.*, 1973, **12**, 2166

171. Cassar, L., Eaton, P.E., and Halpern, J., *J. Am. Chem. Soc.*, 1970, **92**, 3515

172. Katz, T.J. and Acton, N., *Tetrahedron Lett.*, 1967, **27**, 2601

173. Katz, T.J. and Cerefice, S., *J. Am. Chem. Soc.*, 1969, **91**, 2405

174. Herrisson, J.L. and Chauvin, Y., *Makromol. Chem.*, 1971, **141**, 161

175. Grubbs, R.H., Burk, P.L., and Carr, D.D., *J. Am. Chem. Soc.*, 1975, **97**, 3265

176. Grubbs, R.H., Carr, D.D., Hoppin, C., and Burk, P.L., *J. Am. Chem. Soc.*, 1976, **98**, 3478

177. Katz, T.J. and Rothchild, R., *J. Am. Chem. Soc.*, 1976, **98**, 2519

178. Jafarpour, L. and Nolan, S.P., *Organometallics*, 2000, **19**, 2055

179. Hinderling, C., Adlhart, C., and Chen, P., *Angew. Chem. Int. Ed.*, 1998, **37**, 2685

180. Grubbs, R.H. *in* ***Comprehensive Organometallic Chemistry***, Wilkinson, G., Sir, Ed., *Alkene and Alkyne Metathesis Reactions*, Vol. 8, Pergamon Press, Oxford, 1982, p. 499

181. Love, J.A., Sanford, M.S., Day, M.W., and Grubbs, R.H., *J. Am. Chem. Soc.*, 2003, **125**, 10103

182. Young, D., 1998. Introduction to Computational Chemistry. [Web] http://www.ccl.net/cca/documents/dyoung/topics-orig/compchem.html [Date of access: 18/01/06]

183. Wikipedia, 2007. Molecular modelling. [Web] http://en.wikipedia.org/wiki/Molecular_modelling [Date of access: 2 March 2007]

184. Hehre, W.J., Yu, J., Klunzinger, P.E., and Lou, L., ***A Brief Guide to Molecular Mechanics and Quantum Chemical Calculations***, Irvine Wavefunction, Inc., California, 1998

185. Janse van Rensburg, W., ***Contrathermodynamic Isomerisation of Internal Olefins by Exploring the Migratory Aptitude of Various Substrates. The Significance of Concurring Molecular Modeling***, Ph.D thesis, UOFS, 2001

186. Jordan, R.B., ***Reaction Mechanisms of Inorganic and Organometallic Systems***, Oxford University Press, New York, 1998

187. Bray, M.R., Deeth, R.J., and Paget, V.J., *Prog. Reaction Kinetics*, 1996, **21**, 169

188. Jensen, F., ***Introduction to Computational Chemistry***, Wiley, New York, 1999

189. Ziegler, T. and Versluis, L., *Adv. Chem. Ser.*, 1992, **230**, 75

190. Ziegler, T., *Chem. Rev.*, 1991, **91**, 651

191. Ziegler, T., *Pure Appl. Chem.*, 1991, **63**, 873

192. Ziegler, T., *Can. J. Chem.*, 1995, **73**, 743

193. Koga, N. and Morokuma, K., *Top. Phys. Organomet. Chem.*, 1989, **3**, 1

194. Koga, N. and Morokuma, K., *Chem. Rev.*, 1991, **91**, 823

195. Musaev, D.G., Matsubara, T., Mebel, A.M., Koga, N., and Morokuma, K., *Pure Appl. Chem.*, 1995, **67**, 257

196. Musaev, D.G. and Morokuma, K., *Adv. Chem. Phys.*, 1996, **95**, 61

197. Torrent, M., Solà, M., and Frenking, G., *Chem. Rev.*, 2000, **100**, 439

198. Koga, N. and Morokuma, K. *in* ***Theoretical Aspects of Homogeneous Catalysis***, Van Leeuwen, P.W.N.M., Morokuma, K., and Van Lenthe, J.H., Eds., *Alkene Migratory Insertions and C-C Bond Formations*, Kluwer Academic, Dordrecht, The Netherlands, 1995, p. 65

199. Koga, N. and Morokuma, K. *in* ***Theoretical Aspects of Homogeneous Catalysis***, Van Leeuwen, P.W.N.M., Morokuma, K., and Van Lenthe, J.H., Eds., *Carbonyl Migratory Insertions*, Kluwer Academic, Dordrecht, The Netherlands, 1995, p. 93

200. Siegbahn, P.E.M. and Blomberg, M.R.A. *in* ***Theoretical Aspects of Homogeneous Catalysis***, Van Leeuwen, P.W.N.M., Morokuma, K., and Van Lenthe, J.H., Eds., *Oxidative Addition Reactions*, Kluwer Academic, Dordrecht, The Netherlands, 1995, p. 15

201. Hofmann, P., Hämmerle, M., and Unfried, G., *New J. Chem.*, 1991, **15**, 769

202. Hofmann, P. and Hämmerle, M., *Angew. Chem. Int. Ed. Engl.*, 1989, **28**, 908

203. Torrent, M., Duran, M., and Solà, M., *Chem. Commun.*, 1998, 999

204. Torrent, M., Duran, M., and Solà, M., *Organometallics*, 1998, **17**, 1492

205. Torrent, M., Duran, M., and Solà, M., *J. Am. Chem. Soc.*, 1999, **121**, 1309

206. Sakaki, S. and Dedieu, A., *Inorg. Chem.*, 1987, **26**, 3278

207. Sakaki, S., Aizawa, J.T., Koga, N., Morokuma, K., and Ohkubola, K., *Inorg. Chem.*, 1989, **28**, 103

208. Jegat, C., Fouassier, M., Tranquille, M., Mascetti, J., Tommasi, I., Aresta, M., Ingold, F., and Dedieu, A., *Inorg. Chem.*, 1993, **32**, 1279

209. Hutschka, F., Dedieu, A., Eichberger, M., Fornika, R., and Leitner, W., *J. Am. Chem. Soc.*, 1997, **119**, 4432

210. Sakaki, S. and Musashi, Y., *J. Chem. Soc., Dalton Trans.*, 1994, 3047

211. Sakaki, S. and Musashi, Y., *J. Chem. Soc., Dalton Trans.*, 1998, 577

212. Sakaki, S. and Okhubo, K., *Inorg. Chem.*, 1988, **27**, 2020

213. Sakaki, S. and Okhubo, K., *Inorg. Chem.*, 1989, **28**, 2583

214. Sakaki, S. and Okhubo, K., *Organometallics*, 1989, **8**, 2970

215. Sakaki, S. and Musashi, Y., *Inorg. Chem.*, 1995, **34**, 1914

216. Koga, N. and Morokuma, K., *J. Phys. Chem.*, 1990, **94**, 5454

217. Hutschka, F., Dedieu, A., and Leitner, W., *Angew. Chem. Int. Ed. Engl.*, 1995, **34**, 1742

218. Pomelli, C.S., Tomasi, J., and Solà, M., *Organometallics*, 1998, **17**, 3164

219. Klein, R. and Schmid, R. *in* ***Applied Homogeneous Catalysis with Organometallic Compounds***, Cornils, B. and Herrmann, W.A., Eds., *Molecular Modeling in Homogeneous Catalysis*, Vol. Vol. 2: Developments, Wiley, New York, 1996, p. 654

220. Dedieu, A., Sakaki, S., Strich, A., and Siegbahn, P.E.M., *Chem. Phys. Lett.*, 1987, **133**, 317

221. Nakamura, S. and Dedieu, A., *Chem. Phys. Lett.*, 1984, **111**, 243

222. Axe, F.U. and Marynick, D.S., *Chem. Phys. Lett.*, 1987, **141**, 455

223. Siegbahn, P.E.M. and Svensson, M., *Chem. Phys. Lett.*, 1993, **216**, 147

224. Ziegler, T., Versluis, L., and Tschinke, V., *J. Am. Chem. Soc.*, 1986, **108**, 612

225. Rappe, A.K., *J. Am. Chem. Soc.*, 1987, **109**, 5605

226. Tatsumi, K., Nakamura, A., Hofmann, P., Stauffert, P., and Hoffmann, R., *J. Am. Chem. Soc.*, 1985, **107**, 4440

227. Axe, F.U. and Marynick, D.S., *J. Am. Chem. Soc.*, 1988, **110**, 3728

228. McKee, M.L., Dai, C.H., and Worley, S.D., *J. Phys. Chem.*, 1988, **92**, 1056

229. Koga, N. and Morokuma, K., *Organometallics*, 1991, **10**, 946

230. Versluis, L. and Ziegler, T., *J. Am. Chem. Soc.*, 1990, **112**, 6763

231. Blomberg, M.R.A., Karlsson, C.A.M., and Siegbahn, P.E.M., *J. Phys. Chem.*, 1993, **97**, 9341

232. Koga, N. and Morokuma, K., *Chem. Rev.*, 1991, **91**, 823

233. Xiao-Guang, Z., Yin-Sheng, X., and Xie-Xian, G., *J. Mol. Catal.*, 1988, **43**, 381

234. Ren-Hu, W. and Yin-Sheng, X., *J. Mol. Catal.*, 1989, **54**, 478

235. Rosi, M., Sgamellotti, A., Tarantelli, F., and Floriani, C., *J. Chem. Soc., Dalton Trans.*, 1988, 249

236. Pacchioni, G., Fantucci, P., Koutecky, J., and Ponec, V., *J. Catal.*, 1988, **112**, 34

237. Dedieu, A. *in* ***The Challenge of d and f Electrons: Theory and Computation***, Salahub, D.R. and Zerner, M.C., Eds., *ACS Symposium Series 384*, American Chemical Society, Washington, DC, 1989, p. 58

238. Dedieu, A. and Nakamura, S. *in* ***Quantum Chemistry: The Challenge of Transition Metals and Coordination Chemistry***, Veillard, A., Ed., *NATO ASI Series*, Vol. 176, Reidel, Dordrecht, The Netherlands, 1986, p. 277

239. Koga, N. and Morokuma, K. *in* ***Transition Metal Hydrides***, Dedieu, A., Ed., *Chapter 6*, Wiley, New York, 1992,

240. Tsipis, C.A., *Coord. Chem. Rev.*, 1991, **108**, 163

241. Koga, N., Daniel, C., Han, J., Fu, X.Y., and Morokuma, K., *J. Am. Chem. Soc.*, 1987, **109**, 3455

242. Daniel, C., Koga, N., Han, J., Fu, X.Y., and Morokuma, K., *J. Am. Chem. Soc.*, 1988, **110**, 3773

243. Koga, N., Obara, S., Kitaura, K., and Morokuma, K., *J. Am. Chem. Soc.*, 1985, **107**, 7109

244. Dedieu, A. and Strich, A., *Inorg. Chem.*, 1979, **18**, 2940

245. Dedieu, A., *Inorg. Chem.*, 1980, **19**, 375

246. Dedieu, A., *Inorg. Chem.*, 1981, **20**, 2803

247. Dedieu, A. and Hyla-Krispin, I., *J. Organomet. Chem.*, 1981, **220**, 115

248. Roe, R.C., *J. Am. Chem. Soc.*, 1983, **105**, 7770

249. Siegbahn, P.E.M., *J. Am. Chem. Soc.*, 1993, **115**, 5803

250. Siegbahn, P.E.M., *Chem. Phys. Lett.*, 1993, **205**, 290

251. Siegbahn, P.E.M., *J. Organomet. Chem.*, 1994, **478**, 83

252. Bogdan, P.L., Irwin, J.J., and Bosnich, B., *Organometallics*, 1989, **8**, 1450

253. Brown, J.M. and Evans, P.L., *Tetrahedron*, 1988, **44**, 4905

254. Duca, D., Baranyai, P., and Vidoczy, T., *J. Comput. Chem.*, 1998, **19**, 396

255. Duca, D., La Manna, G., and Russo, M.R., *Phys. Chem. Chem. Phys.*, 1999, **1**, 1375

256. Dedieu, A., Strich, A., and Rossi, A. *in* ***Quantum Theory of Chemical Reactivity***, Daudel, R., Pullman, A., Salem, A., and Veillard, A., Eds., Vol. 2, Reidel, Dordrecht, The Netherlands, 1981, p. 193

257. Koga, N. and Morokuma, K. *in* ***The Challenge of d and f Electrons: Theory and Computation***, Salahub, D.R. and Zerner, M.C., Eds., *ACS Symposium Series 394*, American Chemical Society, Washington, DC, 1989, p. 77

258. Woo, T.K., Fan, L.Y., and Ziegler, T., *Organometallics*, 1994, **13**, 2252

259. Rappe, A.K. and Goddard, W.A., III, *J. Am. Chem. Soc.*, 1982, **104**, 448

260. Brookhart, M. and Green, M.L.H., *J. Organomet. Chem.*, 1983, **250**, 395

261. Axe, F.U. and Coffin, J.M., *J. Phys. Chem.*, 1994, **98**, 2567

262. Weiss, H., Ehrig, M., and Ahlrichs, R., *J. Am. Chem. Soc.*, 1994, **116**, 4919

263. Meier, R.J., Vandoremaelle, G.H.S., Iarlori, S., and Buda, F., *J. Am. Chem. Soc.*, 1994, **116**, 7274

264. Lohrenz, J.C.W., Woo, T.K., and Ziegler, T., *J. Am. Chem. Soc.*, 1995, **117**, 12793

265. Lohrenz, J.C.W., Woo, T.K., Fan, L.Y., and Ziegler, T., *J. Organomet. Chem.*, 1995, **497**, 91

266. Niu, S. and Hall, M.B., *Chem. Rev.*, 2000, **100**, 353

267. Vyboishchikov, S.F. and Thiel, W., *Chem. Eur. J.*, 2005, **11**, 3921

268. Tobisch, S., *Acc. Chem. Res*, 2002, **35**, 96

269. Cundari, T.R., *Chem. Rev.*, 2000, **100**, 807

270. Ivanova, A., Tadjer, A., and Gospodinova, N., *J. Phys. Chem. B*, 2006, **110**, 2555

271. Vanka, K., Xu, Z., Seth, M., and Ziegler, T., *Top. Catal.*, 2005, **34**, 143

272. Marshall, E.L., Gibson, V.C., and Rzepa, H.S., *J. Am. Chem. Soc.*, 2005, **127**, 6048

273. Beddie, C., Hollink, E., Wei, P., Gauld, J., and Stephan, D.W., *Organometallics*, 2004, **23**, 5240

274. Tellmann, K.P., Humphries, M.J., Rzepa, H.S., and Gibson, V.C., *Organometallics*, 2004, **23**, 5503

275. Khoroshun, D.V., Musaev, D.G., Vreven, T., and Morokuma, K., *Organometallics*, 2001, **20**, 2007

276. Chen, Y. and Liu, X., *Polymer*, 2005, **46**, 9434

277. Tobisch, S. and Ziegler, T., *Organometallics*, 2005, **24**, 256

278. Spencer, L.P., Altwer, R., Wei, P., Gelmini, L., Gauld, J., and Stephan, D.W., *Organometallics*, 2003, **22**, 3841

279. Belanzoni, P., Sgamellotti, A., Re, N., and Floriani, C., *Inorg. Chem.*, 2000, **39**, 1147

280. Belanzoni, P., Fantacci, S., Re, N., Rosi, M., Sgamellotti, A., and Floriani, C., *Inorg. Chem.*, 1997, **36**, 2018

281. Fan, L., Krzywicki, A., Somogyvari, A., and Ziegler, T., *Inorg. Chem.*, 1996, **35**, 4003

282. Abraham, S.P., Samuelson, A.G., and Chandrasekhar, J., *Inorg. Chem.*, 1993, **32**, 6107

283. Blok, A.N.J., Budzelaar, P.H.M., and Gal, A.W., *Organometallics*, 2003, **22**, 2564

284. de Bruin, T.J.M., Magna, L., Raybaud, P., and Toulbout, H., *Organometallics*, 2003, **22**, 3404

285. Yu, Z.-X. and Houx, K.N., *Angew. Chem. Int. Ed.*, 2003, **42**, 808

286. Janse van Rensburg, W., Grové, C., Steynberg, J.P., Stark, K.B., Huyser, J.J., and Steynberg, P.J., *Organometallics*, 2004, **23**, 1207

287. Ulman, M. and Grubbs, R.H., *Organometallics*, 1998, **17**, 2484

288. Ulman, M. and Grubbs, R.H., *J. Org. Chem.*, 1999, **64**, 7202

289. Adlhart, C. and Chen, P., *Helv. Chim. Acta.*, 2003, **86**, 941

290. Volland, M.A.O., Adlhart, C., Kiener, C.A., Chen, P., and Hofmann, P., *Chem. Eur. J.*, 2001, **7**, 4621

291. Cavallo, L., *J. Am. Chem. Soc.*, 2002, **124**, 8965

292. Hansen, S.M., Rominger, F., Metz, M., and Hofmann, P., *Chem.-Eur. J.*, 1999, **5**, 557

293. Adlhart, C. and Chen, P., *Angew. Chem. Int. Ed.*, 2002, **41**, 4484

294. Coalter III, J.N., Bollinger, J.C., Eisenstein, O., and Caulton, K.G., *New J. Chem.*, 2000, **24**, 925

295. Coalter III, J.N., Spivak, G.J., Gerard, H., Clot, E., Davidson, E.R., Eisenstein, O., and Caulton, K.G., *J. Am. Chem. Soc.*, 1998, **120**, 9388

296. Coalter III, J.N., Bollinger, J.C., Huffman, J.C., Werner-Zwanziger, U., Caulton, K.G., Davidson, E.R., Gerard, H., Clot, E., and Eisenstein, O., *New J. Chem.*, 2000, **24**, 9

297. Fomine, S., Vargas, S.M., and Tlenkopatchev, M.A., *Organometallics*, 2003, **22**, 93

298. Bernardi, F., Bottoni, A., and Miscione, G.P., *Organometallics*, 2003, **22**, 940

299. Ferrando, G., Gerard, H., Spivak, G.J., Coalter III, J.N., Huffman, J.C., Eisenstein, O., and Caulton, K.G., *Inorg. Chem.*, 2001, **40**, 6610

300. Burdett, K.A., Harris, L.D., Margl, P., Maughon, B.R., Mokhtar-Zadeh, T., Saucier, P.C., and Wasserman, E.P., *Organometallics*, 2004, **23**, 2027

301. Costabile, C. and Cavallo, L., *J. Am. Chem. Soc.*, 2004, **126**, 9592

302. Hansen, S.M., Rominger, F., Metz, M., and Hofmann, P., *Chem. Eur. J.*, 1999, **5**, 557

303. Janse van Rensburg, W., Steynberg, P.J., Meyer, W.H., Kirk, M.M., and Forman, G.S., *J. Am. Chem. Soc.*, 2004, **126**, 14332

304. Forman, G.S., McConnell, A.E., Tooze, R.P., Janse van Rensburg, W., Meyer, W.H., Kirk, M.M., Dwyer, C.L., and Serfontein, D.W., *Organometallics*, 2005, **24**, 4528

305. Dinger, M.B. and Mol, J.C., *Adv. Synth. Catal.*, 2002, **366**, 671

306. Stüer, W., Wolf, J., and Werner, H., *J. Organomet. Chem.*, 2002, **641**, 203

307. Romero, P.E. and Piers, W.E., *J. Am. Chem. Soc.*, 2005, **127**, 5032

308. Jordaan, M., Van Helden, P., Van Sittert, C.G.C.E., and Vosloo, H.C.M., *J. Mol. Catal. A: Chem.*, 2006, **254**, 145

309. Forman, G.S., McConnell, A.E., Hanton, M.J., Slawin, A.M.Z., Tooze, R.P., Janse van Rensburg, W., Meyer, W.H., Dwyer, C., Kirk, M.M., and Serfontein, D.W., *Organometallics*, 2004, **23**, 4824

310. Janse van Rensburg, W., Steynberg, P.J., Kirk, M.M., Meyer, W.H., and Forman, G.S., *J. Organomet. Chem.*, 2006, **691**, 5312

Experimental 3

3.1 GENERAL

3.1.1 Reagents and solvents

The complexes $RuCl_2(PCy_3)L(=CHPh)$ [L = PCy_3 or H_2IMes] and substrate 2-(hydroxymethyl)-pyridine were purchased from Fluka and used as they were. The following complexes were synthesized for use as starting materials for the synthesis of the hemilabile complexes and used without further purification: $RuCl_2(PCy_3)Py_2(=CHPh)$ from $RuCl_2(PCy_3)_2(=CHPh)$ and $RuCl_2(H_2IMes)Py_2(=CHPh)$ from $RuCl_2(PCy_3)(H_2IMes)(=CHPh)$. 1-Octene (Aldrich) was passed through a column of basic alumina and stored on molecular sieves (4Å) under N_2. Chlorobenzene (Merck) and pentane (Merck) were refluxed with CaH_2 and distilled over 4Å molecular sieves under N_2. Dichloromethane (Merck) was refluxed with $CaCl_2$ and distilled over 4Å molecular sieves under N_2. THF (Aldrich), toluene (Aldrich) and diethyl ether (Labchem) were refluxed with Na/benzophenone and distilled over 4Å molecular sieves under N_2. Thallium ethoxide, butyl-lithium, pyridine-2-carboxylic acid, 2-hydroxypyridine, 2-(2-hydroxyethyl)pyridine, 2-(hydroxyme-thyl)tetrahydropyran, 8-quinolinol, furan-2-carboxylic acid, guaiacol, 2-(diphenylphosphino)benzoic acid, 2-thiophene carboxylic acid and 2-thiophene carboxamide were purchased from Aldrich and used as received. Afrox supplied all the gasses used during the study.

3.1.2 Apparatus

All reactions were carried out under an argon (Ar) or N_2 atmosphere using standard Schlenk and vacuum techniques. A schematic representation of the experimental setup is given in **Figure 3.1**. Initially a moisture trap, filled with 4Å molecular sieves, was placed between the gas inlet and bubbler 2 to avoid any moisture entering the reaction vessel from the N_2 gas. Due to the generation of oxygen from the molecular sieves (§ 3.1.2.4), the trap was removed and argon was used directly from a cylinder during the synthesis of ruthenium complexes. The double manifold allows for the evacuation of air and flushing with inert gas of the Schlenk glassware as well as the evaporation of small amounts of liquids via condensation into the cooling traps.[1] The setup usually includes two bubblers containing silicon oil, one (bubbler 2) to indicate the gas flow from the inert gas source, and the second (bubbler 1), with an anti suck-back valve, to prevent air from flowing in from the environment when evacuating and flushing the Schlenk glassware with inert gas and to avoid pressure build-up in the system.[1] One of the solvent traps was cooled with a mixture of acetone and dry ice to prevent any solvents from entering the vacuum pump.

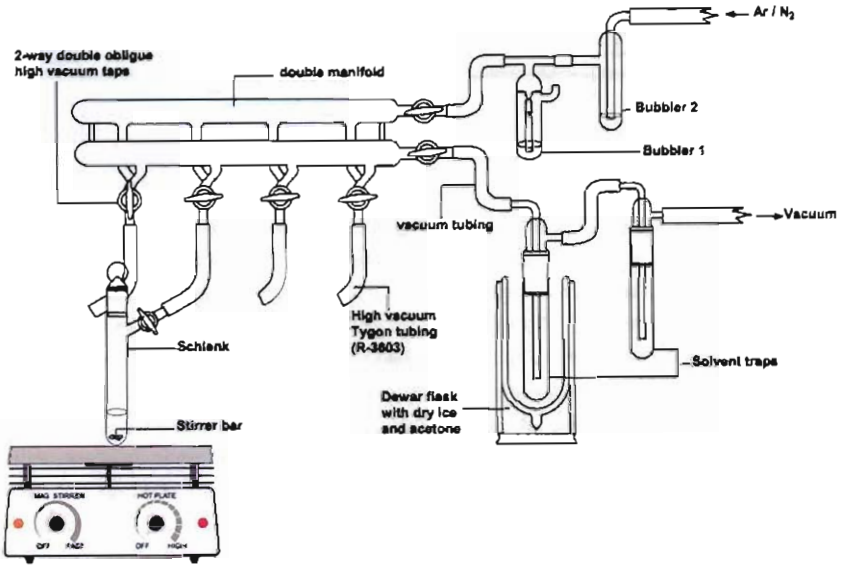

Figure 3.1 Experimental setup for performing a reaction in a Schlenk tube.

Syringes (GASTIGHT® (Hamilton) and disposable (Norm-ject)) were assembled and fitted with stainless steel or terumo needles and flushed with a stream of Ar before transferring liquids to the Schlenk tube.

3.1.2.1 General procedure for the removal of solvents under vacuum

Solvents were removed under vacuum via condensation from a Schlenk tube into one of the solvent traps (cooled with acetone/dry ice) of the manifold. Care was taken not to suck the liquid into the tubing and the manifold. Firstly, the Schlenk tube was evacuated with the valve closed and then one of the following two procedures was used to remove the solvent:

1. *With stirring:* the valve was carefully opened until slightly open (never opened fully) while stirring magnetically.
2. *Without stirring*: the Schlenk tube was tilted in a slightly horizontal position to increase the surface area of the liquid, while pointing the valve to the top of the fume cupboard. The valve was then carefully opened until slightly open (never opened fully).

When the liquid started to cool down and/or convectional streams (in clear liquids) formed, it was an indication that condensation of the solvent was taking place. The valve was opened wider

when no condensation was visible with sinking liquid level. The Schlenk tube was also slightly heated (with non-volatile solvents) to speed up the process. When the liquid was removed completely, the tube was allowed to warm to room temperature. The tube was then flushed with Ar and disconnected from the manifold.

3.1.2.2 General procedure for the filtration of a suspension under inert gas

One of the following procedures was used for the filtration of a suspension under inert gas:

1. Filtration via a sintered funnel (**Figure 3.2**)

A Schlenk tube was connected to a sintered funnel as shown in **Figure 3.2**. The system was evacuated and then flushed with argon. The suspension to be filtered was then transferred into the sinter filter vessel via a syringe and the filtrate collected in the Schlenk tube.

2. Filtration via a syringe filter

The suspension was drawn into a gas-tight syringe under inert gas conditions. A commercially available syringe filter (Whatman GD/X (polypropylene membrane, pore size 0.45 um, diam. 25mm (Aldrich) or Acrodisc (membrane GHPP, 0.45 um, diam. 25mm (Aldrich or Separations)) was placed quickly between the syringe and a new stainless steel needle. The contents of the syringe were then slowly filtered into another Schlenk tube. The syringe filter with precipitate was discarded.

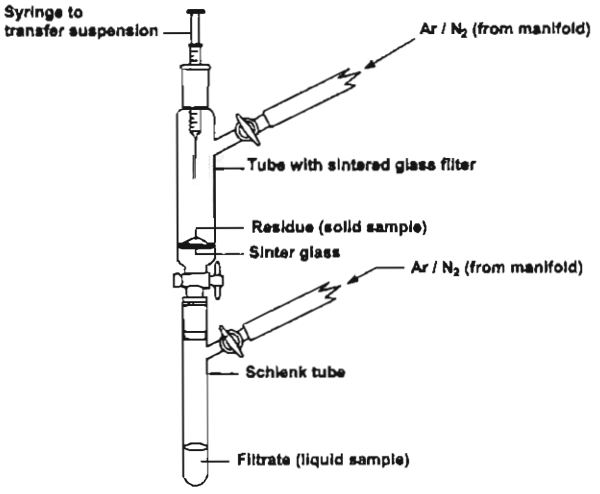

Figure 3.2 Filtration of a suspension under inert gas via a sintered funnel.

3.1.2.3 General procedure for pump freezing solvents

A Schlenk tube was quarter-filled with activated 4Å molecular sieves before adding the deuterated solvent to ⅔ above the level of the sieves. The Schlenk tube was suspended in liquid nitrogen, with the valve closed, to completely freeze the solvent. The Schlenk tube was removed from the liquid nitrogen and then carefully evacuated until the first liquid droplets formed. The Schlenk tube was then flushed with Ar until the solvent completely liquefied. The procedure, from suspending the tube in liquid nitrogen, was repeated twice.

3.1.2.4 Detection of oxygen generated from molecular sieves

It is well known that **Gr1** and **Gr2** exhibit both high reactivity and high tolerance toward functional groups. In addition, the precatalysts are only mildly sensitive to oxygen, since a slow decomposition of **Gr1** and **Gr2** in solution was experimentally observed.[2] For example, for **Gr2** this is visualised as a change in colour in the reaction mixture, which turns from red to greenish-brown. Therefore, the presence of large amounts of oxygen in the reaction mixture can be detrimental to any attempt to manipulate the Grubbs systems. In order to ensure that no oxygen would be present during the synthesis of the new complexes, the gasses, as well as the experimental setup as seen in **Figure 3.1**, which originally had a moisture trap between the gas inlet and bubbler 2, were tested for the presence of oxygen with and without the trap present. A colourless $[Cu(NH_3)_2]^+$ solution was used to test for the presence of oxygen in the system, since it is known that this solution will readily absorb oxygen to form the blue $[Cu(NH_3)_4]^{2+}$ complex.[3] The solution was prepared in a Schlenk tube under an inert atmosphere, so that no atmospheric oxygen could influence the testing process. The Schlenk tube was then connected to the manifold via a Pasteur pipette, while still maintaining a closed system, and the gas bubbled through the solution. With the moisture trap present, the solution turned dark blue within seconds, while only a light blue solution formed after several hours when the trap was removed. This indicated that oxygen was generated from the molecular sieves in the moisture trap, which was therefore removed from the setup.

Synthesis of $[Cu(NH_3)_2]^+$ solution

3 g cupric sulphate was added to *ca.* 40 mL ammonia in a Schlenk tube to form a blue teraaminecopper $[Cu(NH_3)_4]^{2+}$ solution. 2 g copper turnings were added to the solution and left for 2-3 days until the solution was colourless. The Cu^{II}-ion was therefore reduced to Cu^{I} by metallic copper according to eq. 3.1.[3,4]

$$[Cu(NH_3)_4]^{2+} + Cu^0 = 2\,[Cu(NH_3)_2]^+ \qquad (3.1)$$

3.2 SYNTHESIS OF THE LIGAND SALTS

The following alcohols, carboxylic acids and an amide (**Table 3.1**) were investigated as possible hemilabile ligands for the synthesis of hemilabile ruthenium carbene complexes. The tertiary alcohols **L1-L4** (**Table 3.1**) were synthesised according to literature following a simple two-step synthesis route,[5] while all other ligands were purchased and used as received.

The literature survey revealed that lithium,[6] thallium,[7-10] silver,[11,12] potassium[13] and sodium[14] salts have been previously used to manipulate the ruthenium carbene complexes. The thallium salts were more generally used than the others. Due to the toxicity of thallium ethoxide and the instability of the resulting thallium salts, other possibilities were first explored. However, among the various salts investigated for manipulation of **Gr1** and **Gr2**, the thallium and lithium salts proved to be the most efficient and were subsequently used in all the substitution reactions.

Table 3.1 Potential hemilabile ligands that was investigated

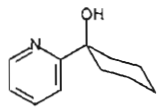

L1

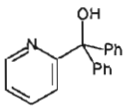

L2

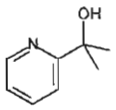

L3

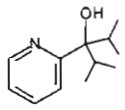

L4

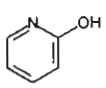

L5

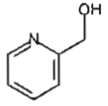

L6

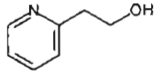

L7

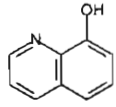

L8

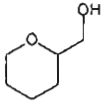

L9

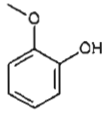

L10

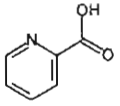

L11

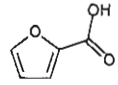

L12

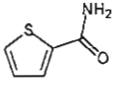

L13

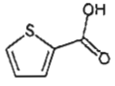

L14

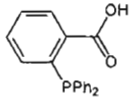

L15

3.2.1 Synthesis of pyridinyl alcoholato ligands

The reaction was performed in a round bottom flask under Ar, which was initially flushed with a stream of Ar for 5 min before adding the reagents. After lithiation of 2-bromopyridine at the ortho-position, the resulting organometallic species underwent a nucleophilic attack at the carbonyl group of the ketone followed by the protonation of the resulting lithium salt (eq. 4.1 and eq. 4.2).

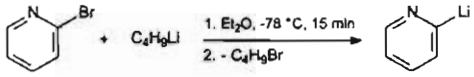

(4.1)

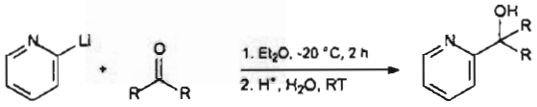

(4.2)

Through the use of various symmetric ketones (**Table 3.2**), the steric and electronic characteristics of these ligands could be changed. The deprotonated alcohols have been previously described[5] as chelating, anionic bidentate ligands, which complex a metal centre with a coordinative bond (through the nitrogen of the pyridine ring) and a covalent single bond (through the alcoholate oxygen of the former hydroxyl group). These ligands form a five-membered ring when bound to the metal centre, which is generally thermodynamically more stable than six-membered rings.[15] The ligands **L1-L4** have been previously complexed to molybdenum to give highly active catalytic systems for the oxidation of 1-octene with elemental oxygen at atmospheric pressure.[5] Denk et al.[6] incorporated **L1** and **L3** into a second generation Grubbs carbene variant for ROMP of norbornene at 60 °C. The analogous **Gr1**-system with **L1** was also synthesised, but not tested for any catalytic activity.

Table 3.2 Reaction of selected ketones with 2-pyridyllithium

Used ketone	Resulting alcohol	Ligand	#
Cyclohexanone	1-(2'-pyridyl)cyclohexanol	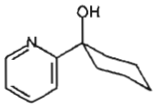	L1
Benzophenone	1,1-Diphenyl-1-(2'-pyridyl)methanol	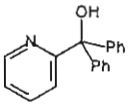	L2
Propan-2-one	2-(2'-pyridyl)propan-2-ol	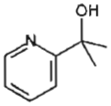	L3
2,4-Dimethylpentan-3-one	2,4-Dimethyl-3(2'-pyridyl)pentan-3-ol	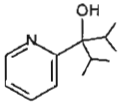	L4

3.2.1.1 General procedure for the synthesis of L1-L4

100 mL diethyl ether was cooled to -78 °C. After addition of 100 mmol (10 mL of a 10 M or 40 mL of a 2.5 M) butyllithium solution in hexane to the cooled ether, a yellow solution was formed. Addition of 95 mmol (9.05 mL) of 2-bromopyridine in 25 mL diethyl ether to the yellow solution proceeded over a period of 15 min. While adding the 2-bromopyridine the colour of the solution changed from yellow to dark-red. After stirring the reaction mixture at -78 °C for 15 min, it was allowed to warm up to -20 °C. The desired ketone (105 mmol) was added to the reaction mixture at -20 °C. The solution was stirred for 2 h at -20 °C and then allowed to warm to room temperature. After careful hydrolysis, the ether phase was extracted with 5 x 20 mL of a 2 M HCl solution. After neutralisation of the water phase with a 2 M NaOH solution, the phase was extracted with diethyl ether. After drying the ether phase with $MgSO_4$, it was decanted and allowed to slowly evaporate. A light-yellow solution resulted, which was treated with activated charcoal and filtered. Colourless crystals were obtained for **L1** and **L2**, while **L3** and **L4** were colourless oils.

3.2.1.2 Spectroscopic data of the ligands L1-L4

The spectral data of these ligands (§ 3.1.3.1) were comparable to literature, which only provided ^{1}H-NMR data.[5]

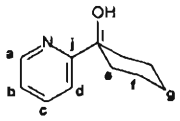

L1

IR-spectra: (KBr, cm^{-1}) ν_{maks} 3415 (O-H stretch), 3069 – 3020 (C-H stretch, aromatic), 2932 – 2855 (C-H stretch, aliphatic), 1593 – 1570 (C=C and C=N stretch).

^{1}H-NMR data: [$CDCl_3$, 300 MHz, ppm]: δ_H 8.487 (1H, d, H_a), 7.657 (1H, dd, H_c), 7.365 (1H, d, H_d), 7.143 (1H, dd, H_b), 4.812 (1H, s, OH), 1.9-1.6 (10H, *m*, CH).

^{13}C-NMR data: [$CDCl_3$, 75 MHz]: δ_C 22.09 (C_f), 25.56 (C_g), 30.51 (C_e), 72.73 (C_i), 118.87 (C_c), 121.71 (C_b), 136.78 (C_a), 147.43 (C_d), 166.113 (C_j).

MS-spectrum: (MSD): 177 *m/z*

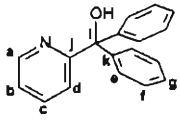

L2

IR-spectra: (KBr, cm^{-1}) ν_{maks} 3347 (O-H stretch), 3054 – 3018 (C-H stretch, aromatic), 1591 – 1571 (C=C and C=N stretch).

^{1}H-NMR data: [$CDCl_3$, 300 MHz, ppm]: δ_H 8.574 (1H, d, H_a), 7.612 (1H, dd, H_c), 7.3-7.19 (11H, d, H_d + Phenyl rings), 7.103 (1H, dd, H_b), 6.258 (1H, s, OH).

^{13}C-NMR data: [$CDCl_3$, 75 MHz]: δ_C 80.829 (C_i), 122.300 (C_b), 122.880 (C_d), 127.270 (C_g), 127.884 (C_f), 128.122 (C_e), 136.342 (C_c), 146.113 (C_a), 147.704 (C_k), 163.228 (C_j).

MS-spectrum: (MSD): 261 *m/z*

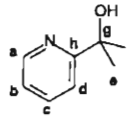

L3

IR-spectra: (KBr) ν_{maks} 3200 (O-H stretch), 3200 – 3100 (C-H stretch, aromatic), 2990 – 2890 (C-H stretch, aliphatic), 1593 – 1570 (C=C and C=N stretch).

^{1}H-NMR data: [$CDCl_3$, 300 MHz]: δ_H 8.469 (1H, d, H_a), 7.646 (1H, dd, H_c), 7.340 (1H, d, H_d), 7.150 (1H, dd, H_b), 5.022 (1H, s, OH), 1.512 (6H, s, CH_3).

^{13}C-NMR data: [$CDCl_3$, 75 MHz]: δ_C 30.592 (C_e), 71.679 (C_g), 118.87 (C_b), 121.71 (C_d), 136.889 (C_c), 147.415 (C_a), 165.990 (C_h).

MS-spectrum: (MSD): 137 *m/z*

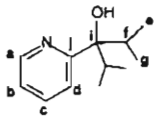

L4

IR-spectra: (KBr) ν_{maks} 3383 (O-H stretch), 3080 – 3057 (C-H stretch, aromatic), 2966 – 2876 (C-H stretch, aliphatic), 1593 – 1570 (C=C and C=N stretch).

^{1}H-NMR data: [$CDCl_3$, 300 MHz]: δ_H 8.484 (1H, d, H_a), 7.636 (1H, dd, H_c), 7.240 (1H, d, H_d), 7.173 (1H, dd, H_b), 5.534 (1H, s, OH), 2.288 (2H, dt, CH), 0.752 (2H, dd, CH_3).

^{13}C-NMR data: [$CDCl_3$, 75 MHz]: δ_C 16.686 (C_g), 17.492 (C_e), 34.244 (C_f), 79.668 (C_i), 120.610 (C_b), 121.637 (C_d), 135.856 (C_c), 146.821 (C_a), 161.520 (C_j).

MS-spectrum: (MSD): 193 *m/z*

3.2.2 Synthesis of sodium salts

Alcohols can react with sodium ethoxide (method 1), metallic sodium (method 2) or sodium hydride (method 3) to produce the corresponding sodium salt.[16,17] The resulting salts are called alkoxides, with the general formula RO^-M^+. These alkoxide ions (RO^-) are very good nucleophiles.[18] Carboxylic acids react with strong bases, such as sodium ethoxide, and metals to form carboxylate salts in which the hydrogen of the -OH group is replaced with the metal ion (method 1).[19]

Due to the magnitude of possible sodium sources, a variety of methods were investigated for the synthesis of the sodium salts of the corresponding alcohol and carboxylic acid ligands. The sodium salts of only a small selection of the ligands in **Table 3.1** were initially investigated and then terminated, because the synthesis of the new hemilabile ruthenium carbene complexes deemed unsuccessful with the use of these salts after several attempts at different ambient temperatures (§ 3.4.1). The experimental setup as described in § 3.1.2 was used for the synthesis of the sodium salts.

a) Method 1

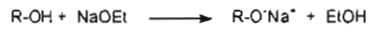

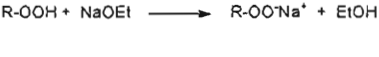

1.8 mmol (0.122g) NaOEt was added to a solution of *ca.* 2 mmol (see **Table 3.3** for specifications) alcohol or carboxylic acid in 5-10 mL THF under Ar. The reaction mixture was stirred for 3 h after which all the solvent was removed under reduced pressure (§ 3.1.2.1) and the precipitate dried under vacuum. The yields and product properties of the salts are given in **Table 3.3**.

b) Method 2

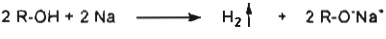

1.8 mmol (0.0414 g) Na was added to a solution of 2 mmol (see **Table 3.3** for specifications) alcohol in 5-10 mL THF under Ar. The reaction mixture was stirred until all the Na was dissolved. The formation of small bubbles of hydrogen gas was an indication that the reaction was taking place. All the solvent was then removed under reduced pressure (§ 3.1.2.1) and the precipitate dried under vacuum. The yields and product properties of the salts are given in **Table 3.3**. This method was not used for the carboxylic acids, since more reactive metals, such as Mg, are needed to produce the carboxylate salt with formation of hydrogen gas.[19]

c) Method 3

1.8 mmol (0.0432 g) NaH was added to a solution of 2 mmol (see **Table 3.3** for specifications) alcohol in 5-10 mL THF under Ar. The reaction mixture was stirred until all the NaH was dissolved. The formation of small bubbles of hydrogen gas was an indication that the reaction was taking place. All the solvent was removed under reduced pressure (§ 3.1.2.1) and the precipitate dried under vacuum. The yields and properties of the salts are given in **Table 3.3**. **S2** was not used for any manipulation reactions, due to difficulties experienced during the weighing process, as the ligand was too sticky.

Table 3.3 Synthesised sodium salts of the alcohols and carboxylic acids

Salt	Method #	$Mass_{Ligand}$ (g) ($Mass_{Na\text{-}source}$)	Yield (%)	Product
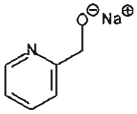 **S1**	2	0.214 (0.048)	23	Light-yellow powder with orange gel on sides of Schlenk
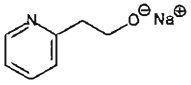 **S2**	2	0.246 (0.094)	-	Orange sticky gel – (could not be weighed for further reactions)
	3	0.246 (0.048)	3	
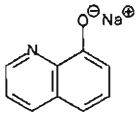 **S3**	1	0.328 (0.158)	70	Yellow powder (light sensitive)
	3	0.580 (0.200)	80	
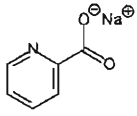 **S4**	1	0.288 (0.156)	85	Beige powder
	1	0.251 (0.122)	86	
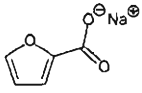 **S5**	1	0.256 (0.160)	78	White powder

3.2.3 Synthesis of thallium salts

The yields and properties of the salts are summarised in **Tables 3.4** to **3.5**. Due to the instability of the thallium salts in air and moisture, no analysis was performed.

Table 3.4 Synthesised thallium salts of the amide, carboxylic acid and alcohol ligands of **Table 3.1**.

Salt	$Mass_{Ligand}$ (g)	TlOEt (mL)	Yield	Product
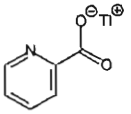 **S6**	0.246	0.142	95	White powder
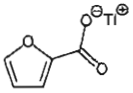 **S7**	0.224	0.142	-	Black residue
	0.220	0.140	90	White powder (unstable)
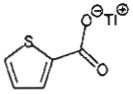 **S8**	0.261	0.412	85	Beige, fine crystals that turn pink after a few hours and were therefore discarded
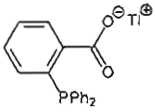 **S9**	0.361	0.084	85	White powder
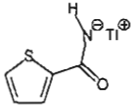 **S10**	0.254	0.117	85	White powder
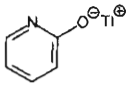 **S11**	0.205	0.142	95	Beige, fine crystals

Table 3.5 Synthesised thallium salts of the alcohol ligands of Table 3.1.

Salt	$Mass_{Ligand}$ (g)	TlOEt (mL)	Yield	Product
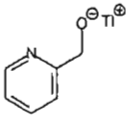 **S12**	0.218	0.140	-	Beige, thick oil
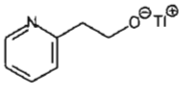 **S13**	0.250	0.140	-	Brown, thick oil
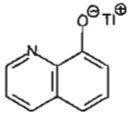 **S14**	0.290	0.143	95	Yellow powder
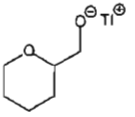 **S15**	0.697	0.425	-	Grey, thick oil
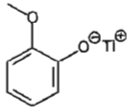 **S16**	0.249	0.140	92	White flakes
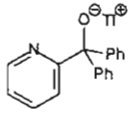 **S17**	0.518	0.140	95	White powder
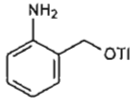 **S18**	0.251	0.146	85	Green crystals

Thallium ethoxide (TlOEt) (*ca.* 1.8 mmol, 0.449 g) was added dropwise to a solution of *ca.* 2 mmol ligands **L1-12** in THF (10 – 20mL) at room temperature under an inert atmosphere. In most cases, after the addition of TlOEt, a precipitate formed immediately and the reaction mixture was stirred for 2 h at room temperature. The solvent was then removed under reduced pressure to give the thallium salts in quantitative yields. Where no precipitate formed after addition of the TlOEt, the solution was stirred for 2 h with subsequent removal of the solvent under reduced pressure giving the desired salt as a powder. The salts were immediately used in the synthesis of ruthenium carbene complexes without further purification.

3.2.4 Synthesis of lithium salts

The yields and properties of the salts are given in **Table 3.6** and **3.7**.

20 mL THF was added to 2 mmol of the desired alcohol or carboxylic acid (**Table 3.1**) at room temperature under Ar. 2 mmol (0.2 mL of a 10 M or 0.9 mL of a 2.5 M solution in hexane) BuLi was added dropwise to the reaction mixture. In most cases after the addition of BuLi, a precipitate formed immediately and the reaction mixture was stirred for 2 h at room temperature. The solvent was then removed under reduced pressure to give the lithium salts in quantitative yields.

If no precipitate formed after addition of the BuLi, the solution was stirred for 2 h with formation of the desired salt after removal of the solvent under reduced pressure. After washing the salt with 2 x 5 mL pentane, the solvent was removed with a syringe and the salt dried under vacuum. No analysis of the salts was performed.

Table 3.6 Synthesised lithium salts of the alcohol ligands of **Table 3.1**.

Salt	#	$Mass_{Ligand}$ (g)	V_{BuLi} (mL)	Yield	Product
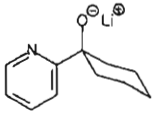	**S19**	0.280	0.150 (10 M BuLi)	90	Orange-brown, fine crystals
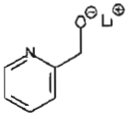	**S20**	0.218	0.200 (10 M BuLi)	-	Orange powder

Table 3.7 Synthesised lithium salts of the carboxylic acid and remaining alcohol ligands of **Table 3.1**.

Salt	#	$Mass_{Ligand}$ (g)	V_{BuLi} (mL)	Yield	Product
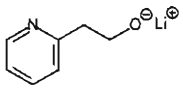	**S21**	0.250	0.200 (10 M BuLi)	-	White, sticky residue
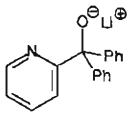	**S22**	0.4115	0.660 (2.5 M BuLi)	95	Beige powder
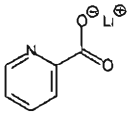	**S23**	0.294	0.900 (2.5 M)	90	White powder
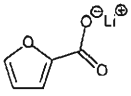	**S24**	0.268	0.15 (10 M)	85	Light-yellow-orange powder
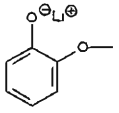	**S25**	0.22mL	0.200 (10M)	95	Beige powder
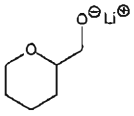	**S26**	0.226mL	0.200 (10M)	95	Beige powder
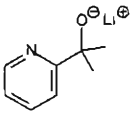	**S27**	0.397	0.200 (10M)	97	Orange flakes
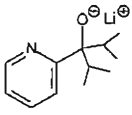	**S28**	0.400	0.200 (10M)	97	Light-yellow flakes

3.3 SYNTHESIS OF $RuCl_2(L)(C_5H_5N)_2(=CHPh)$

The synthesis of the following starting complexes was adapted from literature.[20,21]

3.3.1 $RuCl_2(PCy_3)(C_5H_5N)_2(=CHPh)$ (Gr1-Py)

Gr1 (455 mg, 0.553 mmol) was dissolved in toluene (4 mL), with subsequent addition of an excess pyridine (5 mL, 0.062 mol). The reaction was stirred for 20 min during which time a colour change from purple to light-green was observed. The reaction mixture was transferred into 54 mL of cold (-10 °C) pentane, and a green solid precipitated. The precipitate was filtered, washed with 4 x 50 mL of pentane, and dried under vacuum to afford **Gr1-Py** as a green powder (330 mg, 85% yield).

3.3.2 $RuCl_2(H_2IMes)(C_5H_5N)_2(=CHPh)$ (Gr2-Py)

Gr2 (230 mg, 0.271 mmol) was dissolved in toluene (4 mL), with subsequent addition of an excess pyridine (3.5 mL, 0.043 mol). The reaction was stirred for 20 min during which time a colour change from red to light-green was observed. The reaction mixture was transferred into 54 mL of cold (-10 °C) pentane, and a green solid precipitated. The precipitate was filtered, washed with 4 x 50 mL of pentane, and dried under vacuum to afford **Gr2-Py** as a green powder (180 mg, 92% yield).

3.4 SYNTHESIS OF HEMILABILE RUTHENIUM CARBENE COMPLEXES

3.4.1 Use of sodium salts

3.4.1.1 $RuCl(PCy_3)(O\text{^}N)(=CHPh)$ (O^N = L11)

a) Method 1

6 mL THF was added to a combined mixture of 0.6 mmol (132.5 mg) **Gr1** with 0.19 mmol (28 mg) **S4** while stirring vigorously. A colour change of purple to brownish-green was observed after 3 h. The reaction was stirred a further 12 h and a mixture of 2 mL toluene with 10 mL DCM was added. The reaction mixture was transferred to a second Schlenk via a syringe filter and the volume reduced to *ca.* 1 mL. A green precipitate formed after addition of 30 mL cold pentane to the concentrated reaction mixture. TLC analysis indicated the presence of 3 products. The products were separated by means of column chromatography with a 3 mL hexane : 6 mL EtOAc eluent mixture. NMR analysis of the products indicated that no carbenes were present.

b) Method 2

6 mL THF was added to a combined mixture of 0.02 mmol (20 mg) **Gr1** with 0.23 mmol (34 mg) **S4** while stirring vigorously. After stirring the reaction mixture for 1h at 45 °C, a green precipitate started to form. The reaction mixture was stirred for a further 3 h and the mixture filtered via a sinter filter (**Figure 3.2**). NMR analysis of the precipitate indicated that no carbene was present. The reaction was repeated, but not reproducible since no precipitate formed during the reaction.

c) Method 3

10 mL THF was added to a combined mixture of 0.16 mmol (133 mg) **Gr1** with 0.30 mmol (45 mg) **S4** while stirring vigorously. After stirring the reaction mixture for 1h at 35 °C, a green solution with white precipitate formed. The reaction mixture was stirred for a further 3 h. The reaction mixture was transferred to a second Schlenk via a sinter filter (**Figure 3.2**) and the volume of the filtrate reduced to *ca.* 1 mL. A green precipitate formed after addition of 30 mL cold pentane to the concentrated filtrate. NMR analysis of the white precipitate indicated that no carbene was present, but one carbene was present in the green precipitate fraction.

3.4.1.2 $RuCl(PCy_3)(O\hat{}N)(=CHPh)$ (O^N = L6, L8)

10 mL THF was added to a combined mixture of 0.06 mmol (50 mg) **Gr1** with 0.07 mmol (10 mg) **S1** or **S3** while stirring vigorously. A colour change of purple to dark-green was observed for the reaction with **S1** and brownish-yellow for the reaction with **S3** after 3 h. The reaction was stirred for a further 12 h after transferring the reaction mixture to a second Schlenk via a syringe filter. The volume of the reaction mixture was reduced to *ca.* 1 mL and 30 mL cold pentane added. No NMR analysis was performed for these complexes, due to very low yields.

3.4.1.3 $RuCl(PCy_3)(O\hat{}N)(=CHPh)$ (O^N = L12)

10 mL DCM was added to a combined mixture of 0.18 mmol (145 mg) **Gr1** with 0.23 mmol (31 mg) **S5** while stirring vigorously. The reaction mixture was stirred for 6 h at 45 °C and transfered to a second Schlenk via a syringe filter. The volume of the filtrate was then reduced to *ca.* 1 mL. A purple precipitate formed after addition of 30 mL cold pentane to the concentrated reaction mixture, which was identified as the starting carbene **Gr1**. The reaction was repeated in THF to give a black solution after 24 h.

It was evident that the sodium salts could not be successfully used for the replacement of one PCy_3 and Cl^- ligand on **Gr1** with a chelating ligand. Therefore, the following step was to test the thallium and lithium salts (§ 3.4.2), which deemed to be more successful.

3.4.2 Use of thallium and lithium salts

The first step, which was determined by the solubility of the ligand salts in THF, was the addition of the salt to the starting ruthenium alkylidene complex (**Gr1**, **Gr2**, **Gr1-Py** or **Gr2-Py**):

1. If the salt was soluble in THF, a solution of 2 mmol salt in THF (5 mL) was added dropwise to a solution of 2 mmol starting ruthenium alkylidene in THF (5-10 mL).
2. If the salt was insoluble in THF, 10-15 mL THF was added to the combined mixture of 2 mmol salt and 2 mmol starting ruthenium alkylidene while stirring vigorously.

The reaction was stirred at room temperature (RT) for 1 h. If the TLC indicated that the starting complex was not being consumed, by indication of new spots on the TLC, the reaction mixture was heated to 30 – 45 °C, or kept at RT with addition of a spatula point salt. The reaction mixture was then stirred until the TLC indicated that the starting complex was not present any more. One of the following procedures was then followed:

Procedure 1: No precipitate forms during the reaction

After evaporation of the solvent, the residue was dissolved in a minimal amount of toluene. The metal chloride, i.e. lithium chloride, was then removed by filtration via a syringe filter and the volume of the filtrate reduced to 0 mL (§ 3.1.2.1). After adding 1 mL THF to the residue, cold pentane
(10-15 mL) was layered onto the THF and the Schlenk placed in the fridge to await precipitation of the desired complex. After removal of the pentane via syringe, the desired complex was washed with cold pentane, filtered and then dried under vacuum. In most instances, the solid thus obtained still contained impurities. Therefore the purification method was modified to include sonification of the complex in 5-10 mL pentane for 10 min after the initial wash process followed by removal of the pentane via syringe. The solid obtained was then dried under vacuum.

Procedure 2: Precipitate forms during the reaction

The reaction mixture was transferred to a second Schlenk via a syringe filter to remove the metal chloride, i.e. thallium chloride, that formed. The volume of the filtrate was reduced to *ca.* 1 mL (§ 3.1.2.1) and 10-15 mL cold pentane layered onto the filtrate. The reaction vessel was then placed in the fridge awaiting precipitation of the desired complex. After removal of the pentane via syringe, the desired complex was washed with cold pentane, filtered and dried under vacuum. Similar to procedure 1, the method was modified after it was found that the complex still contained impurities. The complex was therefore sonificated in 5-10 mL pentane for 10 min after the initial wash process followed by removal of the pentane via syringe. The solid obtained was then dried under vacuum.

A summary of the reactions investigated in this study, with the use of the above procedures, is given in **Table 3.9 – Table 3.22**. The reactions were repeated several times at different periods of the year with consistent results, with the exception of **C9**. The synthesis of **C9** resulted in either an oily residue containing no carbene, or a brown powder with the desired carbene that was inseparable from the other impurities, or a green powder with only the desired carbene present. Due to the apparent air and moisture sensitivity of the **C9**, the synthesis could not be successfully repeated.

The carbene signals, as well as ^{31}P NMR signals are reported for the individual complexes. The carbene and ^{31}P NMR signals of the starting complexes together with the ^{31}P-signals of the free PCy_3 ligand, the oxidised form of PCy_3 ($O{=}PCy_3$) and the proposed[22,23] decomposition product of the Grubbs systems are given in **Table 3.8**.

Table 3.8 Assignment of carbene and ^{31}P NMR signals

Carbene signal/ppm	^{31}P-signal/ppm	Assignment
20.034 (s)	35.638	**Gr1**
19.188 (s)	28.928	**Gr2**
19.981 (d)	38.195	**Gr1-Py**
19.225 (s)	-	**Gr2-Py**
-	50.457	$O{=}PCy_3$
-	11.260	Free PCy_3
-	24 – 26	$[Ru(PCy_3)_2ClPhCO]$
	47 –48	$[Ru(PCy_3)_2ClHCO]$
	22 – 23	$[Ru(PCy_3)(H_2IMes)ClPhCO]$
	46 – 47	$[Ru(PCy_3)(H_2IMes)ClHCO]$

Mol et al.[22] identified $[Ru(PCy_3)_2ClPhCO]$ as the metathesis inactive impurity at δ 25.4 ppm in the ^{31}P NMR spectrum, which forms on reaction of **Gr1** with primary alcohols, water and oxygen in solution. The hydride species $[Ru(PCy_3)_2ClHCO]$, where Ph is substituted with H, appears at δ 47.55 ppm in the ^{31}P NMR spectrum.[22] Further studies showed that the second generation Grubbs system (**Gr2**) also reacts with primary alcohols, water and oxygen to form carbonyl ruthenium complexes.[23] These systems have been shown to be excellent 1-alkene isomerisation catalysts at elevated temperatures.[22,23]

Table 3.9 Synthesised complexes from **Gr1**.

Complex	SC_m/mg	Salt used (S_m/mg)	Reaction T/°C	$m_{product}$/mg Yield [a] /%	Product	Carbene signal/ppm	^{31}P/ppm
	182.6	**S6** (75)		10 (-)	Green powder	-	-
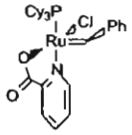 **C1**	200	**S6** (84.5)	RT	65 (42)	Green powder	19.942 (s) 19.756 (d) 19.556 (d)	50.58 43.37 31.88 30.20 27.99 17.65 11.87
	209.5	**S243** (42.5)	35	118 (74)	Brown powder	-	50.91 48.59 34.24 29.99
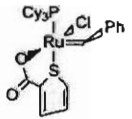 **C2**	168.8	**S8** (100)	RT	12 (-)	Brown powder	None	49.38 30.302 31.65 26.57
	200	**S8** (92)		2 (-)	Grey residue	-	-

SC_m: mass of the starting Ru=C
S_m: mass of the salt used in the synthesis
[a] Yields were only provided for complexes containing carbenes

Table 3.10 Synthesised complexes from Gr1.

Complex	SC_m/mg	Salt used (S_m/mg)	Reaction T /°C	$m_{product}$/mg Yield [a] /%	Product	Carbene signal/ppm	^{31}P/ppm
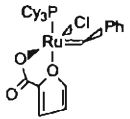 C3	358.4	S24 (52)	RT	322.5 (90)	Purple powder	19.94 (s)	35.63
	100	S7 (44)		2 (-)	Grey residue	-	-
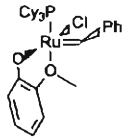 C4	116	S16 (33)	RT	1 (-)	White residue	-	-
	189.6	S25 (30.5)		17 (12)	Brown residue	20.02	51.87 36.27 35.26 24.97 11.84
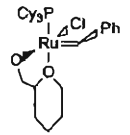 C5	226.2	S14 (100)	RT	2 (-)	Brown residue	-	-
	165	S26 (24.5)		18 (14)	Green powder	20.02	51.99 46.02 36.20 35.17 24.92 11.82

SC_m: mass of the starting Ru=C
S_m: mass of the salt used in the synthesis
[a] Yields were only provided for complexes containing carbenes

Table 3.11 Synthesised complexes from **Gr1**.

Complex	SC_m/mg	Salt used (S_m/mg)	Reaction T/°C	$m_{product}$/mg (Yield [a] /%)	Product	Carbene signal/ppm	^{31}P/ppm
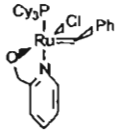 **C6**	233	**S20** (47)		34 (20)	Dark-green powder	20.74 (d) 20.04 (s)	50.46 38.69 35.63 24.34
	200	**S20** (82.8)	RT	47 (-)	Brown powder	None	33.57 17.18 11.26
	255.5	**S20** (50)		32 (-)	Greenish-brown powder	None	53.34 41.89 36.25 11.87
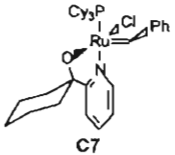 **C7**	154.9	**S19** (34)		15 (-)	Greyish-green powder	None	50.63 29.55
	141	**S19** (78)	RT	8 (-)	Greyish-green powder	None	50.78 34.03 29.54
	235	**S19** (112.6)		141 (60)	Green powder	17.77 (d)	41.55
	478.7	**S19** (130)		317.5 (85)	Dark-brown powder	17.77 (d)	40.69

SC_m: mass of the starting Ru=C
S_m: mass of the salt used in the synthesis
[a] Yields were only provided for complexes containing carbenes

Table 3.12 Synthesised complexes from **Gr1**.

Complex	SC_m/mg	Salt used (S_m/mg)	Reaction T/°C	$m_{product}$/mg (Yield [a] /%)	Product	Carbene signal/ppm	^{31}P/ppm
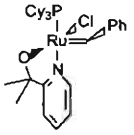 C8	406.6	**S27** (80)	25	150 (47)	Dark-brown powder	17.54 (d)	42.33
	250	**S26** (72.6)	RT	12 (7)	Brown powder	17.82 (d)	51.14 29.92 32.11
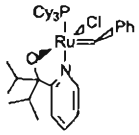 C9	412	**S26** (110)		120 (35)	Green powder	17.83 (d)	39.99
	956.5	**S26** (290.5)	RT = 12	15 (-)	Brown powder	None	50.96 46.02 35.09 34.14 32.10 30.18 11.78

SC_m: mass of the starting Ru=C
S_m: mass of the salt used in the synthesis
[a] Yields were only provided for complexes containing carbenes

Table 3.13 Synthesised complexes from **Gr1**.

Complex	SC_m/mg	Salt used (S_m/mg)	Reaction T /°C	$m_{product}$/mg (Yield [a] /%)	Product	Carbene signal/ppm	^{31}P/ppm
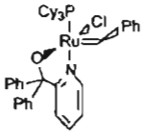 **C10**	197.4 in benzene	**S17** (115)		40 (22)	Brown powder	17.67 (d)	50.35 41.09
	104.7	**S22** (51)	RT	24 (25)	Brown powder	17.67 (d)	40.49
	210	**S22** (70.68)		120 (61)	Greyish-brown powder	17.62 (d)	41.07
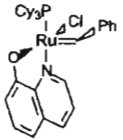 **C11**	115.2	**S14** (50.5)		71 (77)	Brown, crystalline residue	20.01 (s) 19.43 (d) 19.04 (d)	50.67 41.19 36.29 35.24 33.38 29.73 25.03 19.90 11.96
	300	**S14** (143.5)	RT	13 (-)	Brown, oily residue	-	-
	134.6	**S14** (59)		41.6 (39)	Brown powder	19.51 (d)	49.72 32.69 24.34 11.26

SC_m: mass of the starting Ru=C
S_m: mass of the salt used in the synthesis
[a] Yields were only provided for complexes containing carbenes

Table 3.14 Synthesised complexes from **Gr1**.

Complex	SC_m/mg	Salt used (S_m/mg)	Reaction T /°C	$m_{product}$/mg (Yield [a] /%)	Product	Carbene signal/ppm	^{31}P/ppm
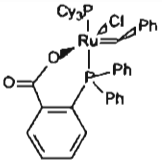 C12	158.4	**S9** (129.3)	RT	1 (-)	Brown residue	-	-
	142	**S9** (91.6)		18 (13)	Green powder	19.94(s)	55.46 49.74 35.64
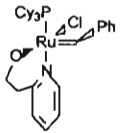 C13	76.7	**S13** (32.6)	RT	18 (-)	Green powder	None	49.85 25.38
	183.8	**S13** (74.6)		25 (-)	Green powder	None	49.76 34.59 25.38
	204	**S21** (60)		30 (19)	Green powder	19.94 (s)	50.24 35.64 28.98 25.37 24.33
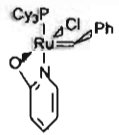 C14	240	**S11** (138)	RT	-	Black solution	-	-

SC_m: mass of the starting Ru=C
S_m: mass of the salt used in the synthesis
[a] Yields were only provided for complexes containing carbenes

Table 3.15 Synthesised from **Gr1-Py**.

Complex	SC_m/mg	Salt used (S_m/mg)	Reaction T/°C	$m_{product}$/mg (Yield/ [a] %)	Product	Carbene signal/ppm	^{31}P/ppm
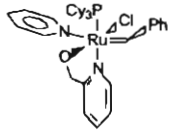 **C15**	100	**S20** (25)	RT	20 (-)	Orange, crystalline residue	None	51.18 46.65 37.04
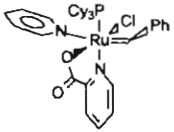 **C16**	135.3	**S23** (30.6)		33 (24)	Green powder	20.11 (d) 19.83 (d)	50.86 37.03 33.70
	92.5	**S6** (45)	RT	35 (38)	Green powder	20.27 (d) 20,11 (d) 19.95 (d) 19.81 (d) 19.58 (d)	50.79 43.49 41.93 34.07 33.72 33.49
	200	**S6** (95)		100 (49)	Green powder	19.82 (d)	34.10
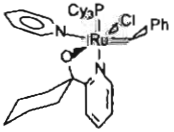 **C17**	124	**S19** (48.1)	RT	20 (15)	Reddish-brown powder	17.75 (d)	50.39 44.21 40.86 26.68

SC_m: mass of the starting Ru=C
S_m: mass of the salt used in the synthesis
[a] Yields were only provided for complexes containing carbenes

Table 3.16 Synthesised complexes from **Gr1-Py**.

Complex	SC_m/mg	Salt used (S_m/mg)	Reaction T /°C	$m_{product}$/mg (Yield/ [a]%)	Product	Carbene signal/ppm	^{31}P/ppm
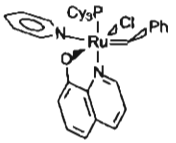 **C18**	20	**S14** (17)	RT	5 (-)	Brown powder	-	-
	300	**S14** (180.4)		50 (16)	Brown powder	20.23 (s) 19.41 (d) 18.00 (s)	50.03 43.39 41.94 41.16 32.69 26.23
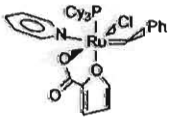 **C19**	91	**S7** (44)	RT	40 (44)	Green powder	20.13 (d) 19.84 (dd) 18.93 (d)	50.68 44.02 37.95 26.86 25.88
	202.7	**S24** (35.8)		30 (-)	Green powder	None	26.22
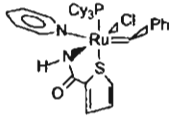 **C20**	105.2	**S10** (65.3)	RT	15 (-)	Brown powder	None	50.67 30.82 29.93 26.70

SC_m: mass of the starting Ru=C
S_m: mass of the salt used in the synthesis
[a] Yields were only provided for complexes containing carbenes

Table 3.17 Synthesised complexes from **Gr1-Py**.

Complex	SC_m/mg	Salt used (S_m/mg)	Reaction T /°C	$m_{product}$/mg (Yield [a]/%)	Product	Carbene signal/ppm	^{31}P/ppm
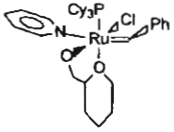 **C21**	162.4	**S15** (79)	RT	15 (-)	Black residue	-	-
	113	**S15** (56.1)		15 (-)	Brown powder	None	49.79 26.22 24.13
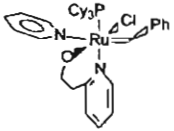 **C22**	200	**S13** (131.9)	RT	18 (-)	Caramel powder	None	49.83 25.38
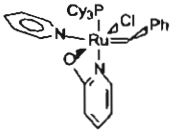 **C23**	66.8	**S11** (30)	RT	15 (-)	Blue-greyish residue	None	50.77 48.49 44.03 40.96 39.37 30.19 29.31 16.23

SC_m: mass of the starting Ru=C
S_m: mass of the salt used in the synthesis
[a] Yields were only provided for complexes containing carbenes

Table 3.18 Synthesised complexes from Gr2.

Complex	SC_m/mg	Salt used (S_m/mg)	Reaction T/°C	$m_{product}$/mg (Yield [a]/%)	Product	Carbene signal/ppm	^{31}P/ppm
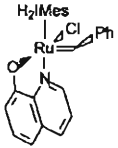 C24	102.7	S14 (62.8)		22.6 (28)	Brown powder	19.09 (s) 18.94 (s) 18.33 (s)	Not analysed
	70	S14 (45)	RT	12.5 (-)	Brown powder	None	Not analysed
	200	S14 (150)		41.8 (26)	Orange-brown powder	18.43 (s)	None
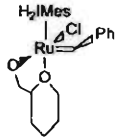 C25	180	S26 (30.5)	40	40 (-)	Brown powder	None	51.55 46.83 30.02 (other smaller peaks)
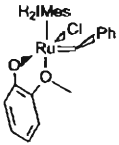 C26	190	S25 (28.5)	40	25 (17)	Brown residue	19.123(s)	51.17 35.22 29.50

SC_m: mass of the starting Ru=C
S_m: mass of the salt used in the synthesis
[a] Yields were only provided for complexes containing carbenes

Table 3.19 Synthesised complexes from **Gr2**.

Complex	SC_m/mg	Salt used (S_m/mg)	Reaction T/°C	$m_{product}$/mg (Yield [a]/%)	Product	Carbene signal/ppm	^{31}P/ppm
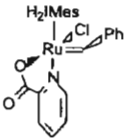 C27	211.6	**S6** (102.8)	RT	70 (43)	Green powder	19.18 (s) 18.57 (s) 18.08 (s)	Not analysed
	147.6	**S6** (75)	30	54 (47)	Green powder	19.04 (s) 18.62 (s) 18.30 (s)	Not analysed
	120.9	**S6** (46.9)	35	40 (43)	Green powder	23.03 (d) 18.65 (s) 18.19 (s)	Not analysed
	155.6	**S23** (26.9)	45	50 (42)	Green powder	19.19 19.11 18.62 18.16	50.752 34.299 29.916 8.632
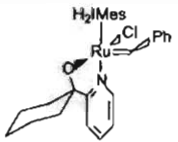 C28	200	**S19** (57)	40	112.8 (67)	Light-green powder	17.96 (s)	None
	527	**S19** (120)		370 (84)	Forest-green powder	18.02 (s)	None

SC_m: mass of the starting Ru=C
S_m: mass of the salt used in the synthesis
[a] Yields were only provided for complexes containing carbenes

Table 3.20 Synthesised complexes from **Gr2**.

Complex	SC_m/mg	Salt used (S_m/mg)	Reaction T/°C	$m_{product}$/mg (Yield [a]/%)	Product	Carbene signal/ppm	^{31}P/ppm
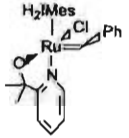 **C29**	470.2	**S27** (90)	40	205 (55)	Dark-green powder	17.82 (s)	None
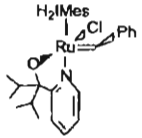 **C30**	192	**S28** (48)	40	6 (-)	Dark-green powder	-	-
	308	**S28** (82)	35	150 (57)	Dark-green (almost black) powder	18.52 (s)	None
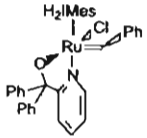 **C31**	189	**S22** (59.7)		62.5 (33)	Light-green powder	17.18 (s)	None
	155	**S22** (51.6)	40	112 (75)	Light-green powder	Not analysed	
	164	**S22** (58.0)		140 (91)	Light-green powder		

SC_m: mass of the starting Ru=C
S_m: mass of the salt used in the synthesis
[a] Yields were only provided for complexes containing carbenes

Table 3.21 Synthesised complexes from **Gr2**.

Complex	SC_m/mg	Salt used (S_m/mg)	Reaction T/°C	$m_{product}$/mg (Yield [a]/%)	Product	Carbene signal/ppm	^{31}P/ppm
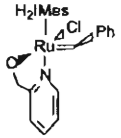 **C32**	330	**S20** (55)	35	30 (-)	Dark-brown, almost black powder	None	24.33

Table 3.22 Synthesised complexes from **Gr2-Py**.

Complex	SC_m/mg	Salt used (S_m/mg)	Reaction T/°C	$m_{product}$/mg (Yield [a]/%)	Product	Carbene signal/ppm	^{31}P/ppm
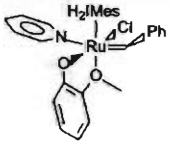 **C33**	76.8	**S16** (40)	RT	15 (20)	Reddish-brown powder	None	Not analysed
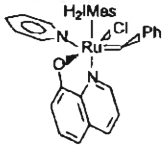 **C34**	65.5	**S14** (35)	RT	21 (31)	Reddish-brown powder	None	Not analysed

SC_m: mass of the starting Ru=C
S_m: mass of the salt used in the synthesis
[a] Yields were only provided for complexes containing carbenes

The characterisation of the complexes that were successfully synthesised, i.e. had a carbene signal present in the ^{1}H NMR, will be discussed in Chapter 4. Reasons for the unsuccessful synthesis of the other complexes will also be provided. It should be noted that the reactions were not just repeated within the same week, but also at different times of the year. Therefore, even with improvement of experimental skills, various reactions remained unsuccessful, indicating that a number of the ligands decompose the Grubbs carbenes.

3.5 METATHESIS REACTIONS

3.5.1 General procedures for the metathesis of 1-octene

The metathesis of 1-octene in the presence of **Gr1** was performed on a small- (§ 3.5.1.1) and large-scale (§ 3.5.1.2) experimental setup. The small-scale reaction was done to characterise the products formed during the reaction by GC/MSD without quenching the reaction. Esters, aldehydes and ketones are usually visible in the GC/MSD analysis of the samples that are quenched with tert-butyl-hydrogen peroxide (**Chromatogram 3.4**). This is most likely due to the reaction of the precatalyst with the peroxide before being completely deactivated. The characterisation results aided us in postulating a mechanistic model (§ 3.7.3) for the 1-octene metathesis reaction in the presence of **Gr1**.

In the rest of the study, the activity investigations of the hemilabile Grubbs precatalysts were executed on the large-scale setup (§ 3.5.1.2), as implemented by the Sasol Technology R&D team of Dr. Wolfgang Meyer,[24] in order to compare the activity of our novel complexes with analogous systems investigated under similar experimental conditions.[25,26]

3.5.1.1 Small-scale reaction

The procedure for the small-scale metathesis experiment is illustrated in **Figure 3.3**. The reaction flask (❶) was thoroughly flushed with Ar (❷) before weighing **Gr1** (13.2 mg, 1 mol) into the reaction flask (❸). Chlorobenzene (1.25 mL) and 1-octene (2.5 mL, 1000 mol) were then added with Hamilton GASTIGHT® syringes to the reaction flask (❹ and ❺). Chlorobenzene served as solvent and internal standard for quantification of the GC results. Following the addition, the reaction flask was placed in the autoinjector sample tray (❻) at 25 °C and the progress of the reaction was monitored by GC/FID. Aliquots (0.2 µL) of the reaction mixture were injected at approximately 40 min intervals with the autoinjector. After 3 h, the same volume was analysed by GC/MSD to characterise the mixture. The response factor of an authentic sample of each major alkene component was determined and used in the conversion calculations.

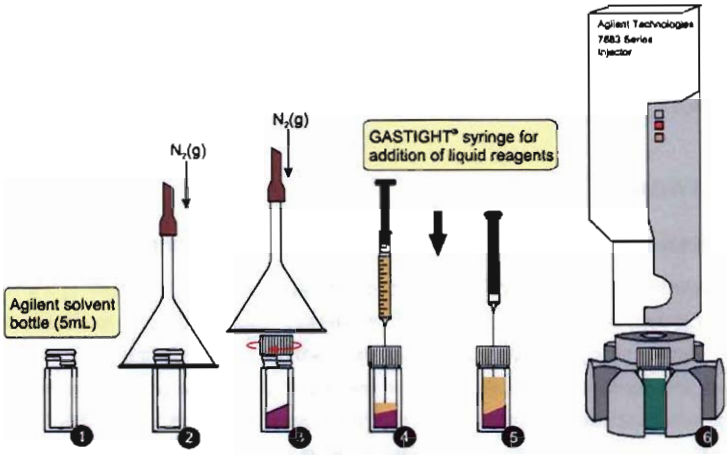

Figure 3.3 Experimental setup for performing a small-scale metathesis reaction.

3.5.1.2 Large-scale reaction (100 mL reaction flask – ethene liberated)

The metathesis reactions were carried out in a 100 mL 3-necked flask fitted with a Liebig-condensor and Ar inlet line as illustrated in **Figure 3.4**. The flask was flushed for 5 min with a steady stream of Ar before adding the reagents. The condenser was cooled by water that was cooled to 2 °C by an external cooling unit (HAAKE EK 51-1 cold finger with HAAKE B circulation bath). The reaction temperatures were obtained by controlling the temperature of an oil bath with an electronic temperature controller (Heidolph MR 3001K), while using a thermometer to control the temperature of the reaction mixture.

Initially, the influence of reaction temperature and precatalyst concentration on the activity of selected first and second generation hemilabile complexes was investigated to determine the optimum reaction temperature and precatalyst concentration where these systems showed high metathesis activity. Consequently, a comparative study between the remaining hemilabile complexes and **Gr1** and **Gr2** was done with regards to their 1-octene metathesis activity at the optimum temperature and concentration.

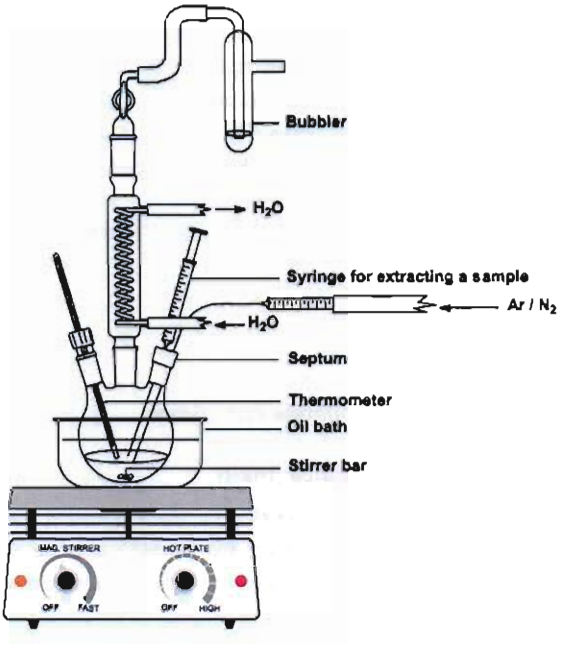

Figure 3.4 Experimental setup for performing a metathesis reaction.

In a typical metathesis experiment, the ruthenium carbene precatalyst (0.015 mmol) was added to a solution of 20 mL 1-octene (0.127 mol) and 1 mL nonane that was preheated to 60 °C. Nonane served as an internal standard for quantification. Samples (0.3 mL) were extracted in various time intervals of 5 to 30 min. The samples were then added to a GC vial (1 mL) filled with a solution of 2 drops tert-butyl-hydrogen peroxide and 0.3 mL toluene. Toluene was used to make up the volume of the sample in order to extract 0.2 µL aliquots with the autoinjector. The tert-butyl-hydrogen peroxide was used to quench the reaction. The progress of the metathesis reaction was monitored by GC/FID. The sample collected after 3 h was also analysed by GC/MSD to characterise the mixture. The presence of esters, aldehydes and ketones were noted for all the samples quenched with tert-butyl-hydrogen peroxide, as illustrated in **Chromatogram 3.4** (§ 3.6.2.2).

3.5.1.3 NMR Investigation of the 1-octene metathesis reaction

A 1 mL NMR tube was placed in a Schlenk tube and the air removed under vacuum. The Schlenk was then flushed with Ar, and the procedure repeated twice. The precatalyst (0.031 mmol) was weighed out into the NMR tube and again placed in the Schlenk to put the sample under Ar. Deuterated solvent (0.75 mL $CDCl_3$) was added to the sample and the tube was closed and shaken to dissolve the solids. The 1-octene (0.05 mL) was added just before inserting the NMR tube into the instrument to keep the initial reaction time of the precatalyst with the alkene as short as possible. The reaction was monitored at 30 to 50 °C over 5 h, with spectra obtained at regular time intervals. The peak integration values of the formed carbenes were normalised against the benzylidene proton signal.

3.6 ANALYTICAL METHODS

3.6.1 Characterisation of hemilabile complexes

3.6.1.1 Nuclear Magnetic Resonance (NMR)

^{1}H-NMR (300, 400 or 500 mHz) and ^{31}P-NMR (121, 162 or 202 mHz) spectra were obtained by using a Varian Gemini 300 (NWU), Varian 400 (SASOL) and the Bruker Avance 500 Spectrometer (SASOL). NMR samples were prepared by dissolving the precatalyst (15 – 30 mg) in a suitable deuterated solvent.

The deuterated solvent was pump freezed before use (§ 3.1.2.3).

3.6.1.2 Infrared spectroscopy (IR)

IR-spectra were obtained by using a Nicolet FTIR 550 spectrophotometer. The pellets were prepared by thoroughly mixing the sample (0.005 g) with dry KBr (0.28 g), which was then pressed into a disc. For liquid samples, the KBr pellets were first pressed into a disc and a drop of liquid was added onto the disc. The spectra were taken at a resolution of 4 cm^{-1} over a wave number range of 400 – 4000 cm^{-1} and number of scans = 10.

3.6.1.3 Elemental analysis (CHN analysis)

Elemental analysis (C, H, N) was obtained on a Leco CHNS 932 analyser with a VTF-900 furnace by Dr. Naidoo at the University of KwaZulu-Natal, Howard College. Samples were also analysed at LCR by Mr. M Philphott from whom the instrumental specifications could not be obtained.

The carbon (C) values of some of the complexes were lower than expected. This is most likely due to a dilution effect from $CDCl_3$ present in the samples, which caused a lower %C than expected from a pure sample. The $CDCl_3$ was present in the samples as a result of the addition of NMR samples to the complex after NMR analysis, drying it under vacuum and not washing the complex afterwards. A correction was therefore made to the C values with the help of the solvent correction CHN calculator program (v1.30) from Heriot-Watt University.[27] The program calculates the possible solvent content of a sample and adjusts the CHN analysis accordingly.

3.6.2 Progress of the metathesis reaction

3.6.2.1 Gas Chromatography (GC)

Samples of the metathesis reactions were quenched with a solution of 2 drops *tert*-butyl-hydrogen peroxide and 0.5 mL toluene in a GC autosampler vial (1 mL) and analysed on an Agilent 6890 gas chromatograph equipped with an Agilent 7683 autoinjector, HP-5 capillary column (30 m x 320 µm x 0.25 µm) and a flame ionisation detector (FID). The general GC settings were as follows:

Inlet temperature	:	200 °C
N_2 carrier gas flow rate	:	2 mL min^{-1} at 20 °C
Injection volume	:	0.2 µL (auto injection)
Split ratio	:	50:1
Oven programming	:	60 to 110 °C at 25 °C min^{-1}
		110 °C for 16 min
		110 to 290 °C at 25 °C min^{-1}
		290 °C for 10 min
Detector	:	FID at 250 °C
H_2 flow rate	:	40 mL min^{-1} at 20 °C
Air flow rate	:	450 mL min^{-1} at 20 °C

A representation of a typical chromatogram of an unquenched sample of the 1-octene metathesis with **Gr1**, after 60 min at 25 °C, is given in **Chromatogram 3.1**. **Chromatogram 3.2** represents a typical chromatogram of a quenched sample of the 1-octene metathesis reaction with a first generation hemilabile complex (**C7**), after 60 min at 60 °C. A similar chromatogram (not shown here) was obtained for the reaction with second generation hemilabile systems, with the exclusion of the $O{=}PCy_3$ peak, since no phosphines are present in these systems. The self-metathesis of 1-octene typically leads to the formation of two isomers, *cis*- and *trans*-7-tetradecene, which combined with ethene (not observed by GC) represent the PMP of the reaction.

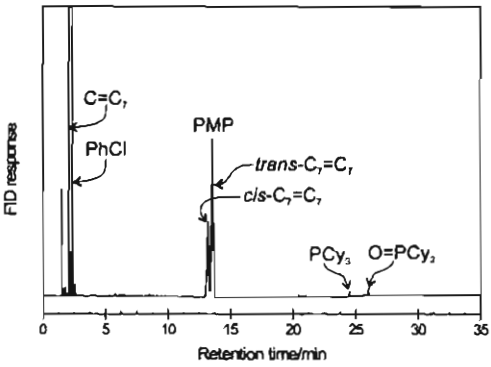

Chromatogram 3.1 GC/FID chromatogram of the reaction mixture of 1-octene in the presence of **Gr1** at 25 °C after 1 h (solvent = chlorobenzene, 1-octene/Ru = 1000, FID response enlarged). (small-scale reaction)

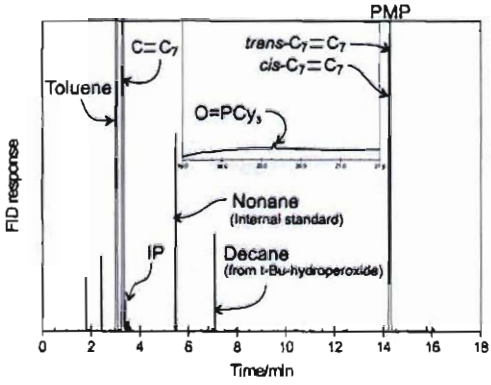

Chromatogram 3.2 GC/FID chromatogram of the reaction mixture of 1-octene in the presence of **Gr1Cy** at 60 °C after 1 h (no solvent, 1-octene/Ru = 9000, FID response enlarged, inset of phosphine region). (large-scale reaction).

The internal standard method (with nonane as internal standard) was used to determine the mole percentage 1-octene converted to the primary and secondary metathesis products (PMP and SMP), respectively. The GC response factor (rf) was calculated from a calibration curve plotted of A_{nonane}/A_{octene} against V_{nonane}/V_{octene}, for solutions with different volume ratios 1-octene to nonane (**Table 3.22**). The internal standard was kept constant. A response factor of 1.03 for 1-octene was calculated from the slope of the calibration curve. The calibration results obtained are shown in **Table 3.22** and represented graphically in **Figure 3.5**.

Table 3.22 Table of GC calibration data for 1-octene with nonane as internal standard

Volume Ratio (nonane : 1-Octene)	V_{nonane}/V_{octene}	A_{nonane}/A_{octene}
0.25 : 1.00	0.25	0.25
0.25 : 0.75	0.33	0.34
0.25 : 0.50	0.50	0.51
0.25 : 0.25	1.00	1.03

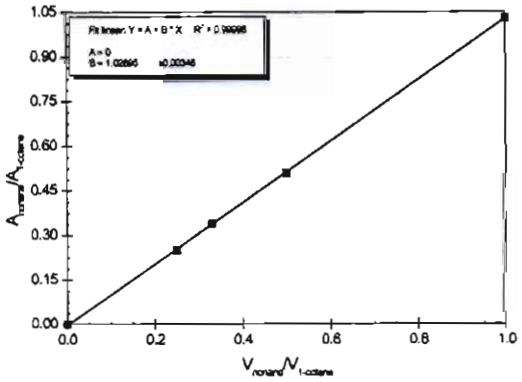

Figure 3.5 Calibration curve for determining the GC response factor.

The following equation was used to determine the mol percentage (mol%) conversion of 1-octene to 7-tetradecene:

$$mol\%C_8 = 100 \times rf \times \frac{V_{is}}{V_{C8}} \times \frac{A_{C8}}{A_{is}}$$

C_8	=	1-octene
rf	=	GC response factor
V_{is}	=	Volume of the internal standard at t = 0
V_{C8}	=	Volume of the 1-octene at t = 0
A_{C8}	=	Area of 1-octene
A_{is}	=	Area of internal standard

The following equation was used to determine the mol percentage 7-tetradecene or other alkenes formed during the reaction:

$$mol\%C_n = 2 \times rf \times \left(V_{is} \frac{A_{Cn}}{A_{is}} \right) \times \frac{\rho_{Cn}}{M_{Cn}} \times \left(\frac{M_{C8}}{\rho_{C8} \times V_{C8}} \right) \times 100$$

C_n	=	alkene
rf	=	GC response factor
V_{is}	=	Volume of the internal standard at t = 0
V_{C8}	=	Volume of the 1-octene at t = 0
A_{Cn}	=	Area of the alkene
A_{is}	=	Area of internal standard
M_{Cn}	=	Molecular mass of C_n
M_{C8}	=	Molecular mass of 1-octene
ρ_{Cn}	=	Density of C_n
ρ_{C8}	=	Density of 1-octene

3.6.2.2 Gas Chromatography/Mass Spectrometry (GC/MS)

For product verification, the reaction mixtures were also analysed using an Agilent 6890 gas chromatograph equipped with an Agilent 7683 autosampler, HP-5 capillary column and an Agilent 5973 mass selective detector (MSD). The same oven program was used with either a 6 min solvent delay or the detector switched off between 5.5 and 5.8 min to exclude the toluene or chlorobenzene. He was used as carrier gas with a 1 mL min^{-1} flow rate at 20 °C.

A typical example of the chromatogram obtained under the above-mentioned conditions is illustrated in **Chromatogram 3.3** for a small-scale reaction sample not quenched with tert-butyl-hydrogen peroxide. **Chromatogram 3.4** illustrates a typical chromatogram obtained for a large-scale reaction sample quenched by *tert*-butyl-hydrogen peroxide. The alkene products in **Chromatogram 3.4** are denoted $C_{\#}$, with # indicating the chain length of the alkene. Apart from the allocated internal and terminal alkenes forming during the 1-octene metathesis reaction, various by-products also formed as depicted by the letters **a – i** in **Chromatogram 3.4**, of which not all are necessarily associated with the reaction. **Table 3.23** gives the product assigned to the individual letters.

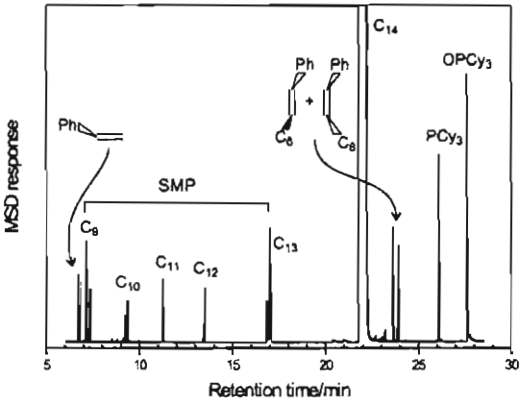

Chromatogram 3.3 GC/MSD chromatogram of the reaction mixture of 1-octene in the presence of **Grl** at 25 °C after 3 h (solvent = chlorobenzene, 1-octene/Ru = 1000, solvent delay = 6 min, small scale reaction, MSD response enlarged).

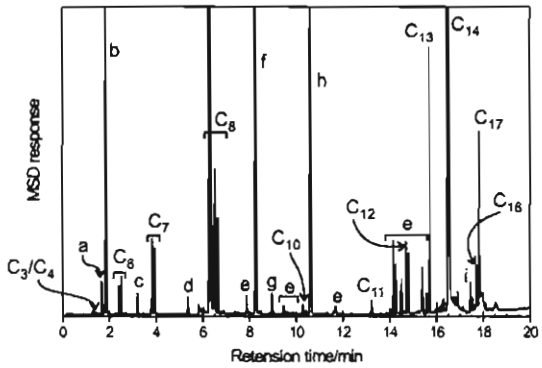

Chromatogram 3.4 GC/MSD chromatogram of the reaction mixture of 1-octene in the presence of **Gr2** at 35 °C after 3 h (No solvent, 1-octene/Ru = 9000, detector off between 5.4 - 5.8 min to exclude toluene, large-scale reaction, MSD response enlarged).

Table 3.23 Assigning the by-products observed in **Chromatogram 3.3** to the given letters a – i.

Product #	Product assignment
a	Acetone (Wash solvent for autosampler syringe)
b	2-methyl-2-propanol
c	Benzene
d	*tert*-butyl-hydrogen peroxide (to quench reaction)
e	Various ketones and aldehydes formed during the reaction
f	Nonane (internal standard)
g	Styrene
h	Decane (solvent of *tert*-butyl-hydrogen peroxide)
i	*cis*- and *trans*-1-phenyl-1-octene (or hexyl styrene),

3.7 COMPUTATIONAL METHODS

3.7.1 Hardware

Two types of hardware were used for the molecular modelling: a personal computer with one CPU and two clusters with 4 and 52 CPU's, respectively.

The specifications of the personal computer (HP) was as follows:

Operating system : Microsoft Windows© 2000 with Service Pack 4
Processor : Intel Pentium 4 2.8 GHz
Memory : 1GB RAM

The specifications of the clusters were as follows:

a) 4 CPU cluster (HP Proliant CP4000):

1 x Master node: HP DL380 – 1 x 2.0 GHz XEON
1 GB RAM, 2 x 36.4 GB HDD
2 x Compute nodes: HP DL360 – 2 x 2.4 GHz XEON
1 GB RAM, 1 x 72.8 GB HDD
Operating system on compute nodes: Redhat Enterprise Linux 2.4.18-3
Cluster operating system: OSCAR software

b) 52 CPU cluster (HP Proliant CP4000 Linux Beowulf with Procurve Gb/E Interconnect on compute nodes):

1 x Master node: HP DL385 – 2 x 2.8 MHz AMD Opteron 64,
2 GB RAM, 2 x 72 GB HDD
12 x Compute nodes: HP DL145G2 – 2 x 2.8 MHz AMD Opteron 64,
2 GB RAM, 2 x 36 GB HDD
Operating system on compute nodes: Redhat Enterprise Linux 4
Cluster operating system: HPC CMU v3.0 cluster

This cluster was only recently obtained (November 2006) and therefore it was only available for a short period of time to start with vibrational calculations, as well as intrinsic reaction path (IRP) calculations for TS studies, which are usually time consuming.

3.7.2 Computational details: Software

All computational results in this study were calculated by using the DMol^3 DFT (Density Functional Theory) code[28-30] as implemented in Accelrys Materials Studio® 3.2.[31] DFT was used since it usually gives realistic geometries, relative energies and vibrational frequencies for transition metal compounds. The non-local generalised gradient approximation (GGA) functional by Perdew and Wang (PW91)[32] was used for all geometry optimisations. The convergence criteria for these optimisations consisted of threshold values of 2 x 10^{-5} Ha, 0.004 Ha/Å and 0.005 Å for energy, gradient and displacement convergence, respectively, while a self consisted field (SCF) density convergence threshold value of 1 x 10^{-5} Ha was specified. The multiplicity was specified as auto, in order to determine the ground spin state using a spin-unrestricted calculation. DMol^3 utilizes a basis set of numeric atomic functions, which are exact solutions to the Kohn-Sham equations for the atom.[33] These basis sets are generally more complete than a comparable set of linearly independent Gaussian functions and have been demonstrated to have small basis set superposition errors.[33] In this study a polarised split valence basis set, termed double numeric polarised (DNP) basis set has been used. All geometry optimisations employed highly efficient delocalised internal coordinates.[34] The use of delocalised coordinates significantly reduces the number of geometry optimisation iterations needed to optimise larger molecules, compared to the use of traditional Cartesian coordinates.

Some of the geometries optimised were also subjected to full frequency analyses at the same GGA/PW91/DNP level of theory to verify the nature of the stationary points. Equilibrium geometries were characterised by the absence of imaginary frequencies. Preliminary transition state (TS) geometries were obtained by the integrated linear synchronous transit/quadratic synchronous transit (LST/QST) algorithm available in Materials Studio® 3.2. This approach was used before in computational studies in homogeneous trimerisation[35] and metathesis.[36] These preliminary structures were then subjected to full TS optimisations using an eigenvector following algorithm. For selected transition state geometries confirmation calculations, involving intrinsic reaction path (IRP) calculations, were performed in which the path connecting reagents, TS and products were mapped. The IRP technique used in Materials Studio® 3.2 also corresponds to the intuitive minimum energy pathway (MEP) connecting two structures and is based on the nudged elastic band (NEB) algorithm of Henkelman and Jonsson.[37] The IRP calculations, performed at the same GGA/PW91/DNP level of theory, ensured the direct connection of transition states with the respective reactant and product geometries. Most of the transition structure geometries that were subjected to vibrational analysis exhibited more than one imaginary frequency in the reaction coordinate. This indicates that the structures need to be refined and TS optimisations need to be done. In most cases, one of the imaginary frequencies was representative of a possible transition structure and should therefore be investigated further.

All results were mass balanced for the isolated system in the gas phase. The energy values that are given in the results are the electronic energies at 0 K and therefore only the electronic effects were in consideration in this study.

The following aspects were investigated with the use of molecular modelling:

- The effect of ligand dissociation (L_2), i.e. precatalyst initiation, on the mechanism of activation of benzylidene-type precatalysts $RuCl_2(L)(L_1)$(=CHPh) (L = PCy_3, H_2IMes, L_1 = PCy_3) by a dissociative pathway. This approach was chosen due to the fact that the presence of the respective ligands (L and L_1) has a significant impact on the initiation rates.[38] Therefore, the initiation and activation steps of the dissociative mechanism were investigated for selected precatalysts with different hemilabile ligands (**L1-L4**), whereby the labile atom (L_1) dissociates or L dissociates as compared to **Gr1** and **Gr2**.

- Calculation of the formation energies of the individual hemilabile complexes from **Gr1** and **Gr2** according to Scheme 4.10 (see Chapter 4). These energies can gave an indication of the stability of the formed complexes.

- The mechanism of 1-octene metathesis with **Gr1** was investigated to gain insight into the observed experimental results. At the GGA-PW91/DNP level, the complete geometry optimisation and the activation energy of various activation steps and catalytic cycles in the dissociative mechanism (§ 6.2.3) were performed.

3.7.3 Model system and notations

Conceptually, the productive metathesis of 1-octene in the presence of Grubbs carbene complexes is illustrated in **Scheme 3.1** and **3.2**. This mechanistic model is mainly based on the dissociative mechanism proposed by Grubbs et al.,[21,39] modelled by Chen et al.[40] and our experimental results.

The generic labels **A** – **I** were given to the individual ruthenium carbene and derived species involved in the reaction mechanism. The mechanism consist of the initial loss of PCy_3 from the precatalyst (**A**) to yield $RuCl_2(L)$(=CHPh) (L = PCy_3 or H_2IMes) (**B**). The different stereochemical approaches of 1-octene towards the catalytically active species (**B**, **F1**, **F3** and **F4**) lead to four activation steps (**1** to **4** notations in **Scheme 3.1**) and six catalytic cycles (**a** and **b** notations in **Scheme 3.2**). To identify which step is under consideration, a numerical suffix (**1** to **4**) is associated with the labels **C** to **I** (e.g. **C1** to **F1** represented activation step 1) and the additional alphabetic suffixes **a** and **b** indicate the different catalytic cycles. Transition states are denoted analogously, e.g. **G3a-H3a** is the transition state for the conversion of **G3a** to **H3a**.

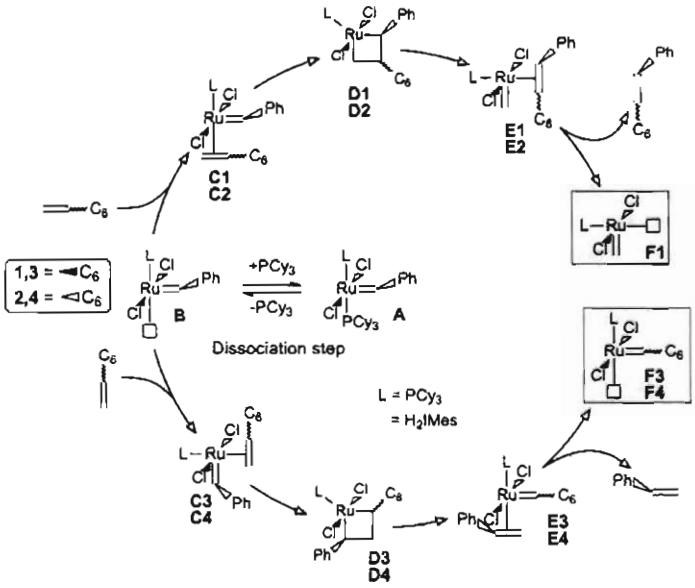

Scheme 3.1 Dissociation (A to B) and activation (B to F) steps in the mechanism of productive 1-octene metathesis using $RuCl_2(PCy_3)_2(=CHPh)$.

The mechanism is initiated by the dissociation of a phosphine ligand from the 16-electron benzylidene complex **A** to form the 14-electron active species **B** (**Scheme 3.1**). This is followed by activation steps (**Scheme 3.1**) and catalytic cycles (**Scheme 3.2**) based on the stereochemical approaches of the 1-octene towards the different carbene species. These steps/cycles consists of several successive formal [2+2] cycloadditions to form a metallacyclobutane, and cycloreversions to form the respective catalytically active species. Before the precatalyst can enter the catalytic cycle, there is an initiation phase (activation) in which the precatalyst first has to be converted from the benzylidene complex (**A**) to the methylidene (**F1**, the second activation step will also yield **F1**) or heptylidenes (**F3** and **F4**). This takes place through the coordination of 1-octene to the metal centre of the 14-electron intermediate to form a π-complex, which undergoes a formal [2+2] cycloaddition to form a metallacyclobutane ring, which in turn can revert to a new π-complex. The liberation of the alkene from the new π-complex leads to the new catalytically active alkylidene species that enters the catalytic cycle.

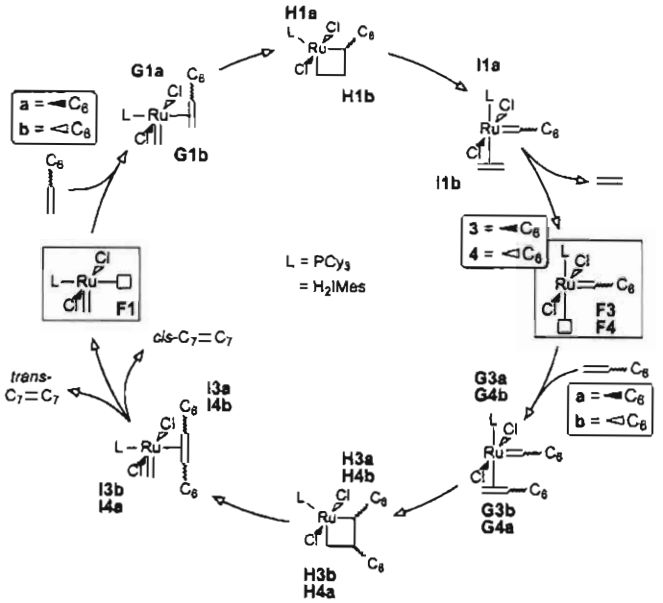

Scheme 3.2 Catalytic cycles in the mechanism of productive 1-octene metathesis using $RuCl_2(PCy_3)_2(=CHPh)$.

Activation steps 1 and 2 leads to the formation of the methylidene complex with the liberation of *cis*- and *trans*-1-phenyl-1-octene. In the other two activation steps, styrene is liberated to form the heptylidene species with the alkyl chain of the carbene facing out of (**F3**) or into (**F4**) the plane, depending on the coordination orientation of 1-octene relative to the phenyl ring of the carbene that is facing into the plane. Within the catalytic cycles, the heptylidene is converted to the methylidene, which is then again converted back to the heptylidenes until all the 1-octene has been consumed or the precatalyst has decomposed. During the conversion of the heptylidene to the methylidene, cis- and *trans*-7-tetradecene is formed, while ethene forms when the methylidene is converted to the heptylidene.

The dissociation and activation steps given in **Scheme 3.1** were applied to the first and second generation hemilabile ruthenium alkylidene complexes [RuCl(L)(O^N)(=CHPh)] (L = H_2IMes (**Gr2Cy**) or PCy_3 (**Gr1Cy**), O^N = 1-(2'-pyridinyl)cyclohexan-1-olate)), bearing a chelating pyridinyl alcoholate ligand to give **Scheme 3.3** and **3.4**. The notation used in **Scheme 3.1** was

applied to both schemes, with the addition of a subscript N or L to the generic labels A – F in **Scheme 3.3** and **3.4** respectively. The subscript N refers to the dissociation of the labile N-atom of the O,N-ligand, while L refers to the dissociation of L (L = PCy_3 or H_2IMes) from the hemilabile complexes. The model in **Scheme 3.3** consists of the initial dissociation of the labile N-atom of the O,N-ligand from **Gr1Cy** or **Gr2Cy** (A_N) to yield $RuCl_2(L)(O^N\text{-open})(=CHPh)$ (L = PCy_3 or H_2IMes) (B_N). In the second model (**Scheme 3.4**), the precatalysts initiate through the initial loss of L (L = PCy_3 or H_2IMes) from A_L to yield $RuCl_2(O^N)(=CHPh)$ (B_L). The same mechanistic considerations as described above for the Grubbs carbenes were followed for both models of the hemilabile complexes and will be further discussed in Chapter 6.

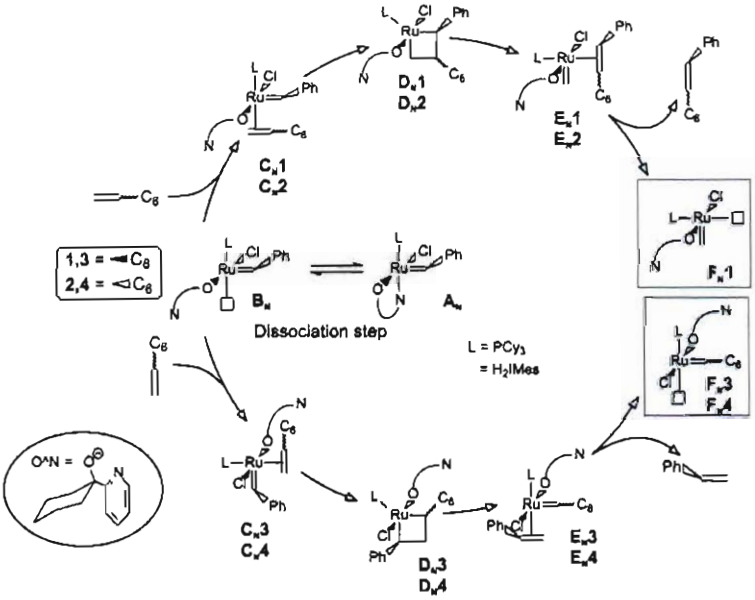

Scheme 3.3 Dissociation (A_N to B_N) and activation (B_N to F_N) steps in the mechanism of productive 1-octene metathesis using $RuCl_2(L)(O^N)(=CHPh)$ (L = PCy_3 or H_2IMes, O^N = 1-(2'-pyridinyl)cyclohexan-1-olate).

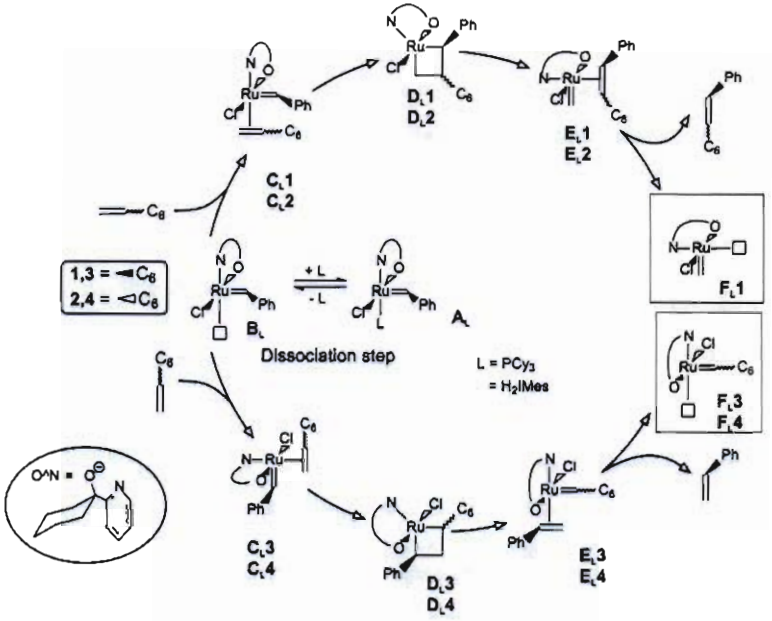

Scheme 3.4 Dissociation (A_L to B_L) and activation (B_L to F_L) steps in the mechanism of productive 1-octene metathesis using $RuCl_2(L)(O\text{^}N)(=CHPh)$ (L = PCy_3 or H_2IMes, O^N = 1-(2'-pyridinyl)cyclohexan-1-olate).

3.8 REFERENCES

1. Casey, M., Leonard, J., Lygo, B., and Procter, G., ***Advanced Practical Organic Chemistry***, Blackie, Glasgow, 1990

2. Buchowicz, W. and Mol, J.C., *J. Mol. Catal. A: Chem.*, 1999, **148**, 97

3. Sharpe, A.G., ***Inorganic Chemistry***, Longman, London, 1986

4. Cotton, F.A. and Wilkinson, G., ***Advanced Inorganic Chemistry***, Fifth Edition, Wiley, New York, 1988

5. Herrmann, W.A., Lobmaier, G.M., Priermeier, T., Mattner, M.R., and Scharbert, B., *J. Mol. Catal. A: Chem.*, 1997, **117**, 455

6. Denk, K., Fridgen, J., and Herrmann, W.A., *Adv. Synth. Catal.*, 2002, **344**, 666

7. Chang, S., Jones II, L., Wang, C., Henling, L.M., and Grubbs, R.H., *Organometallics*, 1998, **17**, 3460

8. Conrad, J.C., Amoroso, D., Czechura, P., Yap, G.P.A., and Fogg, D.E., *Organometallics*, 2003, **22**, 3634

9. De Clercq, B. and Verpoort, F., *Adv. Synth. Catal.*, 2002, **344**, 639

10. De Clercq, B. and Verpoort, F., *Tetrahedron Lett.*, 2001, **42**, 8959

11. Nieczypor, P., Buchowicz, W., Meester, W.J.N., Rutjes, F.P.J.T., and Mol, J.C., *Tetrahedron Lett.*, 2001, **42**, 7103

12. Buchowicz, W., Mol, J.C., Lutz, M., and Spek, A.L., *J. Organomet. Chem.*, 1999, **588**, 205

13. Amoroso, D., Snelgrove, J.L., Conrad, J.C., Drouin, S.D., Yap, G.P.A., and Fogg, D.E., *Adv. Synth. Catal.*, 2002, **344**, 757

14. Coalter III, J.N., Bollinger, J.C., Eisenstein, O., and Caulton, K.G., *New J. Chem.*, 2000, **24**, 925

15. Hancock, R.D., *Acc. Chem. Res.*, 1986, **58**, 1445

16. McMurry, J., ***Organic Chemistry***, Brooks/Cole, California, 1992

17. Loudon, G.M., ***Organic Chemistry***, Reading, Mass. : Addison-Wesley, London, 1984

18. Sweeting, L.M., 1998. Alkoxides, RO⁻. [Web] http://pages.towson.edu/ladon/orgrxs/reagent/bases.htm#RO [Date of access: 25/01/2006]

19. Clark, J., 2004. Carboxylic acids as acids. [Web] http://www.chemguide.co.uk/organicprops/acids/acidity.html [Date of access: 26/01/2006]

20. Sanford, M.S., Love, J.A., and Grubbs, R.H., *Organometallics*, 2001, **20**, 5314

21. Sanford, M.S., Love, J.A., and Grubbs, R.H., *J. Am. Chem. Soc.*, 2001, **123**, 6543

22. Dinger, M.B. and Mol, J.C., *Organometallics*, 2003, **22**, 1089

23. Dinger, M.B. and Mol, J.C., *Eur. J. Inorg. Chem.*, 2003, 2827

24. Meyer, W.H. 2004. Verbal communication with regards to the experimental setup of large-scale reactions for the metathesis of alkenes as performed at Sasol. Sasol Technology R&D, Sasolburg

25. Forman, G.S., McConnell, A.E., Hanton, M.J., Slawin, A.M.Z., Tooze, R.P., Janse van Rensburg, W., Meyer, W.H., Dwyer, C., Kirk, M.M., and Serfontein, D.W., *Organometallics*, 2004, **23**, 4824

26. Forman, G.S., McConnell, A.E., Tooze, R.P., Janse van Rensburg, W., Meyer, W.H., Kirk, M.M., Dwyer, C.L., and Serfontein, D.W., *Organometallics*, 2005, **24**, 4528

27. Unknown, 2006. Heriot-Watt University EPS - Chemistry: Solvent Correction CHN calculator Version 1.30. [Web] http://www.che.hw.ac.uk/research/services/solvent.html [Date of access: 28 August 2006]

28. Delley, B., *J. Chem. Phys.*, 1990, **92**, 508

29. Delley, B., *J. Phys. Chem.*, 1996, **100**, 6107

30. Delley, B., *J. Chem. Phys.*, 2000, **113**, 7756

31. Unknown, 2001-2005. [Web] http://www.accelrys.com [Date of access: 03/04/2004]

32. Perdew, J.P. and Wang, Y., *Phys. Rev.*, 1992, **B45**, 13244

33. Delley, B., ***Modern Density Functional Theory: A Tool for Chemistry***, Seminario, J.M., Politzer, P. *Theoretical and Computational Chemistry*, Vol. 2, Elsevier, Amsterdam, The Netherlands, 1995

34. Andzelm, J., King-Smith, R.D., and Fitzgerald, G., *Chem. Phys. Lett.*, 2001, **335**, 321

35. Janse van Rensburg, W., Grové, C., Steynberg, P.J., Stark, K.B., Huyser, J.J., and Steynberg, P.J., *Organometallics*, 2004, **23**, 1207

36. Janse van Rensburg, W., Steynberg, P.J., Meyer, W.H., Kirk, M.M., and Forman, G.S., *J. Am. Chem. Soc.*, 2004, **126**, 14332

37. Henkelman, G. and Jonsson, H., *J. Chem. Phys.*, 2000, **113**, 9978

38. Vyboishchikov, S.F., Bühl, M., and Thiel, W., Prof., *Chem. Eur. J.*, 2002, **8**, 3962

39. Sanford, M.S., Ulman, M., and Grubbs, R.H., *J. Am. Chem. Soc.*, 2001, **123**, 749

40. Adlhart, C. and Chen, P., *J. Am. Chem. Soc.*, 2004, **126**, 3496

Synthesis: Hemilabile Ru=C complexes 4

4.1 INTRODUCTION

Although a number of factors, *inter alia* steric and electronic effects of the coordinated ligands, can influence the activity of the catalytically active species in a chemical reaction, two main aspects remain of utmost importance: (a) coordination of the ligand to the metal centre, and (b) the application of the coordination complexes in metal catalysed reactions.[1] Therefore, when designing a new catalytic system or ligand for a specific metal, one should keep in mind the type of reaction it will be applied to. Thus, the focus of this study was the development of new Grubbs-type precatalysts with a hemilabile ligand for application in the metathesis of linear alkenes.

Hemilabile ligands are more frequently being used in coordination and organometallic chemistry, as a result of their ability to reversibly create and/or occupy a vacant coordination site at the metal (**Scheme 4.1**).[2,3] The reaction intermediates are therefore stabilised with subsequent enhancement of the catalytic activity of the complexes.[4,5] It is presumed that these ligands act as chelating ligands at room temperature and at elevated temperatures will liberate one coordination site 'on demand' of a competing substrate, such as an alkene *inter alia* norbornene.[5,6] The incorporation of hemilabile ligands into the Grubbs carbene complexes should therefore increase the stability and, hopefully, the activity of these systems for 1-alkene metathesis.

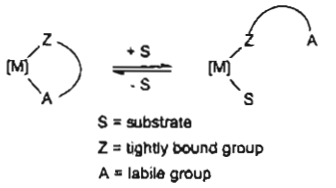

Scheme 4.1 Schematic representation of the concept of hemilability.[2,3]

A number of ruthenium carbene systems with hemilabile ligands for application in ROMP and RCM have been published (**Figure 4.1**).[5-11] Grubbs,[7] and later Verpoort,[8,9] introduced bidentate O,N-chelated Schiff-base ligands on **Gr1** and **Gr2** to give complexes **11** and **13**. The thermal stability and activity of **10** towards ROMP and RCM were increased through the combination of the Schiff-base ligand with a NHC ligand to give **13**.[6,9,12] 2-Pyridinylcarbinol (**HL**) is another type of O,N-chelated ligand, which has been well established in tungsten (VI) catalyst precursors for ROMP reactions.[13]

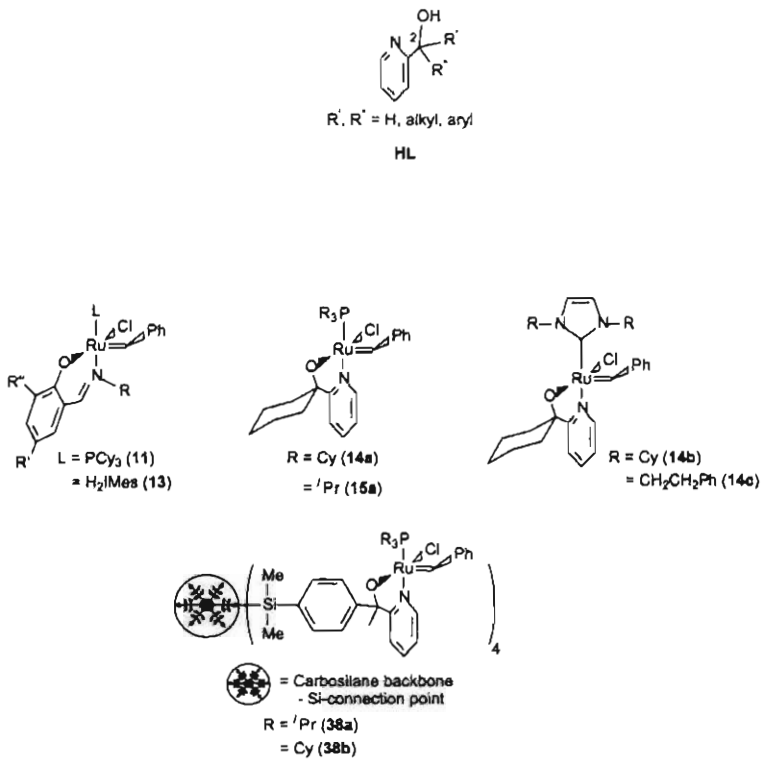

Figure 4.1 Established hemilabile ruthenium precatalysts for alkene metathesis.[6,7,9-12]

Several groups incorporated this type of ligand into the **Gr1** and various second generation Grubbs systems to give complexes **14**, **15** and **38**, which were shown to be active for RCM and/or ROMP.[6,10,11] Although Denk et al.[6] have synthesised **14a**, they did not report on its metathesis activity. Complex **14a** was only used as an intermediate in the synthesis of **14b** and **14c**, which catalysed the ROMP of norbornene and cyclooctene, respectively in 78% and 98% yield within 60 min. This type of ligands has also found application in the design of periphery-functionalised dendritic precatalysts (**38**) for RCM reactions.[11] Van Koten et al.[11] reported a 100% conversion of diethyl diallyl malonate to diethyl-3-cyclopentene carboxylate after 30 min at 80 °C.

The 2-pyridinylcarbinol-containing ruthenium carbene precatalysts are therefore very active for metathesis reactions. To my knowledge, the catalytic activity of these types of systems towards the self-metathesis of linear alkenes has not been previously investigated or reported. We[14] have recently published our findings on the metathesis of 1-octene in the presence of **14a** and the **Gr2**-analogues at 60 °C.

In this study, a variety of chelating ruthenium carbene complexes were prepared with modifications to the literature methods (see Chapter 3). The hemilability of these systems could not be determined with any certainty, but ^{1}H NMR investigations of the 1-octene metathesis reaction in the presence of **C7** and **C28**, suggested hemilabile activity of the pyridinyl alcoholate ligands (see Chapter 5). The hemilability of the other ligands could not be verified during this study, due to the unsuccessful incorporation of these ligands into the Grubbs carbenes. Observations during the synthesis, as well as spectroscopic data, are reported within the following sections. The application of the precatalysts towards the metathesis of 1-octene will be discussed in Chapter 5.

4.2 SYNTHESIS OF PYRIDINYL ALCOHOLATO LIGANDS

The results of the synthesis of the pyridinyl alcoholate ligands have been given in Chapter 3, with the spectral data available in Appendix C1.

4.3 SYNTHESIS OF HEMILABILE GRUBBS CARBENE COMPLEXES

A variety of pyridinyl alcohol as well as carboxylic acid bidentate ligands (see **L1 – L15** § 3.2) were investigated in order to determine the influence of ring size, steric bulk and electronic factors on the synthesis and catalytic activity of the new Ru=C precatalysts **C1 – C32**.

Firstly, bidentate ligands that can form 4- to 6-membered chelate rings with the Ru-centre were investigated. It was found that the 5-membered chelate rings were more stable than the 4- and 6-membered chelate rings. Secondly, carboxylic acid systems in which the labile donor atom was varied, *inter alia* O,N-, O,O-, O,P- and O,S-ligands, were investigated to determine the influence of electronic effects on the synthesis of the precatalysts. Finally, the influence of steric bulk was investigated by varying R' and R'' in **HL** (pyridinyl alcohol). **Scheme 4.2** and **4.3** illustrates the various first and second generation chelating Grubbs systems investigated during the course of this study. The red circles represent the complexes that were successfully synthesised and tested for metathesis activity, while the green circles are the complexes that formed a carbene complex, but could not be isolated and therefore contained various impurities during catalytic activity investigations. The blue circles represent the complexes that were synthesised from the Grubbs carbenes as intermediates for the hemilabile Grubbs-pyridine complexes.

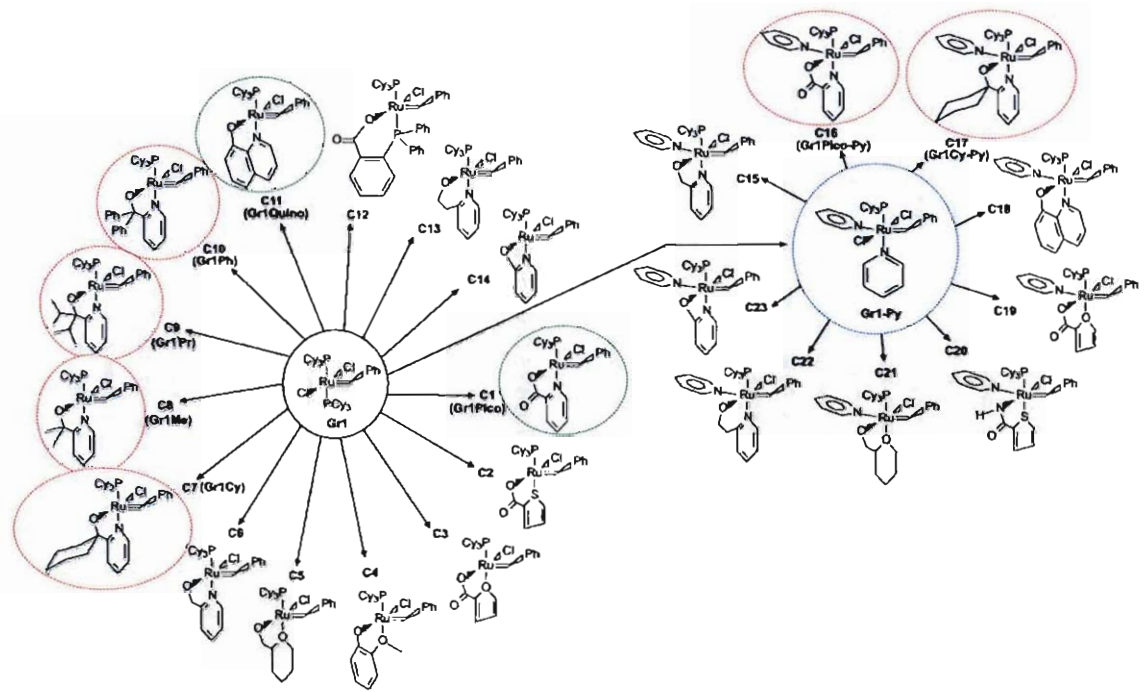

Scheme 4.2 Schematic representation of the first generation Grubbs and Grubbs-pyridine systems investigated [red circles = successfully synthesised carbene complexes, green circles = impure carbene complexes, blue circles = Grubbs pyridine intermediates for synthesis of hemilabile pyridine carbene complexes].

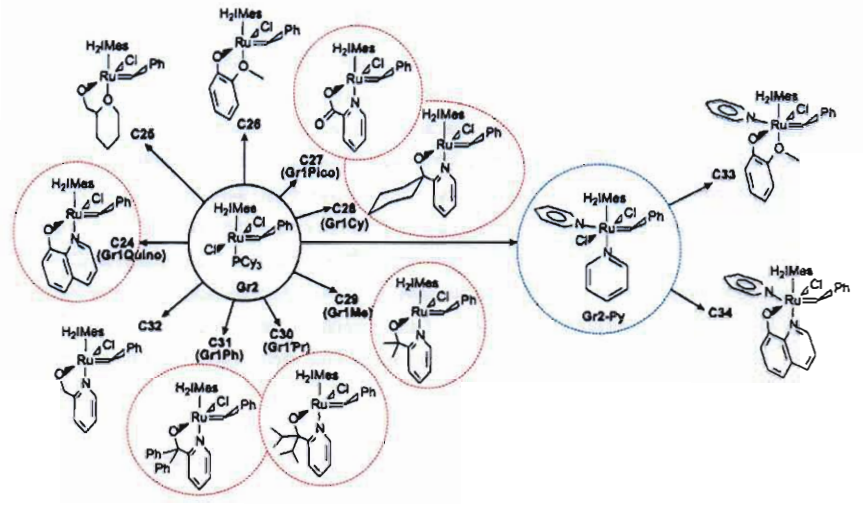

Scheme 4.3 Schematic representation of the second generation Grubbs and Grubbs-pyridine systems investigated [red circles = successfully synthesised carbene complexes, blue circles = Grubbs pyridine intermediates for synthesis of hemilabile pyridine carbene complexes].

The procedure followed for the synthesis of the precatalysts **C1** to **C32** consisted of stirring **Gr1** or **Gr2**, respectively, with a metal salt **S** of the corresponding alcohol or carboxylic acid. The salt was obtained through the reaction of the alcohol or carboxylic acid with either butyllithium, thallium ethoxide or a sodium related source to give the desired metal salt (**Scheme 4.4**).[6,15]

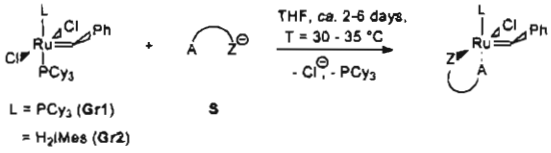

Scheme 4.4 Schematic representation of the synthesis of precatalysts **C1** to **C32**

The reaction was stirred between 2 and 6 days in tetrahydrofuran (THF) at room temperature for **Gr1** and 35 °C for **Gr2**, depending on the salt used. The progress of the reactions was monitored by TLC to determine whether any substrate was present in the reaction mixture, and therefore the reactions were stirred for a longer period than what was reported by Denk et al.[6] The formation of MCl (M = Li, Tl or Na) drove the reaction and was removed either through filtration or, when MCl was soluble in THF, removed through extraction of the product with toluene.The high solubility of LiCl in THF may be the reason why reactions with these salts took up to 2 days to complete. The free phosphine was removed by sonification (10 min) of the raw product in pentane with the subsequent removal of the pentane by syringe. The complexes were finally obtained in moderate (from Li-salts) to low (from Tl- and Na-salts) yields as microcrystalline powders through recrystallisation from THF/pentane. However, if the complexes were found to be soluble in pentane, the mixture was sonificated for 10 min, followed by slow vacuum condensation of pentane to produce the desired complex in moderate yield.

A large number of the systems that were investigated could not be successfully synthesised after numerous attempts, i.e. no carbene signal was observed in the ^{1}H NMR. These systems are shown without circles in **Scheme 4.2** and **4.3**. Several factors can contribute to the unsuccessful synthesis of catalytic complexes, since not only do the reagents, metal and ligand play a role during the synthesis, but also the choice of solvent, molarity, temperature and reaction time. Another important factor to consider is the ligand-to-metal ratio, which can have a vast effect on the structure of the obtained complexes. Too much ligand can lead to undesired systems in which two or more ligands are coordinated to the metal, especially when bidentate, heteronuclear chelating ligands are incorporated into the system. On the other hand, insufficient addition of the ligand will lead to low yields and incomplete formation of the desired complex.

Due to the large number of systems that were unsuccessfully synthesised, only a select few will be discussed to illustrate the reasons why they were unsuccessful. Appendix C1 contains the ^{1}H NMR spectra of all the successfully synthesised complexes with the rest given in Appendix C2, as discussed in this chapter. The spectroscopic data of all the complexes not discussed here will be included on a CD (Appendix C3) to indicate that the absence of a carbene signal deemed them unsuccessful.

4.3.1 Unsuccessful syntheses

It was noted for the reaction of **Gr1** and **Gr2**, respectively, with the O,O-ligand salts, that the Grubbs carbenes either remained unchanged (**Gr1** + **S24**, **Table 3.10**, **Spectrum C.65** and **C.66**) or decomposed to form Ru(PCy_3)(L)(Cl)(R)(CO) (L = PCy_3 or H_2IMes, R = Ph or H), free PCy_3 and O=PCy_3 with little or no carbene (either Grubbs or new complex) present afterwards (see

Table 3.9 – 3.21, Chapter 3 and **Spectrum C.65 – C.73**). However, an additional large ^{31}P NMR peak at δ 36.5 ppm and 29.5 ppm was observed for **C4** and **C26**, synthesised respectively from the reaction of **Gr1** (δ 35.6 ppm) and **Gr2** (δ 35.2 ppm) with the thallium (Tl) or lithium (Li) salts of **L10**. This unidentified complex showed no hydride or carbene resonances in the ^1H NMR. It is postulated that the product **39** (**Scheme 4.5**) formed, which is supported by the ^1H NMR (**Spectrum C.67**, **C.68**, **C.71** and **C.72** in Appendix C2). A strong singlet appeared at *ca.* δ 2.2 – 2.4 ppm for H_b, due to the electron-withdrawing effect of the oxygen attached to C_b (**Scheme 4.5**). Another strong singlet appeared at *ca.* δ 0.2 – 0.5 ppm, which might be assigned to H_a, due to the influence of the Ru-centre on C_a, together with the electron donating effect of phenyl.

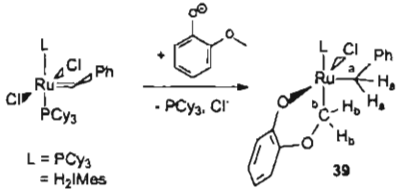

Scheme 4.5 Possible decomposition product of the Grubbs carbenes in the presence of guaiacol (**L10**).

However, Fogg et al.[16] recently successfully incorporated a chelating sulfonato-aryloxide (**Scheme 4.6**) and catecholato (**Scheme 4.7**) ligand, which are two O,O-chelating ligands, into **Gr2-Py**. A five- and six-membered chelated Ru=C complex resulted, whereby both chlorine-groups were substituted, accompanied by the dissociation of one of the pyridine ligands. This suggested that O,O-chelating ligands would more easily facilitate the displacement of a pyridine ring than a bulky, more basic PCy_3 ligand. Therefore, reactions of **Gr2-Py** and **Gr1-Py** with the lithium and thallium salts of **L9** and **L10** were investigated, but no carbene signals were observed. This reaction was not investigated further, and therefore alternative ligands were considered.

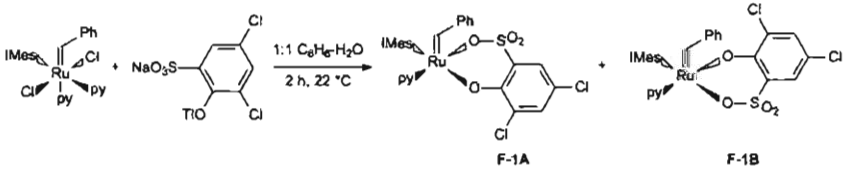

Scheme 4.6 Synthesis of a chelating sulfonato-aryloxide derivative of a second generation Grubbs system.[16]

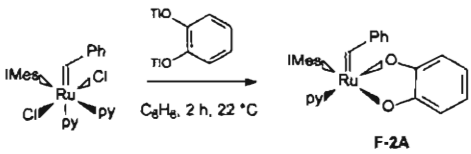

F-2A

Scheme 4.7 Synthesis of a chelating catecholato derivative of a second generation Grubbs system.[16]

Subsequently, a number of O,N-ligands were investigated to determine whether the synthesis, as well as the stability and activity (discussed in Chapter 5), of the precatalysts would improve by changing the donor ability of the labile atom. This was done since it has been shown that O,N-ligands can improve the stability and activity of the Grubbs carbenes towards various metathesis reactions.[6,7,9-12]

During the synthesis of **C14**, additional **S11** (Tl-salt of 2-hydroxypyridine) was added due to the presence of **Gr1** in the reaction mixture after 24 h, according to TLC analysis. This might have caused an **S11**/**Gr1** molar ratio of 1.5 to 2, leading to complexes other than the desired **C14**. Fogg et al.[17] recently indicated that the reaction of **Gr1** with 2 mol phenoxide anion, which is analogous to **S11**-anion, yields alkylidyne **41** via the deprotonation of the benzylidene ligand and liberation of phenol (see **Scheme 4.8**). Although Fogg et al.[17,18] mentioned that modelling studies were performed on these systems; no results have to my knowledge been published. It was suggested that the modelling results showed that the bulky trialkylphosphine ligands within the five-coordinate intermediates (**40** and **42**) would force the aryloxide oxygen into the proximity of the benzylidene proton. The steric pressure would then be relieved through the elimination of an alcohol to produce the alkylidyne.[17,18] Therefore, due to the absence of a carbene α-H (H_α) signal in the ^{1}H NMR of **C14** (**Spectrum C.75** and **C.76**, Appendix C2) and the similarity of the phenoxide and pyridinyloxide anion, it was thought that carbyne **46** might have formed according to route **a-b** in **Scheme 4.9**.

Unfortunately, due to an insufficient amount of sample no ^{13}C NMR spectrum could be obtained, which might have indicated the presence or absence of a quaternary carbyne carbon to support our postulations. According to Fogg et al.,[17] the nucleophilicity of the aryloxide does not have an influence on the formation of the alkylidyne, since they have shown that the treatment of **Gr1** with $TlOC_6F_5$ produces the alkylidyne **43** (**Scheme 4.8**), while the corresponding reaction with *tert*-butoxide produced the alkylidene **44**.[19]

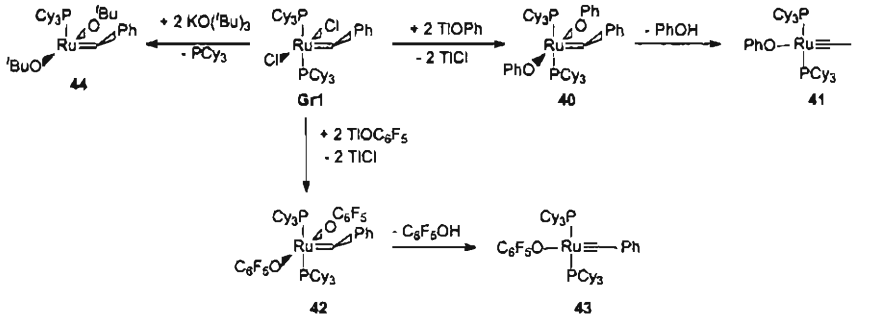

Scheme 4.8 Reaction of **Grl** with phenoxides or alkoxides.[17]

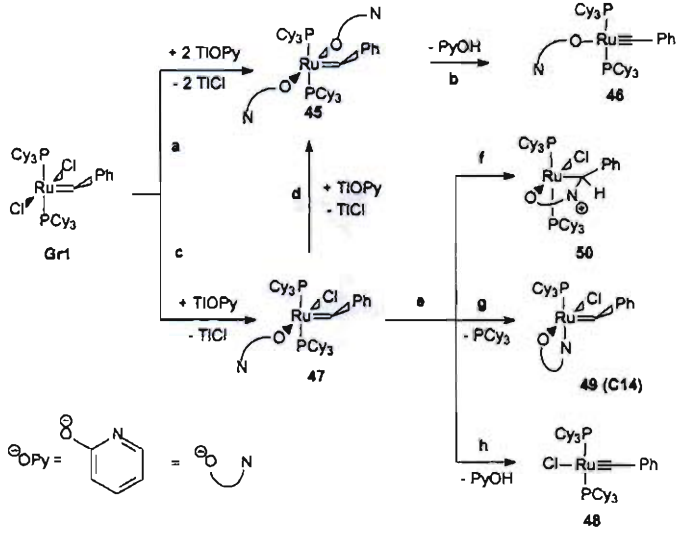

Scheme 4.9 Various reaction routes for the reaction of **Grl** with a pyridinyloxide anion (°OPy).

Therefore, since the nucleophilicity of 2-hydroxy-pyridine (pKa = 11.65) is similar to phenol (pKa = 10), as measured by its pKa value, it might suggest that a similar reaction could occur. However, our modelling results (GGA/PW91/DNP) on the intermediates **40**, **42** and **45** clearly indicated that the PCy_3 ligands do not exert enough steric pressure to force the aryloxide oxygen into proximity of the benzylidene proton, as suggested by Fogg et al.[17] **Figure 4.2** illustrates the distances obtained from the aryloxide oxygen to the benzylidene proton for the intermediates **40** (2.241 Å), **42** (2.294 Å) and **45** (2.330 Å) in this study.

45

40

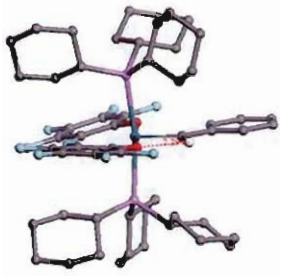

42

Figure 4.2 Optimised geometries for the intermediates **40**, **42** and **45**. The hydrogen atoms on the ligands are omitted for clarity and the unit of the indicated bond lengths are angstrom (Å).

Due to insufficient information on the computational details of their studies, their results cannot be fully evaluated. It was, however, communicated[20] to me that the OFF (Open Force Field) code (a low level of theory - molecular mechanics) was used in contrast to the DMol^3 code (a high level of theory - DFT) used in this study. OFF usually contains a database of molecular mechanics force fields to support the property prediction modules of the molecular modelling software program.[21] If the bond distances and angles of the individual metal-ligand bonds were obtained with a high level of theory and then used as parameters in OFF, the structures could be accurately optimised.[22,23] However, Fogg[20] could not elaborate on which molecular modelling software they used, since their workstation was non-operational and no results were published. The danger of using a low level of theory is that, although the geometry optimisation of the structures might be accurate, the energies are totally overestimated. Dr. Steynberg[24] suggested that a conformational search should be done on the various structures to obtain the global minimum structure for re-evaluation, due to the contrasting results. However, this was not investigated at the time of completing this study, due to time constraints. Another important comment to make is that one cannot just mention modelling results in articles without either including it as supporting material, or keeping a record of it for other authors to view. This prevents others to reproduce or evaluate the results, which might suggest that the results were questionable to start with, otherwise it would have been included in the article.

The energy profile (**Figure 4.3**) of the reaction of **Gr1** with **S11** was modelled and compared to the proposed[17] reaction of **Gr1** with a phenoxide ion (see **Scheme 4.8**). Although the thermodynamic effects caused by the precipitation of TlCl (s) were not included in the calculations, which were based on gas phase reactions, the relative electronic energies of the complexes were comparable to determine reaction trends.[25] To do an estimation on the thermodynamic effect of the salt, the thallium was replaced by a hydrogen atom (it is standard practice in molecular modelling to use truncated systems), which resulted in only a 2% difference in the reaction energies. This supported the fact that the salt was irrelevant and no thermodynamic effects were included. The energy required for the substitution of two chloride ligands in **Gr1** with phenoxide ligands was -2.27 kcal/mol, while 25.42 kcal/mol was needed for substitution with pyridinyloxide ligands (**Figure 4.3**). This indicated that a stable intermediate was initially formed during the reaction with thallium phenoxide, while the reaction with the thallium pyridinyloxide might require some form of heat. No additional energy was required for the formation of carbyne **46** from intermediate **45**, while 23.08 kcal/mol was needed to form **41** from **40**. The modelling results indicate that the formation of **41** from **40** according to **Scheme 4.8** is unfavourable. Coalter et al.[26] reported that an unprecedented phosphine loss results from the reaction of **Gr1** with phenoxide, yielding a four-coordinate carbene Ru(=CHPh)$(OR)_2$L. This indicates that another route to **41** might be involved, contrary to the proposed scheme of Fogg and coworkers.[17] Additionally, if

energy in the form of heat is applied to the reaction of **Gr1** with thallium pyridinyloxide, it might result in the decomposition of **Gr1**, since it is known to be thermally unstable.[27,28]

Therefore the carbyne might not have formed, but due to insufficient spectroscopic data on the identity of the formed product, this route can not be completely excluded. Other reaction possibilities were also suggested, as illustrated in **Scheme 4.9**, for the reaction of **Gr1** with thallium pyridinyloxide with an **S11/Gr1** molar ratio of 1. The energy profiles of these reactions were modelled and compared to the reaction of **Gr1** with thallium phenoxide and pyridinyloxide with an **S12/Gr1** = 2 (see **Figure 4.3** and **4.4** respectively). The substitution of one Cl ligand with a pyridinyloxide (13.23 kcal/mol) is more favourable than the substitution of two of the Cl ligands (25.42 kcal/mol). Additionally, the formation of **50** is endergonic by 108.22 kcal/mol, compared to the formation of **46** (22.90 kcal/mol), **48** (26.68 kcal/mol) and **49** (15.74 kcal/mol) from **Gr1**. This indicates that this is not a viable explanation for the absence of the H_α-signal in the ^1H NMR. The formation of carbyne **48** is unfavourable, due to an additional 13.45 kcal/mol energy required for the deprotonation of the carbene with loss of 2-hydroxypyridine. Complex **49**, which is the desired carbene, requires an additional 2.45 kcal/mol to form, most likely due to the strain of the 4-membered chelate ring formed upon coordination of the N-atom of the O,N-ligand.

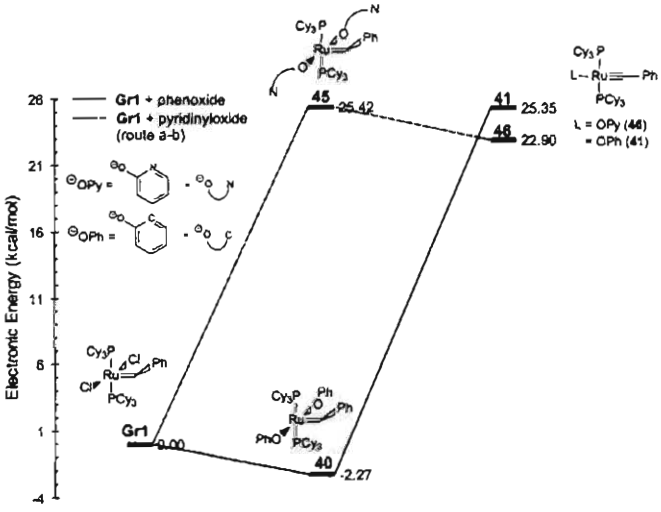

Figure 4.3 Electronic energy profiles of the various reaction routes for the reaction of **Gr1** with a pyridinyloxide anion (OPy), compared to the reaction with a phenoxide anion (OPh).

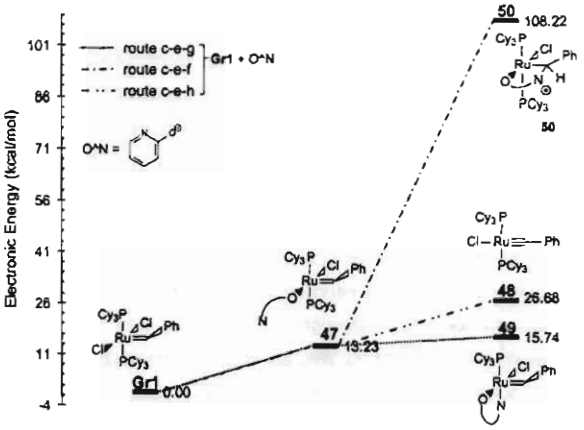

Figure 4.4 Electronic energy profiles of the various reaction routes for the reaction of **Gr1** with a pyridinyloxide anion (OPy).

The chelate ring size of **C14** was increased by increasing the chain length of the alcohol moiety on the pyridine ring of the chelating O,N-ligand. This resulted in the investigation of **L6** (2-(hydroxymethyl)pyridine) and **L7** (2-(2-hydroxyethyl)pyridine), which could potentially form a 5-membered (**C6**) and 6-membered (**C13**) chelate ring with the Ru-centre, respectively. Similar to **C14** (4-membered chelated complex), no H_α resonance signals were observed for either of the complexes (**Spectrum C.77 – C.78**, Appendix C2). Compared to **C7 – C10**, which were successfully synthesised, these systems differ only in the R groups on C_2 of HL, and additionally the size of the chelate ring formed with the Ru-centre for **C13**. The lack of steric bulk on C_2 of **L6** and **L7** might have brought the hydrogens on C_2 into proximity of the benzylidene proton, due to free rotation around the O-C_2 bond. This indicates that steric shielding of C_2 is required to prevent the decomposition of the carbene moiety through a possible exchange of H-atoms on C_2 with H_α. A deuterium labelling study should therefore be considered to determine whether this exchange is possible. One possibility is to replace the H-atoms on C_2 of **L6** with deuterium before reacting the salt with the Grubbs carbenes or to replace H_α with deuterium. To determine what effect electronic variations of HL would have on the syntheses of the new complexes, a range of carboxylic acids with different labile donor groups were investigated. **Gr1** remained mostly unchanged during the reaction with the thallium salts of the O,P-, O,O- and O,S-carboxylic acids, producing a mixture of

decomposition products of which the identities could not be determined. The reaction of **Gr1** or **Gr2** with the thallium or lithium salt of picolinic acid (**L11**, the anion hereafter referred to as pyca), resulted in multiple H_α signals being observed for **C1** and **C27** in the ^{1}H NMR (**Spectrum C.55 – C.58** and **C.61 – C62** respectively, Appendix C1). None of these carbenes could be individually isolated, due to their solubility in THF and other solvents used for recrystallisation. Cavell et al.[29,30] mentioned in a study of Pd-complexes containing pyridine-carboxylate chelating ligands (pyca and analogues), that the pyridine of pyca was unable to displace phosphines more basic than PPh_3 e.g. PCy_3. Contrary to Cavell, Hahn et al.[31] successfully incorporated two pyridinecarboxylate ligands into **Gr2** with the use of the silver salt of **L11** at 60 °C, to produce a halide free complex with two 5-membered chelated rings after 6 h. To my knowledge, no first generation analogues have been previously reported. The reported conditions necessary to displace PCy_3 with the pyridine ring of pyca in **Gr2** will initiate the decomposition of **Gr1**, since it is known to be thermally unstable.[27,28,32] Therefore, since the synthesis of **C1** was performed at 25 – 35 °C and **Gr1** contains two PCy_3 groups, pyca might only be coordinated through the O-atom by substitution of one or both Cl ligands on **Gr1**. However, the identity of the different carbene complexes associated with the H_α signals in the ^{1}H NMR could not be obtained due to insufficient spectroscopic data. Similarly, the synthesis of **C27** was performed at too low a temperature (25 – 45 °C), which might have resulted in more than one pyca coordinated to the Ru-centre in a monodentate fashion. Contrary to the reaction with the thallium and lithium salts of **L11**, only one H_α resonance was observed from reacting **Gr1** with the sodium salt of **L11** at 35 °C. The ^{1}H NMR of the resulting carbene (**Spectrum C.59 – C.60** in Appendix C1) suggested more than one pyca was coordinated to the Ru=C, since the integration values accounted for more than the required H's of **C1**. However, the ^{31}P NMR indicated the presence of a number of impurities after several purification attempts. This made assignment of the ^{1}H and ^{31}P NMR peaks difficult and therefore the structure could not be determined with any certainty.

The above discussions for the unsuccessful synthesis of selected individual complexes can also be applied to the complexes with analogous chelating ligands that were unsuccessfully synthesised, and will therefore not be discussed in any further detail. Although the synthesis of **C11** and **C24** was to some extent successful (**Spectrum C.33 – C.35** and **C.51 – C.53** in Appendix C1), the synthesis and purification steps were made difficult by the fact that these two complexes were partially soluble in most of the alkane solvents used during the purification steps (§ 4.3.2 for purification details). Complexes **C7 – C10**, as well as the second generation analogues were successfully synthesised and will be characterised in § 4.3.2.

Sanford et al.[33] synthesised a second generation complex that contained two substitutionally labile pyridine ligands (**51**, hereafter referred to as **Gr2-Py**), which could be easily displaced with a wide variety of phosphines. They predicted that other incoming ligands might react similarly,

providing that they are not too sterically hindered and are electron rich, since they found that no reaction occurred with P(*o*-tolyl)$_3$ (cone angle (θ) of 194 ° compared to PCy_3 with θ = 170 °)[34] or the electron-poor phosphine $P(C_6F_5)_3$. As a result of their success, a select few of the O,O- and O,N-chelating ligands were incorporated into **Gr2-Py** and the **Gr1** analogous **Gr1-Py**, to determine whether the substitution of the pyridine rings would be more facile compared to PCy_3. Unfortunately, only **C16** and **C17** were successfully synthesised, while no H_α resonance signals were observed for the other pyridine derived complexes. No microanalysis was done on these two samples, since they both contained impurities in the form of $O{=}PCy_3$ and starting material or decomposition products of **Gr1-Py**. Additional information regarding the ease of synthesis and stability of the complexes were obtained from calculating the formation energy (E_{d2}) of each complex (**Scheme 4.10**).

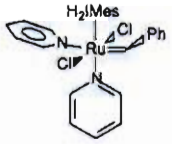

51

L = PCy_3, H_2IMes

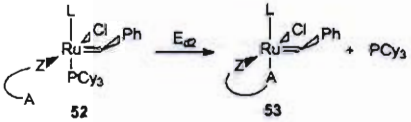

52 **53**

$$E_{d2} = E_{products} - E_{reagents}$$

$$= (E_{53} + E_{PCy3}) - E_{52}$$

with E_{d2} the formation energy
$E_{reagents}$ the electronic energy of the reagents
$E_{products}$ the electronic energy of the products
E_{52} the electronic energy of complex 52
E_{53} the electronic energy of complex 53
E_{PCy3} the electronic energy of complex PCy_3

Scheme 4.10 Calculation of the formation energy of the chelating complexes.

The electronic reaction energies of the reactants and products were used for calculating E_{d2}. In practice the electronic reaction energies correspond to a static system at 0 K, which is not an accurate comparison to experiment. Therefore, Gibbs free energy (ΔG) corrections still need to be done to the electronic energies for vibrational, translational and rotational energies of the molecules to determine the thermodynamic properties of the reaction. This would have required the computationally expensive calculation of vibrational modes of atoms in the molecule, which could not be done due to time constraints. However, preliminary mechanistic trends can be obtained from a PES constructed from the electronic energies of a system, for example identifying the more thermodynamically or kinetically favoured intermediates in a reaction mechanism, evaluating the possibility of synthesising complexes, etc. The energies of the individual species under investigation are usually lower after ΔG corrections are made, with some exceptions,[35] which indicate that the electronic energies are usually sufficient for evaluating systems.

Due to the observed precipitation of TlCl during the reaction of **Gr1** with the thallium salts, it was assumed that the O-atom had already coordinated to the Ru-centre (**52**) as illustrated in **Scheme 4.10**. Therefore, the formation energy of the complex was calculated as the energy required for coordination of A to the Ru-centre through dissociation of PCy_3 to produce **53**.

The formation energies of the various hemilabile complexes investigated in this study are summarised in **Table 4.1** and **4.2**. From the calculated E_{d2} energies, it is predicted that the synthesis of the first generation O,O-chelating complexes (endothermic E_{d2} values) would be difficult compared to the second generation analogues (exothermic E_{d2} values). This indicates that reactions of **Gr1** with the O,O-ligands requires heat, which would lead to the decomposition of the carbene moiety, since it is known that **Gr1** is thermally unstable.[27,28] The high negative (exothermic) E_{d2} values for the first (**C7** to **C10**) and second (**C28** to **C32**) generation O,N-chelated Grubbs systems (**Table 4.1**) indicate that the coordination of the labile N-atom should be favourable. The formation energies of the pyridine related complexes and **Gr2**-analogues of **Table 4.2** could not be determined at the time of completing this study. The ease of synthesis, as predicted by the calculated formation energies, does not always prevail, in view of the fact that, although the synthesis of **C6**, **Gr1Pico** and **C26** was predicted to be possible, (low E_{d2} values) the opposite resulted. This is due to the fact that solvent effects, steric effects, air and moisture sensitivity of complexes, etc., are not taken into consideration during these calculations.

Table 4.1 Comparing the formation energies (E_{d2}) of first and second generation chelating complexes

First generation system		E_{d2} (kcal/mol)	Second generation system		E_{d2} (kcal/mol)
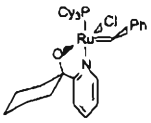	Gr1Cy	-13.05	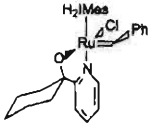	Gr2Cy	-22.11
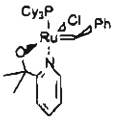	Gr1Me	-12.18	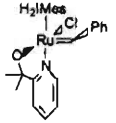	Gr2Me	-28.28
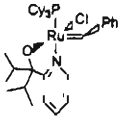	Gr1^{i}Pr	-33.83	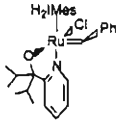	Gr2^{i}Pr	-47.03
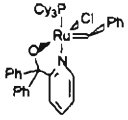	Gr1Ph	-19.84	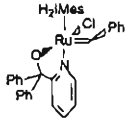	Gr2Ph	-38.06
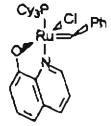	Gr1Quino	-8.95	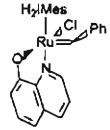	Gr2Quino	-13.36
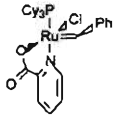	Gr1Pico	-5.29	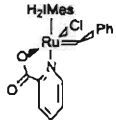	Gr2Pico	-3.05
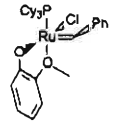	C4	6.43	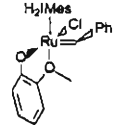	C26	-0.01
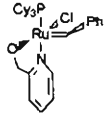	C6	-12.73	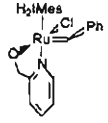	C32	-14.48

Table 4.2 Formation energies (E_{d2}) of various other first generation chelating complexes investigated in this study.

First generation system		E_{d2} (kcal/mol)
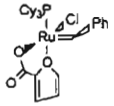	C3	21.69
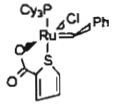	C2	18.94
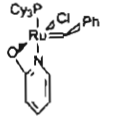	C14	15.74
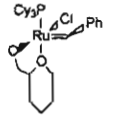	C5	2.24
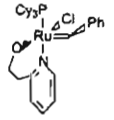	C13	-3.11
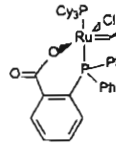	C12	-3.87

4.3.2 Characterisation of the successfully synthesised complexes

In the following section the characterisation of the complexes that were successfully synthesised, i.e. had a carbene signal present in the ^{1}H NMR, will be discussed. Throughout the course of this investigation a higher success rate, i.e. higher yield and more pure complexes, were obtained from reacting the Grubbs carbenes with a lithium salt, compared to the thallium and sodium salts (§ 3.4). Therefore, all complexes discussed in this section were synthesised from the reaction of **Gr1** or **Gr2** with a lithium salt of the chelating pyridinyl alcoholate ligand.

The ^{1}H and ^{31}P NMR spectra of the starting materials, i.e. **Gr1**, **Gr2**, **Gr1-Py** and **Gr2-Py** are illustrated in **Spectrum C.13 – C.20** in Appendix C1, which were comparable to literature.[33,36-38] These spectra were included to serve as reference point for the newly synthesised complexes. The new complexes were characterised with the use of CHN analysis, together with ^{1}H, ^{31}P and COSY NMR. The slow diffusion of pentane into a saturated solution of the complexes in THF failed to produce suitable crystals for X-ray analysis.

The ^{1}H, ^{31}P and COSY NMR spectra of the following first generation hemilabile complexes: Benzylidene-chloro(tricyclohexylphosphine)-[1-(2'-pyridinyl)cyclohexan-1-olato]ruthenium, Benzylidene-chloro(tricyclohexylphosphine)-[1-(2'-pyridinyl)propan-2-olato]ruthenium, Benzylidene-chloro(tricyclohexylphosphine)-[1-(2'-pyridinyl)-2,4-dimethylpentan-3-olato]ruthenium, Benzylidene-chloro(tricyclohexylphosphine)-[1-(2'-pyridinyl)-1,1-diphenyl-methanolato]ruthenium, Benzylidene-chloro(tricyclohexylphosphine)-[8-quinolinolato]ruthenium, Benzylidene-chloro(tricyclohexylphosphine)pyridine-[pyridine-2-carboxylato]ruthenium and Benzylidene-chloro(tricyclohexylphosphine)pyridine-[1-(2'-pyridinyl)cyclohexan-1-olato]ruthenium,

are illustrated in **Spectrum C.21** to **C.38** in Appendix C1 with **Gr1Pico-Py** in **Spectrum C.62** to **C.64** in Appendix C2. For selected complexes, P-H correlation spectra were obtained to confirm assignment of the phosphorous peak to the corresponding H_{α} resonance. The ^{1}H and ^{31}P NMR chemical shifts of these systems are respectively summarised in **Table 4.3 – 4.8**. The yield, product description and CHN analysis of each complex are given beneath the NMR table of each complex to further support the successful synthesis of these complexes. The ^{1}H NMR resonance signals that are not assigned and are not a solvent signal are presumably impurities *inter alia* unreacted ligand, decomposed complex or oxidised PCy_3 ($O{=}PCy_3$). According to the ^{31}P NMR, **Gr1Cy**, **Gr1Me** and **Gr1Ph** were 98 – 100% pure, while **Gr1^{i}Pr**, **Gr1Quino**, **Gr1Pico-Py** and **Gr1Cy-Py** had *ca.* 20 – 50% impurities present in the sample. No microanalysis was done on the impure samples. Overlap of resonance signals in the aliphatic region, due to the large amount of CH_2-protons of PCy_3 that resonates in this region,[35] caused difficulties in assigning the resonance signals to the aliphatic protons. The task of assigning the resonance signals to the aromatic protons was made easier with COSY NMR. As a result of the air and moisture sensitivity of **Gr1^{i}Pr**, no COSY spectra could be obtained. ^{1}H NMR analysis of **Gr1^{i}Pr** indicated that a carbene signal was present (δ 17.83 ppm), while analysis of the complex 2 h after a small crack was detected in the Schlenk tube showed that no carbene was present anymore. The decomposition of **Gr1^{i}Pr** was probably a result of air or moisture entering the Schlenk tube through the crack after vacuum drying the combined NMR sample with **Gr1^{i}Pr**. All attempts to repeat the synthesis of **Gr1^{i}Pr** failed. The absence of a COSY made it difficult to assign chemical shifts to the aromatic protons as well as determine the multiplicity of the signals, due to overlap of the signals (**Spectrum**

C.29). No COSY NMR or CHN analysis was obtained for **Gr1Cy-Py**, due to loss of sample after purification attempts. Thus, due to the presence of impurities, assignment of ^{1}H NMR peaks in the aliphatic and aromatic region was not attempted. It was also noted that only a minute amount of carbene (H_{α}, 1H (d) δ 17.76 ppm) was present, since the signal was enlarged 10-fold. The ^{31}P NMR indicated the presence of various peaks at δ 26.6, 40.9 and 44.2 ppm, which could not be assigned with any certainty to the carbene comples. Although no COSY NMR could be obtained for **Gr1Pico-Py**, the assignment of ^{1}H NMR signals was facilitated with the help of Dr. W. H. Meyer, who previously synthesised and characterised the complex with the aid of a COSY spectrum.[40]

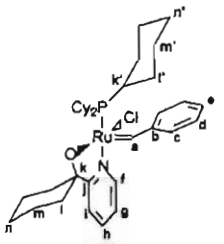

Table 4.3. ^{1}H and ^{31}P NMR data[a] of **Gr1Cy**

Phosphor / Hydrogen	δ[b] (dpm)
P of PCy_3	41.5
a	17.85 (d)
c	7.085 (d)
d	6.965 (dd)
e	7.380 (t)
f	8.95 (bs)
g	6.900 (dd)
h	6.965 (dd)
i	7.025 (d)
CH_2 of PCy_3 & C_8H_{10}	0.850 - 2.450 (43H's + Cy)

[a] ^{1}H spectrum: 300 MHz, ^{31}P spectrum: 121 MHz
[b] Solvent $CDCl_3$. s = singlet, d = doublet, t = triplet and m = multiplet.

Yield:	317.5 mg (0.465 mmol, 85%)			
Product:	dark-brown microcrystalline powder			
CHN analysis:	$C_{36}H_{53}ClNOPRu$ (683.76 g/mol)			
	C_{Calc}	63.24%	C_{Exp}	62.82%
	H_{Calc}	7.81%	H_{Exp}	8.05%
	N_{Calc}	2.05%	N_{Exp}	1.77%

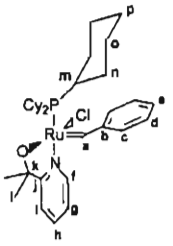

Table 4.4. ^{1}H and ^{31}P NMR data[a] of **Gr1Me**

Phosphor / Hydrogen	δ^{b} (dpm)
P of PCy_3	42.333
a	17.565 (d)
c	7.265 (d)
d	6.885 (d)
e	7.355 (t)
f	9.145 (d)
g	6.945 (dd)
h	7.015 (dd)
I	7.045 (d)
CH_3 (O^N ligand) + CH_2 of PCy_3	0.9-2.4 (39H's)

[a] ^{1}H spectrum: 300 MHz, ^{31}P spectrum: 121 MHz

[b] Solvent $CDCl_3$. s = singlet, d = doublet, t = triplet and m = multiplet.

Yield:	150 mg (0.233 mmol, 47%)			
Product:	dark-brown microcrystalline powder			
CHN analysis:	$C_{33}H_{49}ClNOPRu$ (643.25 g/mol)			
	C_{Calc}	61.62%	C_{Exp}	61.14%
	H_{Calc}	7.68%	H_{Exp}	7.28%
	N_{Calc}	2.18%	N_{Exp}	1.81%

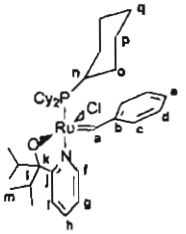

Table 4.5. ^{1}H and ^{31}P NMR data[a] of **Gr1^{i}Pr**

Phosphor / Hydrogen	δ^{b} (dpm)
P of PCy_3	39.987
a	17.825 (d)
c	7.76-6.71 (m)
d	7.76-6.71 (m)
e	7.35 (t)
f	9.01 (bs)
g	6.90 (dd)
h	7.76-6.71 (m)
i	6.98 (d)
CH_3 (O^N ligand) + CH_2 of PCy_3	0.9-2.2 (45H's)
CH (O^N ligand)	2.22 (m, 2H's)

[a] ^{1}H spectrum: 300 MHz, ^{31}P spectrum: 121 MHz

[b] Solvent $CDCl_3$. s = singlet, d = doublet, t = triplet and m = multiplet.

Yield:	120 mg (0.172 mmol, 35%)			
Product:	Green microcrystalline powder			
CHN analysis:	$C_{37}H_{57}ClNOPRu$ (699.36 g/mol)			
	C_{Calc}	63.54%	C_{Exp}	-
	H_{Calc}	8.21%	H_{Exp}	-
	N_{Calc}	2.00%	N_{Exp}	-

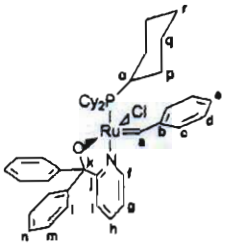

Table 4.6. ^{1}H and ^{31}P NMR data[a] of Gr1Ph

Phosphor / Hydrogen	δ^{b} (dpm)
P of PCy_3	40.481
a	17.637 (d)
c	6.545 (d)
d	7.01 (dd)
e	7.203 (t)
f	9.615 (d)
g	7.14 (dd)
h	7.343 (dd)
i	6.78 (d)
l	7.10 and 7.27 (d)
m	7.01 and 7.14 (dd)
n	7.34 (dd)
CH_2 of PCy_3	0.6-2.5 (m (33H's))

[a] ^{1}H spectrum: 300 MHz, ^{31}P spectrum: 121 MHz

[b] Solvent $CDCl_3$. s = singlet, d = doublet, t = triplet and m = multiplet.

Yield:	120 mg (0.156 mmol, 61%)			
Product:	dark-brown microcrystalline powder			
CHN analysis:	$C_{43}H_{53}ClNOPRu$ (767.40 g/mol)			
	C_{Calc}	67.30%	C_{Exp}	66.86%
	H_{Calc}	6.96%	H_{Exp}	6.88%
	N_{Calc}	1.83%	N_{Exp}	1.62%

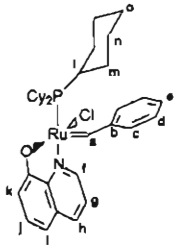

Table 4.7. ^{1}H and ^{31}P NMR data[a] of **Gr1Quino**

Phosphor / Hydrogen	δ^{b} (dpm)
P of PCy_3	32.69
a	19.42 (d)
c	7.16 (m)
d	6.84 – 6.94 (m)
e	7.24 – 7.34 (m)
f	7.86 (d)
g	6.98 (br d)
h	6.76 (d)
i	6.84-6.94 (m)
j	6.98 (br d)
k	8.38 (d)
CH_2 of PCy_3	0.7 – 2.2 (m)

[a] ^{1}H spectrum: 300 MHz, ^{31}P spectrum: 121 MHz

[b] Solvent $CDCl_3$. s = singlet, d = doublet, t = triplet and m = multiplet.

Yield:	41.6 mg (0.064 mmol, 39%)			
Product:	brown powder			
CHN analysis:	$C_{43}H_{45}ClNOPRu$ (651.23 g/mol)			
	C_{Calc}	62.71%	C_{Exp}	-
	H_{Calc}	6.96%	H_{Exp}	-
	N_{Calc}	2.15%	N_{Exp}	-

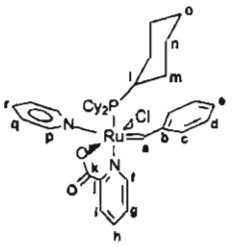

Table 4.8. ^{1}H and ^{31}P NMR data[a] of Gr1Pico-Py

Phosphor / Hydrogen	δ^{b} (dpm)
P of PCy_3	34.10
a	19.82 (d)
c	8.01 (bd)
d	6.83 (t)
e	7.34 (t)
f	8.31 (d)
g	7.20 (m)
h	7.63 (t)
i	7.54 (d)
p	8.11 (d)
q	7.20 (m)
r	8.01 (bd)
CH_2 of PCy_3 & C_6H_{10}	0.9 – 2.2 (m)

[a] ^{1}H spectrum: 300 MHz, ^{31}P spectrum: 121 MHz

[b] Solvent $CDCl_3$. s = singlet, d = doublet, t = triplet and m = multiplet. bd refers to observation of a broad doublet

Yield: 100 mg (0.141 mmol, 49%)

Product: Green powder

The ^{1}H, ^{31}P and COSY NMR spectra of the following first generation hemilabile complexes:
Benzylidene-chloro(1,3-bis-(2,4,6-trimethylphenyl)-2-imidazolidinylidene)-[1-(2'-pyridinyl)cyclohexan-1-olato]ruthenium,
Benzylidene-chloro(1,3-bis-(2,4,6-trimethylphenyl)-2-imidazolidinylidene)-[1-(2'-pyridinyl)propan-2-olato]ruthenium,
Benzylidene-chloro(1,3-bis-(2,4,6-trimethylphenyl)-2-imidazolidinylidene)-[1-(2'-pyridinyl)-2,4-dimethylpentan-3-olato]ruthenium,
Benzylidene-chloro(1,3-bis-(2,4,6-trimethylphenyl)-2-imidazolidinylidene)-[1-(2'-pyridinyl)-1,1-diphenyl-methanolato]ruthenium,
Benzylidene-chloro(1,3-bis-(2,4,6-trimethylphenyl)-2-imidazolidinylidene)-(2-pyridinecarboxy-lato)-ruthenium and
Benzylidene-chloro(1,3-bis-(2,4,6-trimethylphenyl)-2-imidazolidinylidene)-[8-quinolinolate]ruthenium

are illustrated in **Spectrum C.39** to **C.54** in Appendix C1 with **Gr2Pico** in **Spectrum C.60** to **C.61** in Appendix C2. No suitable crystals for X-ray analysis could be obtained through the slow diffusion of pentane into a saturated solution of the complexes in THF. It was, however, noted that crystal chunks formed for some of the second generation complexes after placing the pentane/THF mixture in the fridge for *ca.* 12 h, but due to insufficient experience in crystal growth, no suitable crystals could be obtained. The ^{1}H NMR chemical shifts of the second generation hemilabile complexes are, respectively, summarised in **Table 4.9 – 4.13**. The resonance signals, which are not represented in the tables and are not a solvent signal, are most likely impurities from the synthesis procedure *inter alia* unreacted ligand or decomposed complex. No attempts were made to assign the ^{1}H NMR signals of **Gr2Pico**, due to the presence of impurities and 4 carbene complexes resulting in signal overlap.

The yield, product description and CHN analysis of each complex are given beneath the NMR table of each complex to further support the successful synthesis of these complexes.

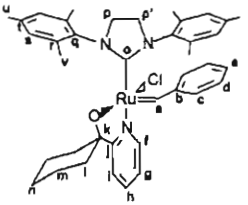

Table 4.9. ^{1}H NMR data[a] of **Gr2Cy**

Hydrogen	δ[b] (dpm)
a	17.962 (s)
c	7.245 (d)
d	6.88 (dd)
e	7.045-7.145 (m)
f	9.55 (d)
g	6.78 (dd)
h	7.045-7.15 (m)
i	6.60 (d)
l	1.25
m	1.45 — (10H's)
n	1.65
p/p'	3.85 (4H's, m)
s/s'	6.66/6.88 (bs, 4H's)
u	2.15
v	2.40 — (18H's, 3 x s)
v'	2.55

[a] ^{1}H spectrum: 300 MHz

[b] Solvent $CDCl_3$. s = singlet, d = doublet, t = triplet and m = multiplet.

Yield:	370 mg (0.521 mmol, 84%)			
Product:	forest-green microcrystalline powder			
CHN analysis:	$C_{39}H_{47}ClN_3ORu$ (710.33 g/mol)			
	C_{Calc}	65.94%	C_{Exp}	66.45%
	H_{Calc}	6.67%	H_{Exp}	6.58%
	N_{Calc}	5.92%	N_{Exp}	5.29%

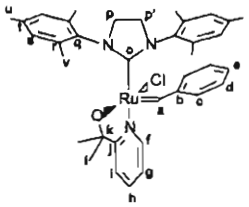

Table 4.10. ^{1}H NMR data[a] of **Gr2Me**

Hydrogen	δ^{b} (dpm)
a	17.815 (s)
c	7.15 (d)
d	6.85 (dd)
e	7.05 (dd)
f	9.15 (d)
g	6.75 (dd)
h	7.1 (dd)
i	6.6 (d)
l	1.2 (s (6H's))
p/p'	4.015 (4H's)
s/s'	6.85 / 6.7 (4H's)
u	2.2
v	2.6 (18H's 3xs)
v'	2.8

[a] ^{1}H spectrum: 300 MHz

[b] Solvent $CDCl_3$. s = singlet, d = doublet, t = triplet and m = multiplet.

Yield:	205 mg (0.436 mmol, 55%)			
Product:	green microcrystalline powder			
CHN analysis:	$C_{36}H_{43}ClN_3ORu$ (670.28 g/mol)			
	C_{Calc}	64.51%	C_{Exp}	64.03%
	H_{Calc}	6.47%	H_{Exp}	5.99%
	N_{Calc}	6.27%	N_{Exp}	5.81%

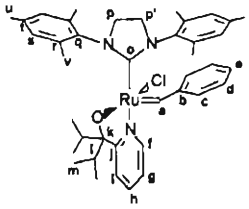

Table 4.11. ^{1}H NMR data[a] of Gr2^{i}Pr

Hydrogen	δ[b] (dpm)
a	18.52 (s)
c	7.65 (d)
d	7.35 (dd)
e	7.55 (dd)
f	9.65 (d)
g	7.15 (dd)
h	7.55 (dd)
i	7.05 (d)
l	2.15 (dt (2H's))
m	0.1-0.5 (2xd (6H's))
n	1.0-1.35 (2xd (6H's))
p/p'	4.45 (4H's)
s/s'	7.15 / 7.35 (4H's)
u	2.59
v	2.89 (18H's 3xs)
v'	3.05

[a] ^{1}H spectrum: 300 MHz

[b] Solvent $CDCl_3$. s = singlet, d = doublet, t = triplet and m = multiplet.

Yield:	150 mg (0.207 mmol, 57%)			
Product:	green microcrystalline powder			
CHN analysis:	$C_{40}H_{51}ClN_3ORu$ (726.39 g/mol)			
	C_{Calc}	66.14%	C_{Exp}	65.68%
	H_{Calc}	7.08%	H_{Exp}	6.73%
	N_{Calc}	5.78%	N_{Exp}	5.08%

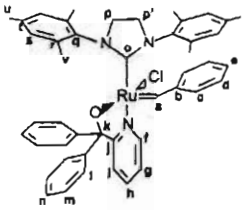

Table 4.12. [1]H NMR data[a] of Gr2Ph

Hydrogen	δ[b] (dpm)
a	17.183 (s)
c	6.43 (d)
d	6.77 (dd)
e	7.19 (dd)
f	9.67 (d)
g	7.036 (dd)
h	7.19 (dd)
l	6.64 (d)
l	7.12-7.19 m (10H's)
m	
n	
p/p'	4.05 (4H's)
s/s'	6.71 / 6.99 (4H's)
u	2.20
v	2.30 (18H's 3xs)
v'	2.65

[a] [1]H spectrum: 300 MHz

[b] Solvent $CDCl_3$. s = singlet, d = doublet, t = triplet and m = multiplet.

Yield:	140 mg (0.176 mmol, 91%)			
Product:	light-green microcrystalline powder			
CHN analysis:	$C_{46}H_{47}ClN_3ORu$ (794.42 g/mol)			
	C_{Calc}	69.55%	C_{Exp}	69.97%
	H_{Calc}	5.96%	H_{Exp}	6.33%
	N_{Calc}	5.29%	N_{Exp}	5.16%

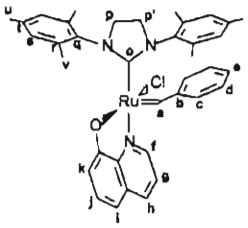

Table 4.13. ^{1}H NMR data[a] of **Gr2Quino**

Hydrogen	δ[b] (dpm)
a	18.25 (s)
c	6.85 (d)
d	6.72-6.65 (m)
e	7.35 (t)
f	7.75 (d)
g	7.05-6.89 (m)
h	6.40 (d)
i	6.72-6.65 (m)
j	7.05-6.89 (m)
k	8.58 (d)
p/p'	3.95 (4H's)
s/s'	6.52 (bs, 2H's) and 6.33 (bs, 2H's)
u	2.25
v	2.05 (18H's 3xs)
v'	1.95

[a] ^{1}H spectrum: 300 MHz

[b] Solvent $CDCl_3$. s = singlet, d = doublet, t = triplet and m = multiplet.

Yield:	41.8 mg (0.062 mmol, 26%)			
Product:	orange-brown powder			
CHN analysis:	$C_{37}H_{39}ClN_3ORu$ (678.26 g/mol)			
	C_{Calc}	65.52%	C_{Exp}	65.04%
	H_{Calc}	5.80%	H_{Exp}	5.40%
	N_{Calc}	6.20%	N_{Exp}	6.13%

Three carbene complexes formed during the synthesis of **Gr2Quino**, as seen in the ^{1}H NMR spectrum (**Spectrum 4.1**) of **Gr2Quino** before purification. The absence of **Gr2** in the ^{31}P NMR spectrum (**Spectrum 4.2**) illustrates that **Gr2** has been completely converted to the three new carbene species of which two were completely soluble in pentane, with the third only partially soluble. As a result of the solubility differences of the 3 carbenes in pentane, two product layers were formed upon slow vacuum condensation. The dark-brown top-layer contained the carbene species that were soluble in pentane, with H_a resonance signals at δ 19.09 and 18.92 ppm. The bottom orange-brown layer contained the partially soluble **Gr2Quino** with a H_a resonance signal at δ 18.31 ppm, (**Spectrum 4.3**) with no PCy_3 peaks present in the ^{31}P NMR spectrum (see Appendix C1, **Spectrum C.52**). Microanalysis of the orange-brown powder corresponds to the expected composition of **Gr2Quino**.

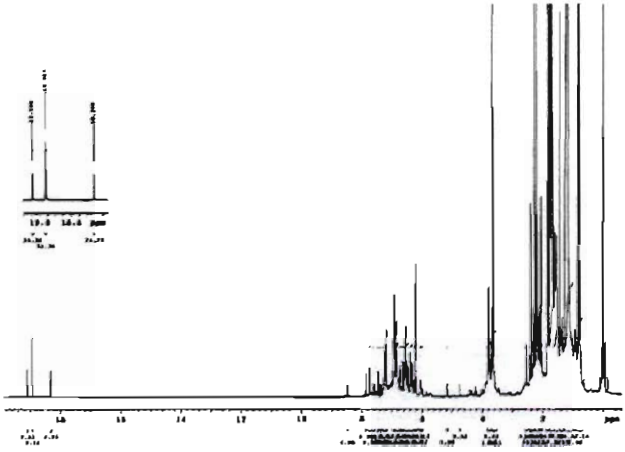

Spectrum 4.1 ^{1}H NMR spectrum of the reaction mixture of **Gr2** with the lithium salt of 8-quinolinol (L8) before purification.

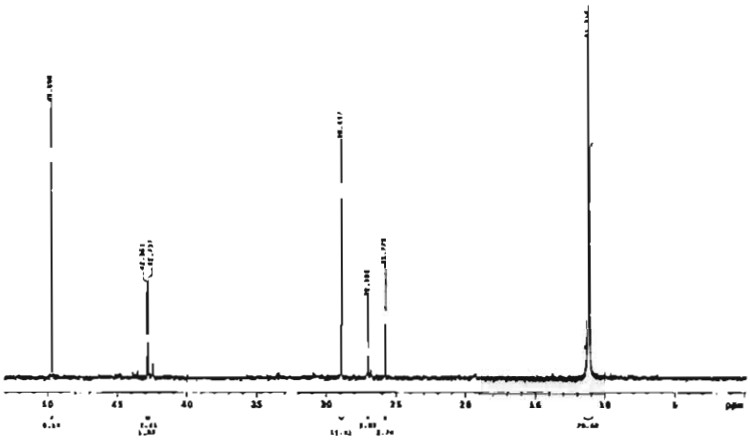

Spectrum 4.2 ^{31}P NMR spectrum the reaction mixture of **Gr2** with the lithium salt **L8** before purification.

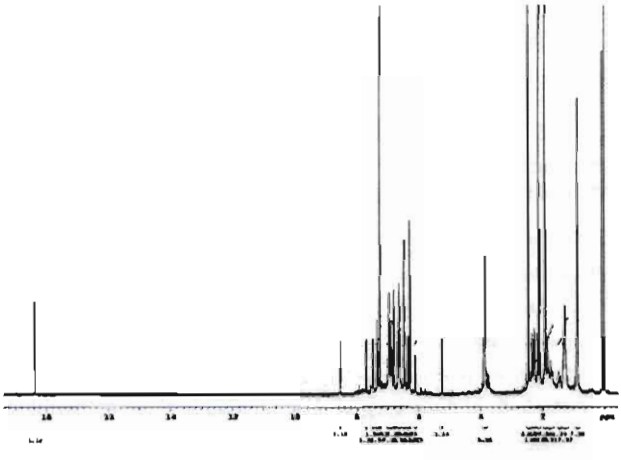

Spectrum 4.3 ^{1}H NMR spectrum of the orange-brown product formed after purification of the reaction mixture of **Gr2** with the lithium salt **L8**.

The infrared (IR) spectra of the various first and second generation complexes are illustrated in **Spectrum** D.1 – D.7 in Appendix D. The IR spectra of the hemilabile complexes are compared with the free chelating ligands and **Gr1** or **Gr2**, respectively, to obtain information regarding the coordination of the chelating ligands. The IR spectra of these complexes contain many sharp bands of different intensities due to additional vibrations arising from the coordinated benzylidene moiety together with the Cl^-, PCy_3 and/or NHC ligands. Therefore, these spectra are complex in nature and no attempts have been made to assign the individual bands in the fingerprint region. Consequently, a general assignment of the most important bands in the spectra of the ligands and respective complexes are given below.

Peaks at 1606 and 1604 cm^{-1} are assigned to the C=N stretch vibrations of the pyridine ring, while C=C stretch vibrations appears at 1430 – 1450 cm^{-1}. The sharp band appearing at 1260 – 1265 cm^{-1} in all the second generation systems is assigned to the C-N stretching vibration of the NHC ligand. The aromatic and aliphatic C-H stretch vibrations appear at 2800 – 2950 cm^{-1}, while the P-C vibrations of PCy_3 appear at 1443 – 1445 cm^{-1}.[39]

It has been reported[41] that, upon coordination of pyca to a Ni-centre to form a 5-membered chelate ring, an increase of 14 – 18 cm^{-1} was observed in the IR frequency of the pyridine ring deformations as compared to the free ligand. Upon coordination of the various pyridinyl alcoholato ligands to the Ru-centre, a positive shift of 5 – 7 cm^{-1} was observed for the C=N stretch vibrations, compared to the free ligands. This might be an indication of coordination of the pyridyl nitrogen to the Ru-centre. No IR data was obtainable for analogous ruthenium complexes to which our data could be compared to confirm our observations.

4.3.2.1 Discussion of the NMR results of the successfully synthesised complexes

The ^1H NMR chemical shifts of the carbene α-H signal (denoted H^* in the structures) and pyridine α-H signal (denoted as H^1 in the structures) for the first and second generation systems are summarised in **Table 4.14** and **4.15**, respectively, with inclusion of the ^{31}P signals for the first generation systems in **Table 4.14**. The H_α signals for the first generation hemilabile complexes are strongly shifted upfield relative to **Gr1** and appeared as doublets. This indicates that the dihedral angle P-Ru-C_α-H_α in these systems must be close to 0° or 180° and that only one PCy_3 group is left.[42] Various authors who investigated chelating systems observed the H_α signal as a doublet. The chelating complexes varied from our systems in that the chelating ligand is attached to the carbene as illustrated in structure **54**, rather than via X as seen in structure **55**.

Table 4.14 Selected ^{1}H and ^{31}P NMR signals of the first generation hemilabile complexes in comparison to the free O,N-ligands and **Gr1**.

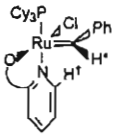

Catalytic system	δ_{H^*} (ppm)[a]	δ_{H^*} (ppm)[a]	$\delta_{H^\dagger}$ (ppm)[b]	δ_P (ppm)
Gr1	20.03 (s)	-	-	35.6
Gr1Cy	17.85 (d)	8.95 (d)	8.48 (d)	41.5
Gr1^{i}Pr	17.83 (d)	9.15 (bs)	8.52 (d)	39.9
Gr1Me	17.57 (d)	9.15 (d)	8.49 (d)	42.3
Gr1Ph	17.64 (d)	9.62 (d)	8.50 (d)	40.5

[a] carbene α-H signal (denoted H*) and pyridine α-H signal (denoted as H†) of the hemilabile complexes

[b] pyridine α-H signal (denoted as H†) of the pyridinyl carbinol ligands

Table 4.15 Selected ^{1}H NMR signals of the second generation hemilabile complexes in comparison to the free O,N-ligands and **Gr2**.

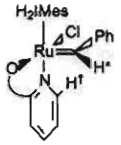

Catalytic system	δ_{H^*} (ppm)[a]	δ_{H^*} (ppm)[a]	$\delta_{H^\dagger}$ (ppm)[b]
Gr2	19.19 (s)	-	-
Gr2Cy	17.96 (s)	9.55 (d)	8.48 (d)
Gr2^{i}Pr	18.52 (s)	9.65 (d)	8.52 (d)
Gr2Me	17.82 (s)	9.15 (d)	8.49 (d)
Gr2Ph	17.18 (s)	9.67 (d)	8.50 (d)
Gr2Quino			8.77 (d)

[a] carbene α-H signal (denoted H*) and pyridine α-H signal (denoted as H†) of the hemilabile complexes

[b] pyridine α-H signal (denoted as H†) of the pyridinyl carbinol ligands

L^1 = PCy_3, H_2IMes
L^2 = O, N

54

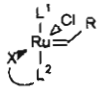

L^1 = PCy_3, H_2IMes
L^2 = O, N

55

Grubbs et al.[43,44] proposed a Karplus-type relation between the dihedral angle P-Ru-C_α-H_α and the observed coupling constant $J_{P,H}$ for first generation Grubbs systems. In general, this relation implies that the magnitude of the coupling between phosphine ligands and the α-proton of a carbene unit depends on their relative spatial orientation or geometry. Although the decoupler was off during the acquisition of the ^{31}P NMR spectra no P-H_α coupling was observed. Relative to **Gr1**, the ^{31}P NMR resonances of **Gr1Cy**, **Gr1Me**, **Gr1^{i}Pr** and **Gr1Ph**, which appeared as singlets, were strongly shifted upfield, indicating that the chelating O,N-ligands have strong effects on the chemical shifts of the relevant NMR resonances. Similar to the first generation hemilabile complexes, a strong upfield shift is observed in the H_α signals of the second generation hemilabile complexes. Relative to **Gr2**, the H_α signals also appeared as singlets. As expected, no ^{31}P NMR resonances were observed, since no phosphorous group should theoretically be coordinated to the Ru-centre after substitution with the O,N-chelated ligands.

The calculated Hirshfeld charges of selected atoms of the first and second generation Ru=C hemilabile systems and free pyridinyl carbinol ligands are given in **Table 4.16**. The upfield shift of the H_α" peak in the ^1H NMR of the first and second generation hemilabile complexes, compared to **Gr1** and **Gr2** (**Table 4.14** and **4.15**), is due to a change in the electronic environment induced by the chelating ligand. The change in the electron environment of H_α" is mainly caused by the donation of the free electron pair of the N-atom to the carbene moiety upon coordination with the Ru-centre. This is evident from the reduced electron density on the O- and N-atoms of the ligand after coordination with the Ru-centre, which is distributed to C_α. The charges on the carbene moiety of **Gr1** (-0.069) and **Gr2** (-0.069) decreased by *ca.* 0.04, with a simultaneous increase of *ca.* 0.09 in the electrophilic character of the Ru-centre. This suggests that the hemilabile complexes might be more active due to the high susceptibility of the Ru-centre for nucleophilic attack from *inter alia* an alkene. Additionally, a downfield shift in the pyridine α-H signal was observed for the first and second generation hemilabile complexes, indicating that the electronic environment of the ligand has changed. This implies that the N-atom has coordinated to the Ru-centre, since a

downfield shift of a proton resonance signal is indicative of reduced electron density of the attached C-atom.[39] When comparing the calculated Hirshfeld charges of the N-atoms of the free ligand to the coordinated N-atoms, it is seen that the coordinated atoms are much more positively charged. Therefore, the electron density of the pyridine ring has been distributed towards the Ru=C moiety, supporting the downfield shift of α-H^1.

Table 4.16 Calculated Hirshfeld charges of selected atoms of the Ru=C systems and free carbinol ligands

Catalyst \ Atom	Ru	$=C_\alpha$	N	O	Free ligand \ Atom	N	O
Gr1	0.212	-0.069	-	-		-	-
Gr2	0.187	-0.069	-	-		-	-
Gr1Me	0.298	-0.108	-0.068	-0.237	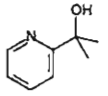	-0.177	-0.535
Gr2Me	0.319	-0.096	-0.074	-0.246			
Gr1Ph	0.295	-0.099	-0.069	-0.238	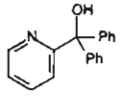	-0.181	-0.535
Gr2Ph	0.316	-0.088	-0.073	-0.244			
Gr1Cy	0.298	-0.108	-0.068	-0.235	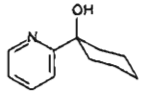	-0.175	-0.503
Gr2Cy	0.320	-0.097	-0.074	-0.244			
Gr1^{i}Pr	0.301	-0.111	-0.065	-0.230	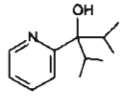	-0.127	-0.224
Gr2^{i}Pr	0.323	-0.095	-0.072	-0.235			
Gr2Quino	0.313	-0.069	-0.081	-0.220	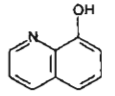	-0.165	-0.167

4.4 REFERENCES

1. Pretorius, M., ***Bi- and Tridentate Ligands and their use in Catalysis***, Ph.D thesis, Rand Afrikaans University, 2004

2. Bielawski, C.W., ***Tailoring Polymer Synthesis with Designer Ruthenium Catalysts***, Ph.D thesis, California Institute of Technology, 2003

3. Slone, C.S., Weinberger, D.A., and Mirkin, C.A., *Progr. Inorg. Chem.*, 1999, **48**, 233

4. Noack, C.L., ***Studies in Coordination Chemistry***, Ph.D thesis, Griffith University, 2003

5. Meyer, W.H., Brull, R., Raubenheimer, H.G., Thompson, C., and Kruger, G.J., *J. Organomet. Chem.*, 1998, **553**, 83

6. Denk, K., Fridgen, J., and Herrmann, W.A., *Adv. Synth. Catal.*, 2002, **344**, 666

7. Chang, S., Jones II, L., Wang, C., Henling, L.M., and Grubbs, R.H., *Organometallics*, 1998, **17**, 3460

8. De Clercq, B. and Verpoort, F., *J. Mol. Catal. A: Chem.*, 2002, **180**, 67

9. De Clercq, B. and Verpoort, F., *Adv. Synth. Catal.*, 2002, **344**, 639

10. Van der Schaaf, P.A., Muhlbach, A., Hafner, A., and Kolly, R., 1999. Heterocyclyl ligand containing ruthenium and osmium catalysts. Patent: *WO 99/29701*

11. Wijkens, P., Jastrzebski, J.T.B.H., Van der Schaaf, P.A., Kolly, R., Hafner, A., and Van Koten, G., *Org. Lett.*, 2000, **2**, 1621

12. De Clercq, B. and Verpoort, F., *Tetrahedron Lett.*, 2002, **43**, 9101

13. Van der Schaaf, P.A., Abbenhuis, R.A.T.M., van der Noort, W.P.A., De Graaf, R., Grove, D.M., Smeets, W.J.J., Spek, A.L., and Van Koten, G., *Organometallics*, 1994, **13**, 1433

14. Jordaan, M. and Vosloo, H.C.M., *Adv. Synth. Catal.*, 2007, **349**, 184

15. Herrmann, W.A., Lobmaier, G.M., Priermeier, T., Mattner, M.R., and Scharbert, B., *J. Mol. Catal. A: Chem.*, 1997, **117**, 455

16. Monfette, S. and Fogg, D.E., *Organometallics*, 2006, **25**, 1940

17. Conrad, J.C., Amoroso, D., Czechura, P., Yap, G.P.A., and Fogg, D.E., *Organometallics*, 2003, **22**, 3634

18. Conrad, J.C., Snelgrove, J.L., Eeelman, M.D., Hall, S., and Fogg, D.E., *J. Mol. Catal. A: Chem.*, 2006, **254**, 105

19. pK_a values: perfluorophenol, 5.52 (Birchall, J.M. and Haszeldine, R.N., *J. Chem. Soc.*, 1959, 3653); phenol, 10 and *tert*-butyl alcohol, 18 (Streitwieser, A.J. and Heathcock, C.N., ***Introduction to Organic Chemistry***, 2nd ed., McMillan: New York, 1981)

20. Fogg, D.E. (dfogg@uottawa.ca) 23 October 2006. Communication with regards to their modelling results. E-mail to: Jordaan, M. (chemr@puk.ac.za (at time of communication))

21. Accelrys, 2006. Cerius2. [Web] http://www.msi.umn.edu/sdvl/software/MolecularModeling.html [Date of access: 23 February 2007]

22. Steynberg, P.J. 2007. Verbal communication with regards to OFF. Sasol Technology R&D, Sasolburg

23. Unknown, 2006. Molecular Mechanics. [Web] http://www.sdsc.edu/~kimb/molmech.html [Date of access: 23 February 2007]

24. Steynberg, P.J. 2007. Verbal communication with regards to possible conformational studies. Sasol Technology R&D, Sasolburg

25. Janse van Rensburg, W. 2006. Verbal communication with regards to reactions in which precipitation of salts occurs. Sasol Technology R&D, Sasolburg

26. Coalter III, J.N., Bollinger, J.C., Eisenstein, O., and Caulton, K.G., *New J. Chem.*, 2000, **24**, 925

27. Lehman, S.E., Jr., Schwendeman, J.E., O'Donnell, P.M., and Wagener, K.B., *Inorg. Chim. Acta.*, 2003, ***345***, 190

28. Mahahle, M.M.D., ***Isomerisation of Alkenes using Metal Carbenes and Related Transition Complexes***, Ph.D thesis, Potchefstroom University for Christian Higher Education, 2005

29. Jin, H., Cavell, K.J., Skelton, B.W., and White, A.H., *J. Chem. Soc., Dalton Trans.*, 1995, 2159

30. Hoare, J.L., Cavell, K.J., Skelton, B.W., and White, A.H., *J. Chem. Soc., Dalton Trans.*, 1996, 2197

31. Hahn, F.E., Paas, M., and Frohlich, R., *J. Organomet. Chem.*, 2005, **690**, 5816

32. Ulman, M. and Grubbs, R.H., *J. Org. Chem.*, 1999, **64**, 7202

33. Sanford, M.S., Love, J.A., and Grubbs, R.H., *Organometallics*, 2001, **20**, 5314

34. Tolman, C.A., *Chem. Rev.*, 1977, **77**, 313

35. Janse van Rensburg, W., Steynberg, P.J., Kirk, M.M., Meyer, W.H., and Forman, G.S., *J. Organomet. Chem.*, 2006, **691**, 5312

36. Schwab, P., Grubbs, R.H., and Ziller, J.W., *J. Am. Chem. Soc.*, 1996, **118**, 100

37. Sanford, M.S., Love, J.A., and Grubbs, R.H., *J. Am. Chem. Soc.*, 2001, **123**, 6543

38. Scholl, M., Ding, S., Lee, C.W., and Grubbs, R.H., *Org. Lett.*, 1999, **1**, 953

39. Silverstein, R.M. and Webster, F.X., ***Spectrometric Identification of Organic Compounds***, 6th Ed., Wiley, New York, 1998

40. Unknown 2003. Synthesis of **Gr1-PyPico** at Sasol during vacation work under supervision of Dr. Meyer. Sasol Technology R&D, Sasolburg

41. Desjardins, S.Y., Cavell, K.J., Jin, W., Skelton, B.W., and White, A.H., *J. Organomet. Chem.*, 1996, **515**, 233

42. Fürstner, A., Thiel, O.R., and Lehman, S.E., *Organometallics*, 2002, **21**, 331

43. Dias, E.L., Nguyen, S.T., and Grubbs, R.H., *J. Am. Chem. Soc.*, 1997, **119**, 3887

44. Nguyen, S.T. and Grubbs, R.H., *J. Am. Chem. Soc.*, 1993, **115**, 9858

Alkene metathesis: Experimental investigation

5

5.1 INTRODUCTION

The ruthenium carbene complexes developed by the Grubbs group, $RuCl_2PCy_3L(=CHPh)$ (L = PCy_3 (**Gr1**) and L = NHC (**Gr2**)) are among a limited number of well-defined catalytic systems that initiate the metathesis of terminal alkenes.[1-3] These systems are of interest because of their high metathesis activity, stability towards polar functional groups and ease of manipulation.[3-8] The lifetime and reactivity of **Gr1** have been improved through the replacement of one phosphine ligand by a more bulky and basic N-heterocyclic carbene ligand to produce **Gr2**.[9,10] The higher activity of **Gr2** can also be attributed to electronic and steric effects that influence the dissociation of the phosphine ligand as well as the ratio of alkene to phosphine coordination during the mechanistic cycle (see Chapter 6).[11]

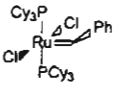

Gr1

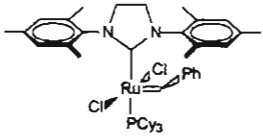

Gr2

A number of manipulations to the Grubbs precatalysts were investigated during this study in an attempt to improve the efficiency of **Gr1** and **Gr2** towards the metathesis of 1-octene. **Figure 5.1** illustrates the various parameters that influence the efficiency of a precatalyst as defined by Grubbs and coworkers.[12] They define 'selectivity' as the ability of a precatalyst to react with certain types of alkenes, 'activity' as the reaction-rate observed with a given precatalyst and 'stability' as the lifetime of the precatalyst during the course of the reaction. The degree of activity can be expressed in terms of the turnover number (TON), while the turnover frequency (TOF in h^{-1}) can be used to describe the overall efficiency of a precatalyst.[13] In this study the effective TON, which is the total number of 1-octene molecules converted to metathesis products per molecule of the precatalysts, was used to describe the degree of activity. This was used in view of the fact that Dinger and Mol[3] pointed out that the total TON of 1-octene couldn't be calculated with any degree of certainty because the metathesis events cannot be accurately followed. The term 'reactivity' will be used to describe the activity of a given precatalyst qualitatively in terms of the mol% PMP formed. 'Selectivity' and 'stability' will be used as described by Grubbs.

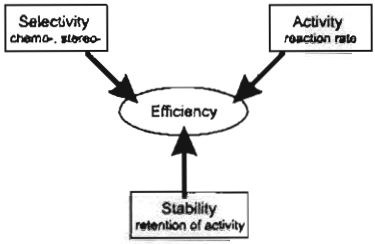

Figure 5.1 Parameters that influence the efficiency of precatalysts.[12]

In this study a number of successfully synthesised O,N-chelated ruthenium carbene complexes (see **Figure 5.2**) were tested for 1-octene metathesis activity at elevated temperatures in the absence of any solvent. ^{1}H NMR studies of the 1-octene metathesis reaction were also done to gain insight into the mechanism of the reaction with the first and second generation Grubbs systems and their hemilabile analogues.

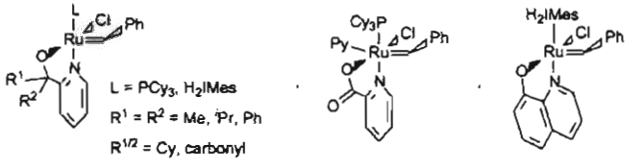

Figure 5.2 O,N-chelating ruthenium carbene complexes investigated for the metathesis of 1-octene.

5.2 METATHESIS OF 1-OCTENE WITH RUTHENIUM CARBENE COMPLEXES

During the metathesis of 1-octene, a mixture of products can form due to alkene isomerisation and metathesis (self- and cross metathesis) reactions, which can occur simultaneously as the reaction proceeds (**Table 5.1**).[14,15] As a result of double bond isomerisation, secondary cross metathesis between the various alkenes can take place yielding a range of C_2 – C_{14} alkene products. Therefore, three major groups of products can be identified, i.e. primary metathesis products (PMP), isomerisation products (IP) and secondary metathesis products (SMP). All the possible side reactions that can occur during the metathesis of 1-octene as a result of cross-metathesis of the isomerisation products are illustrated in Appendix E.

Table 5.1 Possible reactions of 1-octene in the presence of metathesis precatalysts.

Reaction	Substrate[a]	Products[a]	
Primary metathesis			
Self-metathesis	$C=C_7$	$C=C + C_7=C_7$	(PMP)[b]
Isomerisation	$C=C_7$	$C_2=C_6 + C_3=C_5 + C_4=C_4$	(IP)[c]
Secondary metathesis			
Cross-metathesis	$C=C_7 + C_2=C_8$	$C_2=C_7 + C=C_8 + C=C_2 + C_8=C_7$	(SMP)[d]
Self-metathesis	$C_2=C_6$	$C_2=C_2 + C_6=C_6$	

[a] Hydrogens are omitted and geometrical isomers not shown for simplicity.

[b] Primary metathesis products (PMP) refers to the homometathesis products of 1-octene i.e. $C_7=C_7$ and C=C.

[c] Isomerisation products (IP) refers to the double bond isomerisation reaction of terminal to internal alkenes.

[d] Secondary metathesis products (SMP) refers to the metathesis of the isomerisation products of 1-octene.

Initially, the influence of temperature on the catalytic conversion of 1-octene to 7-tetradecene in the presence of **Gr1** and **Gr2** was investigated to provide a benchmark against which the new systems could be evaluated. Additionally, the metathesis of 1-octene in the presence of **Gr1Cy** and **Gr2Cy** was investigated to determine optimum conditions for high reactivity with limited side-reactions. These conditions were applied to the remaining hemilabile complexes and compared to **Gr1** and **Gr2**. Additionally, NMR investigations of the 1-octene metathesis reaction in the presence of **Gr1**, **Gr2**, **Gr1Cy** and **Gr2Cy** were done to gain insight into the mechanism.

5.2.1 Metathesis in the presence of Gr1 and Gr2

5.2.1.1 Optimisation of reaction conditions

The activity of **Gr1** and **Gr2** towards the metathesis of 1-octene was measured at a temperature range of 35 – 80 °C with a 1-octene/Ru molar ratio of 9000. Samples (0.3 mL) were withdrawn by syringe at regular time intervals and quenched with a solution of toluene (0.3 mL) and *tert*-butyl-hydrogen peroxide (2 drops). The reaction mixture was monitored by GC/FID to determine which different products formed during the metathesis of 1-octene; these products were identified by GC/MSD. The initiation rate constants (k_{init}/mol s^{-1}) were determined as a function of the mol 7-tetradecene formed over time. It should be noted that the 1-octene already contained 0.85% 4-octene, 0.10% 3-octene and 0.05% 2-octene which could not be removed from the

reaction mixture. Therefore, the reported IP's exclude the initial isomers present in the reaction mixture, but the cross-metathesis of the irremovable isomers could have contributed to the observed SMP percentages.

During the course of this study, I received different batches of **Gr1** and **Gr2** from the suppliers, which differed in the texture of the precatalyst, i.e.

Batch 1: light-purple (**Gr1_B1**) and light-brown (**Gr2_B1**) fine powder
Batch 2: dark-purple (**Gr1_ B2**) and dark-brown (**Gr2_ B2**) microcrystalline powder

It was interesting to note that different reactivity results were obtained from the two batches, since one should expect the behaviour of the precatalysts to be similar throughout the different batches (see **Table 5.3**).

Tabel 5.3 Catalytic reactivity and selectivity of the two batches Grubbs precatalysts towards the metathesis of 1-octene at 60 °C (1-octene/Ru = 9000, no solvent) after 420 min.

Precatalyst	PMP/%	SMP/%	IP/%	%S[a]	k_{init} (mol s^{-1})
Gr1_B1	39.1	0.7	8.4	81.12	3.78×10^{-5}
Gr1_B2	21.2	0.3	4.8	80.61	4.65×10^{-5}
Gr2_B1	65.0	37.1	0.3	63.48	1.36×10^{-4}
Gr2_B2	81.6	3.6	0.0	95.77	1.89×10^{-4}

[a] Selectivity towards PMP

A decrease in the PMP formation was observed for **Gr1_B2** with a simultaneous decrease in SMP and IP formation compared to **Gr1_B1**. The PMP formation pattern between the **Gr2** batches differed as illustrated in **Figure 5.3**. For batch 1, a drop in reactivity from 75 to 60% was observed after 10 min with a slight increase in reactivity to reach 65% PMP after 7 h. In contrast, batch 2 showed no drop in activity after reaching 75% PMP formation within 10 min. A similarly slow continuous increase in activity was observed in which 81% PMP's were obtained after 7 h. The drop in reactivity for **Gr2_B1** might be attributed to secondary metathesis reactions occurring as the reaction proceeds. A dramatic decrease in SMP formation from 36 to 4% was observed in the presence of **Gr2_B2**, with no IP formation. Although the IP formation in the presence of **Gr2_B1** is negligibly small, it was noted that there was an increase in IP formation to a maximum of 0.8% after an initial induction period of 15 min, followed by a slow decrease to 0.3% (see **Figure 5.4**). The IP formation contributed to the SMP formation due to cross-metathesis of the IP's.

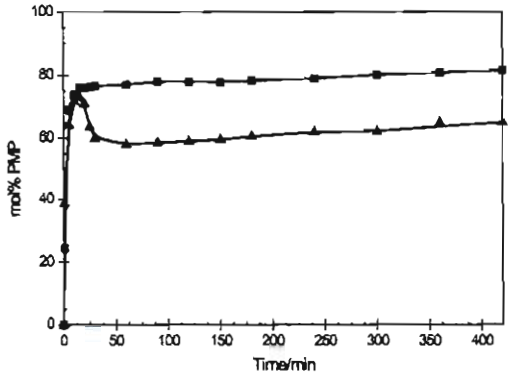

Figure 5.3 PMP formed during the metathesis of 1-octene in the presence of the different batches Gr2 at 60 °C.
[▲ Gr2_B1 ■ Gr2_B2]

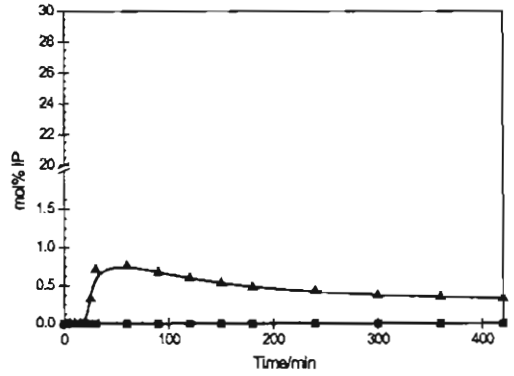

Figure 5.4 IP formed during the metathesis of 1-octene in the presence of the different batches Gr2 at 60 °C.
[▲ Gr2_B1 ■ Gr2_B2]

All further investigations were carried out with Batch 2 precatalysts, since only a limited amount of the first batch was initially available, and lower SMP and IP formations were obtained with the second batch of precatalysts. For simplicity, **Grl_B2** and **Gr2_B2** will be referred to as **Grl** and **Gr2**, respectively, in the following sections. The influence of reaction temperature on the metathesis of 1-octene in the presence of **Grl** and **Gr2** are illustrated in **Figure 5.5** to **5.7** and **Figure 5.8** to **5.10**, respectively. **Table 5.4** summarises the catalytic activity and selectivity of these systems over a temperature range of 35 – 80 °C. As illustrated in **Figure 5.5** and **5.8**, not only the reaction rate, but also the lifetime of the precatalyst is influenced by temperature, since at temperatures above 35 °C, both systems are inactive for PMP formation after *ca.* 15 min. According to Forman et al.,[16] **Grl** is usually intolerant of reaction temperatures above 50 °C, leading to a shorter lifetime of the precatalyst. A similar trend was observed in this study as illustrated in **Figure 5.5**. At temperatures above 35 °C, a maximum of only 20% PMP's was formed within 5 min, relative to 40% formed at 35 °C over a time period of 180 min. This indicates that an increase in temperature decreases the lifetime of **Grl**, most likely due to catalyst decomposition and/or competing side reactions. The shape of the curves in **Figure 5.5** and **5.8** reveals important information concerning the reaction mechanism of **Grl**- and **Gr2**-catalysed alkene metathesis. At temperatures above 35 °C, an initial period of high activity is observed for both catalytic systems within the first 10 min to produce 20% and 80% PMP, respectively. After this period, the reaction rate slows down dramatically and continues to completion at a much slower rate within 7 h. Regardless of the initial induction period of **Gr2** at temperatures below 40 °C, which is consistent with slower precatalyst initiation, a higher degree of reactivity is displayed relative to **Grl**, i.e. 61% relative to 41% PMP after 420 min.

Tabel 5.4 Catalytic activity and selectivity of **Grl** towards the metathesis of 1-octene at 35 – 80 °C (1-octene/Ru = 9000, no solvent) after 420 min.

Precatalyst	T/°C	PMP/%	SMP/%	IP/%	%S[a]	k_{init} (mol s^{-1})	TON
Grl	35	40.8	0.3	0.4	98.31	1.24×10^{-5}	4136
	60	21.2	0.3	4.8	80.61	4.65×10^{-5}	2175
	70	18.6	0.3	8.7	67.39	6.37×10^{-5}	2020
	80	20.5	0.3	25.3	44.47	7.41×10^{-5}	2056
Gr2	35	60.8	1.3	0.0	97.91	2.40×10^{-5}	6601
	60	81.6	3.6	0.0	95.77	1.89×10^{-4}	8881
	70	82.2	11.3	0.0	87.91	3.08×10^{-4}	8929
	80	78.8	12.8	0.1	85.93	3.68×10^{-4}	8988

[a] Selectivity towards PMP

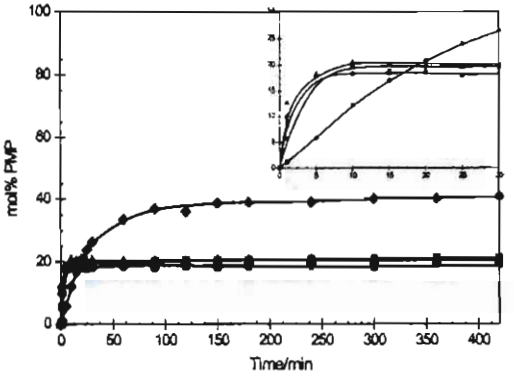

Figure 5.5 PMP formed during the metathesis of 1-octene in the presence of **Gr1** at various temperatures (enlarged inset of the first 30 min).
[◆ 35 °C ■ 60 °C ● 70 °C ▲ 80 °C]

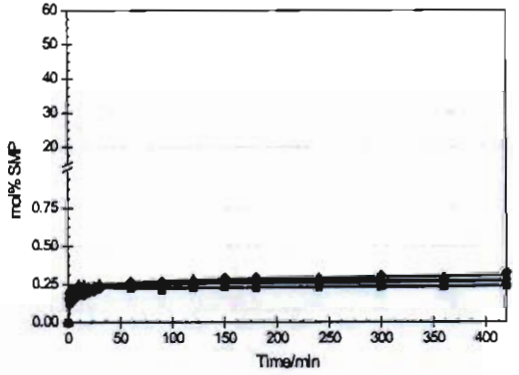

Figure 5.6 SMP formed during the metathesis of 1-octene in the presence of **Gr1** at various temperatures (break inserted between 1 and 20 mol% SMP).
[◆ 35 °C ■ 60 °C ● 70 °C ▲ 80 °C]

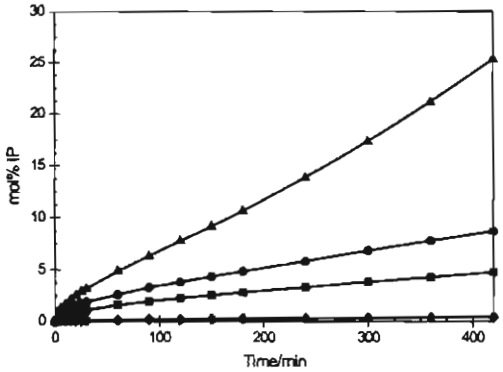

Figure 5.7 IP formed during the metathesis of 1-octene in the presence of Gr1 at various temperatures.
[◆ 35 °C ■ 60 °C ● 70 °C ▲ 80 °C]

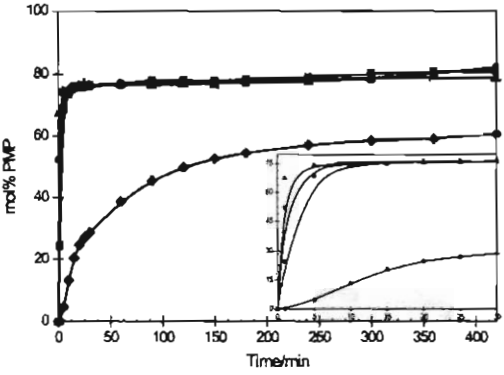

Figure 5.8 PMP formed during the metathesis of 1-octene in the presence of Gr2 at various temperatures (enlarged inset of the first 30 min).
[◆ 35 °C ■ 60 °C ● 70 °C ▲ 80 °C]

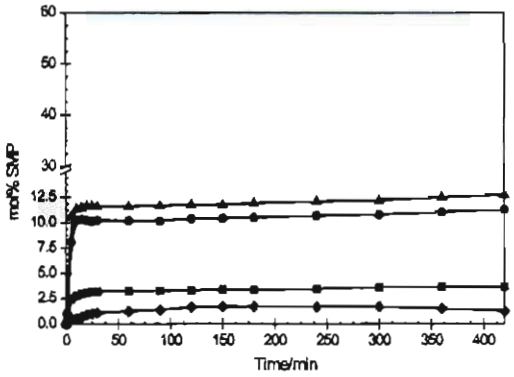

Figure 5.9 SMP formed during the metathesis of 1-octene in the presence of **Gr2** at various temperatures (break inserted between 15 and 30 mol% SMP).
[◆ 35 °C ■ 60 °C ● 70 °C ▲ 80 °C]

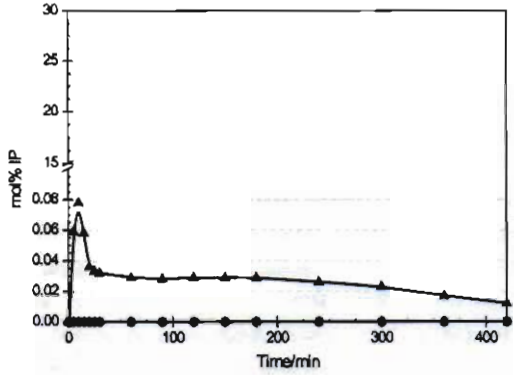

Figure 5.10 IP formed during the metathesis of 1-octene in the presence of **Gr2** at various temperatures (break inserted between 1 and 15 mol% IP).
[◆ 35 °C ■ 60 °C ● 70 °C ▲ 80 °C]

All reactions carried out at temperatures above 60 °C only produced a maximum of 20% PMP's for **Gr1** and 80% for **Gr2**. A TON of 6601 for **Gr2**, relative to 4136 for **Gr1** at 35 °C, indicates that **Gr2** exhibits superior activity over **Gr1**. Increasing the reaction temperature from 35 to 60 °C sharply decreases the activity and selectivity of **Gr1** towards the formation of PMP (see **Figure 5.11**). In contrast, **Gr2** showed a steady increase in PMP formation up to 70 °C with a decrease in reactivity when the temperature increased above 70 °C (see **Figure 5.11**). Although a steady increase in the TON was observed for **Gr2** at elevated temperatures with a steady decrease in selectivity, a sharp reduction in both selectivity and TON was noted for **Gr1** at temperatures above 60°C (**Table 5.4**). This supports the fact that the replacement of one PCy_3 with an NHC ligand has improved the activity, selectivity and stability of **Gr1**. The relative stability of the precatalysts at different temperatures can be illustrated by plotting ln([1-octene]) as a function of time.[12] According to Grubbs et al.,[12] the curvature of the logarithmic plot is indicative of pseudo first-order rate kinetics (linear plot) or decomposition of the precatalyst over the course of the reaction. Graphical representations of the stability of **Gr1** and **Gr2**, respectively, are illustrated in **Figure 5.12** and **5.13** for the first 120 min of the reaction. At temperatures above 35 °C, the stability of **Gr1** and **Gr2** is sharply reduced, since both systems already start to decompose within the first 10 min with a temperature increase of 10 – 25 °C. The reduced stability of these systems at high temperatures prevents high efficiency due to increased IP and SMP formation. It is known that alkene isomerisation is a major side-reaction of ruthenium catalysed metathesis reactions.[2,17-21] In contrast to findings of Lehman et al.,[2] **Gr1** significantly promotes the isomerisation of terminal alkenes at temperatures above 50 °C with a 1-octene/Ru molar ratio of *ca.* 9000. An exponential increase in IP, with no significant SMP formation (see **Figure 5.14** and **5.15**), was observed during the metathesis of 1-octene in the presence of **Gr1** as the temperature increased. Lehman's observation was made at a 1-octene/Ru molar ratio of 1000, where he noted that only **Gr2** promoted the isomerisation of 1-octene at a temperature of 50 – 60 °C. In contrast, at low **Gr2**-concentrations a linear increase in SMP formation was observed with an increase in temperature, with no significant IP's present in the reaction mixture. This indicates that the isomers are immediately consumed for cross-metathesis reactions. It was also noted that, in the presence of **Gr2** at 80 °C, the mol% IP increases to a maximum within the first 10 min, followed by a sharp decrease to *ca.* 0% within 30 min as the reaction proceeded (**Figure 5.10**), most probably due to cross-metathesis of the IP's to form SMP's. It is known that **Gr1** and **Gr2** are thermally decomposed to hydride species.[19] In this study Argon was used as inert gas, which is known to contain trace amounts of oxygen as contaminants (§ 3.1.2.4). In the presence of oxygen, **Gr1** and **Gr2** can form a carbonyl species (**56** and **57**), which is converted to the corresponding hydride species (**58** and **59**) upon reaction with a terminal alkene.[22] This could be the cause of the isomerisation of 1-octene through a hydride mechanism.[2,17-20] Therefore, this study indicates that **Gr1** is catalytically active for the isomerisation of terminal alkenes at high temperatures even at low precatalyst concentrations, while SMP formation is limited. On the other hand, at low **Gr2**-

concentrations, cross-metathesis occurs concurrently with the isomerisation of 1-octene, since no significant IP's were observed.

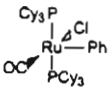

56

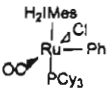

57

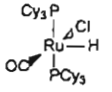

58

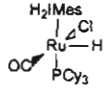

59

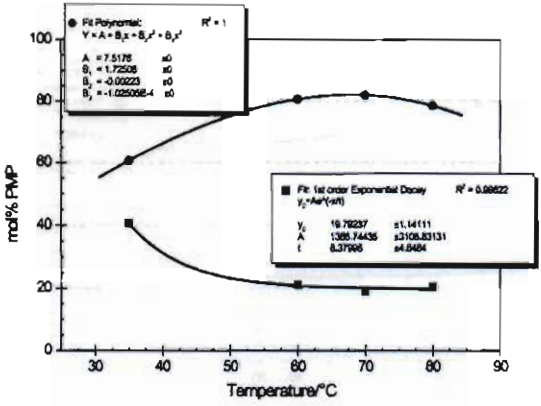

Figure 5.11 The observed trend for the mol% PMP with an increase in reaction temperature during the metathesis of 1-octene in the presence of precatalysts **Gr1** and **Gr2** after 420 min.
[■ Gr1, ● Gr2]

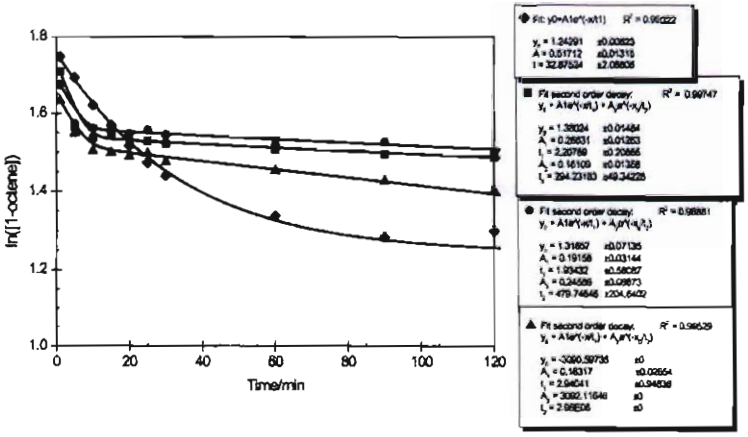

Figure 5.12 Logarithmic plot of Gr1 to describe its relative stability as a function of time.
[◆ 35 °C ■ 60 °C ● 70 °C ▲ 80 °C]

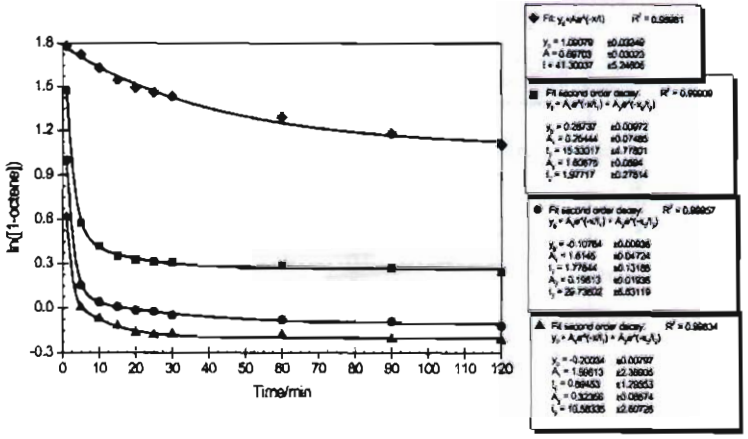

Figure 5.13 Logarithmic plot of Gr2 to describe its relative stability as a function of time.
[◆ 35 °C ■ 60 °C ● 70 °C ▲ 80 °C]

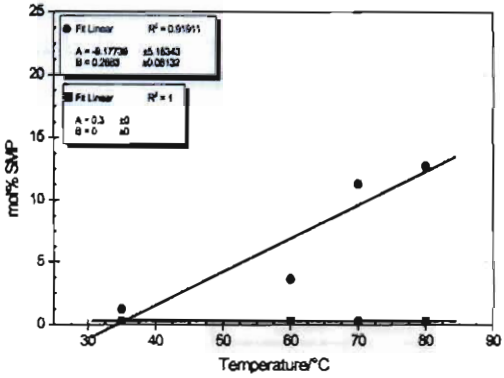

Figure 5.14 A linear increase in the mol% SMP with an increase in temperature during the metathesis of 1-octene in the presence of precatalysts **Gr1** and **Gr2** after 420 min.
[■ Gr1 ● Gr2]

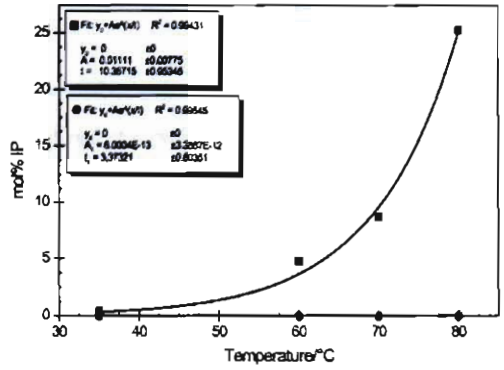

Figure 5.15 An exponential increase in the mol% IP with an increase of temperature during the metathesis of 1-octene in the presence of precatalysts **Gr1** and **Gr2** after 420 min.
[■ Gr1 ● Gr2]

The rate of initiation (k_{init}/mol s^{-1}) for the formation of 7-tetradecene increased linearly with temperature for both catalytic systems (**Figure 5.16**). The sharp increase in the slope of the curve for **Gr2** i.e. 9.82 x 10^{-6} (mol s^{-1} K^{-1}) relative to 1.70 x 10^{-6} (mol s^{-1} K^{-1}) for **Gr1**, indicates that **Gr2** is catalytically more active than **Gr1** at elevated temperatures.

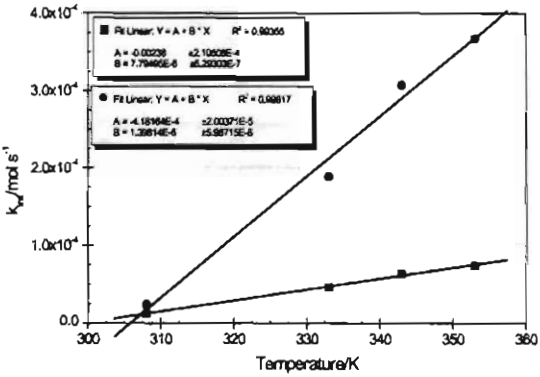

Figure 5.16 Linear increase in k_{init} as a function of temperature.
{■ Gr1 ● Gr2}

It is well known that the Arrhenius equation (Equation 5.1) can be used to describe the temperature dependence of the first-order rate constant, k, for determining the activation energy (E_a).

$$\ell n\, k = \ell n\, A - \frac{E_a}{RT} \qquad \text{(Eq. 5.1)}$$

with *k* the measured first-order rate constant, E_a the experimental activation energy, A the pre-exponential factor, R the gas constant and T the temperature. The two units, E_a and A, are known as the Arrhenius parameters. The rate constants of a reaction can be predicted from the Arrhenius equation at a specific temperature if a linear graph is obtained for *ln k* as a function of 1/T. According to Frost et al.,[22] there are situations where a nonlinear curve is obtained for the Arrhenius plot, in which two competing reactions with different activating energies may occur

simultaneously. This results in a curve with two parts, with each part approaching linearity as illustrated in **Figure 5.17**. The graph representing the rate constants in the Arrhenius equation for **Gr1** and **Gr2** is given in **Figure 5.18**. Although both graphs are curved in an opposite direction to the illustrated graph in **Figure 5.17**, similar conclusions can be made. It is evident from the experimental results that SMP and/or IP formation is a major competing reaction occurring at temperatures above 70 °C for both **Gr1** and **Gr2**, with PMP formation limited. This supports the shape of the graphs in **Figure 5.18**, in which two parts are identified, both approaching linearity. This indicates that, at high temperatures, the competing side-reactions are significantly influencing the activity and selectivity of the precatalyst. Therefore, if you look at the first part of the graph, excluding the data at temperatures above 70 °C, a linear graph is obtained in which the side-reactions are negligibly small (**Figure 5.19**). From the data in **Table 5.4**, the activation energy was calculated as 42.03 kJ mol^{-1} for **Gr1**, and 65.33 kJ mol^{-1} for **Gr2** with a pre-exponential factor of 1.70 x 10^2 min^{-1} and 2.98 x 10^6 min^{-1}, respectively. The second part of the graph in **Figure 5.18** was not considered further, since insufficient information was available to obtain E_a values.

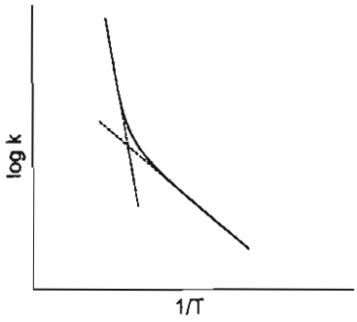

Figure 5.17 Graphical representation of a nonlinear curve for the Arrhenius plot.[22]

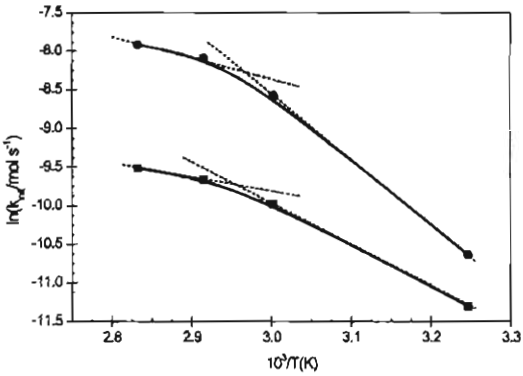

Figure 5.18 Arrhenius plot for the 1-octene metathesis reaction in the presence of **Gr1** and **Gr2**.
[■ Gr1 ● Gr2]

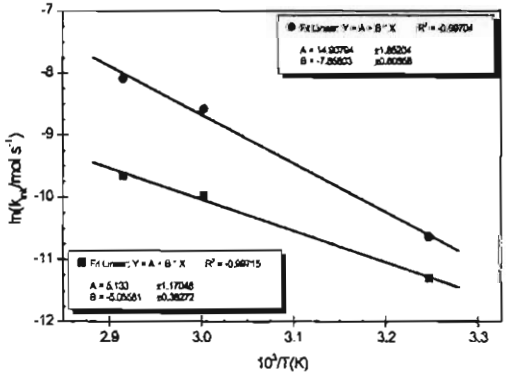

Figure 5.19 Arrhenius plot for the 1-octene metathesis reaction in the presence of **Gr1** and **Gr2**, with the exclusion of T = 80 °C.
[■ Gr1 ● Gr2]

5.2.1.2 NMR investigation

I investigated the metathesis of 1-octene in the presence of **Grl** and **Gr2** with ^{1}H NMR to gain some insight into the reaction mechanism. The ^{1}H NMR spectra obtained during these investigations are presented in Appendix F.

NMR investigation: metathesis with Grl

The metathesis of 1-octene was investigated in the presence of **Grl** at 30 °C and 50 °C in $CDCl_3$, with a 1-octene/Ru molar ratio of 10. P van Helden[23] investigated the reaction at 30 °C as part of his honours study in 2004 in support of the current study. The involvement of the three carbene species are clearly illustrated in **Figure 5.20** for the reaction at 30 °C. The H_α signal (denoted H*) of the benzylidene **Grl** appears at δ 20.02 ppm, of the heptylidene $[RuCl_2(PCy_3)_2(=CHC_6H_{13})]$ at δ 19.31 ppm and the methylidene $[RuCl_2(PCy_3)_2(=CH_2)]$ at δ 18.95 ppm. The shift of the H_α peak of the benzylidene to lower field to produce a doublet and a singlet is due to the change in the electronic environment of the ligand attached to the carbene carbon. Due to the fast initiation rate ($9.6 \pm 0.2\ s^{-1}$)[24] of **Grl** during the metathesis reaction, all three carbene signals are already present after 14 min. The change in the size of the H_α signals of the three carbene species involved in the metathesis of 1-octene with time is given in **Figure 5.21**. The size of the benzylidene signal gradually decreases (**Figure 5.21(a)**), suggesting the conversion of the benzylidene to the heptylidene and methylidene; after 300 min all of the **Grl** has been converted (see also **Figure 5.20**).

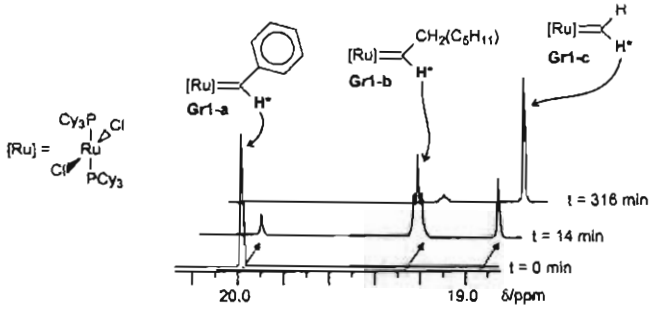

Figure 5.20 ^{1}H NMR spectra of the carbene proton region at different time intervals of a 1-octene/**Grl** reaction mixture in $CDCl_3$ at 30 °C.

(a) δ = 20.015 ppm

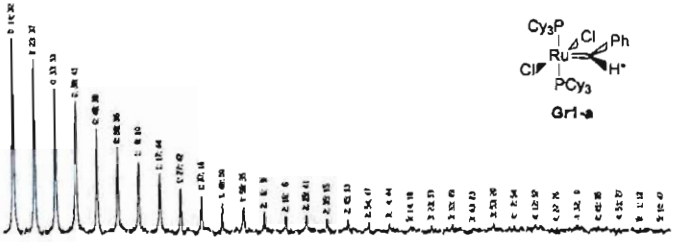

(b) δ = 19.310 ppm

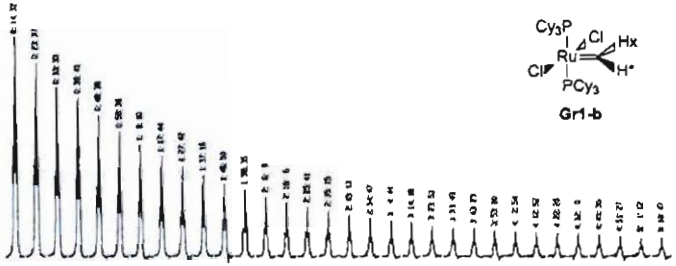

(c) δ = 18.954 ppm

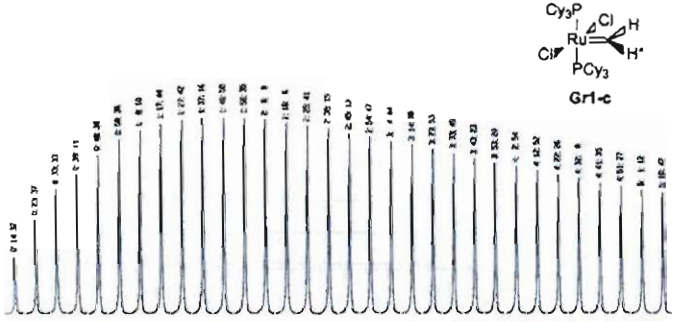

Figure 5.21 ^{1}H NMR signals at different time intervals of the H_α's in a 1-octene/Grl reaction mixture in $CDCl_3$ at 25 °C.

[(a) Ru=CHPh, (b) Ru=CHHx, (c) $Ru=CH_2$]

The simultaneous decomposition of the benzylidene to some other species cannot be ruled out. The sharp increase to a maximum of the heptylidene signal within 14 min is followed by a gradual decrease as the reaction proceeds (**Figure 5.21(b)**), while the methylidene signal gradually increases to a maximum within 2 h, followed by a slow decrease (**Figure 5.21(c)**), possibly due to catalyst decomposition. In the presence of 1-octene, it seems that the benzylidene is rapidly converted to the heptylidene, while the formation of the methylidene proceeds at a much slower rate at 30 °C. Ulman et al.[25] also observed that the alkylidene is generally more reactive in comparison to the methylidene in the metathesis of alkenes with **Grl**.

The reaction was also performed at 50 °C to determine the influence of temperature on the formation of the individual carbene species. The involvement of the three carbene species is illustrated in **Figure 5.22**. As noted, an additional 7 min was needed to obtain the first spectrum at 50 °C, in comparison to 30 °C, to allow for temperature stabilisation of the cold sample inserted into a warm sample tube. It appeared that the benzylidene was more rapidly converted to the methylidene and heptylidene within 20 min at 50 °C in comparison to 30 °C. The change in the size of the H_α signals of the three carbene species involved in the metathesis of 1-octene at 50 °C over time is given in **Figure 5.23**. No benzylidene signal is present after 20 min at the time of obtaining the first spectrum (**Figure 5.23(a)**), suggesting a rapid conversion of the benzylidene to the heptylidene and methylidene (see also **Figure 5.22**).

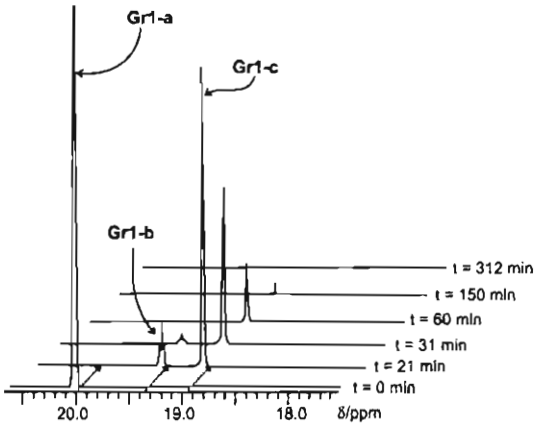

Figure 5.22 ^{1}H NMR spectra of the carbene proton region at different time intervals of a 1-octene/**Grl** reaction mixture in $CDCl_3$ at 50 °C.

The simultaneous decomposition of the benzylidene to some other species cannot be ruled out. The sharp increase to a maximum of the heptylidene and methylidene signal within 20 min is followed by a sharp decrease of the heptylidene to a minimum within 10 min, while the methylidene gradually decreases as the reaction proceeds (**Figure 5.23(b)** and **(c)**). After 300 min, no carbene species are present any more. **Figure 5.24** illustrates the change in the peak integration values of the individual carbene species as a function of time. Due to the fact that 20 min have passed before the first spectrum was obtained and the fast initiation rate of **Gr1**, no substantial conclusions can be made regarding the identity of the initial carbene species that formed during the reaction.

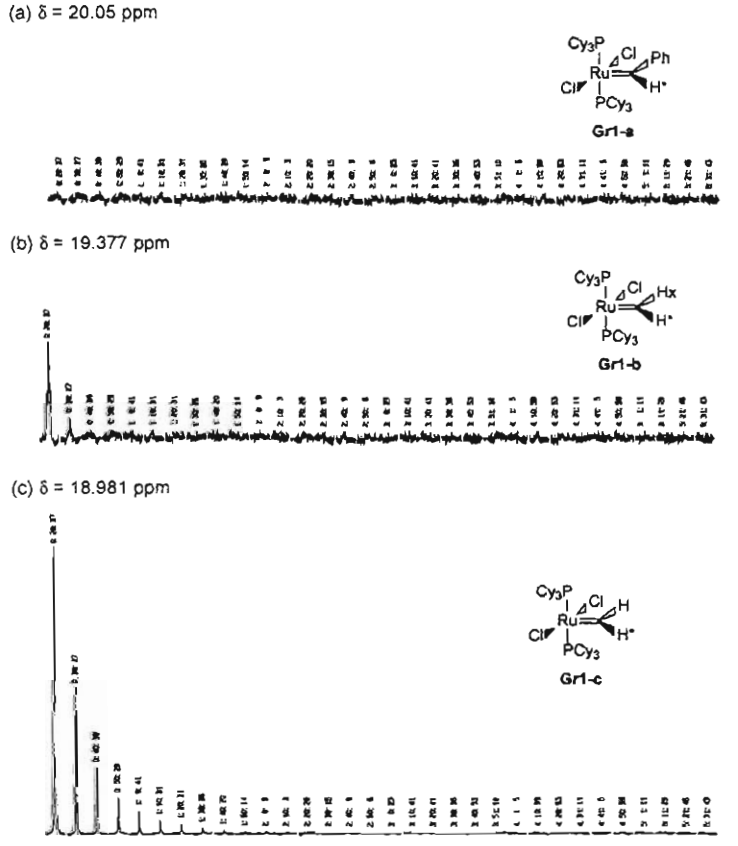

Figure 5.23 ^{1}H NMR signals at different time intervals of the carbene α-H's in a 1-octene/**Gr1** reaction mixture in $CDCl_3$ at 50 °C.

[(a) Ru=CHPh, (b) Ru=C**H**C_6H_{13}, (c) Ru=CH_2].

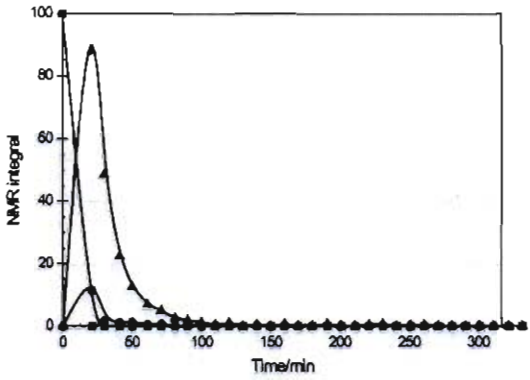

Figure 5.24 The ^{1}H NMR peak integration values of the carbenes involved in the metathesis reaction of 1-octene in the presence of **Gr1** at 50 °C.
[■ δ 20.05 ppm, ● δ 19.38 ppm, ▲ δ 18.98 ppm]

NMR investigation: metathesis with Gr2

The metathesis of 1-octene was investigated in the presence of **Gr2** at 50 °C in $CDCl_3$, with a 1-octene/Ru molar ratio of 10. Contrary to the reaction in the presence of **Gr1**, an additional carbene signal was observed at δ 18.55 ppm (**Figure 5.25**). Mtshatsheni[26] made a similar observation during an NMR investigation of the 1-octene metathesis reaction with 1-octene/**Gr2** = 5 at 25 °C. However, the multiplicity of the split of this signal could not be visually determined and therefore she made no conclusions with regards to the identity of the carbene species.

The H_α signal (denoted H*) of the benzylidene **Gr2** appears at δ 19.21 ppm (singlet), of the heptylidene $[RuCl_2(PCy_3)(H_2IMes)(=CHC_6H_{13})]$ at δ 18.72 ppm (triplet) and the methylidene $[RuCl_2(PCy_3)(H_2IMes)(=CH_2)]$ at δ 17.83 ppm (singlet). The additional carbene signal appears at δ 18.55 ppm (quartet or doublet of doublets). The question arises: is the additional signal a quartet or a doublet of doublets? Since a high degree of isomerisation and secondary metathesis occurs at high concentrations of **Gr2** at elevated temperatures,[2] the appearance of a quartet can be due to the formation of an ethylidene (**60**) and hexylidene (**61**) from 2-octene. The chemical shift of the hexylidene and heptylidene will be similar, since the alkyl chain will not greatly influence the shift of the H_α, while a quartet will appear for the ethylidene H_α. In contrast, a doublet of doublets will imply that a tertiary carbon has to be present in the form illustrated in **62**.

The formation of such a complex is difficult to visualise, since it implies the cyclisation of the alkyl chain of the heptylidene moiety to form **62**. Therefore by reason of the improbability of cyclisation of the alkyl chain occurring and assigning a likely peak intensity ratio of 1:3:3:1 to the signal, a split multiplicity of quartet is assigned to the signal at δ 18.55 ppm.

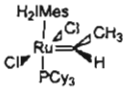

60

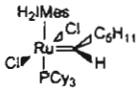

61

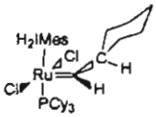

62

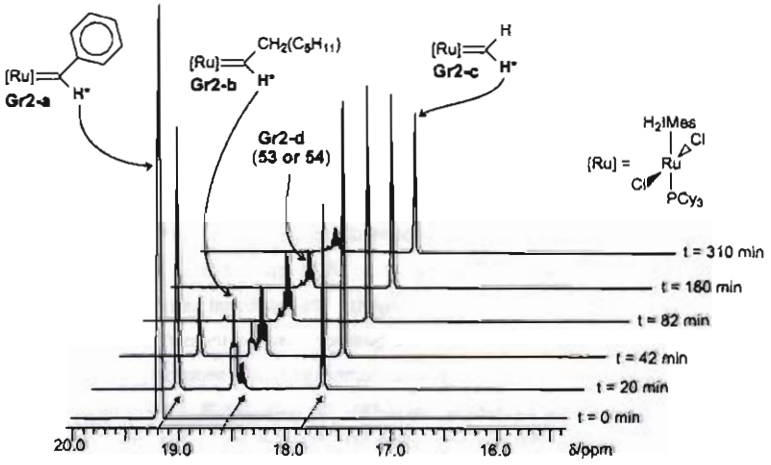

Figure 5.25 ^{1}H NMR spectra of the carbene proton region at different time intervals of a 1-octene/**Gr2** reaction mixture in $CDCl_3$ at 50 °C.

Figure 5.26 illustrates the change in peak integration values for the benzylidene and methylidene species as a function of time. Due to difficulties in separating the triplet and quartet, only a visual plot of the signals could be obtained without integration (see **Figure 5.27(b)**). The plot of the signals at δ 18.72 – 18.46 was differently compiled than the others in order to distinguish between the two signals and to expand the region. The change in the size of the H_α signals of the four carbene species involved in the metathesis of 1-octene in the presence of **Gr2** at 50 °C over time is given in **Figure 5.27**. The size of the benzylidene signal decreases sharply to a minimum within 80 min (**Figure 5.27(a)**); after 90 min all of the **Gr2** has been converted (see also **Figure 5.25**). The simultaneous decomposition of the benzylidene to some other species cannot be ruled out. The methylidene signal increases to a maximum within 40 min, followed by a slow decrease (**Figure 5.27(c)**). From the results obtained by Mtshatsheni,[26] it is noted that, at room temperature, the triplet increases to a maximum within 1 h, followed by a very slow decrease, while after approximately 2 h, an additional carbene signal starts to form. An increase in reaction temperature caused the quartet to sharply increase to a maximum within 60 min, followed by a slow decrease (**Figure 5.27(b)**), while an initial sharp increase to a maximum of the triplet signal within 20 min was followed by a gradual decrease as the reaction proceeded (**Figure 5.27(b)**).

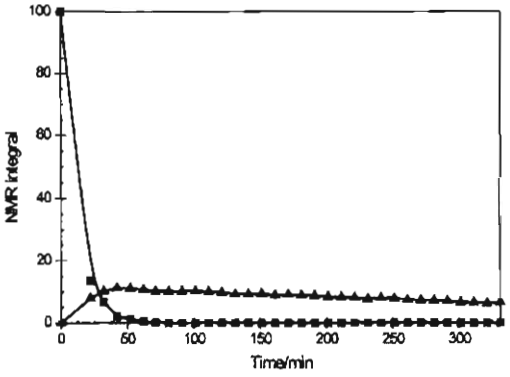

Figure 5.26 The ^{1}H NMR peak integration values of the carbenes involved in the metathesis reaction of 1-octene in the presence of **Gr2** at 50 °C.
[■ δ 19.21 ppm, ▲ δ 18.83 ppm]

(a) δ = 19.21 ppm

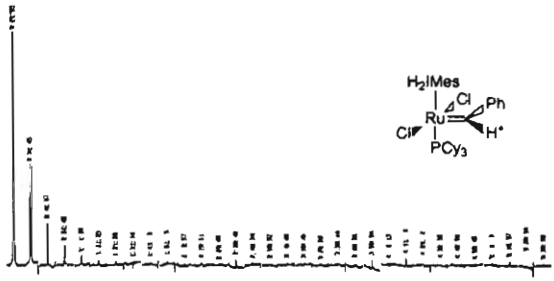

(b) δ = 18.72 – 18.46 ppm

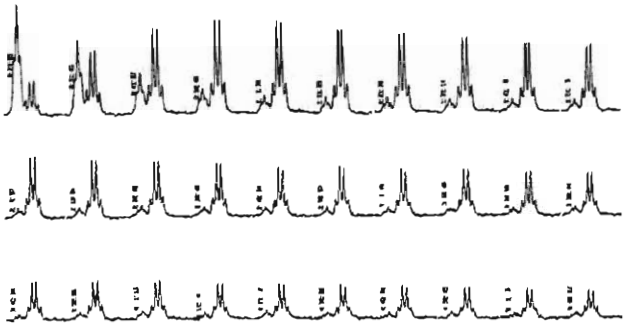

(c) δ = 17.83 ppm

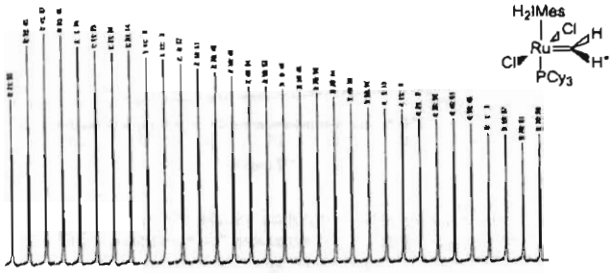

Figure 5.27 ^{1}H NMR signals at different time intervals of the carbene α-H's in a 1-octene/**Gr2** reaction mixture in $CDCl_3$ at 50 °C.

[(a) Ru=CHPh, (b) Ru=CHC$_6$H$_{13}$, (c) Ru=CH$_2$]

5.2.2 Metathesis of 1-octene in the presence of Gr1Cy and Gr2Cy

The following section determines the optimum temperature and 1-octene/Ru molar ratio at which the hemilabile complexes would give high activity, while retaining a high degree of selectivity towards PMP with a limited amount of SMP and IP formation. It was decided to benchmark the **Gr1Cy** and **Gr2Cy** systems, which are analogous to those reported by Denk et al.[28] (**14**) and Van der Schaaf et al.[29] (**15**) for RCM and ROMP reactions, differing in ligand L which is attached to the Ru-centre. Investigations on the self- or cross-metathesis of linear alkenes with these types of systems, to my knowledge, have not been reported in the last decade. However, we have recently published our findings on the self-metathesis of 1-octene with **Gr1Cy** and **Gr2Cy**.[15]

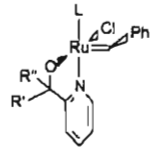

L = PCy_3, R'-R'' = $(CH_2)_5$ **(14a)**

L = 

R' = R'' = Me; R''' = Cy **(14b)**
R' = R'' = Me; R''' = CH_2CH_2Ph **(14c)**
R'-R'' = $(CH_2)_5$; R''' = CH_2CH_2Ph **(14d)**
R'-R'' = $(CH_2)_6$; R''' = Cy **(14e)**

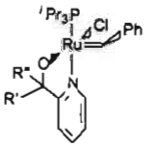

R' = R'' = Me **(15a)**
R' = R'' = Me **(15b)**
R'-R'' = $(CH_2)_5$ **(15c)**
R'-R'' = $(CH_2)_5$ **(15d)**

5.2.2.1 Optimisation of reaction conditions

It has been reported that the phosphine and NHC based ruthenium carbene systems with an O,N-chelating ligand are not very active for RCM and ROMP metathesis reactions at room temperature.[8,26,29] As a result, experiments were carried out at temperatures ranging from 35 – 80 °C to determine the effect of temperature on the 1-octene metathesis activity and selectivity of **Gr1Cy** and **Gr2Cy** at a 1-octene/Ru molar ratio of 9000. Both **Gr1Cy** and **Gr2Cy** showed a rather low activity for the metathesis of 1-octene at 35 °C, i.e. approximately 10% and 3% PMP after 420 min, respectively. It was, however, noted that, at temperatures above 35 °C, **Gr2Cy** only dissolved after 15 min in the 1-octene, while the reaction mixture at 35 °C remained murky for the duration of the reaction. **Gr1Cy** dissolved within a few minutes in the 1-octene at 35 °C. This might suggest that, at low temperatures, **Gr2Cy** might rather act as a heterogeneous catalyst.

Table 5.5 summarises the catalytic activity and selectivity of **Gr1Cy** and **Gr2Cy** towards the metathesis of 1-octene over a temperature range of 35 – 80 °C. Although a linear increase in the activity of **Gr1Cy** towards the formation of PMP was observed with an increase in temperature, an exponential increase in IP and SMP was noted (see **Figure 5.28** to **5.30**). In contrast, **Gr2Cy** shows a sharp increase in PMP formation up to 70 °C, with an even sharper decrease in activity when the temperature increases above 70 °C, with an exponential increase in SMP (see **Figure 5.28** to **5.30**).

The major SMP products were found to be nonene (C_9) and tridecene (C_{13}) for both systems. A 5% and 2.5% increase in C_{13} and C_9 was, respectively, observed for **Gr1Cy** with a 45 °C increase in temperature, while the combined contribution of the other SMP products was increased by 0.5%. An increase in temperature from 35 to 70 °C for **Gr2Cy** resulted in a 20% increase in C_{13}, together with a 15% increase in C_9, with the other SMP products contributing 2% to the total SMP's. It was interesting to note that a further increase of 10 °C for **Gr2Cy** resulted in an additional 20% increase in C_{13}, while C_9 only increased to a maximum of 10% within the first 10 min, followed by a slow decrease to 2%. The observed increase in undecene (C_{12}) to 12% could be a result of cross metathesis between the isomers of C_9, which would explain the observed decline. The presence of 1-propene and 1- and 2-butene was explicitly noted in the reaction samples of **Gr2Cy** at 80 °C; identified by GC/MSD (**Chromatogram 5.1**), while to a lesser degree for both systems at the lower temperatures. These products were not as explicitly observed in the **Gr1**- and **Gr2**-catalysed 1-octene metathesis reaction samples in comparison to **Gr2Cy**. Janse van Rensburg et al.[18] has recently shown that the formation of propene during the metathesis of ethene in the presence of the methylidene intermediates of **Gr1** or **Gr2** species can cause irreversible substrate-induced decomposition of the Ru=C functionality (**Scheme 5.1**). Therefore, the reaction of the methylidene intermediate of **Gr2Cy** with the liberated ethene during the metathesis of 1-octene might lead to the formation of 1-propene and 1- and 2-butene according to the proposed substrate-induced decomposition route. Alternatively, the formation of propene and 1- and 2-butene by cross-metathesis of 1- and 2-octene, followed by the isomerisation of 1-butene (by reversible allyl-hydride formation),[21] cannot be excluded.

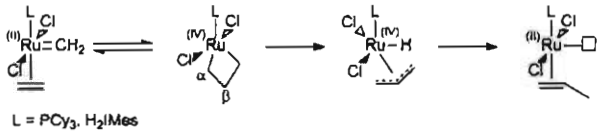

Scheme 5.1 Substrate-induced catalyst decomposition during ruthenium-catalysed alkene metathesis.[18]

Table 5.5 Catalytic activity and selectivity of **Gr1Cy** and **Gr2Cy** towards the metathesis of 1-octene at 35 - 80 °C (1-octene/Ru = 9000, no solvent) after 420 min.

Precatalyst	T/°C	PMP/%	SMP/%	IP/%	%S[a]	k_{init} (mol s^{-1})	TON
Gr1Cy	35	10.2	0.1	0.0	98.67	5.48×10^{-6}	1143
	60	53.2	0.4	0.5	98.34	2.06×10^{-5}	5907
	70	59.6	1.2	1.5	95.97	5.55×10^{-5}	6652
	80	90.3	8.1	2.2	89.80	6.39×10^{-5}	10119
Gr2Cy	35	3.3	0.6	0.0	85.40	6.00×10^{-6}	379
	60	81.1	12.9	0.0	86.28	5.19×10^{-6}	9214
	70	91.8	26.1	0.0	77.83	1.35×10^{-5}	10428
	80	59.9	58.5	0.3	50.46	2.82×10^{-5}	6811

[a] Selectivity towards PMP

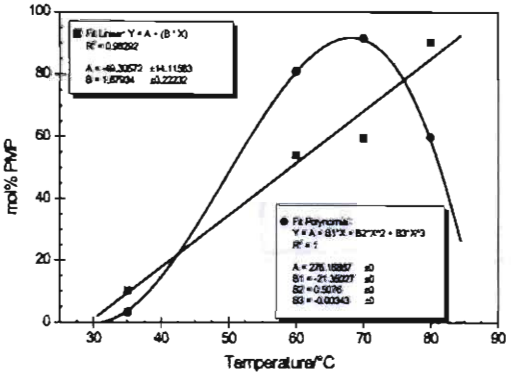

Figure 5.28 The observed trend for the mol% PMP with an increase of temperature during the metathesis of 1-octene in the presence of precatalysts **4a** and **7** after 420 min.
[■ Gr1Cy ● Gr2Cy]

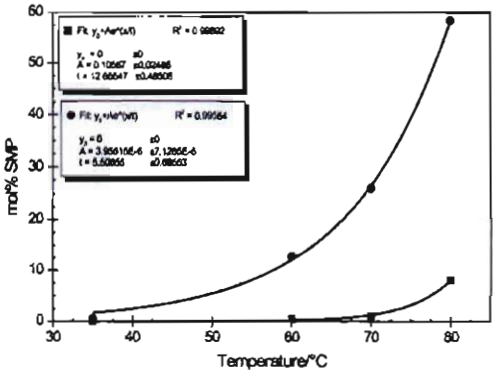

Figure 5.29 An exponential increase in the mol% SMP with an increase in temperature during the metathesis of 1-octene in the presence of precatalysts **Gr1Cy** and **Gr2Cy** after 420 min.
[■ **Gr1Cy** ● **Gr2Cy**

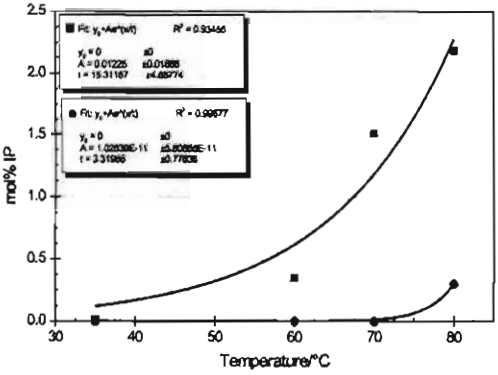

Figure 5.30 An exponential increase in the mol% IP with an increase of temperature during the metathesis of 1-octene in the presence of precatalysts **Gr1Cy** and **Gr2Cy** after 420 min.
[■ **Gr1Cy** ● **Gr2Cy**]

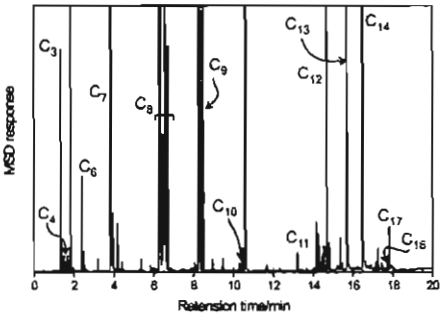

Chromatogram 5.1 GC/MSD chromatogram of the reaction mixture of 1-octene in the presence of **Gr2Cy** at 80 °C after 3 h (No solvent, 1-octene/Ru = 9000, detector off between 5.4 - 5.8 min to exclude toluene, MSD response enlarged, only alkene products labelled – see Chapter 3 for identity of the other products).

It was also noted, that in the presence of **Gr1Cy**, the mol% IP increases to a maximum within the first 10 min, followed by a sharp decrease to *ca.* 0% within 30 min as the reaction proceeds (**Figure 5.31**), most probably due to cross metathesis of the IP's to form SMP's. Although a steady increase in the TON was observed for both **Gr1Cy** and **Gr2Cy** at elevated temperatures, a sharp reduction in the selectivity and TON was noted for **Gr2Cy** at temperatures above 70°C (**Table 5.5**).

The optimum working temperature whereby both catalytic systems gave high activity while retaining a high degree of selectivity towards PMP, with a limited amount of SMP and IP formation, was found to be 60 °C.

The influence of temperature on the relative stability of **Gr1Cy** and **Gr2Cy** are illustrated in **Figure 5.32** and **Figure 5.33**, respectively, as a result of plotting ln([1-octene]) as a function of time. For both systems, a linear plot is obtained at 35 °C as well as at 60 °C for **Gr2Cy**, indicating pseudo first-order rate kinetics over the course of the reaction. The very slight curvature in the logarithmic plot for **Gr1Cy** at temperatures above 35 °C indicates that the precatalyst is starting to gradually decompose. **Gr2Cy** also shows a slight curvature in the logarithmic plot at 70 °C, but at 80 °C the precatalyst is starting to decompose rapidly, which might explain why SMP formation is increasing radically, i.e. approximately a 30% increase with a 10 °C increase in temperature. Although replacing the PCy_3 with a NHC carbene increases the stability, lifetime and reactivity of **Gr1Cy**, the selectivity of the precatalyst decreases with an increase in temperature.

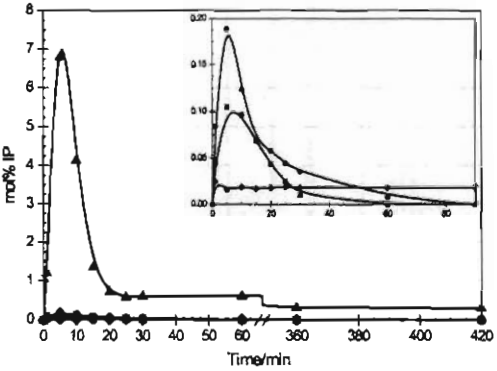

Figure 5.31 The mol% IP formed during the self-metathesis of 1-octene in the presence of **Gr2Cy** over a temperature range of 35 – 80 °C (1-octene/Ru = 9000, enlarged inset of the first 30 min excluding 80 °C).
[◆ 35 °C ■ 60 °C ● 70 °C ▲ 80 °C]

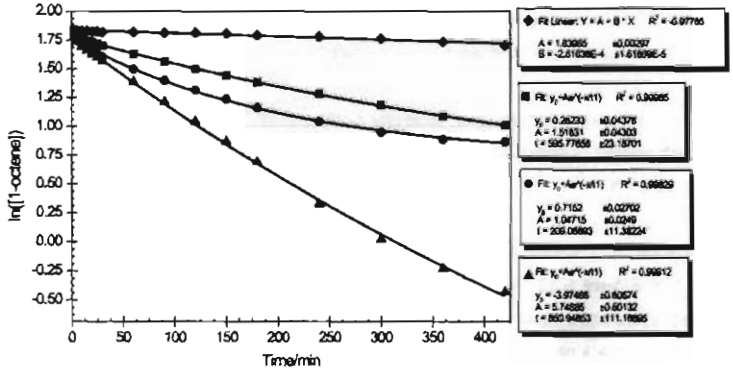

Figure 5.32 Logarithmic plot for **Gr1Cy** as a function of time at various temperatures.
[◆ 35 °C ■ 60 °C ● 70 °C ▲ 80 °C]

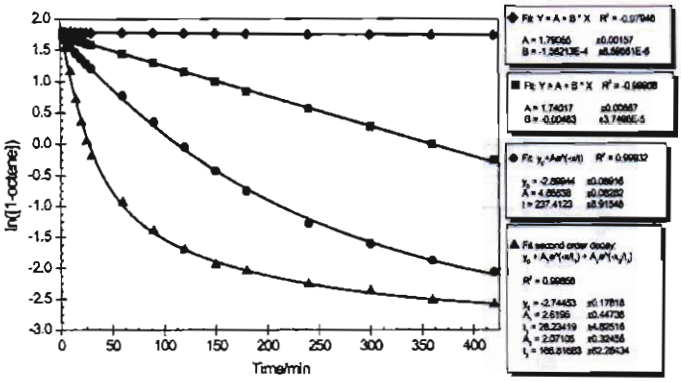

Figure 5.33 Logarithmic plot for **Gr2Cy** as a function of time at various temperatures
[35 °C ■ 60 °C ● 70 °C ▲ 80 °C]

To determine the activation energy of the reaction in the presence of **Gr1Cy** and **Gr2Cy**, the initiation rate constants (k_{init}/mol s^{-1}) for both systems were determined as a function of the mol 7-tetradecene formed over time (**Table 5.5**). A linear increase in k_{init} for the formation of 7-tetradecene was observed in the presence of **Gr1Cy**, while k_{init} increased exponentially for **Gr2Cy** with an increase in temperature (**Figure 5.34**). The graph representing the rate constants in the Arrhenius equation for **Gr1Cy** and **Gr2Cy** is given in **Figure 5.35**. The shape of the curves is identical to the illustrated graphs for **Gr1** and **Gr2** in **Figure 5.18**, in which two parts are identified, both approaching linearity. Similar to the results of the **Gr1**- and **Gr2**-induced 1-octene metathesis, the experimental results for **Gr1Cy** and **Gr2Cy** showed that at temperatures above 70 °C, SMP and/or IP formation significantly increases, with PMP formation being limited. By excluding the data above 70 °C, a linear graph was obtained for the first part of the graphs, in which the side reactions are negligibly small (**Figure 5.37**). From the data in **Table 5.5**, the activation energy was calculated as 117.58 kJ mol^{-1} for **Gr1Cy**, and 139.41 kJ mol^{-1} for **Gr2Cy**, with a pre-exponential factor of 4.95 x 10^{12} min^{-1} and 2.85 x 10^{16} min^{-1}, respectively. The higher activation energy, compared to **Gr1** and **Gr2**, suggests that the initiation of these systems might be due to bond breakage rather than the spontaneous dissociation of a ligand.[29] This might also contribute to the higher stability of these systems relative to **Gr1** and **Gr2**. The second part of the graph was not considered further, since insufficient data was available to obtain E_a values from the graph.

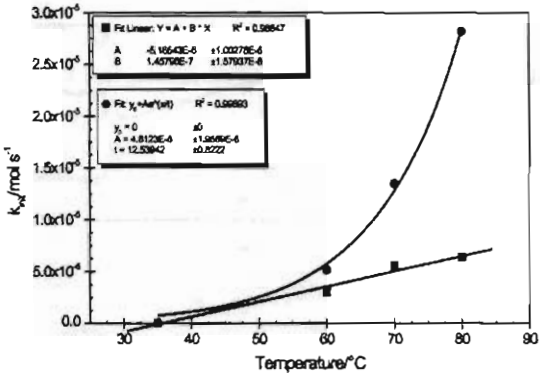

Figure 5.34 Initiation rate (k_{init}) as a function of temperature
[■ Gr1Cy, ● Gr2Cy]

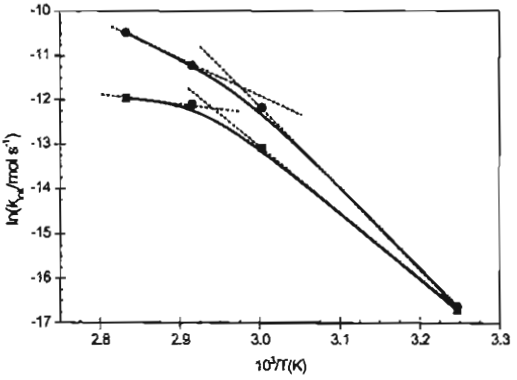

Figure 5.35 Arrhenius plot for the 1-octene metathesis reaction in the presence of Gr1Cy and Gr2Cy.
[■ Gr1Cy ● Gr2Cy]

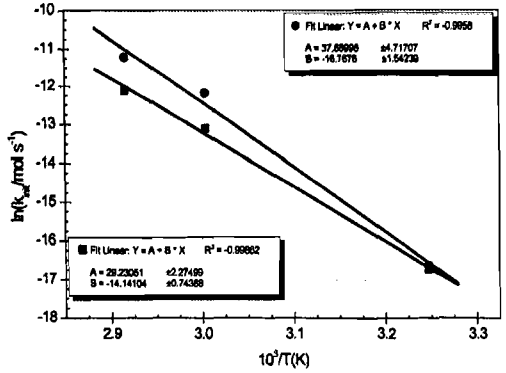

Figure 5.36 Arrhenius plot for the 1-octene metathesis reaction in the presence of **Gr1Cy** and **Gr2Cy**, with the exclusion of T = 80 °C.
[■ **Gr1Cy** ● **Gr2Cy**]

5.2.2.2 Influence of catalyst concentration

I also investigated the influence of the 1-octene/Ru molar ratio on the performance of **Gr1Cy** to determine whether the precatalyst will be active at lower precatalyst concentrations. **Table 5.5** summarises the catalytic activity and selectivity of **Gr1Cy** towards the metathesis of 1-octene at 60 °C, varying the 1-octene/Ru molar ratio from 2000 – 100 000. The activity of **Gr1Cy** towards the formation of PMP increases with a decrease in the 1-octene/Ru molar ratio, as illustrated in **Figure 5.37**, with a simultaneous increase in both the SMP and IP (**Table 5.6**).

Table 5.6 Catalytic activity and selectivity of Gr1Cy towards the metathesis of 1-octene at 60 °C at different 1-octene/Ru molar ratio (no solvent) after 420 min.

1-octene/Ru molar ratio	PMP/%	SMP/%	IP/%	%S[a]	k_{init} (mol s^{-1})	TON
2000	68.0	1.5	0.9	96.59	2.62×10^{-6}	1728
9000	53.2	0.4	0.5	98.34	2.06×10^{-6}	5907
100 000	32.0	0.2	0.5	97.86	5.52×10^{-7}	3569

[a] Selectivity towards PMP

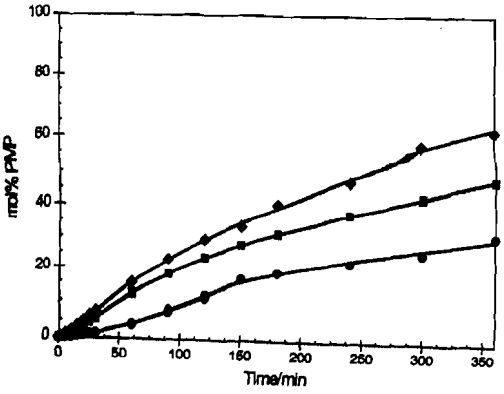

Figure 5.37 Influence of 1-octene/Ru molar ratio on the self-metathesis of 1-octene to 7-tetradecene and ethene (PMP) in the presence of precatalyst **Gr1Cy** at 60 °C.
[◆ 2000 ■ 9000 ● 100 000]

Although the initiation rate of **Gr1Cy** increased with an increase in the precatalyst concentration, a sharp decrease in the TON was observed after reaching a maximum at a 1-octene/Ru molar ratio of 9000. Therefore, in order to have a high activity and selectivity of **Gr1Cy** towards PMP, with a limited amount of SMP and IP, an 1-octene/Ru molar ratio = 9000 was used for further investigations.

5.2.2.3 NMR investigation

In addition, I investigated the metathesis of 1-octene in the presence of **Gr1Cy** and **Gr2Cy** with ^{1}H NMR at 50 °C in $CDCl_3$, to gain some insight into the reaction mechanism. The reaction was not investigated at 30 °C, due to limited availability of the precatalysts. The ^{1}H NMR spectra obtained during these investigations are presented in Appendix F.

*NMR investigation: metathesis with **Gr1Cy** (for simplicity referred to as **C7** in the NMR section)*

The H_α signal (denoted H*) of the coordinated benzylidene **C7** (**C7a-H***) appears at δ 17.846 ppm, of the heptylidene [RuCl(PCy$_3$)(O^N)(=CHC$_6$H$_{13}$)] (**C7ab-H***) at δ 17.002 ppm and the methylidene [RuCl(PCy$_3$)(O^N)(=CH$_2$)] (**C7ac-H***) at δ 16.190 ppm. The shift of the H_α peak of the benzylidene to a lower field to produce a triplet and a doublet is due to the change in the electronic environment of the ligand attached to the carbene carbon.

The change in the size of the pyridine α-H signals over time is illustrated in **Figure 5.38**. The change in the shift in the pyridine α-H signal (denoted as $H^{\dagger}$) was also observed during the course of the reaction, indicating that the electronic environment of the ligand is changing, most probably due to the coordination and decoordination of the N-donor atom as the reaction continues. The pyridine α-H signal of the coordinated benzylidene (**C7a-H†**) appears at δ 9.04 ppm, but the other signals cannot be assigned with certainty to the other intermediates. Only three carbene species were observed during the metathesis of 1-octene in the presence of **C7a** (**Figure 5.39**). Theoretically, six carbenes should be involved, but neither of the H_{α} signals for the uncoordinated **C7a**-related intermediates (**C7a-open-H***, **C7ab-open-H*** and **C7ac-open-H***) was observed. This might be due to the fast nature of the reaction, and the fact that *ca.* 13 min was needed for each NMR spectrum to be recorded over a period of 5 h. The reaction may therefore proceed at such a fast rate that some of the carbene signals are not observed within the time of recording the NMR spectrum. **Figure 5.40** illustrates the change in the peak integration values of the individual carbene species as a function of time. The change in the size of the H_{α} signals of the three carbene species involved in the metathesis of 1-octene over time is given in **Figure 5.41**. The methylidene intermediate seems to follow a different pattern than that reported for **Gr1**,[15] in which it seems the signal increases to a maximum with a gradual decrease without being depleted in the 5 hours as the reaction proceeds (**Figure 5.41(c)**). The benzylidene signal gradually decreases, suggesting the conversion of the benzylidene to the heptylidene and methylidene; after 200 min all of the **Gr1Cy** has been converted. The heptylidene and methylidene signals increase to a maximum, followed by a gradual decrease to a minimum as the reaction proceeds. The simultaneous decomposition of the benzylidene to some other species cannot be ruled out. In the presence of 1-octene it seems as if the benzylidene is simultaneously converted to the heptylidene and the methylidene as the reaction proceeds.

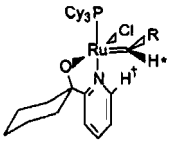

R = Ph (**C7a**)
= Hx (**C7ab**)
= H (**C7ac**)

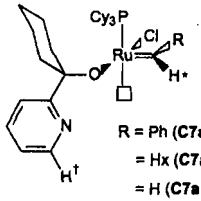

R = Ph (**C7a-open**)
= Hx (**C7ab-open**)
= H (**C7ac-open**)

(a) δ = 9.26 ppm

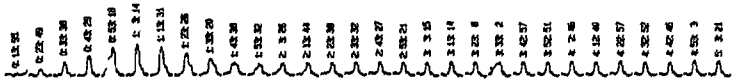

(b) δ = 9.04 ppm (**C7a-H^1**)

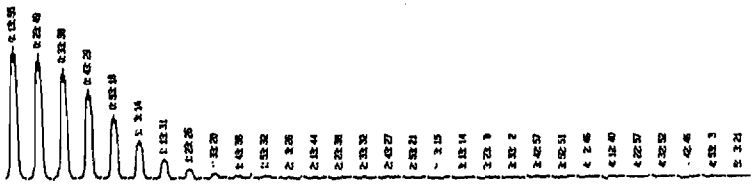

(c) δ = 8.95 ppm

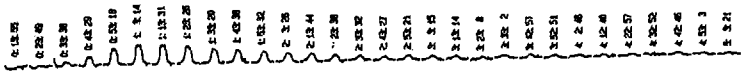

Figure 5.38 ^{1}H NMR signals at different time intervals of the pyridine α-H's in a 1-octene/**C7** reaction mixture in $CDCl_3$ at 50 °C

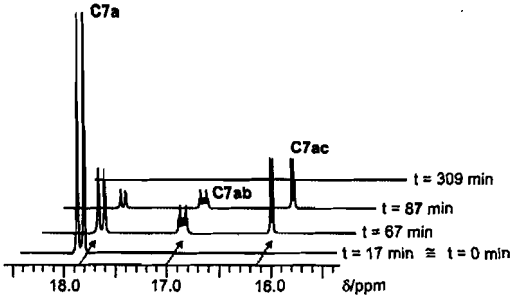

Figure 5.39 ^{1}H NMR spectra of the carbene proton region at different time intervals of a 1-octene/**Gr1Cy** reaction mixture in $CDCl_3$ at 50 °C.

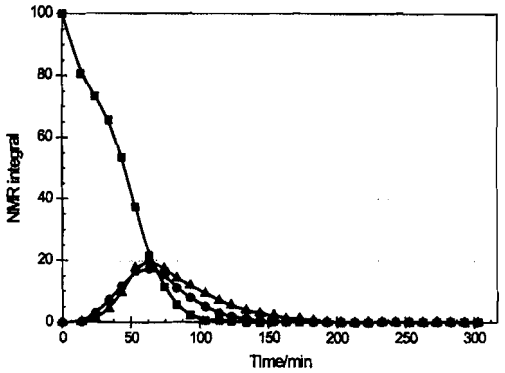

Figure 5.40 The ^{1}H NMR peak integration values (normalised) of the carbenes involved in the metathesis reaction of 1-octene in the presence of **C7**.
[■ δ 17.846 ppm, ● δ 17.002ppm, ▲ δ 16.170 ppm]

(a) δ = 17.846 ppm

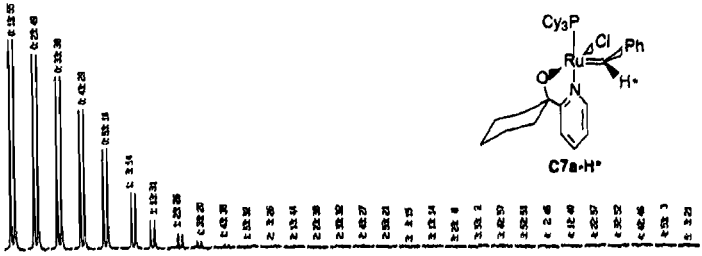

(b) δ = 17.002 ppm

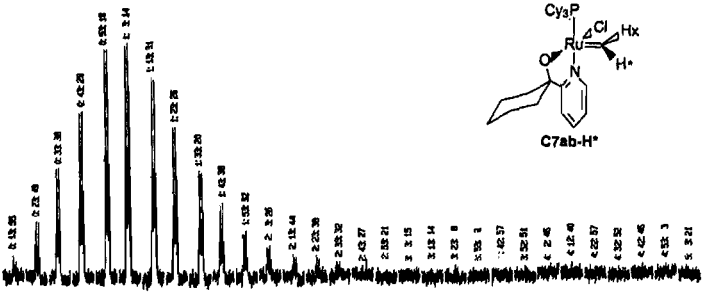

(c) δ = 16.170 ppm

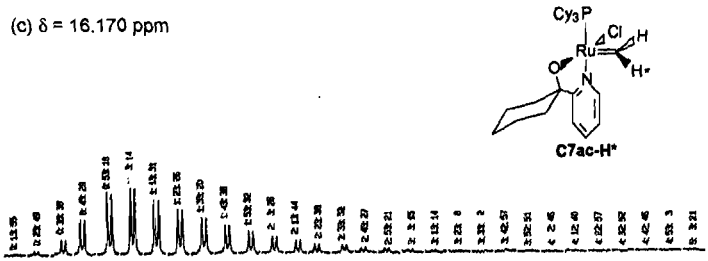

Figure 5.41 ^{1}H NMR signals at different time intervals of the carbene α-H's in a 1-octene/**C7** reaction mixture in $CDCl_3$ at 50 °C

[(a) Ru=CHPh, (b) Ru=CHC_6H_{13}, (c) Ru=CH_2]

*NMR investigation: metathesis with **Gr2Cy** (for simplicity referred to as **C28** in the NMR discussion)*

I also investigated the metathesis of 1-octene in the presence of **C28** with ^{1}H-NMR at 50 °C in $CDCl_3$. In contrast to **Gr1Cy**, five carbene species were observed during the metathesis of 1-octene in the presence of **C28**, which might relate to the open and coordinated intermediates as illustrated in **Figure 5.42**. The H_α signal of the uncoordinated **C28**-related heptylidene intermediate (**C28b-open-H***) was not observed. The H_α signal of the coordinated benzylidene **C28** (**C28-H***) appears at δ 18.053 ppm, of the heptylidene [RuCl(H_2IMes)(O^N)(=CHC_6H_{13})] (**C28b**) at δ 16.711 ppm and the methylidene [RuCl(H_2IMes)(O^N)(=CH_2)] (**C28c**) at δ 16.079 ppm.

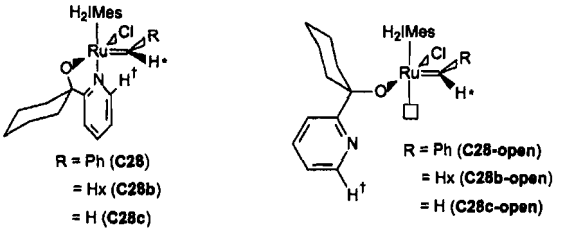

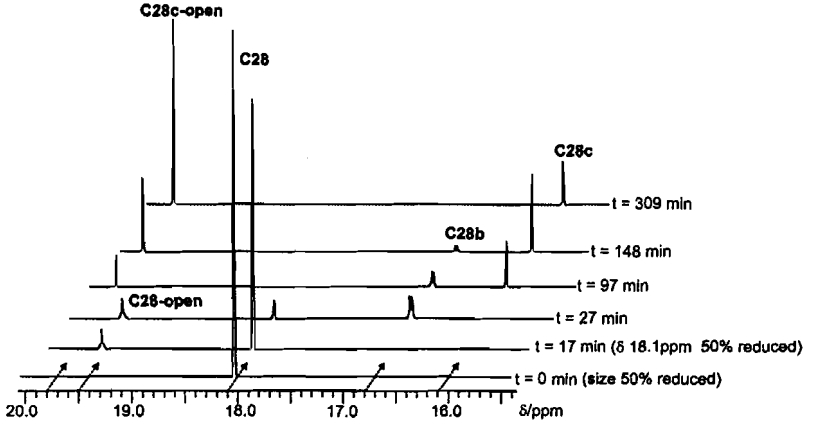

Figure 5.42 ^{1}H NMR spectra of the carbene proton region at different time intervals of a 1-octene/**C28** reaction mixture in $CDCl_3$ at 50 °C.

The shift of the H_α peak of the benzylidene to a lower field to produce a doublet and singlet is due to the change in the electronic environment of the ligand attached to the carbene carbon. The appearance of singlets at δ 19.484 ppm and δ 19.758 ppm can be attributed to the decoordination of the N-donor to produce the open benzylidene (**C28-H'**) and methylidene (**C28c-H'**) intermediates. The downfield shift of the carbene signals is due to the decrease in electron density around the Ru=C moiety and therefore the H_α becomes less shielded. A shift in the pyridine α-H signal was also observed during the course of the reaction (**Figure 5.43**), indicating that the electronic environment of the ligand is changing, most probably due to the coordination and decoordination of the N-donor atom as the reaction continues. The pyridine α-H signal of the coordinated benzylidene **C28** (**C28-H'**) appears at δ 9.476 ppm, but the other signals cannot be assigned with certainty to the coordinated and uncoordinated heptylidene and methylidene intermediates nor the uncoordinated benzylidene. As seen in **Figure 5.43**, a number of the signals are overlapped, which made integration of the signals difficult and therefore no definite trend could be obtained.

Figure 5.44 illustrates the change in the size of the H_α signals of the three main carbene species involved in the metathesis of 1-octene with **C28** over time. The two additional carbene signals that form during the metathesis reaction are given in **Figure 5.45**. The change in the peak integration values of the individual carbene species as a function of time is given in **Figure 5.46**. The form of the graph for signals δ 19.48 ppm and δ 16.71 ppm follows the same pattern, which suggests that these signals might be connected to each other in the form of the uncoordinated and coordinated heptylidene species, respectively. In the presence of 1-octene, it seems that the benzylidene is rapidly converted to the heptylidene, while the formation of the methylidene proceeds at a much slower rate. The individual species seem to follow a similar pattern as was reported for **Gr1**, in which it has been shown that the heptylidene is thermodynamically and kinetically favoured above the methylidene species.[15]

The sharp decrease of the benzylidene signal (**Figure 5.45(a)**) suggests a fast conversion of the benzylidene to either the uncoordinated benzylidene intermediate (**C28-open**) or the heptylidene and methylidene; after 50 min all of the **C28** has been converted. The simultaneous decomposition of the benzylidene to some other species cannot be ruled out. The increase to a maximum of the heptylidene signal within 26 min is followed by a gradual decrease as the reaction proceeds (**Figure 5.45(b)**), while the methylidene signal gradually increases to a maximum within 3 h, followed by a slow decrease (**Figure 5.45(c)**), possibly due to catalyst decomposition or formation of the uncoordinated methylidene intermediate (**C28c-open**), which might be correlated to the gradual formation of the H_α signal at δ 19.76 ppm.

(a) δ = 9.045 ppm

(b) δ = 9.216 ppm

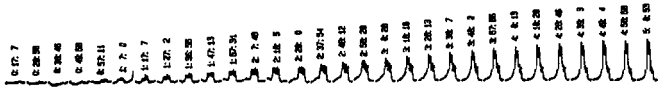

(c) δ = 9.476 ppm (**C28-H^t**)

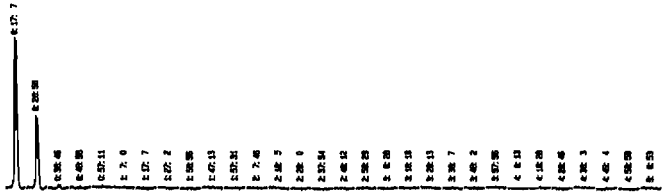

(d) δ = 9.706 ppm

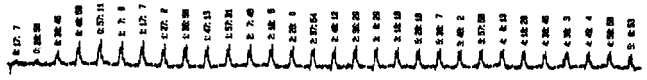

Figure 5.43 ^{1}H NMR signals at different time intervals of the pyridine α-H's in a 1-octene/**C28** reaction mixture in $CDCl_3$ at 50 °C.

(a) δ = 18.05 ppm

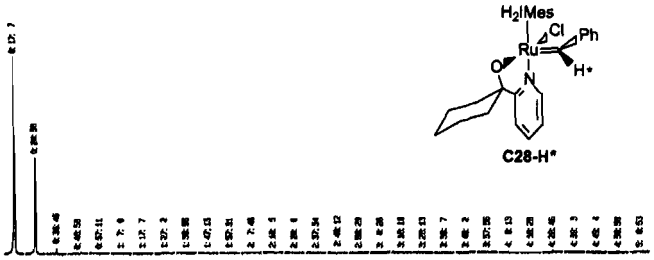

(b) δ = 16.71 ppm

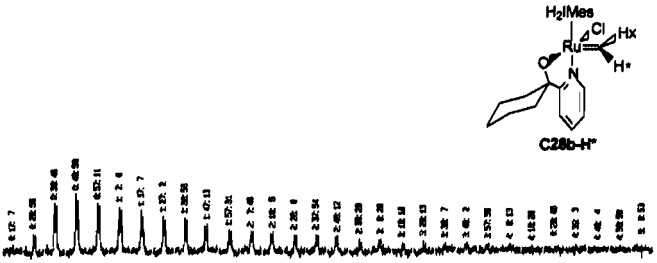

(c) δ = 16.08 ppm

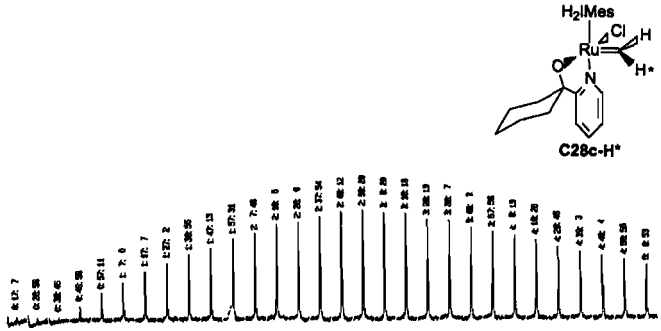

Figure 5.44 ^{1}H NMR signals at different time intervals of the carbene α-H's in a 1-octene/**C28** reaction mixture in $CDCl_3$ at 50 °C.

[(a) Ru=CHPh, (b) Ru=CHC_6H_{13}, (c) Ru=CH_2]

(a) δ = 19.48 ppm

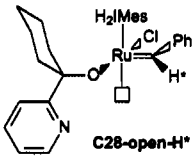

(b) δ = 19.76 ppm

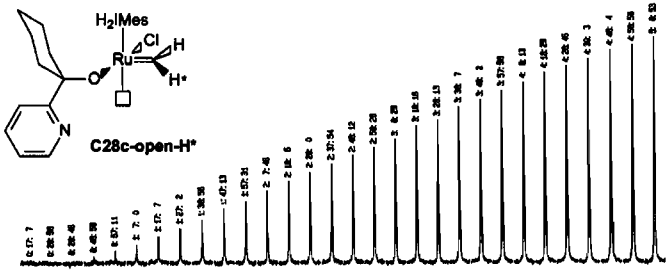

Figure 5.45 ^{1}H NMR signals at different time intervals of the additional carbene α-H's that formed in the 1-octene/**C28** reaction mixture in $CDCl_3$ at 50 °C.
[(a) Ru=CHPh-open (**C28-open-H***) (b) Ru=CH_2-open (**C28c-open-H***)]

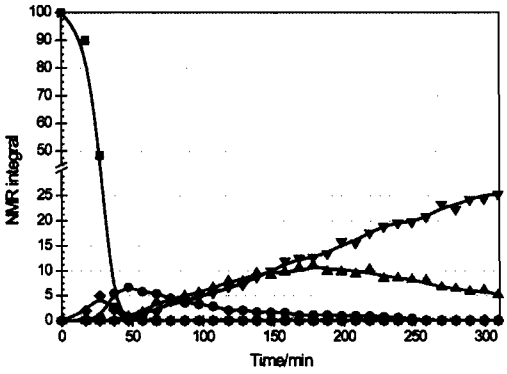

Figure 5.46 The ^{1}H NMR peak integration values (normalised) of the carbenes involved in the metathesis reaction of 1-octene in the presence of **C28**.
[▼ δ 19.758 ppm, ◆ δ 19.484 ppm, ■ δ 18.053 ppm, ● δ 16.711 ppm, ▲ δ 16.079 ppm]

5.2.3 Comparing Grubbs systems with hemilabile Ru=C complexes

In § 5.2.2, optimum conditions were identified to obtain high 1-octene metathesis activity in the presence of a hemilabile complex. Consequently, a comparative study was made between the Grubbs carbenes (**Gr1** and **Gr2**) and the hemilabile complexes with regards to the 1-octene metathesis activities and selectivities at the identified optimum conditions. The fact that most of the activity investigations were not repeated might lead to inaccurate representation of the initiation rates, but the given results can be used to give an initial indication of the reaction kinetics.

5.2.3.1 Metathesis with first generation hemilabile complexes

In **Table 5.7**, the 1-octene metathesis activity and selectivity of the first generation hemilabile precatalysts are compared to **Gr1** after 420 min. The reactions were performed at 60 °C with a 1-octene/Ru molar ratio of 9000. A graphical representation is given in **Figures 5.47** to **5.49**. The catalytic activity of **Gr1^{i}Pr** could not be determined, as a result of its air and moisture sensitivity leading to the decomposition of the system before the reaction could be executed (see Chapter 4).

Table 5.7 Catalytic activity and selectivity of the various first generation hemilabile Ru=C complexes in comparison to **Gr1** at 60 °C (1-octene/Ru = 9000, no solvent) after 420 min.

Precatalyst	PMP/%	SMP/%	IP/%	%S[a]	k_{init} (mol s^{-1})	TON
Gr1	21.2	0.2	4.8	80.92	4.65×10^{-5}	2172
Gr1Ph	30.5	0.0	0.6	98.07	1.26×10^{-6}	3740
Gr1Me	34.1	0.0	0.4	98.84	1.88×10^{-7}	4125
Gr1Cy	53.2	0.4	0.5	98.34	2.06×10^{-6}	5907

[a] Selectivity towards PMP

Although the initiation rate of the hemilabile precatalysts are slower compared to **Gr1**, the TON, selectivity and lifetime of the precatalysts were improved. After 20 h, all the catalysts still showed activity towards the metathesis of 1-octene, i.e. approximately 69, 52 and 42% PMP for **Gr1Cy**, **Gr1Me** and **Gr1Ph**, respectively, while **Gr1** (21% PMP) was inactive (see **Figure 5.47**). The selectivity towards the formation of PMP increased with *ca.* 30% in the presence of the hemilabile complexes compared to **Gr1**. IP formation remained below 1% for the hemilabile **Gr1**-type precatalysts while a 5% increase was observed in the presence of **Gr1**. SMP formation remained below 0.5% for all the systems, including **Gr1**. This indicates that the incorporation of a hemilabile ligand into **Gr1** will improve the lifetime, activity and selectivity of **Gr1** towards 1-alkene metathesis at higher temperatures. Denk et al.[27] and van Koten et al.[30] have also shown that the incorporation of a hemilabile ligand into the Grubbs system improves the activity of the precatalyst for ROMP and RCM reactions.

The relative stability of the precatalysts, as determined by plotting ln([1-octene]) as a function of time, is compared to **Gr1** in **Figure 5.50**. Due to the linear logarithmic plot for **Gr1Me**, compared to the slight curvature in the plots for **Gr1Cy** and **Gr1Ph**, it appears that **Gr1Me** is more stable than the other two systems. However, **Gr1Cy** and **Gr1Ph** decompose very slowly compared to the dramatic decomposition of **Gr1** at 60 °C. This indicates that the hemilabile complexes are more stable than **Gr1**.

Electronic as well as steric effects can play an important role on the behaviour of transition metal precatalysts. Since the development of the cone angle theory by Tolman[31] in the 1970s, it has been shown that steric effects are generally at least as important as electronic effects, and that they can dominate in many cases. Nolan et al.[32,33] has recently defined a spherical volume to describe the steric influence of NHC-type ligands on catalyst activity. Since O,N-chelating ligands cannot be seen in the same light as phosphine or NHC ligands, the atomic volume of the complete system, as determined by DFT calculations, was used to quantify the steric influences of these ligands.

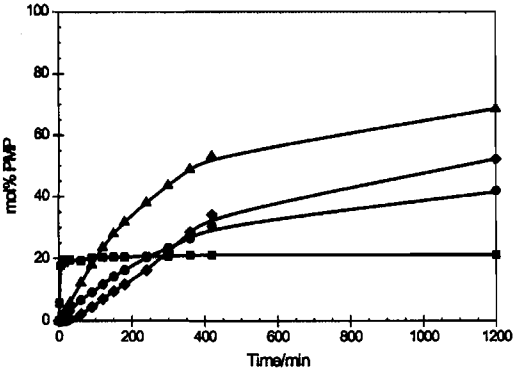

Figure 5.47 PMP formed during the metathesis of 1-octene in the presence of **Gr1** related complexes at 60 °C.
[■ **Gr1** ● **Gr1Ph** ◆ **Gr1Me** ▲ **Gr1Cy**]

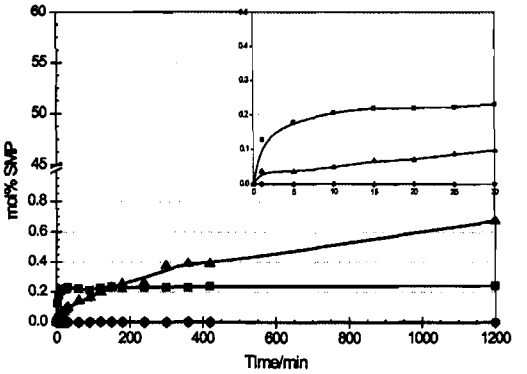

Figure 5.48 SMP formed during the metathesis of 1-octene in the presence of **Gr1** complexes at 60 °C (enlarged inset of the first 30 min).
[■ **Gr1** ● **Gr1Ph** ◆ **Gr1Me** ▲ **Gr1Cy**]

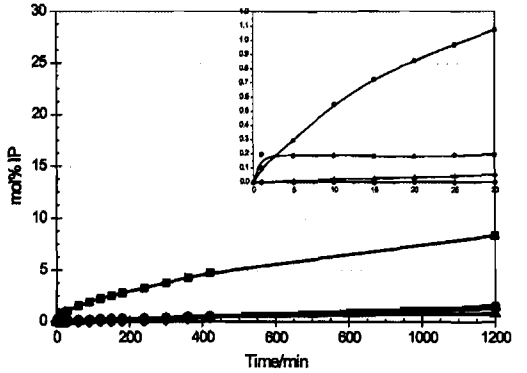

Figure 5.49 IP formed during the metathesis of 1-octene in the presence of **Gr1** related complexes at 60 °C (enlarged inset of the first 30 min).
[■ **Gr1** ● **Gr1Ph** ◆ **Gr1Me** ▲ **Gr1Cy**]

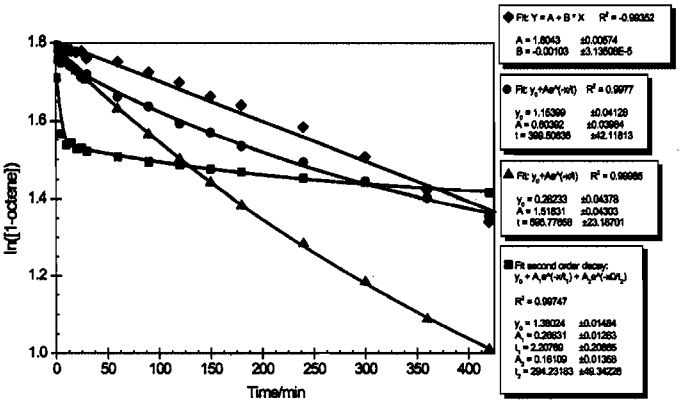

Figure 5.50 Comparing the logarithmic plot of **Gr1** with hemilabile first generation Grubbs analogues at 60 °C
[■ **Gr1** ● **Gr1Ph** ◆ **Gr1Me** ▲ **Gr1Cy**]

The atomic volume of the precatalysts increased in the order **Gr1Me** < **Gr1Cy** < **Gr1Ph** as the steric bulk of the alkyl substituents (R^1 and R^2) on the 2-pyridinylcarbinolate ionic ligand (**HL1**) increased. **Figure 5.51** illustrates the influence of atomic volume on both PMP formation and k_{init}. A linear increase in both PMP formation and initiation rate is observed with an increase in steric bulk. However, a dramatic decrease in activity was observed for **Gr1Ph**. This might be due to the free rotation of the phenyl-rings on C_2 of **HL1**, which increases the steric bulk around the Ru-centre and therefore obstructs coordination of the 1-octene to the Ru=C-moiety. The stability of the complex might also be influenced by electronic effects, which can cause low activity, but was not investigated in much detail during this study.

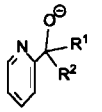

R^1, R^2 = H, alkyl, aryl

HL1

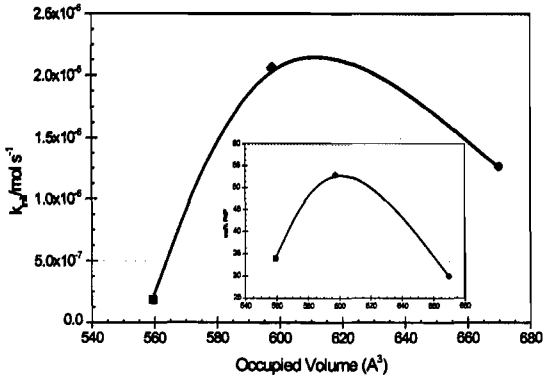

Figure 5.51 Influence of atomic volume on the PMP formation (inset) and k_{init} of the first generation hemilabile complexes.
[■ **Gr1Me** ◆ **Gr1Cy** ● **Gr1Ph**]

Since **Gr1Quino**, **Gr1Cy-Py** and **Gr1Pico-Py** were to some extent successfully synthesised (see Chapter 4), it was deemed necessary to determine the activity of these systems towards 1-octene metathesis. A large quantity of **Gr1Quino** and **Gr1Cy-Py** was lost in the process of purifying the complexes before executing the metathesis reactions, and therefore no data could be obtained for these two systems. On the other hand, after further purification of **Gr1Pico-Py**, the metathesis activity was investigated at 60 °C with a 1-octene/Ru molar ratio of 9000. Although **Gr1Pico-Py** showed a selectivity of 89% towards PMP formation, only 2.5% PMP formation was achieved after 420 min at 60 °C along with 0.3% IP formation. This gives an indication that changing the electronic environment of the C_2 of **HL1** has a dramatic effect on the activity of the ruthenium carbene, and should therefore be investigated in more detail.

5.2.3.2 Metathesis in the presence of second generation hemilabile complexes

In **Table 5.8**, the 1-octene metathesis activity and selectivity after 420 min of the second generation hemilabile precatalysts are compared to **Gr2**. Graphical representations of the 1-octene metathesis reactions at 60 °C with a 1-octene/Ru molar ratio of 9000 are given in **Figure 5.52** to **5.54**.

Similar to the first generation hemilabile complexes, the lifetime and activity of the second generation analogues have been improved, regardless of the slow initiation rate of these systems compared to **Gr2** at 60 °C. However, an approximate 10 – 20% decrease in the selectivity of **Gr2Cy**, **Gr2^{i}Pr** and **Gr2Me** towards the formation of PMP was evident after 420 min, compared to **Gr2**, while the selectivity of **Gr2Ph** slightly increased. After 20 h, all the catalytic systems still showed activity towards the metathesis of 1-octene, i.e. approximately 88, 82, 70 and 93% PMP for **Gr2Cy**, **Gr2Me**, **Gr2Ph** and **Gr2^{i}Pr**, respectively, while **Gr2** (82% PMP) was inactive after *ca.* 7 h (see **Figure 5.52**). Therefore, a 4 – 10 % increase in PMP formation for **Gr2Cy**, **Gr2^{i}Pr** and **Gr2Me** was observed after 20 h compared to a 40% increase for **Gr2Ph**, indicating the high stability and activity of these complexes. The SMP formation for all the precatalysts remained almost unchanged with only a 1 – 2% increase leading to an approximate 2% decrease in the selectivity of **Gr2Cy**, **Gr2^{i}Pr** and **Gr2Me** towards the formation of PMP. However, a 20% increase in the selectivity of **Gr2Ph** was observed after 20 h. The fact that no IP formation was observed after 420 min for the hemilabile complexes or **Gr2**, indicates that cross metathesis occurred simultaneously with the isomerisation of 1-octene. Although the observable IP's for all the complexes remained below 0.2% (**Figure 5.54**), an increase to a maximum within the first5 – 10 min was followed by a sharp decrease to *ca.* 0% within 10 – 30 min as the reaction proceeded (**Figure 5.54**), most probably due to cross metathesis of the IP's to form SMP's. Additionally, a second increase in IP formation is noted for **Gr2Me** within 3 h, followed by a slow decrease to 0% after 7 h (**Figure 5.54**). The major SMP product was found to be tridecene (C_{13}) for all the systems, which is mainly a result of the cross metathesis of 1- and 2-octene (see Appendix E for a detailed outline of all the possible side reactions of 1-octene metathesis).

Table 5.8 Catalytic activity and selectivity of the various hemilabile Ru=C complexes in comparison to **Gr2** at 60 °C (1-octene/Ru = 9000, no solvent) after 420 min.

Precatalyst	PMP/%	SMP/%	IP/%	%S[a]	k_{init} (mol s^{-1})	TON
Gr2Ph	34.0	0.9	0.0	97.42	9.23×10^{-7}	3861
Gr2Me	74.0	21.8	0.0	77.24	4.66×10^{-6}	7644
Gr2Cy	81.1	12.9	0.0	86.28	5.19×10^{-6}	9214
Gr2	81.6	3.6	0.0	95.77	1.89×10^{-4}	8881
Gr2^{i}Pr	87.0	13.0	0.0	87.00	7.54×10^{-6}	11 729

[a] Selectivity towards PMP

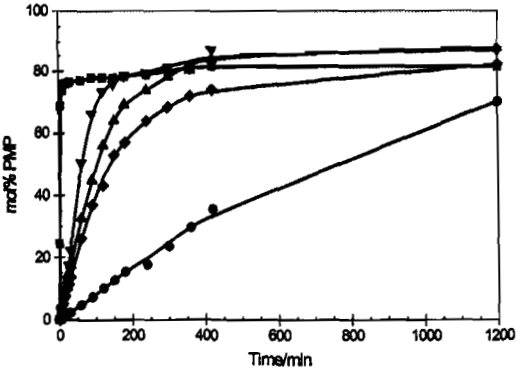

Figure 5.52 PMP formed during the metathesis of 1-octene in the presence of **Gr2** related complexes at 60 °C.
[■ **Gr2** ● **Gr2Ph** ◆ **Gr2Me** ▲ **Gr2Cy** ▼ **Gr2^{i}Pr**]

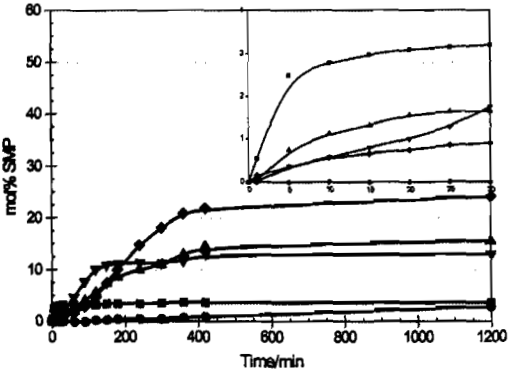

Figure 5.53 SMP formed during the metathesis of 1-octene in the presence of **Gr2** related complexes at 60 °C (enlarged inset of the first 30 min).
[■ **Gr2** ● **Gr2Ph** ◆ **Gr2Me** ▲ **Gr2Cy** ▼ **Gr2^{i}Pr**]

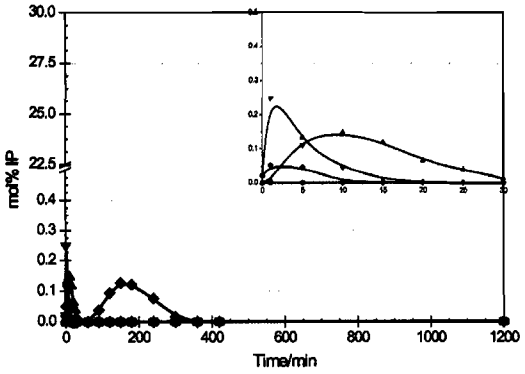

Figure 5.54 IP formed during the metathesis of 1-octene in the presence of **Gr2** related complexes at 60 °C (enlarged inset of the first 30 min).
[■ **Gr2** ● **Gr2Ph** ◆ **Gr2Me** ▲ **Gr2Cy** ▼ **Gr2^{i}Pr**]

The influence of atomic volume on the PMP formation (**Figure 5.55**) and initiation rate (**Figure 5.56**) of the second generation hemilabile Grubbs systems is graphically represented in **Figure 5.55** and **5.56**, respectively. A linear increase in the PMP formation is observed with an increase in steric bulk, while an exponential increase in the initiation rate is noted. However, a similar dramatic decrease in activity is observed for **Gr2Ph** as was observed for **Gr1Ph**, which is likely to also be due to the free rotation of the phenyl-rings on C_2 of **HL1** leading to an increased steric bulk around the Ru-centre.

The stability of the precatalysts is graphically compared to **Gr2** in **Figure 5.57**. The linear plot of **Gr2Ph**, **Gr2Me** and **Gr2Cy**, compared to the curved plots of **Gr2^{i}Pr** and **Gr2**, indicates that the aforementioned systems are more stable. However, despite the high thermal stability of **Gr2Me** and **Gr2Cy**, low selectivities are displayed towards PMP formation. On the other hand, high selectivity and stability is observed for **Gr2Ph** despite its slow activity.

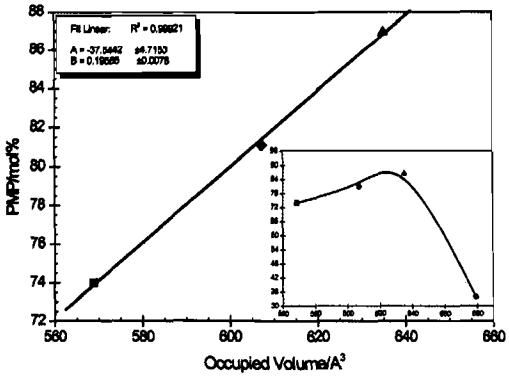

Figure 5.55 Influence of atomic volume on PMP formation of the second generation hemilabile complexes.
[■ **Gr2Me** ◆ **G2Cy** ▲ **Gr2^{i}Pr** ● **Gr2Ph**]

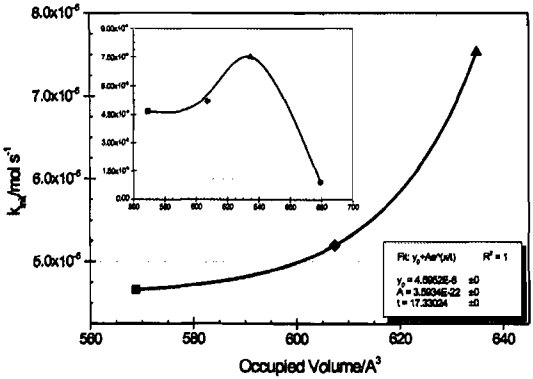

Figure 5.56 Influence of atomic volume on the initiation rate of the second generation hemilabile complexes.
[■ **Gr2Me** ◆ **G2Cy** ▲ **Gr2^{i}Pr** ● **Gr2Ph**]

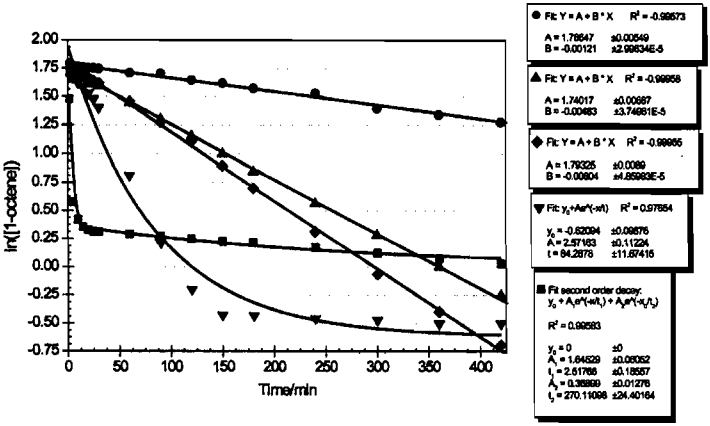

Figure 5.57 Comparing the logarithmic plot of **Gr2** with hemilabile second generation Grubbs analogues at 60 °C
[■ **Gr2** ● **Gr2Ph** ◆ **Gr2Me** ▲ **Gr2Cy** ▼ **Gr2^{i}Pr**]

To determine whether temperature would increase the 1-octene metathesis activity of **Gr2Ph**, which has a very long lifetime at 60 °C, the reaction was investigated at 120 °C. A graphical representation of the reaction progress is given in **Figure 5.58**. An increase in temperature results in a 26% decrease in PMP formation, with a simultaneous 72% increase in SMP formation within 60 min. The mol% IP increases to a maximum within the first 10 min, followed by a sharp decrease to *ca.* 0% within 60 min as the reaction proceeds (**Figure 5.58**). This indicates that the isomerisation activity of **Gr2Ph** increased with an increase in temperature, which led to an increase in SMP formation due to cross-metathesis of the IP's. The isomerisation can probably occur either by reversible allyl-hydride formation, or due to the decomposition of the precatalyst to form a monophosphine Ru-hydride intermediate.[19,21] These mechanisms have been previously explained in much detail for the Grubbs carbenes and are applicable to our system.[18,21]

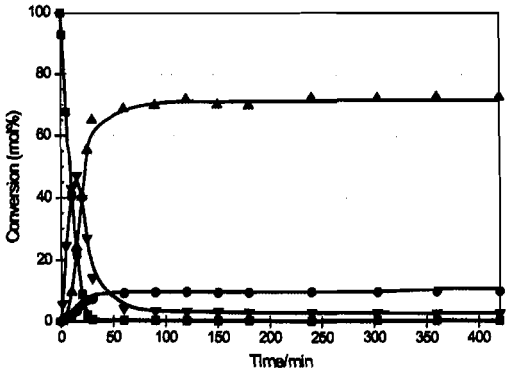

Figure 5.58 Reaction of 1-octene in the presence of **Gr2Ph** at 120 °C (no solvent, 1-octene/Ru = 9000).
[■ 1-Octene ● PMP ▼ IP ▲ SMP]
(4% *trans*-7-tetradecene and 1% *cis*-7-tetradecene after 420min)

A more detailed study should therefore be launched to investigate the alkene isomerisation probability of **Gr2Ph** and the other first and second generation complexes to be able to elaborate in more detail on the above observations.

Since **Gr2Quino** and **Gr2Pico** were to some extent successfully synthesised (see Chapter 4), it was deemed necessary to determine the activity of these systems towards 1-octene metathesis. The metathesis activity of these two systems was investigated at 60 °C with a 1-octene/Ru molar ratio of 9000. Similar to the first generation system **Gr1-PyPico**, the activity of the ruthenium carbene was significantly influenced by varying the electron environment of C_2 on **HL1**. **Gr2Quino** and **Gr2Pico** showed low activity towards the formation of PMP's, with **Gr2Pico** only achieving 0.1% PMP formation compared to 0.4% for **Gr2Quino**.

Table 5.9 Catalytic activity and selectivity of **Gr2Pico** and **Gr2Quino** at 60 °C (1-octene/Ru = 9000, no solvent) after 420 min.

Precatalyst	PMP/%	SMP/%	IP/%	%S[a]	k_{init} (mol s^{-1})	TON
Gr2Pico	0.1	0.0	0.0	100.00	2.41×10^{-7}	1
Gr2Quino	0.4	0.0	0.2	61.61	6.37×10^{-7}	39

[a] Selectivity towards PMP

5.3 REFERENCES

1. Ivin, K.J. and Mol, J.C., ***Olefin Metathesis and Metathesis Polymerization***, Academic Press, San Diego, 1997

2. Lehman, S.E., Jr., Schwendeman, J.E., O'Donnell, P.M., and Wagener, K.B., *Inorg. Chim. Acta.*, 2003, ***345***, 190

3. Dinger, M.B. and Mol, J.C., *Adv. Synth. Catal.*, 2002, **366**, 671

4. Van Schalkwyk, C., Vosloo, H.C.M., and Du Plessis, J.A.K., *Adv. Synth. Catal.*, 2002, **344**, 781

5. Sanford, M.S., Love, J.A., and Grubbs, R.H., *Organometallics*, 2001, **20**, 5314

6. Chang, S., Jones II, L., Wang, C., Henling, L.M., and Grubbs, R.H., *Organometallics*, 1998, **17**, 3460

7. De Clercq, B. and Verpoort, F., *Adv. Synth. Catal.*, 2002, **344**, 639

8. De Clercq, B. and Verpoort, F., *Adv. Synth. Catal.*, 2002, **344**, 1

9. Huang, J., Schanz, H.-J., Stevens, E.D., and Nolan, S.P., *Organometallics*, 1999, **18**, 5375

10. Weskamp, T., Kohl, F.J., Hieringer, W., Gleich, D., and Herrmann, W.A., *Angew. Chem. Int. Ed.*, 1999, **38**, 2416

11. Sanford, M.S., Love, J.A., and Grubbs, R.H., *J. Am. Chem. Soc.*, 2001, **123**, 6543

12. Ritter, T., Hejl, A., Wenzel, A.G., Funk, T.W., and Grubbs, R.H., *Organometallics*, 2006, **25**, 5740

13. Maechling, S., Zaja, M., and Blechert, S., *Adv. Synth. Catal.*, 2005, **347**, 1413

14. Van Schalkwyk, C., ***Die Katalitiese Sintese van Lineêre Alkene via 'n Metatesereaksie***, Ph.D thesis, Potchefstroomse Universiteit vir Christelike Hoër Onderwys, 2001

15. Jordaan, M., Van Helden, P., Van Sittert, C.G.C.E., and Vosloo, H.C.M., *J. Mol. Catal. A: Chem.*, 2006, **254**, 145

16. Forman, G.S., McConnell, A.E., Tooze, R.P., Janse van Rensburg, W., Meyer, W.H., Kirk, M.M., Dwyer, C.L., and Serfontein, D.W., *Organometallics*, 2005, **24**, 4528

17. Ulman, M. and Grubbs, R.H., *J. Org. Chem.*, 1999, **64**, 7202

18. Janse van Rensburg, W., Steynberg, P.J., Meyer, W.H., Kirk, M.M., and Forman, G.S., *J. Am. Chem. Soc.*, 2004, **126**, 14332

19. Mahahle, M.M.D., ***Isomerisation of Alkenes using Metal Carbenes and Related Transition Complexes***, Ph.D thesis, Potchefstroom University for Christian Higher Education, 2005

20. Janse van Rensburg, W., Steynberg, P.J., Kirk, M.M., Meyer, W.H., and Forman, G.S., *J. Organomet. Chem.*, 2006, **691**, 5312

21. Bourgeois, D., Pancrazi, A., Nolan, S.P., and Prunet, J., *J. Organomet. Chem.*, 2002, **643-644**, 247

22. Dinger, M.B. and Mol, J.C., *Organometallics*, 2003, **22**, 1089

23. Frost, A.A. and Pearson, R.G., ***Kinetics and Mechanism: A Study of Homogeneous Chemical Reactions***, Second Edition, Wiley, New York, 1962

24. Van Helden, P. 2004. ***A Computational Study on the Ligand Effects in Alkene Cross-metathesis***, (mini project report written as part of the Honours course at North-West University) PU for CHE, Potchefstroom, 21 p. (unpublished)

25. Love, J.A., Sanford, M.S., Day, M.W., and Grubbs, R.H., *J. Am. Chem. Soc.*, 2003, **125**, 10103

26. Ulman, M. and Grubbs, R.H., *Organometallics*, 1998, **17**, 2484

27. Mtshatsheni, K.N.G., ***Metathesis of Alkenes using Ruthenium Carbene Complexes***, M.Sc dissertation, North-West University (Potchefstroom Campus), 2005

28. Denk, K., Fridgen, J., and Herrmann, W.A., *Adv. Synth. Catal.*, 2002, **344**, 666

29. Van der Schaaf, P.A., Muhlbach, A., Hafner, A., and Kolly, R., 1999. Heterocyclyl ligand containing ruthenium and osmium catalysts. Patent: *WO 99/29701*

30. Breet, E. 2006. Verbal communication with the author. North-West University (Potchefstroom Campus)

31. Wijkens, P., Jastrzebski, J.T.B.H., Van der Schaaf, P.A., Kolly, R., Hafner, A., and Van Koten, G., *Org. Lett.*, 2000, **2**, 1621

32. Tolman, C.A., *Chem. Rev.*, 1977, **77**, 313

33. Huang, J., Schanz, H.-J., Stevens, E.D., and Nolan, S.P., *Organometallics*, 1999, **18**, 2370

34. Hillier, A.C., Sommer, W.J., Yong, B.S., Petersen, J.L., Cavallo, L., and Nolan, S.P., *Organometallics*, 2003, **22**, 4322

Alkene metathesis: Theoretical investigation

6

6.1 INTRODUCTION

The Hérisson-Chauvin metal carbene mechanism is the generally accepted mechanism for the alkene metathesis reaction (**Scheme 6.1**).[1] The mechanism consists of successive [2+2] cycloadditions followed by cycloreversions. This involves the coordination of the alkene to the metal centre to form a π-complex, followed by the formation of a metallacyclobutane intermediate, which in turn can revert to a new π-complex to yield the products after dissociation.

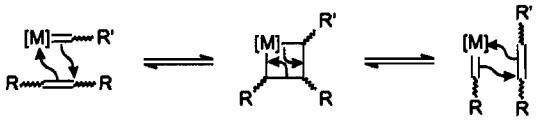

Scheme 6.1 Hérisson-Chauvin metal carbene mechanism.

Theoretical studies can be of immense use to resolve the effect of ligand coordination and to gain deeper insights into the mechanism of catalytic reactions. There has been a few recent studies that calculated mechanistic parameters or combined experimental work with computational studies on the alkene metathesis mechanism with ruthenium carbenes.[2-12] In these studies, the catalytic cycle and ligand dissociation of the methylidene species $RuCl_2(PR_3)_2(=CH_2)$ (**F1** in **Scheme 6.2**) were extensively explored. Many of these studies made use of model PR_3 (R = H, Me) ligands and/or ethene as model substrate with the methylidene complex **F1**, mainly to reduce the computing cost. This leaves room for interpretation concerning the steric and electronic influences of the actual ligands (PCy_3 versus PR_3, (R = H, Me)) and substrates (1-octene versus ethene) with the benzylidene complex (versus methylidene complex) as precatalyst.

Adlhart et al.[3] have postulated a number of mechanistic pathways which can be divided into 2 main categories, i.e. an associative and dissociative mechanism. Recent studies indicate that the dissociative mechanism, which is initiated by the dissociation of a phosphine ligand from $RuX_2(PR_3)_2(=CHR)$ to form a 14-electron species, is preferred.[2,3,13] Chen et al.[4] confirmed this by the identification of the 14-electron species by gas-phase ESI-MS/MS. The rate of phosphine dissociation and initiation of the alkene metathesis reaction by $RuX_2L(PR_3)(=CHR)$-type precatalysts have been investigated theoretically and experimentally by Sanford et al.[2]

Although many aspects of the alkene metathesis mechanism in the presence of **Gr1** were elucidated by various techniques including kinetic measurements,[14,15] there are still aspects that need to be investigated. This includes the determination of the species that are most active in the metathesis reaction as well as elucidating the mechanism followed when the benzylidene, and not the methylidene, is used as precatalyst. We[16] have recently published a conceptual model of the complete mechanism for the productive dissociative mechanism of the 1-octene metathesis reaction in the presence of **Gr1** (**Scheme 6.2** and **6.3**), which will be discussed in the following sections.

In this study, I report on aspects of the mechanism of 1-octene metathesis with **Gr1**, **Gr2**, **Gr1Cy** and **Gr2Cy**. A conceptual model of the complete mechanism in the presence of **Gr1** is presented (see **Scheme 3.1** and **3.2** in Chapter 3) and applied to **Gr2** (**Scheme 3.1** and **3.2**) and the hemilabile complexes **Gr1Cy** and **Gr2Cy** (**Scheme 3.3** in Chapter 3). Due to insufficient crystallographic data for the hemilabile complexes on the coordination position of the O- and N-atoms, it is assumed, according to various publications, that the O,N-ligand coordinates according to **Figure 6.1**.[17-19]

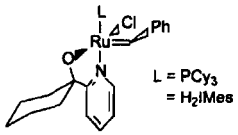

Figure 6.1 Illustration of the coordination positions of the O- and N-atoms of the O,N-ligand.

The conceptual model for **Gr1** was based on the dissociative mechanism proposed by Grubbs et al.,[2,13] modelled by Chen et al.[3] and our experimental results.[16] To experimentally determine the various by-products that form during the catalytic conversion of 1-octene to 7-tetradecene with **Gr1**, the large-scale experimental setup (§ 3.5) was changed to a small-scale setup to exclude quenching of the samples. This was done to eliminate the formation of esters, aldehydes and ketones as a result of quenching the samples with *tert*-butyl-hydrogen peroxide (§ 3.5.1.2). Therefore, the reaction was performed at room temperature (25 °C) at a 1-octene/Ru molar ratio of 1000 in a 5 mL mini reaction bottle with continuous monitoring of the reaction by GC/FID. The various products formed during the reaction were identified by GC/MSD (§ 3.6.2.2). The two isomers, *cis*- and *trans*-7-tetradecene (see **Chromatogram 3.1**, Chapter 3), which form part of the PMP, are the main products of the homometathesis of 1-octene. Although cross-metathesis occurs as a side reaction to produce a range of $C_2 - C_{14}$ alkene products (SMP), this reaction was

not included in the conceptual model since the focus was mainly on the productive metathesis of 1-octene to form 7-tetradecene.

After 3 h, the following by-products were also identified in the reaction mixture with the aid of GC/MSD (see **Chromatogram 3.3**, Chapter 3), i.e. styrene, *cis*- and *trans*-1-phenyl-1-octene (or hexyl styrene), PCy_3 and $O{=}PCy_3$. The presence of PCy_3 in the reaction mixture is consistent with the dissociation step leading to the active 14-electron benzylidene species. Furthermore, the presence of the styrenes is indicative of the formation of ruthenium methylidene and heptylidene species. The different orientation possibilities of 1-octene coordination to the **Gr1** benzylidene metal centre lead to the formation of a heptylidene species with the liberation of styrene, or the methylidene species with the liberation of the hexyl styrenes. Therefore, the observation of the various by-products aided us in composing the mechanistic models for the initiation, activation and catalytic steps of the **Gr1**-catalysed 1-octene metathesis reaction, which will be discussed in detail in the following sections.

For the purpose of this study the minimum structure obtained from the geometry optimisation (GGA/PW91/DNP) of 1-octene was used in further calculations. In this structure, the hexyl chain was "straight" and remained so in most of the optimisations of intermediates. The influence of the various confirmations of 1-octene on the energetics of the reaction pathway was not considered in this study. The optimised structures along with the located transition states for the various transformations for the relevant catalytic systems are presented on the included CD. The car files (hidden files) as well as xsd files of the structures are included together with the outmol data files. The energies of the various starting complexes as well as TS's in the **Gr1**-energy profiles are different than the published[16] values, since after confirmation calculations were performed on a number of the steps, structures were obtained which more closely resembled the desired π-complex and ruthenacyclobutane intermediates. The distances in some of the original structures were too large and/ or did not represent the true equilibrium structure.

6.2 METATHESIS OF 1-OCTENE IN THE PRESENCE OF GRUBBS CARBENES

The quantum mechanical calculations that were employed in this study were applied to the $RuCl_2(PCy_3)L(=CHPh)$ and $RuCl_2L(O\text{^}N)(=CHPh)$ (L = PCy_3 or H_2IMes and O^N = 1-(2'-pyridinyl)-cyclo-hexan-1-olate)) complexes with a closer focus on the *trans* addition of 1-octene to the catalytically active species. For **Gr1**, the coordination of the alkene *trans* with respect to the ligand L is the most favourable pathway, due to the fact that large phosphines, like PCy_3, have a Tolman cone angle of 170° [20,21] and the position *trans* with respect to the carbene would be avoided due to the strong σ-donor effect of the carbene bond. This is shown to be the case according to the

computational studies of Adlhart et al.[3] (ADF program, BP86 functional) in which the coordination of the alkene *trans* towards L is one of the two most favourable pathways in the catalytic cycle. The coordination of the alkene *trans* towards L was applied to the other systems to make a comparison with **Gr1**. The *trans* coordination of the alkene with respect to the ligand L will most probably also reduce steric crowding around the metal, since the steric bulk increases with the incorporation of the O,N-ligands investigated in this study.

According to Janse van Rensburg et al.,[12] the alkylidene CR_2 plane of the precatalysts "**A**" may be orientated either parallel (**A1**) or perpendicular (**A2**) to the Cl-Ru-X plane (X = Cl or O), as illustrated in **Figure 6.2** for Grubbs first and second generation catalysts and their hemilabile analogues. They[12] indicated that, for the methylidene precatalyst of **Gr1** and **Gr2**, different CH_2 orientations could account for the most stable precatalyst complex, i.e. a parallel orientation of CH_2 for **Gr2**, and perpendicular orientation for **Gr1**.

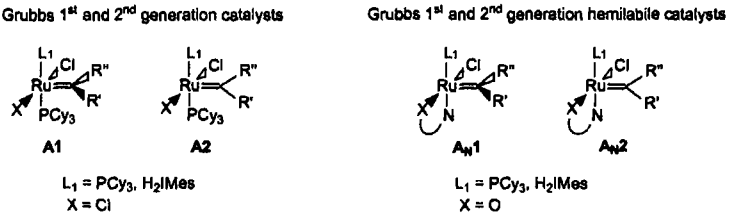

Figure 6.2 Illustration of the possible orientation of the alkylidene moiety for the Ru-carbene precatalysts.

Due to time constraints, the various possibilities were not investigated in this study. Complexes corresponding to **A1** (for **Gr1** and **Gr2**) and $\mathbf{A_N1}$ (for hemilabile complexes) were used as starting complexes before any optimisation attempts were commenced. This resulted either in the spontaneous rotation of the alkylidene moiety toward a perpendicular orientation (as seen for **Gr1Cy** and **Gr2Cy** in **Figure 6.3(b)**) or remained parallel (as seen for **Gr1** and **Gr2** in **Figure 6.3(a)**) after optimisation of the structures. It is interesting to note that the Ph-ring on the alkylidene moiety rotates downward towards the O,N-ligand for **Gr2Cy**, while it does so in the opposite direction for **Gr1Cy**. This is most probably due to the steric influence of the mesityl groups on the NHC ligand, while the Cy groups on PCy_3 can rotate to relief steric crowding.

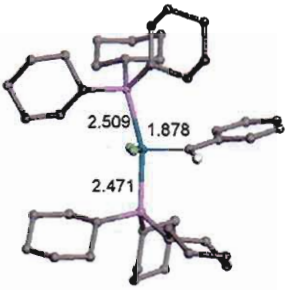

Gr1-A1

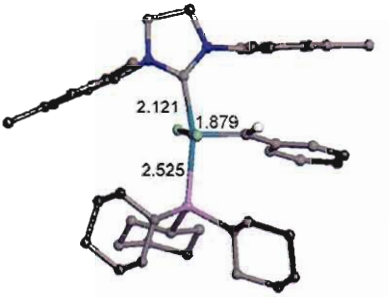

Gr2-A1

Figure 6.3(a) Optimised geometries for the lowest energy **Gr1** and **Gr2** complexes. The hydrogen atoms on the ligands are omitted for clarity and the unit of the indicated bond lengths is angstrom (Å).

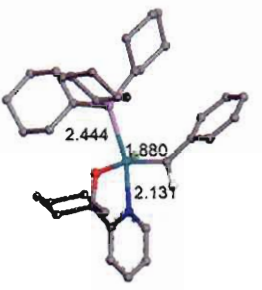

Gr1Cy-A2

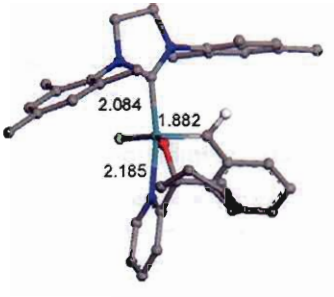

Gr2Cy-A2

Figure 6.3(b) Optimised geometries for the lowest energy **Gr1Cy** and **Gr2Cy** complexes. The hydrogen atoms on the ligands are omitted for clarity and the unit of the indicated bond lengths is angstrom (Å).

In an attempt to get a better idea of the validity of the computational method used in this study, comparisons of key bond lengths and angles of **Gr1** were made. The calculated bond lengths and angles are compared with crystallographic data obtained by Nguyen et al.[22] and calculated values obtained by Adlhart et al.[23] (**Table 6.1**). An acceptable correlation is obtained with bond lengths being overestimated and bond angles generally being underestimated in the calculations.

Table 6.1 Crystallographic and theoretical values of key bond lengths and angles of **Gr1**.

	Nguyen[22]	Calculated[a]	Calculated[23]
Bond Lengths (Å)			
Ru=C	1.838(2)	1.878	1.860
Ru-Cl_{avg}	2.390(1)	2.452	2.420
Ru-P_{avg}	2.416(1)	2.490	2.435
Bond Angles (°)			
Cl-Ru-Cl	168.21(2)	160.97	162.4
P(1)-Ru-P(2)	161.90(2)	163.35	-
Ru=C-R	136.70(2)	136.04	-

[a] DMol^3 GGA/PW91/DNP – full DFT calculation of geometries
Ref. 23 (ADF BP86 – QM/MM calculation of geometries)

In the subsequent sections the individual phases or steps in the mechanism will be discussed in more detail under the following headings:

- Catalyst initiation
- Catalyst activation
- Catalytic cycle

6.2.1 Catalyst initiation

It is generally accepted that the Ru-catalysed alkene metathesis reaction proceeds via a dissociative mechanism, which is initiated by the dissociation of a phosphine ligand from $RuX_2(PR_3)L(=CHR)$ to form a 14-electron species ("**B**").[2,3,13] In this sense catalyst initiation involves the dissociation of PCy_3 for both **Gr1** and **Gr2**.

Catalyst initiation of hemilabile complexes raises a few questions:

a) Since hemilabile ligands are believed[24] to release a free coordination site "on demand" of competing substrates and occupying it otherwise, the following question can be asked: Does the ruthenium centre of the hemilabile complexes become coordinatively unsaturated with or without the influence of the incoming alkene (see **Scheme 6.2**)?

NMR studies of the 1-octene metathesis reaction in the presence of these complexes should be able to give insight into the mechanism *inter alia* monitoring the precatalyst over time in the absence and presence of the alkene with ^{1}H and ^{31}P NMR. From these results, the influence of the alkene on releasing a free coordination site might be obtained. Due to time constraints not all the aspects of this question could be fully addressed. ^{1}H NMR analysis of the 1-octene metathesis reaction in the presence of **Gr2Cy** (§ 5.2.2.3) indicated the presence of 5 carbene species while only 3 were visible in the presence of **Gr1Cy**. Due to insufficient information, no concluding remarks could be made on the influence of the alkene, but it was noticeable that two different mechanisms may be involved for the first and second generation complexes. This should be investigated further.

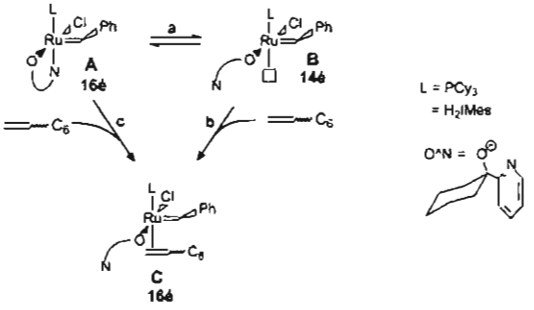

Scheme 6.2 Illustration of the dissociative (**a-b**) and associative (**c**) catalyst initiation steps for **Gr1Cy** and **Gr2Cy**.

To address this question theoretically, a comparative study on the catalyst initiation steps in **Scheme 6.2** is needed to determine which pathway (**a-b** (dissociative) or **c** (associative)) would be more favourable. At the time of completing this study, only the dissociative mechanism was addressed and will be discussed in the following sections.

b) Since the above question was not fully answered and the NMR results suggested that two different mechanisms might be involved for the first and second generation hemilabile precatalysts, a second question can be asked: Does precatalyst initiation for **Gr1Cy** and **Gr2Cy** involve the dissociation of the labile N-atom of the O,N- ligand (**Scheme 6.3 (a)**), or does it rather involve the dissociation of ligand L (with L = PCy_3 or H_2IMes) (**Scheme 6.3 (b)**)?

This was asked due to the fact that, throughout the catalytic investigation of the 1-octene metathesis reaction in the presence of all the first generation hemilabile complexes, the free PCy_3 ligand was experimentally observed with GC/FID. In the following sections, attempts will be made to answer these questions.

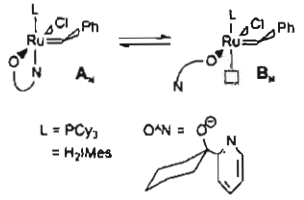

(a) Dissociation of labile N-atom of O,N-ligand

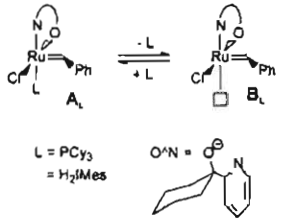

(b) Dissociation of ligand L

Scheme 6.3 Dissociation ("**A**" to "**B**") steps in the mechanism of productive 1-octene metathesis using $RuCl_2(PCy_3)L(O\text{^}N)(=CHPh)$.

Since ligand dissociation proceeds prior to the interaction of the alkene with the ruthenium centre, precatalyst initiation requires the formation of an unsaturated 14-electron complex, "**B**" (**Scheme 3.1** and **6.3**). Similar to precatalysts "**A**", various orientations of the alkylidene moiety in "**B**" is also possible (**Figure 6.4**), but was not explored in this study. Complexes corresponding to "**B1**" were used as starting structures prior to optimisations. Spontaneous formation of the perpendicular alkylidene orientation ("**B2**") resulted during optimisation of the unsaturated **Gr1**, **Gr1Cy** and **Gr2Cy** complexes, while remaining parallel for the second generation Grubbs system (**Gr2-B1**) as illustrated in **Figure 6.5**. The Ph-ring of the alkylidene once again rotates upward towards PCy_3 for the first generation systems while the steric bulk on NHC causes the Ph-ring to rotate downward into the open coordination site for **Gr2Cy**.

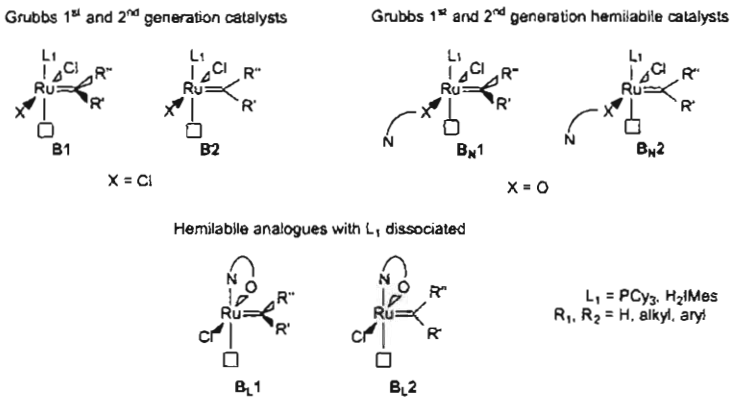

Figure 6.4 Illustration of the possible orientation of the alkylidene moiety for the Ru-carbene unsaturated complexes.

Table 6.2 summarises the calculated electronic (ΔE) energies in kcal/mol for the initiation phase ("A" – "B") of the 1-octene metathesis reaction in the presence of **Gr1**, **Gr2**, **Gr1Cy** and **Gr2Cy** according to the dissociation of the N-atom or L ligand.

Dissociation of PCy_3 from the first generation 16-electron precatalyst complex (**Gr1-A1**) proceeds with ΔE = 21.89 kcal/mol and 25.92 kcal/mol for the second generation precatalyst (**Gr2-A1**). This is in agreement with the experimental kinetic studies by Grubbs[2,13] in which $\Delta H^{\ddagger}$ values of 23.6 ± 0.5 and 27 ± 2 kcal/mol were obtained for **Gr1** and **Gr2**, respectively.

Table 6.2 Calculated electronic (ΔE) energies in kcal/mol for the initiation phase sequence "A" – "B" as catalysed by **Gr1**, **Gr2**, **Gr1Cy** and **Gr2Cy**.

Mechanistic sequence #	Gr1	Gr2	Gr1Cy	Gr2Cy
A	0.0	0.0	0.0	0.0
B_L	21.89[b]	25.92[b]	23.26[b]	61.52[a]
B_N	-	-	20.26	16.08

All energies are reported relative to the respective precatalysts "A" and balanced with the energies of the free ligand where necessary.
[a] Dissociation of L = H_2IMes, no PCy_3 ligands are present in this complex
[b] Dissociation of L = PCy_3

(a) Grubbs first and second generation catalysts

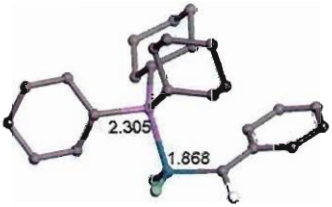

Gr1-B2

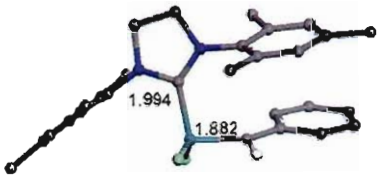

Gr2-B1

(b) Grubbs first and second generation hemilabile analogues

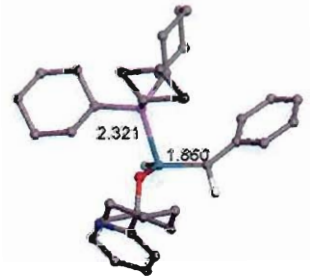

Gr1Cy-B2

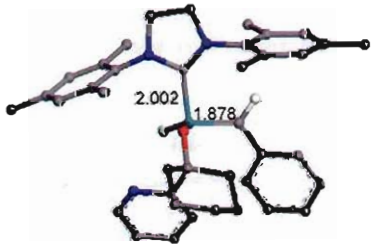

Gr2Cy-B2

Figure 6.5 Optimised geometries for the lowest energy first and second generation Grubbs unsaturated complexes, as well as their hemilabile analogues. The hydrogen atoms on the ligands are omitted for clarity and the unit of the indicated bond lengths is angstrom (Å).

The dissociation of PCy_3 in the first generation hemilabile analogue **Grl Cy-A2** (ΔE = 23.26 kcal/mol) is calculated to be 3 kcal/mol less favourable than the dissociation of the labile N-atom of the O,N-bidentate ligand. This implies that **Grl Cy** might rather initiate via the dissociation of the labile N-atom, which compared to **Grl**, is *ca.* 1.5 kcal/mol more favourable. This suggests that the initiation kinetics of **Grl Cy** should be in the same order as **Grl**, but was shown to be an order of magnitude slower (§ 5.2.3). Although the dissociation of PCy_3 from **Grl Cy-A2** (B_L) is *ca.* 3 kcal/mol less favourable than B_N, it is only 1.5 kcal/mol less favourable than **Grl**, and should therefore not be completely discarded. Only after investigating the complete mechanism, i.e. initiation, activation and catalytic cycle, can concluding remarks be made with regards to which dissociation step B_N or B_L is favoured. The dissociation of H_2IMes in the second generation hemilabile analogue **Gr2Cy-A2** (ΔE = 61.52 kcal/mol) is found to be more unfavourable (45 kcal/mol) than the dissociation of the labile N-atom. This suggests that **Gr2Cy** also initiates via the dissociation of the labile N-atom ((ΔE = 16.08 kcal/mol), which compared to **Gr2**, is *ca.* 10 kcal/mol more favourable. Similarly to **Grl Cy**, the initiation kinetics of **Gr2Cy** was found to be 2 orders of magnitude slower compared to **Gr2**, which is not in agreement with the theoretical study. This is an indication that Gibbs free energy corrections need to be done on the intermediates to include enthalpy and entropy changes. The results will then be more accurately comparable to the experimental work.

The possibility of another mechanistic route dominating *inter alia* an associative coordination of the alkene prior to dissociation of the labile N-atom, could lead to different initiation rates. This should, therefore, be more extensively explored to elucidate the preferred mechanistic pathway of 1-octene metathesis catalysed with a hemilabile complex.

6.2.2 Catalyst activation

After catalyst initiation, an alkene coordinates to the unsaturated intermediate species "B" to form the corresponding π-complexes "C". The coordination of the alkene in the *trans* position can be in two discrete, perpendicular orientations for the various Ru=C systems according to the different initiation steps (**Scheme 6.4**).

In this study, the coordination of the alkene parallel to the Cl-Ru-Cl line and perpendicular or orthogonal to the carbene (C_P) was used in the equilibrium geometry calculations of the π-coordination structures (**C**, **E**, **G** and **I**) for Grl, since the work[3] upon which the conceptual model of **Grl** was based considered this coordination as energetically favourable. If the alkene coordinates in the C_P mode (**Scheme 6.4**), it has to turn approximately 90° to align with the benzylidene carbene bond (C_H mode) to yield the metallacyclobutane intermediate (**C-D**, etc.). In a recent study,[12] it was shown that the coordination of the alkene in the C_H mode is more

energetically favoured. Therefore, for **Gr2**, **Gr1Cy** and **Gr2Cy**, both the C_p-C_{II}-D and C_{II}-D conversion were investigated, while investigation of the C_{II}-D conversion for **Gr1** was still ongoing at completion of this study. For the sake of simplicity, all the π-coordination structures are given in the C_{II} mode and will be referred to as the C_p mode when investigating the C_p-C_{II}-D conversions, while the C_{II} mode will be used when looking at the C_{II}-D conversions.

Since ethene is generally used as substrate in most theoretical studies, we initially modelled the activation steps of **Gr1** with ethene to the corresponding metallacyclobutane intermediate and compared our results with the values obtained by other authors (**Figure 6.6**). This was done to determine the validity of the computational method we used in this study and point out the importance of using the benzylidene precatalyst instead of the methylidene model.

(a) Grubbs 1st and 2nd generation catalysts

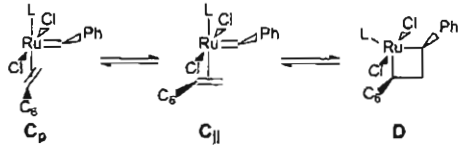

(b) Grubbs 1st and 2nd generation hemilabile analogues: Dissociation of labile N-atom

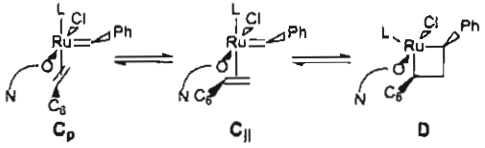

(c) Grubbs 1st and 2nd generation hemilabile analogues: Dissociation of ligand L

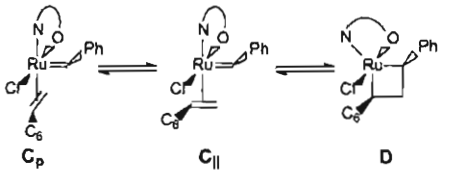

Scheme 6.4 *Trans* alkene coordination in the dissociative pathway for the Grubbs catalysts (L = PCy_3 or H_2IMes).

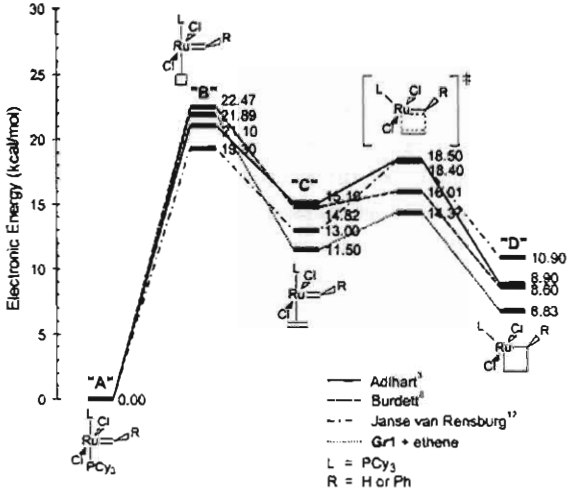

Figure 6.6 A comparison of the calculated and literature-reported electronic energy profiles of the activation steps of ethene metathesis using **Grl**.

The electronic energy profile we calculated (DMol[3], GGA-PW91 functional, DNP basis set) was for the **Grl** benzylidene system, while the electronic energies obtained by Adlhart et al.[3] (ADF program, BP86 functional, triple ξ basis set on ruthenium and a polarised double ξ basis set for all other elements), Burdett et al.[8] (Jaguar 4.1 program, B3LYP hybrid functional, LACVP** basis set) and Janse van Rensburg et al.[12] (DMol[3], GGA-PW91 functional, DNP basis set) were calculated for the **Grl** methylidene. It has been shown that sterically bulky and electron-donating R groups (e.g. alkyl, Ph) lead to higher initiation rates (phosphine dissociation) because they more effectively promote phosphine dissociation, while small and electronically neutral groups (e.g., H) are less effective at labilising the phosphine ligand.[15] This is not significantly clear in **Figure 6.6**. The trend for the formation of the metallacyclobutane ring is similar in all four cases, but a more stable 16-electron complex ("**C**") as well as a 14-electron metallacyclobutane ("**D**") is obtained from the benzylidene complex. It was shown that electron-withdrawing phosphine ligands would destabilise the 14-electron metallacyclobutane intermediate ("**D**") relative to the 14-electron carbene species ("**B**").[3] Therefore, the presence of an electron-donating species will have a stabilisation effect on these complexes. This explains the catalytic activity of the methylidene but lack of activation by the benzylidene.

The coordination of the substrate to the 14-electron species ("**B**" to "**C**") is a step that is in competition with the recoordination of the phosphine ligand ("**B**" to "**A**"). In our model there is only one substrate molecule competing with one phosphine, although in a catalytic system with precatalyst to substrate ratios of 1:500 or more, this competition is statistically favoured towards the substrate. The stoichiometric competition described in our model excludes this statistical competitiveness. The competition can be described by comparing the energy of coordination of the phosphine to the energy of coordination of the substrate by taking the ratio of the respective energy differences. These values are summarised by the ratio $\Delta E_{B\text{-}A}/\Delta E_{B\text{-}C}$ in **Table 6.3** for the metathesis of 1-octene and ethene with **Gr1** and **Gr2**. Grubbs et al.[2,13,25] have demonstrated experimentally that the activity of a metathesis catalyst can be correlated to the ratio of the rates for phosphine recoordination (k_{-1}) and ethene coordination (k_2) to the 14-electron complex "**B**". They have found that k_{-1}/k_2 was 4 orders of magnitude larger for **Gr1** in comparison to **Gr2**, which quantified the better alkene coordination selectivity of **Gr2** to its higher experimentally observed activity. A similar trend is observed from the modelling results in which phosphine recoordination is favoured for **Gr1**, while **Gr2** displays a larger affinity for the coordination of 1-octene. However, it was also noted that the affinity of **Gr1** and **Gr2** towards phosphine slightly increases with an increase in the chain length of the substrate.

Table 6.3 Comparison of electronic energies of the π-coordination intermediate $RuCl_2(PCy_3)L(=CHPh)$ containing ethene and 1-octene.

	Energy Ratio	
L	$\Delta E_{B\text{-}A} / \Delta E_{B\text{-}C}$	$\Delta E_{B\text{-}C}$ (B to C) kcal/mol
Gr1+ethene	2.11	-10.39
Gr1+1-octene	2.39	-9.16
Gr2+ethene	1.63	-15.90
Gr2+1-octene	1.79	-14.45

If the electronic energy profiles of **Gr1** with ethene and 1-octene are compared (**Figure 6.7**), it is clear that the 1-octene does not coordinate as strongly as the ethene to B ("**C**"). The electronic energy of activation of "**C**" to "**D**" with ethene is 2.87 kcal/mol while the value with 1-octene is 13.85 kcal/mol. Adlhart and Chen[23] calculated the activation energy ($\Delta E_o^{\ddagger}$) for the insertion barrier "**C**" to "**D**" with styrene as 12.30 kcal/mol. The activation with 1-octene seems to be the less favourable outcome. The metallocyclobutane intermediates are of similar thermodynamic electronic stability in both cases. The formation of "**D**" form "**C**" is exergonic for both ethene (-4.67 kcal/mol) and for 1-octene (-6.49 kcal/mol), with the rate-limiting step in both cases being the decomposition of the metallacyclobutane ("**D**" to "**E**"). The overall energy change from "**B**" to "**F**" is

endergonic (0.22 kcal/mol) for ethene and exergonic (-3.87) for 1-octene, which can be a small driving force for the 1-octene activation. Thus, if the substrate is changed from a C_2 to a C_8 alkene, deviations in the electronic profiles are observed which could have an impact on the rate of activation of the complexes. One should therefore be careful to directly apply the model with ethene as a simple substrate to systems using larger substrates like 1-octene.

The activation steps for the formation of the methylidene and heptylidene species were investigated in more detail for **Gr1**, **Gr2** as well as the hemilabile **Gr1Cy** and **Gr2Cy** systems to determine which pathway is more favourable. The activation step investigations of the hemilabile complexes will be discussed separately form the Grubbs carbenes in order to distinguish between the different activation phases that formed due to the two distinct initiation phases.

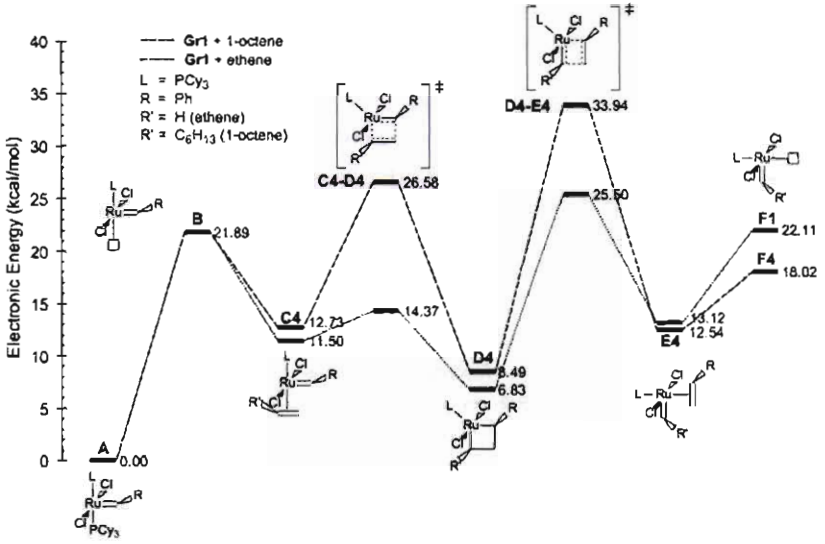

Figure 6.7 Electronic energy profiles of the activation steps of the metathesis of ethene and 1-octene using **Gr1**.

6.2.2.1 Activation phase: Gr1- and Gr2-catalysed metathesis reaction

Figure 6.8 – 6.9 illustrate the activation steps for the C_p mode of **Gr1** and **Gr2**, while **Figure 6.10** illustrates the steps for the C_{II} mode of **Gr2**. Activation step 3 is not shown because of its similarity to activation step 4. Dissociation of the phosphine and association of the alkene are both free of activation enthalpy because they proceed without considerable rearrangement of the complex.

Activation step 4 (**B** to **C4** to **F4**) is kinetically and thermodynamically more favourable than activation steps 1 (**B** to **C1** to **F1**) and 2 (**B** to **C2** to **F1**; note **F2** = **F1**) for both systems in the C_p mode as well as the C_{II} mode of **Gr2**. The rate-limiting step for the formation of the alkylidene species in the presence of **Gr1** is the decomposition of the ruthenacyclobutane ("**D**" to "**E**"), while for **Gr2** it is ruthenacyclobutane formation ("**C**" to "**D**"). The activation energy of the rate-limiting step ("**D**" to "**E**") for heptylidene formation from **Gr1** is 25,45 kcal/mol while methylidene formation requires more than 29 kcal/mol and the overall energy change from "**B**" to "**F**" is -3.87 and approximately 17 kcal/mol, respectively. For **Gr2** in the C_p mode, the activation energy of the rate-limiting step ("**C**" to "**D**") for heptylidene formation is 42.12 kcal/mol while methylidene formation requires more than 50 kcal/mol. The overall energy change from "**B**" to "**F**" for heptylidene formation is 4.47 and for methylidene formation approximately 20 kcal/mol. Therefore, the heptylidene formation is exothermic for **Gr1** and endothermic for **Gr2** from "**B**" to "**F**", which indicates that **Gr2** is thermally more stable than **Gr1**. The calculated activation energy of the rate-limiting step ("**C**" to "**D**") for heptylidene formation in the C_{II} mode of **Gr2** is 31.83 kcal/mol, while methylidene formation requires *ca.* 44 kcal/mol. The overall energy change from "**B**" to "**F**" is similar to the C_p mode since the unsaturated species are identical in both modes.

Whether one reaction pathway is favoured compared to an alternative pathway does not depend on relative energy differences of individual step, but on the absolute energy of the highest transition state.[26] Therefore, for **Gr2**, coordination of the alkene parallel to the carbene and perpendicular or orthogonal to the Cl-Ru-Cl line (C_{II}) seems to be the more energetically favoured pathway, since the activation energy of the rate-limiting step is lower for the C_{II} mode compared to the C_p mode. Interestingly, the decomposition of the ruthenacyclobutane ("**D**" to "**E**") for heptylidene formation as well as methylidene formation in step 2 is barrierless in the C_{II} mode, while respective barriers of 5.08 and 1.63 kcal/mol have to be overcome in the C_p mode. Additionally, during methylidene formation from **Gr2**, barriers of 11 and 15 kcal/mol have to be overcome in activation step 1 for the decomposition of the ruthenacyclobutane ("**D**" to "**E**") in the C_{II} and C_p modes, respectively. This might indicate that **D1**, in which the orientation of the alkyl chain of 1-octene is *trans* relative to the Ph-ring of the benzylidene moiety, is more stable than **D2**, where the alkyl chain is *cis* relative to the Ph-ring. Therefore, due to steric crowding in **D2**, it spontaneously transforms to **E2** in the C_{II} mode with only a small barrier of 1.63 kcal/mol to overcome in

the C_p mode. The fact that heptylidene formation is kinetically and thermodynamically more favourable than the formation of methylidene for both **Gr1** and **Gr2** explains why the ^1H NMR results (§ 5.2.1.2) show a rapid formation of the heptylidene at the onset of the reaction at room temperature.

6.2.2.2 Activation phase: hemilabile Ru=C-catalysed metathesis reaction

a) Metathesis of 1-octene in the presence of Gr1Cy and Gr2Cy

Dissociation of the labile N-atom from Gr1Cy and Gr2Cy

Figure 6.11 and **6.13** illustrate the activation steps for the C_p mode of **Gr1Cy** and **Gr2Cy**, while **Figure 6.12** and **6.14** illustrate the steps for the C_{II} mode according to **Scheme 3.3**. Activation step 3 is not shown for the hemilabile systems because of its similarity to activation step 4. No energy barriers were calculated for the dissociation of the labile N-atom or the association of the alkene since it was assumed that these steps proceed without considerable rearrangement of the complex. This should be investigated further to take the rotation of the hemilabile ligand around the Ru-O-bond into consideration.

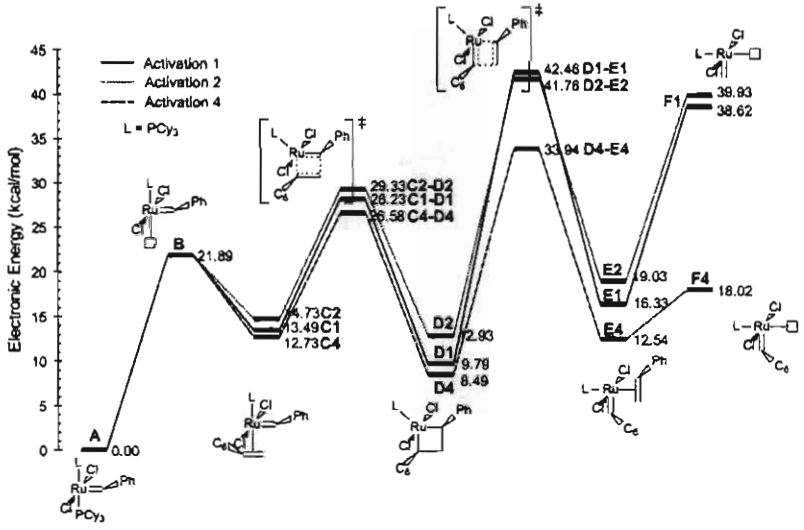

Figure 6.8 Electronic energy profiles of the activation steps in the productive 1-octene metathesis using **Gr1** (only the **C4** to **F4** structures are shown) (C_p mode).

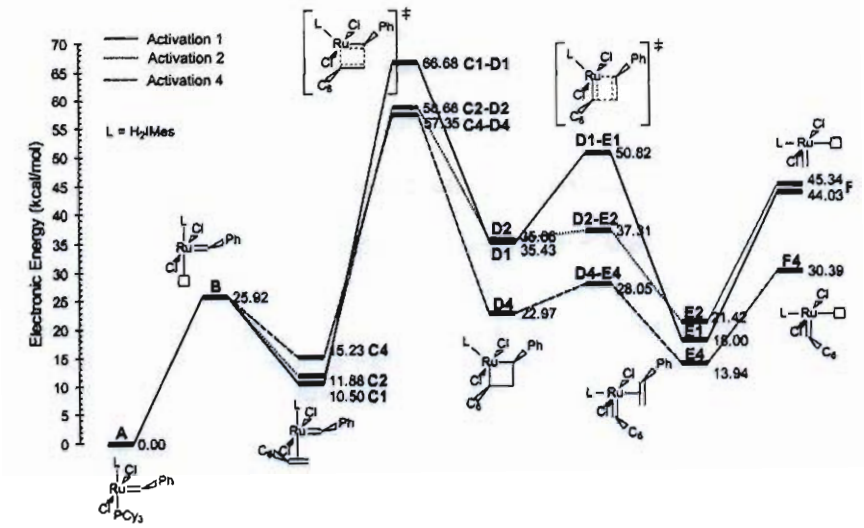

Figure 6.9 Electronic energy profiles of the activation steps in the productive 1-octene metathesis using **Gr2** (only the **C4** to **F4** structures are shown). (C_p mode)

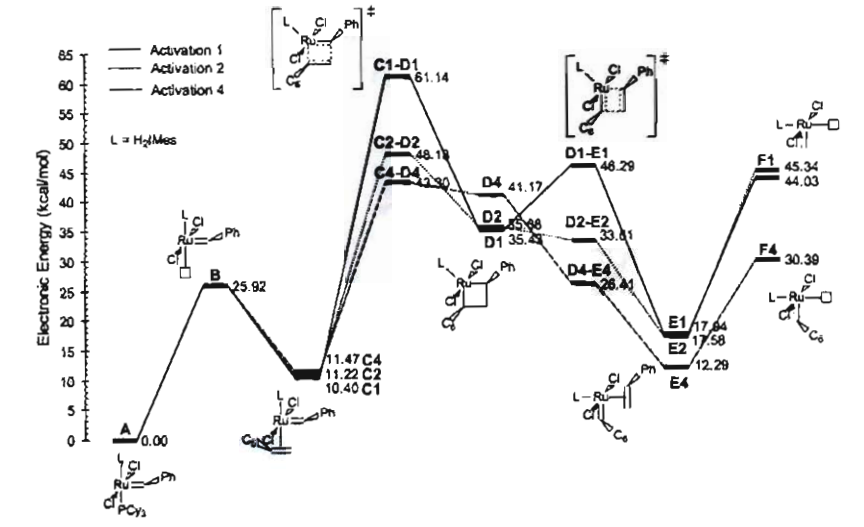

Figure 6.10 Electronic energy profiles of the activation steps in the productive 1-octene metathesis using **Gr2** (only the **C4** to **F4** structures are shown). (C_{ii} mode)

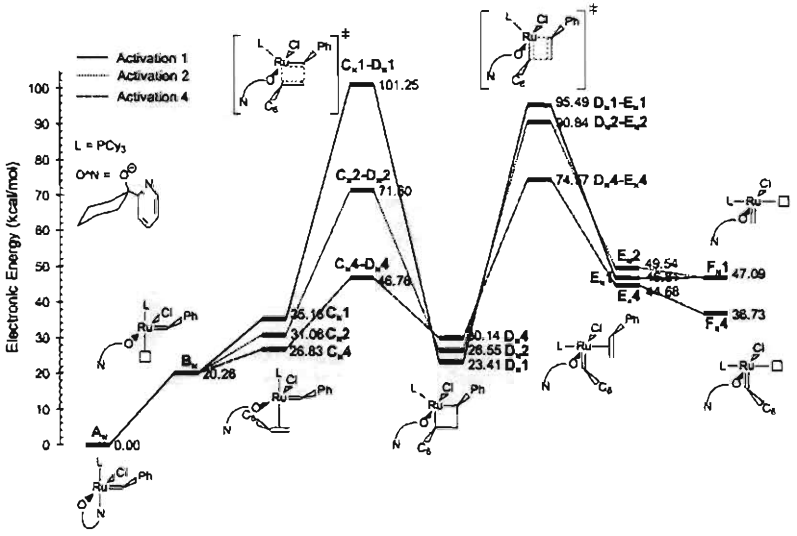

Figure 6.11 Electronic energy profiles of the activation steps in the productive 1-octene metathesis using **Grl Cy** (only the C_N4 to F_N4 structures are shown) (C_p mode).

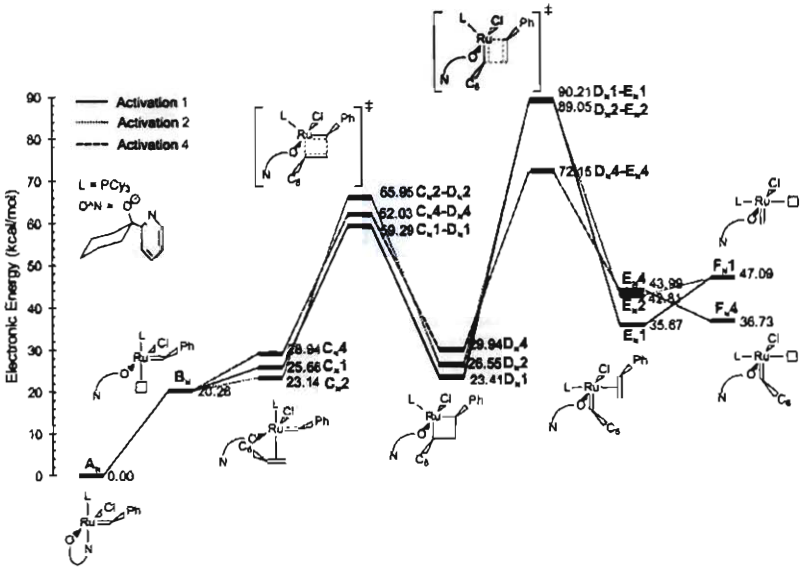

Figure 6.12 Electronic energy profiles of the activation steps in the productive 1-octene metathesis using **Gr1Cy** (only the C_N4 to F_N4 structures are shown). (C_{II} mode)

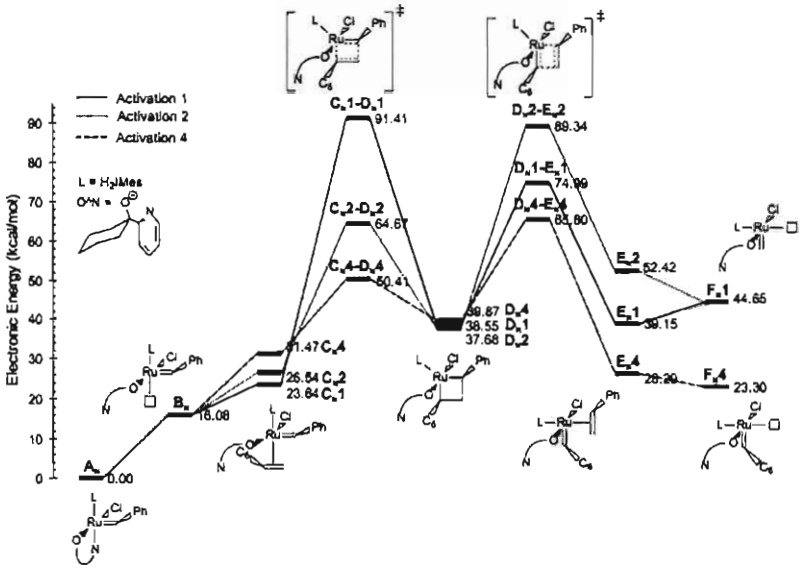

Figure 6.13 Electronic energy profiles of the activation steps in the productive 1-octene metathesis using **Gr2Cy** (only the C_N4 to F_N4 structures are shown) (C_p mode).

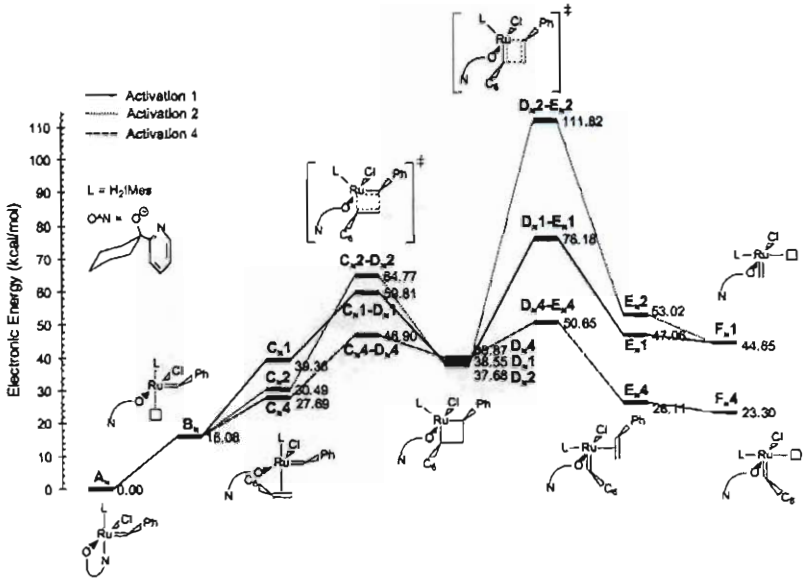

Figure 6.14 Electronic energy profiles of the activation steps in the productive 1-octene metathesis using **Gr2Cy** (only the C_N4 to F_N4 structures are shown) (C_{II} mode).

Activation step 4 (B_N to C_N4 to F_N4) is thermodynamically and kinetically more favourable than activation steps 1 (B_N to C_N1 to F_N1) and 2 (B_N to C_N2 to F_N1; note $F_N2 = F_N1$) for both systems in the C_p and C_{II} mode. However, the modelling results for **Gr2Cy** cannot explain the observed ^{1}H NMR results, in which the carbene signal of F_N1 from **Gr2Cy** is observed to keep growing without being depleted. This indicates that the complete mechanism, with inclusion of the catalytic cycle, should be investigated to make any concluding remarks. It has however been demonstrated by Halpern[27] that the most abundant complex in a solution need not be a part of the most favourable catalytic cycle; it may represent, in fact, a dead end. Therefore, a more in depth study of the complete mechanism is needed. The absence of F_N1 in the ^{1}H NMR study of the 1-octene metathesis reaction with **Gr1Cy**, might suggest that a different mechanistic pathway is followed.

The calculated reaction energy for the formation of the ruthenacyclobutane intermediate (**Gr1Cy-D_N4**) from the π-complex **Gr1Cy-C_N4** in the presence of **Gr1Cy** is endergonic (3.31 kcal/mol) for the C_p mode with activation energy of 31 kcal/mol. In contrast, the formation of "D_N" from the π-complex "C" is exergonic for both activation steps 1 (-11.95 kcal/mol) and 2 (-4.51 kcal/mol) with activation energies of 66 and 45 kcal/mol, respectively. The decomposition of the ruthenacyclobutane ("D_N" to "E_N") is endergonic for both the heptylidene (15 kcal/mol) and methylidene (*ca.* 23 kcal/mol) formation steps with activation energies of *ca.* 45 and 70 kcal/mol, respectively. The coordination of the 1-octene in the C_{II} mode has a *ca.* 2 – 5 kcal/mol decrease in $\Delta E_o^{\ddagger}$ for "D_N" to "E_N" for all 3 activation steps, as well as for "C_N" to "D_N" in step 2. Additionally, a 30 kcal/mol decrease in $\Delta E_o^{\ddagger}$ is observed for the formation of the ruthenacyclobutane in step 1, while step 4 shows a 2 kcal/mol increase. This indicates that the alkene prefers to coordinate to **Gr1Cy** in the C_{II} mode, in which the steric bulk around the Ru-centre is relieved in steps 1 and 2. This is due to the fact that the alkyl chain of 1-octene in steps 1 and 2 is no longer parallel to the Cl-Ru-O line, in which the alkyl chain was directly below the O,N-ligand and thereby adding to the steric bulk around the Ru-centre. The rate-limiting step for the formation of the heptylidene, as well as the methylidene species in the presence of **Gr1Cy**, is the decomposition of the ruthenacyclobutane ("D_N" to "E_N") for both coordination modes.

For **Gr2Cy**, the decomposition of the ruthenacyclobutane ("D_N" to "E_N") in step 4 for both coordination modes, as well as the formation of "D_N" from "C_N" in step 1 for the C_{II} mode is exergonic, i.e. approximately -13 and -1 kcal/mol, respectively. All the other formation or decomposition steps are endergonic for both the C_p and C_{II} modes. In contrast to **Gr1Cy**, different rate-limiting steps are involved for the formation of the heptylidene species from **Gr2Cy** in the C_p and C_{II} modes i.e. "D_N" to "E_N" for C_p and "C_N" to "D_N" for C_{II} with activation energy of 25.93 and 19.21 kcal/mol, respectively. The decomposition of the ruthenacyclobutane ("D_N" to "E_N") is considered the rate-limiting step for the formation of the methylidene species in step 1 ($\Delta E_o^{\ddagger}{}_{D1\text{-}E1}$ = 37.63 kcal/mol) and 2 ($\Delta E_o^{\ddagger}{}_{D2\text{-}E2}$ = 74.14 kcal/mol) in the C_{II} mode as well as step 2 ($\Delta E_o^{\ddagger}{}_{D2\text{-}E2}$ =

51.66 kcal/mol) in the C_p mode. The rate-limiting step for the formation of the methylidene species in step 1 in the C_p mode is the formation of the ruthenacyclobutane with an activation energy of 67.77 kcal/mol. No conclusions can be made regarding the preferred coordination mode of the alkene to **Gr2Cy**, since mixed increasing and decreasing effects are observed with regards to the TS's. This might be due to the fact that the preliminary frequency analysis on the various TS's indicated that only D_N1-E_N1 (263*i* cm^{-1}) and C_N4-D_N4 (120*i* cm^{-1}) in the C_p mode are close to a transition state. This supports the fact that refinements on the reagents and products need to be done, followed by TS confirmations and TS optimisations within the DFT calculations. These are time-consuming computations, which additionally require vibrational mode calculations that were ongoing at the time of completion of this study. The overall energy change from "B_N" to "F_N" for both the C_p and C_{II} mode for heptylidene formation in the presence of **Gr1Cy** and **Gr2Cy** is 16.47 and 7.22 kcal/mol, respectively. For methylidene formation it is between 27 and 29 kcal/mol, respectively. The 1-octene metathesis reaction in the presence of **Gr1Cy** and **Gr2Cy** is therefore strongly endothermic compared to **Gr1** and **Gr2**, which indicates that the hemilabile Ru-carbene complexes are relatively more stable compared to the Grubbs carbenes. The reason why **Gr2Cy** is less endothermic compared to **Gr1Cy**, when the opposite is actually expected, is uncertain at this stage and needs to be investigated further. It might be that ΔG corrections will provide a different answer, as was illustrated[12] for the ethene metathesis reaction with **Gr1**.

Comparison of the activation steps of **Gr1Cy** and **Gr2Cy** for the formation of the heptylidene species in the C_{II} mode (which is more favourable than the C_p mode) (see **Figure 6.15**), suggests that **Gr2Cy** is more active than **Gr1Cy**. Due to the endergonic nature of the sequence "A_N" → "B_N" → "C_N" → "C_N-D_N" (**Figure 6.15**) for both systems, the total barrier for ruthenacyclobutane ("D_N") formation may be correlated to the energy change of "A_N" → "C_N-D_N".[12] The largest barrier is calculated for **Gr1Cy** (62.03 kcal/mol), with **Gr2Cy** (46.90 kcal/mol) exhibiting a much lower barrier. Therefore, relative reaction rates for these catalyst in decreasing order are suggested: **Gr2Cy** > **Gr1Cy**, which is in qualitative agreement with the relative turnover numbers (§ 5.2.2) of these systems.[28]

Dissociation of ligand L from Gr1Cy and Gr2Cy:

It is generally assumed that ruthenium-catalysed metathesis reactions proceed through 14-electron intermediates.[2-4,13] Therefore, the possibility of phosphine or NHC ligand dissociation from the respective first and second generation hemilabile carbenes should not be excluded. Consequently, we have postulated a mechanism for the **Gr1Cy** and **Gr2Cy**-catalysed 1-octene metathesis reaction (**Scheme 3.4** in Chapter 3) whereby the O,N-ligand remains attached to the Ru-centre. Similar to the dissociation of the labile N-atom, a very stable methylidene species is obtained from **Gr1Cy** and **Gr2Cy** after dissociation of L. As seen in **Figure 6.16 (a)** and **(b)**, the

only difference between the optimised heptylidene and methylidene species is the alkyl chain of the alkylidene moiety, which makes this result inexplicable.

The activation steps for the C_p mode of **Gr1Cy** and **Gr2Cy** are graphically represented in **Figure 6.17** and **6.19**, while **Figure 6.18** and **6.20** illustrate the steps for the C_{ll} mode according to **Scheme 3.4**. Activation step 3 is not shown due to its similarity to activation step 4. No energy barriers were calculated for the dissociation of ligand L (L = PCy_3 or H_2IMes) or the association of the alkene, since it proceeds without considerable rearrangement of the complex.

Experimental[2,13] and theoretical evidence[3,9,23,29,30] has shown that the phosphine, and not the NHC carbene dissociates from **Gr2**, indicating that the intermediates for catalysis by first and second generation catalysts are different. Due to the higher binding energy of NHC ligands in comparison to phosphine ligands, the dissociation of the NHC ligand during the initiation step of the mechanistic cycle will result in higher dissociation energy.[2,29] This is most probably due to the increased σ-donor capability and the reduced π-acidity of the NHC ligand[31-33] in comparison to PR_3 ligands, which increase the stability of the second generation catalysts. When applied to the hemilabile second generation systems, it is clearly shown that the dissociation of the NHC ligand, which is 45 kcal/mol higher than the dissociation of the labile N-atom, will be improbable.

The individual steps ("C_L", "D_L" and "E_L") of the current activation phase in the presence of **Gr2Cy** are approximately 10 – 20 kcal/mol higher for both the C_p and C_{ll} modes, compared to the activation phase in which the labile N-atom of the O,N-ligand dissociates (**Figure 6.13** and **6.14**). This indicates that **Gr2Cy** most likely initiates according to **Scheme 3.3** rather than **Scheme 3.4**.

Although the dissociation of PCy_3 from **Gr1Cy** is 3 kcal/mol higher compared to the dissociation of the labile N-atom of the O,N-ligand, more stable intermediates form during the activation phase for both the C_p and C_{ll} modes (**Figure 6.17** and **6.18**). A decrease of approximately 15 – 30 kcal/mol is observed in the energies of the alkene-coordinated π-complexes, together with a 5 – 15 kcal/mol decrease in the metallacyclobutane "**D**" species. A decrease was also noted in the transition states, which varied between 5 to 45 kcal/mol. Additionally, the overall energy changes from "B_L" to "F_L" for both the C_p and C_{ll} modes decrease with 12 kcal/mol. This indicates that **Gr1Cy** most likely initiates according to **Scheme 3.4** rather than **Scheme 3.3**, which explains why only 3 carbene species are observed during the ^{1}H NMR investigation (§ 5.2.2.3). Since it has been shown that **Gr2Cy** initiates according to **Scheme 3.3**, only the activation steps (**Scheme 3.4**) for the 1-octene metathesis reaction with **Gr1Cy**, will be discussed in more detail.

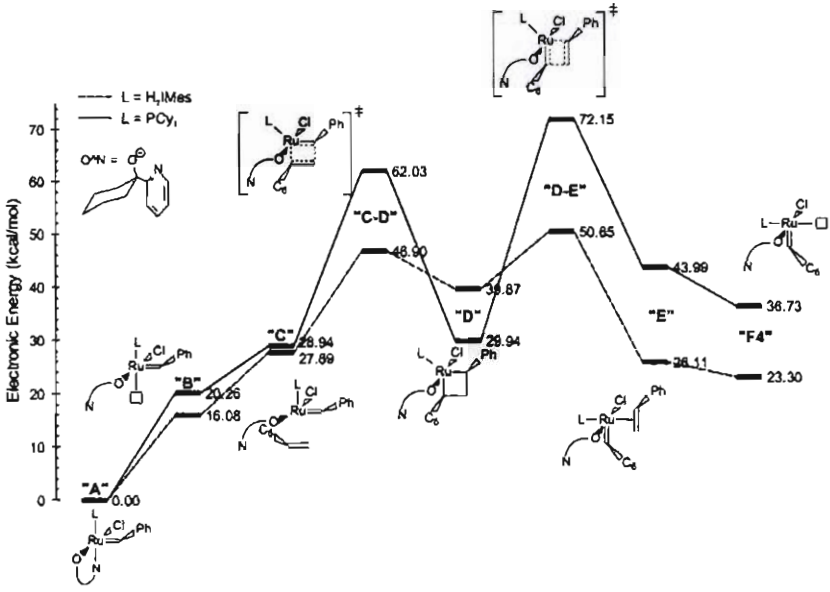

Figure 6.15 Comparison of the electronic energy profiles of the activation steps of **Gr1Cy** and **Gr2Cy** in the productive 1-octene metathesis (C_{α} mode).

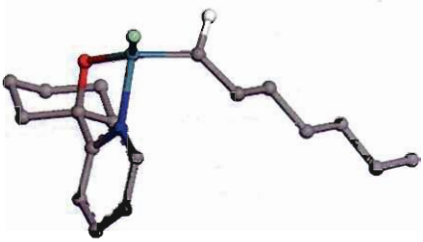

(a) Hemilabile unsaturated heptylidene (F_L4) species after dissociation of L

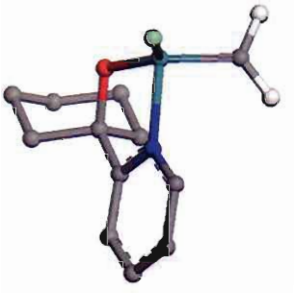

(b) Hemilabile unsaturated methylidene (F_L1) species after dissociation of L

Figure 6.16 Optimised geometries for the heptylidene and methylidene **Gr1Cy** and **Gr2Cy** species after dissociation of L. The hydrogen atoms on the ligands are omitted for clarity.

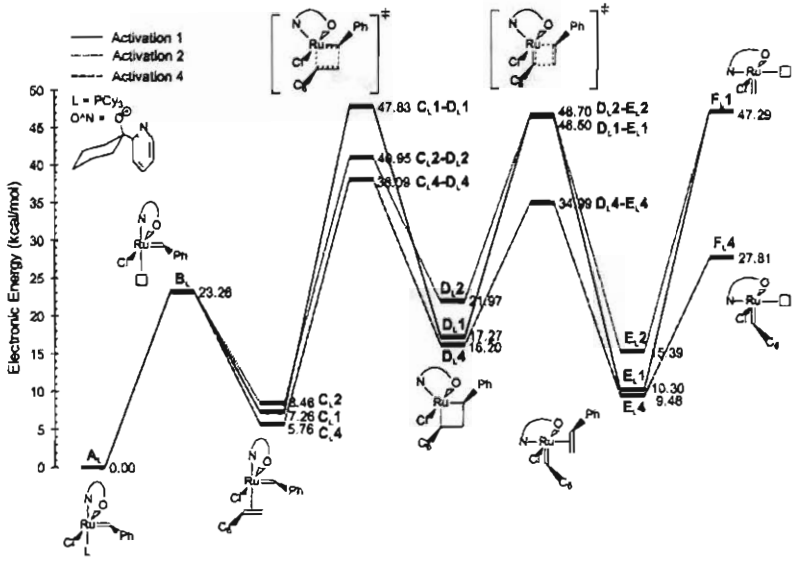

Figure 6.17 Electronic energy profiles of the activation steps in the productive 1-octene metathesis using **Gr1Cy** (only the C_L4 to F_L4 structures are shown) (C_p mode).

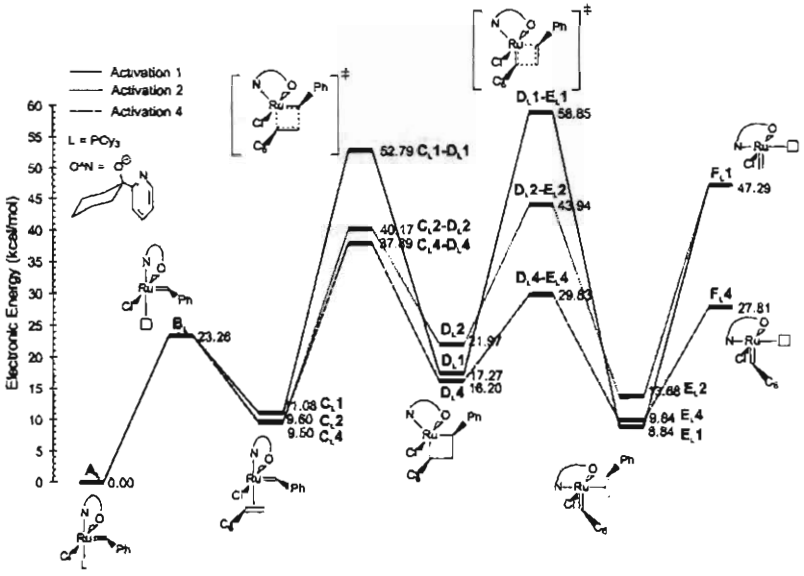

Figure 6.18 Electronic energy profiles of the activation steps in the productive 1-octene metathesis using **Gr1Cy** (only the C_L4 to F_L4 structures are shown) (C_{II} mode).

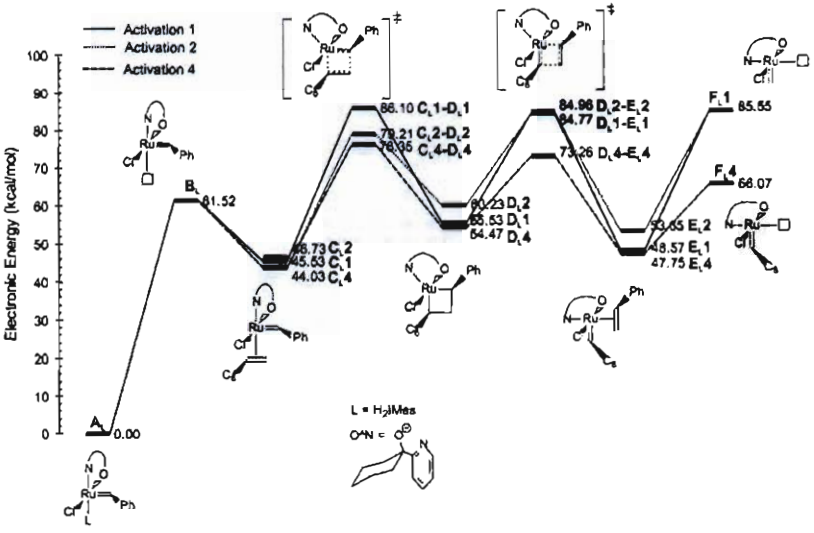

Figure 6.19 Electronic energy profiles of the activation steps in the productive 1-octene metathesis using **Gr2Cy** (only the C_L4 to F_L4 structures are shown) (C_p mode).

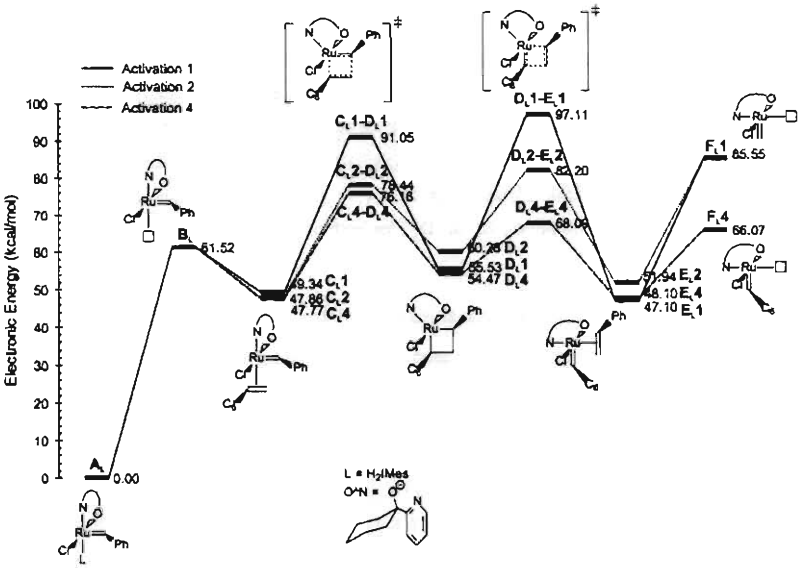

Figure 6.20 Electronic energy profiles of the activation steps in the productive 1-octene metathesis using **Gr2Cy** (only the C_L4 to F_L4 structures are shown) (C_{II} mode).

Activation step 4 (B_L to C_L4 to F_L4) is thermodynamically and kinetically more favourable than activation steps 1 (B_L to C_L1 to F_L1) and 2 (B_L to C_L2 to F_L1; note $F_L2 = F_L1$) for **Gr1Cy** in the C_p and C_{II} mode. The calculated reaction energy for the formation of the ruthenacyclobutane intermediate ("D_L") from the π-complex "C_L" in the presence of **Gr1Cy** is endergonic for the C_p (*ca.* 11 kcal/mol) and C_{II} (*ca.* 9 kcal/mol) mode for all the activation steps. In contrast, the formation of "D_L" from the π-complex "C_L" is exergonic for all the activation steps in the C_p (*ca.* -7 kcal/mol) and C_{II} (*ca.* -8 kcal/mol) mode. The coordination of the 1-octene in the C_{II} mode shows only a slight decrease in the activation energy of the ruthenacyclobutane formation and decomposition steps for activation steps 2 (1.92 kcal/mol decrease) and 4 (3.94 kcal/mol decrease), with a 1 kcal/mol increase for step 1. In contrast, a 12.59 kcal/mol increase was observed in $\Delta E_o^{\ddagger}$ for "D_L" to "E_L" for step 1. This indicates that the alkene can coordinate to **Gr1Cy** in either mode. The rate-limiting step for the formation of the heptylidene ($\Delta E_o^{\ddagger} \approx 30$ kcal/mol) as well as the methylidene ($\Delta E_o^{\ddagger} \approx 30$ to 42 kcal/mol) species in the presence of **Gr1Cy**, from which PCy_3 has dissociated, is the formation of the ruthenacyclobutane ("C_L" to "D_L") for both coordination modes.

b) Metathesis of 1-octene in the presence of Gr1Ph

In an attempt to investigate the activation of the remaining O,N-chelated Ru=C hemilabile complexes, a first glance were given to the **Gr1Ph** system, which was experimentally shown to initiate fairly slow. The dissociation of the N-atom of the pyridine requires 23.68 kcal/mol energy (**Table 6.4**), which is 3.43 kcal/mol higher than **Gr1Cy**, supporting the slower initiation rate of **Gr1Ph** compared to **Gr1Cy** (§ 5.2.3.1). However, the coordination of 1-octene to **Gr1Ph**, either parallel or perpendicular to the carbene (**Figure 6.21 (a)**) to form the heptylidene intermediate, is unfavourable. This is likely due to the steric pressure exerted by the combined bulk of the O,N-ligand and trialkylphosphine ligand (PCy_3) forcing the alkene out of coordination proximity of the Ru=C (see **Figure 6.21 (a)**). Conversely, it was noted that optimisation of the starting complex in which the 1-octene was coordinated parallel to the carbene with the alkyl chain of 1-octene *cis* to the Ph-ring of the benzylidene moiety (**Figure 6.21 (b)**), 1-octene remained within coordination distance of the Ru-centre. The latter will result in the formation of the methylidene intermediate, which has been shown for **Gr1Cy** to be thermodynamically so stable that it will not react any further, indicating that another mechanism is involved.

The steric constraints may be relieved through coordination of the alkene after dissociation of the PCy_3 ligand. Although this was not investigated for **Gr1Ph**, it was shown to be more favourable for **Gr1Cy**. Investigation of the various initiation routes of the remaining hemilabile complexes together with their activation steps were ongoing at the time of completion of this study and will not be discussed further.

(a) Coordination of 1-octene in C_p for formation of heptylidene

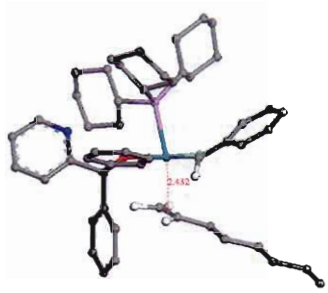

(b) Coordination of 1-octene in C_{II} for formation of methylidene

Figure 6.21 Optimised structures for the coordination of 1-octene to **Gr1Ph** in the C_p and C_{II} modes

Table 6.4 Electronic energies for the 1-octene metathesis reaction with **Gr1Ph** and **Gr1Cy** in the C_{II} mode to form the methylidene active species

Intermediate \ Catalyst	Gr1Ph	Gr1Cy
"A"	0	0
"B"	23.68	20.26
"C"	30.00	25.66

6.2.3 Catalytic cycle

The catalytic cycles for **Gr1**, using the heptylidene **F4**, were further investigated; a 1-octene molecule now coordinates to the catalytically active species to yield **H4** (see **Scheme 3.2**). The catalytic cycles of the other systems were beyond the scope of this study. Stereochemically the coordination of 1-octene can take place in two different modes, the hexyl groups *trans* (**G4a**) and the hexyl groups *cis* (**G4b**), with their respective electronic energy profiles illustrated in **Figure 6.22**.

The energies of "G" and "H", as well as the TS's, are different than the published[16] values, since after confirmation calculations were performed on these steps ("G" to "H"), structures were obtained which more closely resembled the desired π-complex and ruthenacyclobutane. The distances in the original structures were too large and "H" did not represent a true ruthenacyclobutane. The two approaches give rise to transition states with different electronic energies; the *cis*-mode requiring 17.33 kcal/mol and the *trans*-mode only 11.28 kcal/mol. The calculated reaction energy for the formation of the ruthenacyclobutane intermediate ("H") from the π-complex "G" in the presence of **Gr1** is exergonic for the *cis*-route (*ca.* -2.60 kcal/mol) and the *trans*-route (*ca.* -3.24 kcal/mol). The metallacyclobutane intermediates that form (**H3a** and **H3b**) then liberates the PMP's, *trans*-7-tetradecene and *cis*-7-tetradecene, and the methylidene (**F1**).

The *trans*/*cis*-ratio found experimentally (**Chromatogram 6.1**) correlates roughly with the corresponding activation energy ratio.

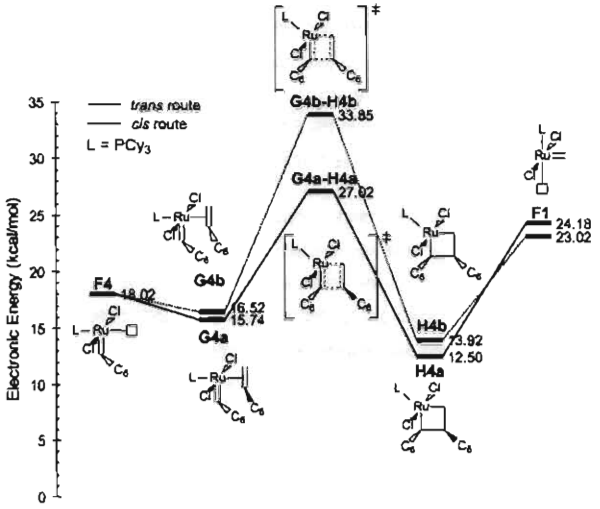

Figure 6.22 Electronic energy profile of the *trans*- and *cis*-routes from the heptylidene F4 to the methylidene F1.

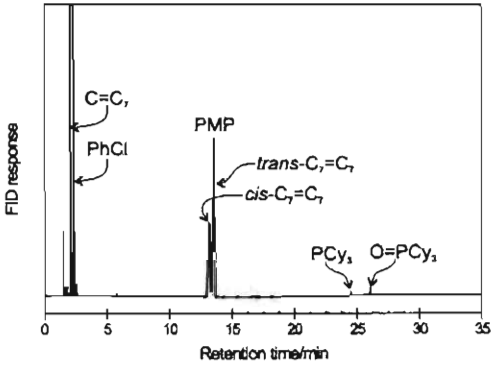

Chromatogram 6.1 GC/FID chromatogram of the reaction mixture of 1-octene in the presence of **Gr1** at 25 °C after 1 h (solvent = chlorobenzene, 1-octene/Ru = 1000, FID response enlarged).

Finally, the completion of the catalytic cycle, **F1** to **F4**, was modelled. The complete electronic energy profile of **A** to **F4** to **F1** to **F4** is illustrated in **Figure 6.23**, with the transition states for the decomposition of the ruthenacyclobutanes **H4** and **H1** now added to the published energy profile.[16] The conversion to the heptylidene (**F1-F4**) is thermodynamically favoured over the conversion to the methylidene (**F4-F1**), with changes in electronic energies of approximately -5 and 6 kcal/mol respectively. The different energies shown in the **F1** to **F4** cycle are due to the formation of *trans*- and *cis*-7-tetradecene carried over in the mass balance used for the calculation.

Only after considering the full mechanistic cycle can a complete picture be obtained with regards to the relative activity of the catalyst, as illustrated for **Gr1** in **Figure 6.23**. The rate-limiting step for the activation step as well as the reaction was identified as the decomposition of the ruthenacyclobutane **D4**. The activation energy for the decomposition of **H4** is *ca.* 2 kcal/mol lower, making this step a potential rate-determining step, indicating that Gibbs free energy (ΔG) corrections need to be made to the electronic energies for vibrational, translational and rotational energies of the molecules. Thereby the thermodynamic properties of the reaction can be calculated, which will more accurately determine the rate determining step of the reaction. This will require the computationally expensive calculation of vibrational modes of atoms in the molecule, which was ongoing at the time of completion of this study. Janse van Rensburg et al.[12] elegantly illustrated this point for the coordination of ethene to **Gr1**, where the electronic energies predicted one coordination mode as the lowest energy, while after ΔG corrections were made, another was shown to be the true lowest equilibrium structure.

6.2.4 References

1. Herrisson, J.L. and Chauvin, Y., *Makromol. Chem.*, 1971, **141**, 161
2. Sanford, M.S., Love, J.A., and Grubbs, R.H., *J. Am. Chem. Soc.*, 2001, **123**, 6543
3. Adlhart, C. and Chen, P., *J. Am. Chem. Soc.*, 2004, **126**, 3496
4. Adlhart, C., Hinderling, C., Baumann, H., and Chen, P., *J. Am. Chem. Soc.*, 2000, **122**, 8204
5. Louie, J. and Grubbs, R.H., *Organometallics*, 2002, **21**, 2153
6. Huang, J., Stevens, E.D., Nolan, S.P., and Petersen, J.L., *J. Am. Chem. Soc.*, 1999, **121**, 2674
7. Vyboishchikov, S.F., Bühl, M., and Thiel, W., Prof., *Chem. Eur. J.*, 2002, **8**, 3962
8. Burdett, K.A., Harris, L.D., Margl, P., Maughon, B.R., Mokhtar-Zadeh, T., Saucier, P.C., and Wasserman, E.P., *Organometallics*, 2004, **23**, 2027

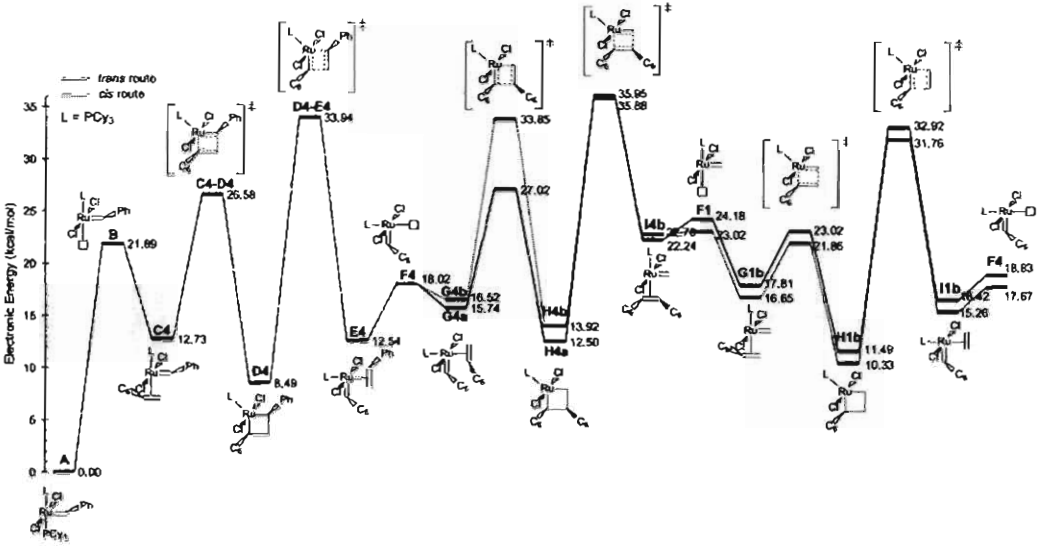

Figure 6.23 Electronic energy profile of a complete pathway in the 1-octene metathesis mechanism using **Gr1** (only *trans* structures are shown from **F4** to **F4**).

9. Cavallo, L., *J. Am. Chem. Soc.*, 2002, **124**, 8965

10. Bernardi, F., Bottoni, A., and Miscione, G.P., *Organometallics*, 2003, **22**, 940

11. Fomine, S., Vargas, S.M., and Tlenkopatchev, M.A., *Organometallics*, 2003, **22**, 93

12. Janse van Rensburg, W., Steynberg, P.J., Kirk, M.M., Meyer, W.H., and Forman, G.S., *J. Organomet. Chem.*, 2006, **691**, 5312

13. Sanford, M.S., Ulman, M., and Grubbs, R.H., *J. Am. Chem. Soc.*, 2001, **123**, 749

14. Dias, E.L., Nguyen, S.T., and Grubbs, R.H., *J. Am. Chem. Soc.*, 1997, **119**, 3887

15. Ulman, M. and Grubbs, R.H., *Organometallics*, 1998, **17**, 2484

16. Jordaan, M., Van Helden, P., Van Sittert, C.G.C.E., and Vosloo, H.C.M., *J. Mol. Catal. A: Chem.*, 2006, **254**, 145

17. Denk, K., Fridgen, J., and Herrmann, W.A., *Adv. Synth. Catal.*, 2002, **344**, 666

18. Van der Schaaf, P.A., Muhlbach, A., Hafner, A., and Kolly, R., 1999. Heterocyclyl ligand containing ruthenium and osmium catalysts. Patent: *WO 99/29701*

19. Wijkens, P., Jastrzebski, J.T.B.H., Van der Schaaf, P.A., Kolly, R., Hafner, A., and Van Koten, G., *Org. Lett.*, 2000, **2**, 1621

20. Tolman, C.A., *Chem. Rev.*, 1977, **77**, 313

21. Bunten, K.A., Chen, L., Fernandez, A.L., and Poe, A.J., *Coord. Chem. Rev.*, 2002, **41-51**, 233

22. Nguyen, S.T. and Trnka, T.M. *in* ***Handbook of Metathesis***, Grubbs, R.H., Ed., *The Discovery and Development of Well-Defined, Ruthenium-Based Olefin Metathesis Catalysts*, Vol. 1, Wiley, 2003, p. 61

23. Adlhart, C. and Chen, P., *Angew. Chem. Int. Ed.*, 2002, **41**, 4484

24. Meyer, W.H., Brull, R., Raubenheimer, H.G., Thompson, C., and Kruger, G.J., *J. Organomet. Chem.*, 1998, **553**, 83

25. Love, J.A., Sanford, M.S., Day, M.W., and Grubbs, R.H., *J. Am. Chem. Soc.*, 2003, **125**, 10103

26. Adlhart, C., ***Intrinsic Reactivity of Ruthenium Carbenes: A Combined Gas Phase and Computational Study***, Ph.D thesis, Eidgenossische Technische Hochschule Zurich, 2003

27. Halpern, J., *Science*, 1982, **217**, 401

28. Jordaan, M. and Vosloo, H.C.M., *Adv. Synth. Catal.*, 2007, **349**, 184

29. Weskamp, T., Kohl, F.J., Hieringer, W., Gleich, D., and Herrmann, W.A., *Angew. Chem. Int. Ed.*, 1999, **38**, 2416

30. Adlhart, C. and Chen, P., *Helv. Chim. Acta.*, 2003, **86**, 941

31. Collman, J.P., Hegedus, L.S., Norton, J.R., and Finke, R.G., ***Principles and Applications of Organotransition Metal Chemistry***, University Science Books: Mill Valley, California, 1987

32. Arduengo III, A.J., *Acc. Chem. Res.*, 1999, **32**, 913

33. Perrin, L., Clot, E., Eisenstein, O., Loch, J., and Crabtree, R.H., *Inorg. Chem.*, 2001, **40**, 5806

Conclusions & Recommendations 7

7.1 INTRODUCTION

The purpose of this study was to develop new ruthenium carbene complexes with hemilabile bidentate ligands (hereafter referred to as Ru=C hemilabile complexes) for application in linear alkene metathesis. The focus was to improve the thermal stability, activity and lifetime of **Gr1** and **Gr2** for the metathesis of linear alkenes. It is known that, despite the high selectivity of **Gr1** during the metathesis of terminal alkenes, its lifetime decreases with an increase in temperature.[1-3] The development of **Gr2** has to some extent dealt with this drawback by providing a catalytic system with excellent activity and lifetime.[4,5] However, the selectivity of **Gr2** decreases at elevated temperatures.[3,6-11] The development of the Ru=C hemilabile complexes were attempted because of the fact that it was recently shown that the activity and selectivity of **Gr1** and various second generation Grubbs systems for ROMP and RCM reactions at elevated temperatures improved through the incorporation of a hemilabile ligand into the system.[12,13]

7.2 SYNTHESIS OF HEMILABILE COMPLEXES

A number of O,O-, O,N-, O,S-, O,P-carboxylate and O,O-, O,N-alcoholate ligands with increased steric and/or electronic properties were investigated as possible hemilabile ligands for incorporation into **Gr1** and **Gr2**. This was achieved by reacting a metal salt of the ligand with **Gr1** or **Gr2**, respectively, at 16 to 35 °C until TLC analysis indicated all of the starting carbene was consumed. Lithium,[12] thallium,[14-17] silver,[18,19] potassium[20] and sodium[21] salts have previously been used to manipulate the ruthenium carbene complexes, of which the thallium salts were more generally used than the others. Due to the toxicity of thallium ethoxide and the instability of the resulting thallium salts, other possibilities were first explored. Therefore, the reaction of **Gr1** with the sodium salts of selected carboxylate and alcoholate ligands were initially investigated but later terminated, since most of the syntheses were unsuccessful. The reactions generally resulted in the decomposition of **Gr1** to form $Ru(PCy_3)(L)(Cl)(R)(CO)$ [L = PCy_3 or H_2IMes, R = Ph or H], free PCy_3 and $O{=}PCy_3$, with little or no carbene (either **Gr1** or new complex) present (§ 3.4.1). Only the reaction of **Gr1** with the sodium salt of pyca resulted in the formation of a new carbene complex. The identity of this carbene could not be determined with any certainty due to insufficient spectroscopic data as a result of impurities and loss of sample during purification.

The next step was therefore to investigate the thallium and lithium salts of the various ligands, since literature has shown that these types of salts are more frequently used to manipulate the Grubbs carbenes.[12,14-17] It was noted that the thallium and lithium salts of the carboxylic acids were

not a viable source for manipulating the Grubbs carbenes. This was due to the fact that the reaction of **Gr1** with the lithium or thallium salts of the carboxylate-ligands resulted in either unreacted **Gr1** (**Gr1** and lithium salt of furoic acid (**S25**), **Table 3.10**), formation of a mixture of carbenes (**Gr1** and thallium salt of pyca (**S7**), **Table 3.9**) or the decomposition of **Gr1** with little or no carbene (**Gr1** or new complex) present afterwards (see **Table 3.9 – 3.21** for the remaining carboxylate complexes). Therefore, since the reaction of **Gr1** with the sodium salt of pyca resulted in the formation of a new carbene, similar results might be obtained from the sodium salts of the remaining carboxylic acids, which should be investigated further. However, according to a recent publication,[22] two pyca ligands were successfully incorporated into **Gr2** at 60 °C, which are harsher conditions than those applied in this study. It might therefore be interesting to investigate the carboxylic acid chelating ligands further to determine the influence of temperature and/or the type of salt used on the successful incorporation of these types of ligands into the Grubbs carbenes.

Although the incorporation of **L9** and **L10**, two O,O-ligands, into **Gr1** and **Gr2** was unsuccessful, it has been previously shown[23] that other O,O-ligands could be successfully incorporated into the Grubbs carbenes. Molecular modelling was used in combination with the experimental work to gain insight into possible reasons for the unsuccessful synthesis of the O,O-chelated ruthenium carbenes. The modelling results (see Chapter 4) suggested that the synthesis of the first generation O,O-chelating complexes would be difficult as a result of the endothermic energy required for coordination of the labile O-atom to the Ru-centre through dissociation of PCy_3. Therefore, since the reactions were performed at RT and the formation of TlCl was visible, with no carbene forming, other decomposition routes might have dominated. The ^{1}H-NMR supported the formation of **39** as a possible decomposition product from the reaction of **Gr1** or **Gr2** with the lithium or thallium salt of **L10** (**Figure 4.2**, § 4.3.1 and **Scheme 7.1**). Therefore, the results suggests that the type of O^O-ligands to be considered for manipulating the Grubbs carbenes in the future are aromatic systems with no alkyl groups attached to the labile donating O-atom. The absence of an alkyl group is necessary to avoid possible reaction of the alkyl group with the carbene moiety, which will lead to decomposition of the carbene.

To theoretically investigate the possibility of **39** forming, a mechanistic route is postulated in **Scheme 7.1**, which should be investigated further to determine its feasibility. Although it is generally accepted that PCy_3 dissociates from the Grubbs carbenes during a metathesis reaction,[24-26] a different mechanism might play a role during synthetic manipulation of the Grubbs carbenes.

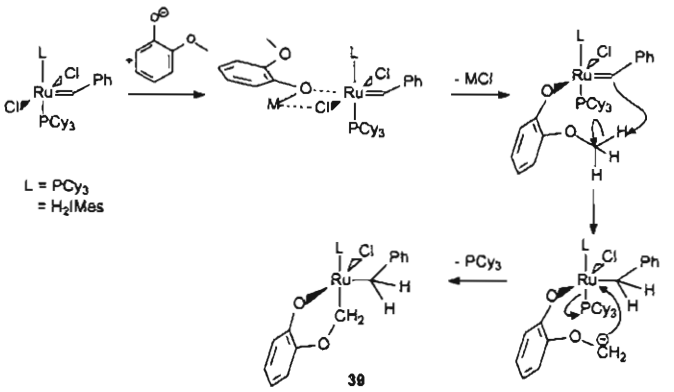

Scheme 7.1 Postulated mechanistic route for the decomposition of the Grubbs carbenes.

Therefore, an associative coordination of the metal-salt to the Ru-centre is proposed leading to the substitution of the Cl-atom with the non-labile O-donor of the O,O-ligand with subsequent formation of the metal chloride salt. The proposed mechanism for formation of **39** is based on a modification for the dehydrogenation of alcohols with **Gr1**, whereby the alkyl group is in close proximity to the carbene moiety to react as proposed by Mol et al.[27] (**Scheme 7.2**). The formation of an aldehyde as suggested during the dehydrogenation of alcohols would be chemically unfavourable and therefore a carbanion is formed. The carbanion can then react with the Ru-centre with subsequent loss of PCy_3.

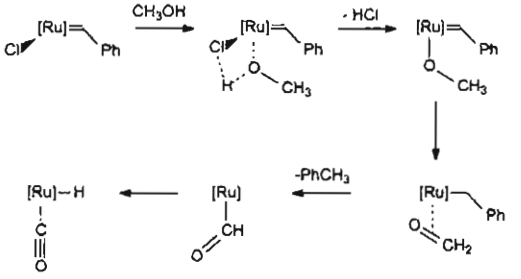

Scheme 7.2 Proposed dehydrogenation of alcohols with **Gr1**.[27]

The synthesis of first and second generation O,N-chelated ruthenium carbene complexes proved to be more successful, indicating that a more stable complex is formed with a neutral N-donor atom compared to a neutral O-donor atom. However, it was observed that the C_2 carbon of **HL** required steric shielding to prevent decomposition of the carbene moiety through a possible exchange of H-atoms with H_α.

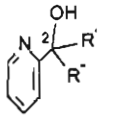

R', R" = H, alkyl, aryl

HL

A deuterium labelling study should provide the necessary information with regards to possible exchange reactions that can occur during the reaction. One possibility is to replace the H-atoms on C_2 of **L6** with deuterium before reacting the salt with the Grubbs carbenes, or to replace H_α with deuterium.

In general, a higher success rate, i.e. higher yield and more pure complexes, were obtained from reacting the Grubbs carbenes with a lithium salt in comparison to the thallium or sodium salts (§3.4). However, it appears that sodium salts, rather than lithium or thallium salts, should be used to incorporate carboxylate ligands into the Grubbs carbenes. The possibility of using silver salts should also be investigated, since reactions of the Grubbs carbenes with these salts appeared to be rather successful, and the toxicity of these salts are lower than that of the thallium salts.

To get an indication of the stability of the complexes during the synthesis process, a ^1H and ^{31}P NMR investigation should be launched in which the reaction is performed in an NMR tube. The reaction is then monitored over time to determine the rate at which the carbene disappears and if new carbenes form at any stage of the reaction. This would give an indication of how the synthesis procedures should be adapted to attempt separation of newly formed carbenes from the mixtures. The viability of such a study should be discussed with the NMR operator, since the formation of the metal salt might severely hamper the ability of obtaining readable spectra, i.e. without significant signal distortions due to saturation of the sample.

7.3 CATALYTIC ACTIVITY

The catalytic activity of the successfully synthesised O,N-chelated ruthenium carbene complexes (**Figure 7.2**) were tested for the metathesis of 1-octene and compared to **Gr1** and **Gr2**.

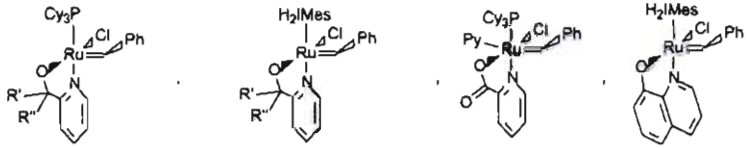

R' = R'' = Me (**Gr2Me**)
= Ph (**Gr2Ph**)
R''' = Cy (**Gr1Cy**)

R' = R'' = Me (**Gr2Me**)
= Ph (**Gr2Ph**)
= ^{i}Pr (**Gr2^{i}Pr**)
R''' = Cy (**Gr1Cy**)
= Carbonyl (**Gr2Pico**)

Gr1Pico-Py

Gr2Quino

Figure 7.2 O,N-chelating ruthenium carbene complexes investigated for the metathesis of 1-octene.

Initially, the influence of reaction temperature and precatalyst concentration on the 1-octene metathesis activity of **Gr1Cy** and **Gr2Cy** was performed and compared to the **Gr1** and **Gr2**. This was done to determine the optimum conditions of which these systems would display high metathesis activity with limited isomerisation and cross metathesis. The influence of temperature on the reactivity of **Gr1Cy** and **Gr2Cy** in comparison to **Gr1** and **Gr2** is illustrated in **Figure 7.3** and **7.4**, respectively.

As expected, **Gr1Cy** and **Gr2Cy** showed low reactivity at 35 °C in comparison to **Gr1** and **Gr2**, due to the additional stabilisation of the chelating ligand. The activity and stability of both systems towards the formation of PMP increased with an increase in temperature relative to **Gr1** and **Gr2**. After 20 h, **Gr1Cy** and **Gr2Cy** still showed activity for the metathesis of 1-octene, while **Gr1** and **Gr2** were inactive. The incorporation of a hemilabile ligand into **Gr1** decreased the degree of SMP and IP formation, while increasing the activity and selectivity. However, the activity and selectivity of the second generation analogue (**Gr2Cy**) dramatically decreased above 70 °C. This was unexpected since it was thought that replacement of the PCy_3 ligand in **Gr1Cy** with an NHC ligand would stabilise **Gr1Cy** even further, as was observed for **Gr1**. The decreased activity is either due to thermal instability to produce a ruthenium hydride intermediate, which can facilitate the isomerisation of alkenes, or another mechanism is involved apart from the assumed dissociation of the labile N-donor of the hemilabile ligand.

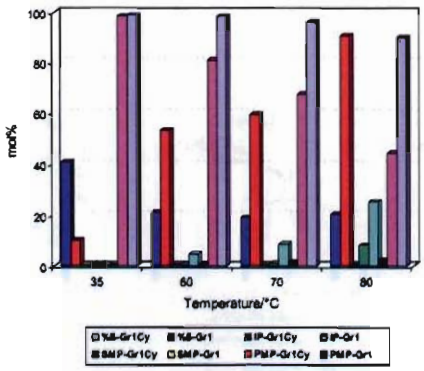

Figure 7.3 The influence of temperature on the reactivity of the **Gr1Cy** in comparison to **Gr1** (no solvent, 1-octene/Ru = 9000).

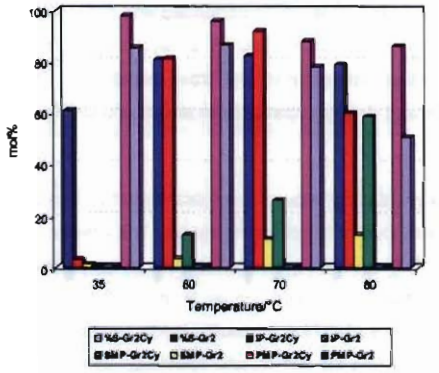

Figure 7.4 The influence of temperature on the reactivity of the **Gr2Cy** in comparisond to **Gr2** (no solvent, 1-octene/Ru = 9000).

This is suggested since it was observed in the ^{1}H NMR investigation of **Gr2Cy** at 50 °C that the aliphatic region of the spectrum dramatically changes as the reaction proceeds (**Spectrum F.4 – F.6** and **F.9 – F.11** for **Gr2** and **Gr2Cy,** respectively in Appendix F). Therefore, an in-depth NMR study should be launched to investigate the following:

- Thermal decomposition of **Gr1**, **Gr2**, **Gr1Cy** and **Gr2Cy**, whereby the rate at which H_α disappears is monitored over time

For a typical thermolytic decomposition study:

Prepare a 0.023 M solution of the carbene complex in C_6D_6 with a drop of pentafluorobenzene (internal standard). Heat the solution to the desired temperature in the NMR probe and acquire spectra at specific intervals. The integral of the carbene proton can then be compared to the integral of pentafluorobenzene to obtain the rate of disappearance of the carbene.

- Monitor the 1-octene metathesis reaction in the presence of **Gr2** and **Gr2Cy** at a temperature range of 35 – 80 °C, to determine whether the NHC ligand participates in the reaction (see § 3.5.1.3 for reaction conditions)

The optimum temperature, for both **Gr1Cy** and **Gr2Cy**, to maintain high selectivity towards PMP and limit the formation of SMP and IP during the metathesis of 1-octene was identified as 60 – 70 °C. A subsequent investigation into the influence of precatalyst concentration on the 1-octene metathesis activities of these two systems revealed that a 1-octene/Ru molar ratio of 9000 was optimum for maintaining a high activity and selectivity towards PMP formation.

Consequently, a comparative study was launched to determine the 1-octene metathesis activities of the remaining Ru=C hemilabile complexes at the above optimum conditions identified for **Gr1Cy** and **Gr2Cy**. However, reaction temperature and precatalyst concentration studies for these complexes should be done to determine whether the current conditions are in actual fact the optimum conditions for them to achieve high selectivity and activity towards PMP formation.

The reactivity of the various first and second generation hemilabile complexes compared to **Gr1** and **Gr2**, are illustrated in **Figure 7.5** and **7.6**, respectively. The hemilabile complexes are arranged in increasing order of molecular volume. A linear increase in the PMP formation was observed for the first and second generation Ru=C complexes with an increase in steric bulk. However, a dramatic decrease in activity was observed for **Gr1Ph** and **Gr2Ph**. This might be due to the free rotation of the phenyl-rings on C_2 of **HL**, which increases the steric bulk around the Ru-centre and therefore obstructs coordination of the 1-octene to the Ru=C-moiety. The low activity of **Gr1Ph** and **Gr2Ph** was thought to involve possible electronic effects, due to the electron donating effect of the phenyl rings on C_2 of **HL**.

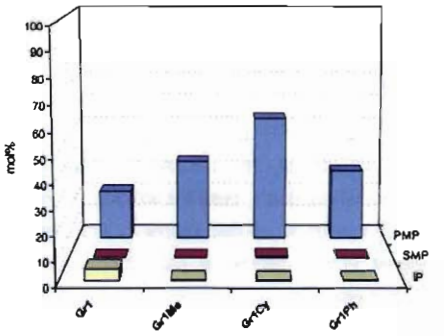

Figure 7.5 Reactivity of the various first generation hemilabile complexes in comparison to **Gr1** (complexes arranged according to increasing steric bulk).

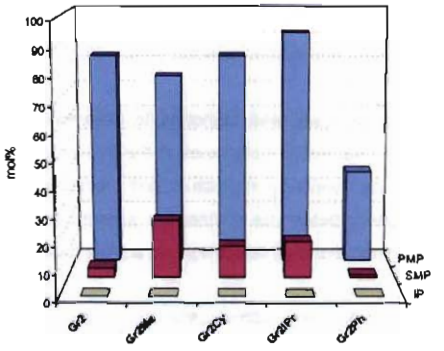

Figure 7.6 Reactivity of the various second generation hemilabile complexes in comparison to **Gr2** (complexes arranged according to increasing steric bulk).

With the help of molecular modelling, the calculated Hirshfeld charges of the various R groups on C_2 were compared to those of the free ligands (see **Table 7.1** and **7.2**, respectively). The results indicated that the electronic effects of the various R-groups are negligibly small.

The only significant electronic effect visible was the stabilisation of the Ru=C-moiety through the donation of electrons from the N-atom of the pyridine ring upon coordination to the Ru=C-moiety. This is evident from the reduced electron density on the O- and N-atoms of the ligand after coordination with the Ru-centre, which is distributed to C_a. The charges on the carbene moiety of **Gr1** (-0.069) and **Gr2** (-0.069) decreased by *ca.* 0.04, with a simultaneous increase of *ca.* 0.09 in the electrophilic character of the Ru-center (0.212 and 0.187 for **Gr1** and **Gr2**, respectively). This suggests that the hemilabile complexes might be more active due to the high susceptibility of the Ru-centre for nucleophilic attack from *inter alia* an alkene.

Table 7.1 Calculated Hirshfeld charges of selected atoms in the first and second generation hemilabile complexes compared to **Gr1** and **Gr2**.

Pre-catalyst[x] \ Atom	G[y]	N	O	Ru	=C	C_a	C_b	Aryl ring of O,N-ligand[z]
	1st	N/A	N/A	0.212	-0.069	N/A	N/A	N/A
	2nd	N/A	N/A	0.238	-0.069	N/A	N/A	N/A
	1st	-0.069	-0.236	0.295	-0.099	0.066	-0.003	-0.047
	2nd	-0.073	-0.244	0.316	-0.088	0.065	-0.004	-0.046
	1st	-0.068	-0.273	0.298	-0.108	0.071	-0.115	N/A
	2nd	-0.074	-0.246	0.319	-0.096	0.069	-0.118	N/A
	1st	-0.065	-0.230	0.301	-0.111	0.070	-0.020	N/A
	2nd	-0.072	-0.235	0.323	-0.095	0.068	-0.022	N/A
	1st	-0.068	-0.235	0.298	-0.108	0.067	-0.070	-0.062
	2nd	-0.074	-0.244	0.320	-0.097	0.066	-0.073	-0.062

[x] [Ru] = [RuCl$_2$L(=CHPh)] with L = PCy_3 (1st) or H_2IMes (2nd)
[y] Indication of first (1st) or second (2nd) generation Grubbs carbene or hemilabile analogues
[z] Average charge of carbons in the Ph or Cy groups on O,N-ligand

Table 7.2 Calculated Hirshfeld charges of selected atoms in the O,N-ligands.

O,N-ligand \ Atom	N	O	C_a	C_b	Aryl ring of O,N-ligand[‡]
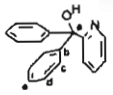	-0.128	-0.220	0.096	-0.004	-0.043
	-0.130	-0.250	0.101	-0.096	N/A
	-0.123	-0.228	0.095	-0.001	N/A
	-0.129	-0.240	0.095	-0.054	-0.047

[‡] Average charge of carbons in the Ph or Cy groups on C_2 of the O,N-ligand

At this point the focus should also be directed to **Gr1Cy**, which contains an O,N-chelated ligand that is bulky and sterically directed, due to loss of free rotation.[28] The steric demand of the 1-(2'-pyridinyl)cyclohexan-1-olato-ligand (**PyCy**) when coordinated to a metal-centre is illustrated in **Figure 7.9**. Conversely, the 1-(2'-pyridinyl)propan-2-olato- (**PyMe2**), 1-(2'-pyridinyl)-2,4-dimethyl-pentan-3-olato- (**Py^{i}Pr2**) and 1-(2'-pyridinyl)-1,1-diphenyl-methanolato-ligands (**PyPh2**) are bulky, but not sterically directed, due to free rotation of the alkyl- and aryl-groups on C_2 of **HL**.

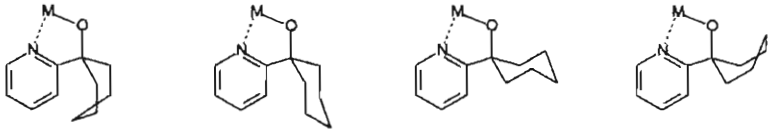

Figure 7.9 Steric demand of the 1-(2'-pyridinyl)cyclohexan-1-olato-ligand when bound to a metal as illustrated by the different conformations of the cyclohexyl group.[28]

Therefore, despite the observed trends for the various hemilabile complexes, the results with regards to steric and electronic effects of the O,N-ligands on the metathesis activity of the precatalysts are inconclusive. This is due to the fact that the one ligand is sterically directed

(PyCy) compared to the free rotation of the others, which can increase steric bulk around the metal centre. As a result of this observation a broader theoretical and/or experimental investigation should be launched, to incorporate a variety of O,N-ligands in which the steric and electronic properties of the ligand are varied. During the theoretical investigation, the R groups should be systematically varied, even if the resulting ligands are fictitious. This will help elucidate the steric and electronic effects of the R-groups with regards to the metathesis activity of the complexes. Typical variations of the R-groups to consider with inclusion of the current ligands are illustrated in Figure 7.10.

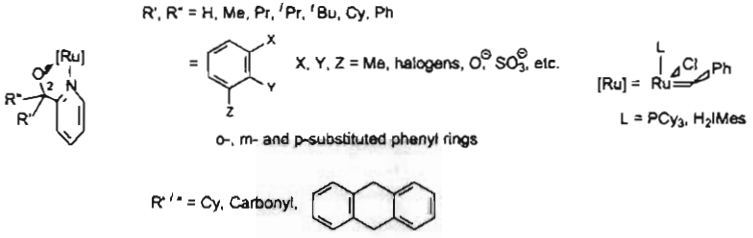

Figure 7.10 A few suggestions for typical ligands to be considered for investigating steric and electronic influences of the R-groups on C_2.

The high thermal stability of the Ru=C hemilabile complexes can be rationalised by the increased electron density of the N-atom of the pyridine ring upon coordination to the Ru-centre, which is delocalised over the Ru=C-moiety and PCy_3 ligand. This delocalisation is elegantly illustrated in Figure 7.11 and 7.12 by comparing the HOMO-orbitals of a representative first (**Gr1Ph**) and second (**Gr2Ph**) generation hemilabile complex with **Gr1** and **Gr2**. All the remaining Ru=C hemilabile complexes displayed similar HOMO orbitals and are illustrated in Appendix G.

The electron density of **Gr1** and **Gr2** appears to be localised over the Ru=C-moiety. However, the 14-electron intermediates of **Gr1** (**Gr1-B**) and **Gr2** (**Gr2-B**) are stabilised by the remaining L-group (PCy_3 or NHC-ligand) after dissociation of the PCy_3. The activity differences of **Gr1** and **Gr2** was initially thought to be as a result of the increased σ-donor ability of NHC to decrease the strength of the Ru-P interaction and therefore facilitate the dissociation of PCy3.[24-26,29,30] However, the high activity of **Gr2** compared to **Gr1** was shown to be as a result of the NHC's ability to promote and stabilise metal-to-alkene back bonding to a much greater extent than the phosphine ligands.[24,31] This supported the theoretical observation of the high affinity of **Gr2** to coordinate an alkene rather than PCy_3 as compared to **Gr1**.

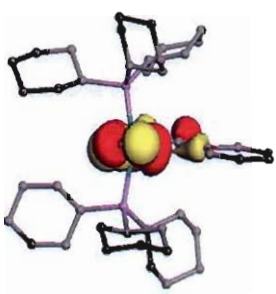

Gr1

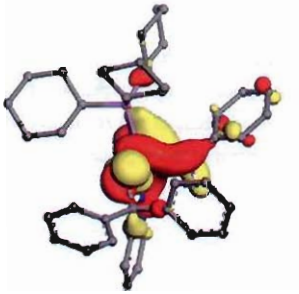

Gr1Ph

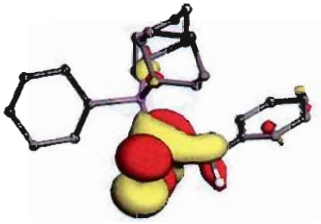

Gr1-B

Figure 7.11 HOMO-orbitals of **Gr1**, **Gr1-B** and a representative first generation hemilabile Ru=C complex (**Gr1Ph**).

Aspects surrounding the activity of the hemilabile complexes are more complex in nature, since NMR studies (see Chapter 5) showed different mechanisms might be involved for the first and second generation hemilabile precatalysts. The calculated Hirshfeld charges of the Ru=C hemilabile complexes (**Table 7.1**) together with the N-Ru bond distances (**Table 7.3**), implies that the N-atom is more strongly coordinated to the Ru-centre in the first generation complexes as compared to the second generation analogues. Therefore, if the complexes initiate through the dissociation of the labile N-atom of the O,N-ligand, the **Gr2**-systems would initiate more rapidly compared to the **Gr1**-systems. This was observed experimentally from the k_{init} results (§ 5.2.3.1). However, no apparent trend could be observed to relate the Ru-N distances to electronic or steric effects. The dissociation of the PCy_3 in the first generation precatalysts as a result of the increased electron density of the Ru=C moiety cannot be ruled out at this stage and should be investigated further.

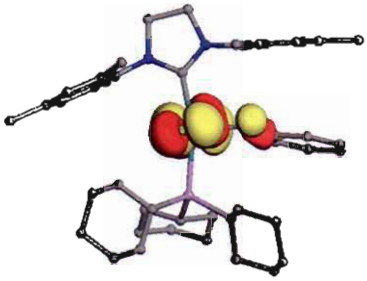

Gr2

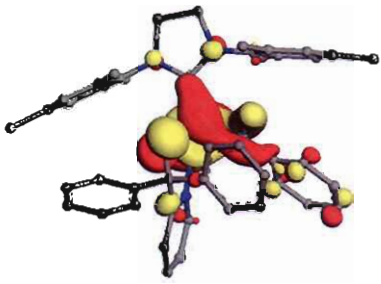

Gr2Ph

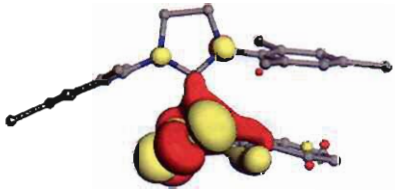

Gr2-B

Figure 7.12 HOMO-orbitals of **Gr2**, **Gr2-B** and a representative second generation hemilabile Ru=C complex (**Gr2Ph**).

Table 7.3 Selected bond lengths of the first and second generation hemilabile precatalysts.

Precatalyst[‡] \ Bond length	G[#]	Ru=C	Ru-N	Ru-O	Ru-L
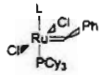	1st	1.878	N/A	N/A	2.471
	2nd	1.870	N/A	N/A	2.121
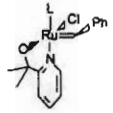	1st	1.880	2.136	2.007	2.441
	2nd	1.883	2.180	2.016	2.087
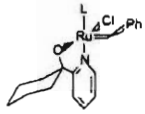	1st	1.880	2.131	2.012	2.444
	2nd	1.882	2.185	2.011	2.084
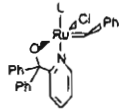	1st	1.875	2.151	2.025	2.443
	2nd	1.882	2.186	2.039	2.085
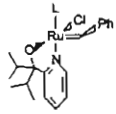	1st	1.880	2.130	2.005	2.451
	2nd	1.885	2.171	2.015	2.095

[‡] [Ru] = [RuCl$_2$L(=CHPh) with L = PCy_3 (1st) or H_2IMes (2nd)]
[#] Indication of first (1st) or second (2nd) generation Grubbs carbene or hemilabile analogues

With the help of the frontier molecular orbital (FMO) Fukui function as developed by Parr and Yang,[32] the reactivity of the various complexes with respect to nucleophilic attack can be theoretically justified. It is generally accepted that the Grubbs carbenes initiate through the loss of PCy_3 to obtain the catalytically active 14-electron intermediate **B**.[24,25,33-36] As illustrated in **Figure 7.9** for the first and second generation intermediates of **B**, the calculated positions exhibiting nucleophilic Fukui functions (*f*+; i.e., positions activated for nucleophilic attack) are illustrated by the map of *f*+ on the electron isodensity surface of **B** (**Gr1-B-*f*+** and **Gr2-B-*f*+** in **Figure 7.13** for the first and second generation intermediates, respectively). The relative concentration of red in "**B**"-*f*+ indicates that Ru, benzylidene carbon and the Cl (in decreasing order) should in principle be susceptible to favourable interaction with a nucleophile. From this qualitative picture, it is thus predicted that the alkene would preferentially interact with the Ru=C in **Gr2-B** from a position *trans* to the NHC, since the position *cis* to the NHC is sterically hindered.

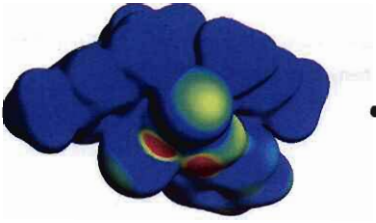

Gr2-B-*f*+

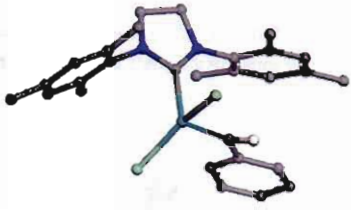

Gr2-B

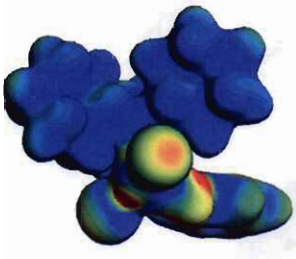

Gr1-B-*f*+

Gr1-B

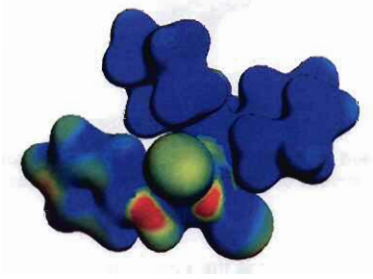

Gr1-180-B-*f*+
(turned at an 180° angle)

Figure 7.13 Optimised geometry of the 14-electron intermediate (B) of **Gr1** and **Gr2**, together with maps of the nucleophilic (*f*+) Fukui functions on the electron isodensity surface of B.

The alkene can interact with the Ru=C in **Gr1-B** from two positions: (a) the position *trans* to the PCy_3 or (b) the position *cis* to the carbene along the bisector line of the Cl-Ru=C angle. The nucleophilic Fukui functions of two representative first and second generation hemilabile complexes (with the rest given in Appendix G) are shown in **Figure 7.14 – 7.15** and **7.16 – 7.17**, respectively, to illustrate the steric effect of the phenyl and cyclohexyl R groups.

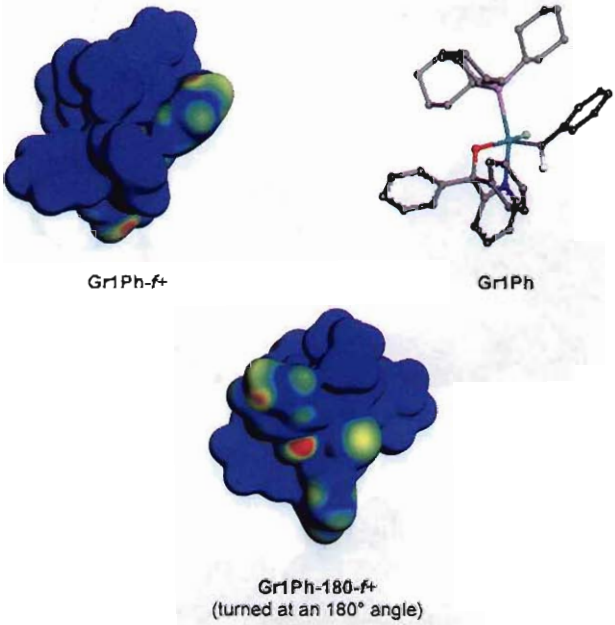

Figure 7.14 Optimised geometry of **Gr1Ph**, together with maps of the nucleophilic (*f+*) Fukui functions on the electron isodensity surface of the complexes.

It is evident that the Ph-rings increase the steric bulk around the Ru-centre and direct the attack of the alkene to the Cl-Ru=C bisector line opposite the O,N-ligand (**Gr1Ph-180-*f+***). This will most likely cause the N-atom of the pyridine ring to decoordinate to allow for formation of the ruthenacyclobutane. However, due to the sterically directed cyclohexyl-group, more than one coordination possibility is revealed (see **Gr1Cy-*f+*** and **Gr1Cy-180-*f+***). Although the coordination position in **Gr1Cy-*f+*** is to some extent hindered, the possibility of coordination after decoordination of the N-atom of the pyridine ring should not be ruled out. Therefore, reduced steric bulk around the Ru-centre, might lead to enhanced activity.

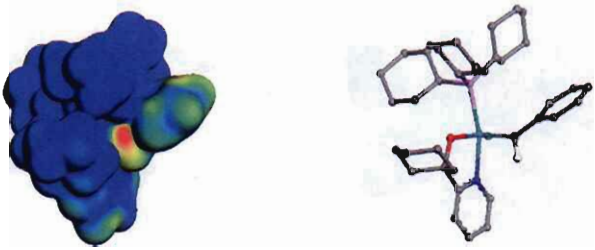

Gr1Cy-*f*+ Gr1Cy

Gr1Cy-180-*f*+
(turned at an 180° angle)

Figure 7.15 Optimised geometry of **Gr1Cy**, together with maps of the nucleophlic (*f*+) Fukui functions on the electron isodensity surface of the complexes.

Similar to the first generation systems, the steric bulk of the O,N-ligand together with increased bulk due to the NHC ligand, leads to obstruction of alkene coordination in **Gr2Ph**. On the other hand, in **Gr2Cy**, coordination of the alkene is possible *cis* to the carbene from the same side as the O,N-ligand (**Gr2Cy-*f*+**). The coordination site on the opposite face (**Gr2Cy-*f*+** as well as **Gr2Ph-180-*f*+**) is too sterically hindered to allow for alkene coordination. These results indicate that, in the second generation systems, the decoordination of the N-atom of the pyridine ring or NHC ligand should precede the coordination of the alkene to the Ru-centre. This suggests that the metathesis of 1-octene in the presence of the second generation hemilabile complexes might proceed according to a dissociative mechanism. Since the molecular modelling indicated that the dissociation of the NHC ligand is improbable, it suggests that the O,N-ligand acts like a hemilabile ligand, i.e. opens and closes a free coordination site if coordinated to the **Gr2**.

Gr2Ph-*f*+ Gr2Ph

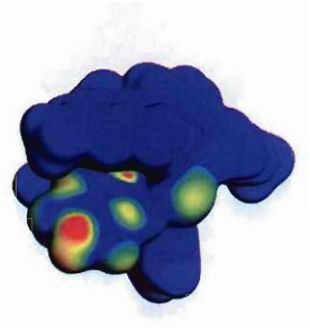

Gr2Ph-180-*f*+
(turned at an 180° angle)

Figure 7.16 Optimised geometry of **Gr2Ph**, together with maps of the nucleophlic (*f*+) Fukui functions on the electron isodensity surface of the complexes.

This is also supported by the ^{1}H NMR study. On the other hand, for the first generation system, coordination of the alkene to the Ru-centre might proceed according to an associative mechanism, since a coordination point is freely available as illustrated by complexes "**90-*f*+**". The ^{1}H NMR investigation of the 1-octene metathesis reactions in the presence of **Gr1Cy** and **Gr2Cy** suggested that different mechanisms were involved for the individual systems. This is due to the fact that only 3 carbene signals were observed for **Gr1Cy**, compared to 5 observed for **Gr2Cy**. It would therefore be interesting to investigate the 1-octene metathesis reaction of the other Ru=C hemilabile complexes with NMR, to determine whether similar mechanistic differences are observed.

Gr2Cy-*f*+ Gr2Cy

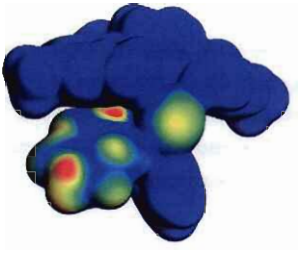

Gr2Cy-180-*f*+
(turned at an 180° angle)

Figure 7.17 Optimised geometry of **Gr2Cy**, together with maps of the nucleophlic (*f*+) Fukui functions on the electron isodensity surface of the complexes

Due to the fact that all the reactions except, the NMR investigations of **Gr1**, **Gr2**, **Gr1Cy** and **Gr2Cy**, were performed neat (without solvent), it would be interesting to see whether a solvent has any influence on the 1-octene metathesis activity of the hemilabile complexes. Monitoring the precatalyst over time in the absence and presence of the alkene with ^{1}H and ^{31}P NMR should be able to give insight into the influence of the alkene and solvent on the release of a free coordination site.

Although only the dissociative mechanism was investigated for the various systems (Chapter 6), the possibility of an associative coordination of the alkene to the Ru-centre should not be excluded. This should be investigated to determine whether different mechanisms play a role in the first and second generation hemilabile complexes. This will also help determine the hemilability of the O,N-ligand.

Since it was shown[37] that the activity and selectivity of **Gr1** improved through the addition of phenol, it would be interesting to see whether the activity of **Gr1Ph** and **Gr2Ph**, which are slow to activate, would improve. The influence of temperature, solvent etc., should also be investigated if proven successful.

Another interesting aspect to investigate theoretically and experimentally would be the influence of alkyl chain length of the substrate. This is suggested since it has been theoretically shown (§ 6.2.2) that the affinity of **Gr1** and **Gr2** towards phosphine increases with an increase in the chain length of the substrate. This implies that the initiation rate of **Gr1** and **Gr2** decreases with an increase in alkyl chain length. However, since only ethene and 1-octene was considered as alkene substrates, the theoretical investigation is inconclusive and other substrates should be considered in a future study.

As a general conclusion for this study, since the thermal stability, activity and lifetime of the Grubbs carbenes have been improved after incorporation of a O,N-chelating ligand, it can be said that the purpose of this study has been achieved. In support of the experimental investigation of the 1-octene metathesis reaction, we also looked at the mechanism from a theoretical point of view, which will be discussed in the following section.

7.4 MECHANISTIC INVESTIGATION

A conceptual model for the productive metathesis of 1-octene in the presence of **Gr1** was constructed based on literature[24,25,34] and experimental results.[38] The 1-octene metathesis reaction in the presence of **Gr1** is described by a dissociative mechanism. The mechanism is supported by the formation of by-products, i.e. styrene, 1-phenyl-1-octene isomers and PCy_3. The model for the initiation and activation of **Gr1** was additionally applied to **Gr2** and adapted for the hemilabile complexes (**Gr1Cy** and **Gr2Cy**) to elucidate observed experimental results.

With the use of DFT calculations, electronic energy surfaces for the metathesis mechanism of the individual precatalysts were constructed and compared. The models used for the mechanistic study incorporated the full ligands as used in an experiment with 1-octene as substrate. Ethene was used as substrate with **Gr1** during a comparative study with literature to determine the influence of substrate and precatalyst when used in calculations. This was done since most theoretical studies use ethene as substrate with the Ru-methylidene instead of Ru-benzylidene (**Gr1**) as precatalyst. The DFT calculations compared very well with calculations by other authors. It was found that the same simple models that efficiently describe the metathesis of simple substrates with a methylidene type precatalyst couldn't be used to describe the reaction of real systems. It is clear that the mechanism of metathesis with actual catalytic systems are complex if

it is done with large substrates like 1-octene, and that electronic effects cannot fully account for effects that are observed e.g. the *cis*/*trans*-isomerisation of the primary metathesis product. Therefore, this reaction cannot just be considered by using a simple model, since both electronic and steric effects are then excluded which will lead to inconclusive results.

The initiation and activation steps of the various precatalysts, with 1-octene as substrate, were investigated to determine the catalytically active species which preferentially forms from the benzylidene precatalyst. ^{1}H NMR studies of the 1-octene metathesis reactions were also done to gain insight into the mechanism of the reaction with **Gr1**, **Gr2** and their hemilabile analogues. The NMR results indicated that the heptylidene was the catalytically active species whicht preferentially formed in the 1-octene metathesis reaction with **Gr1** and **Gr2** at 30 °C, as well as with **Gr2Cy** at 50 °C in $CDCl_3$. In contrast, both the heptylidene and methylidene species formed simultaneously during the 1-octene metathesis reaction with **Gr1Cy** at 50 °C, while the results of **Gr1** and **Gr2** at 50 °C were inconclusive due to the long initial time that passed before the first spectra could be obtained. This is also due to the very fast initiation rate of the Grubbs carbenes at elevated temperatures.[33]

Kinetic information can be obtained from monitoring the disappearance of the benzylidene H_a, since its disappearance is equal to the activation of the precatalyst. Therefore, the rate of disappearance of the benzylidene will be equal to the rate of activation of the precatalyst. **Figure 7.16** gives an indication of the percentage unactivated precatalyst (**Gr1**, **Gr2**, **Gr1Cy** and **Gr2Cy**) present at a certain time in the reaction mixture at 30 and 50 °C. Due to the fast disappearance of the benzylidenes of **Gr1**, **Gr2** and **Gr2Cy** (see **Figure 7.16**) at 50 °C, no valuable kinetic data could be obtained. Therefore, kinetic studies of the hemilabile systems should rather be performed at 35 °C or lower to obtain enough data points for the calculation of activation parameters. The activation rate constants for **Gr1** and **Gr2** at 30 °C, as well as for **Gr1Cy** at 50 °C, are given in **Table 7.4**. It is seen that **Gr1** activates approximately three times faster than **Gr2** at 30 °C, which is expected, since **Gr2** is thermally stable, which implies that it will activate slower at lower temperature. It is noted that the activation rate of **Gr1** has improved after the incorporation of a hemilabile ligand into the system, while the half-lifetime approximately halved, but the results are inconclusive. More kinetic studies should be done at lower temperatures to be able to make valuable remarks with regards to the stability and activity of the hemilabile complexes, compared to **Gr1** and **Gr2**.

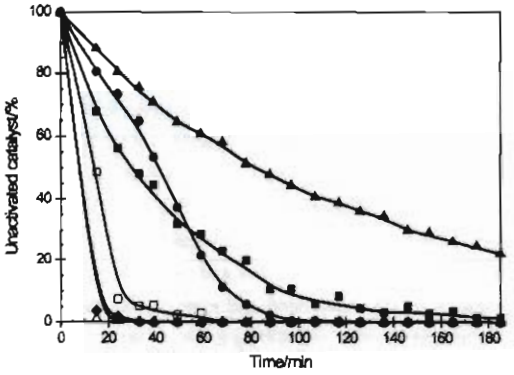

Figure 7.16 Activation of 1-octene metathesis in the presence of **Gr1**, **Gr2**, **Gr1Cy** and **Gr2Cy** (1-octene/Ru = 10, 0.07 mL $CDCl_3$) at different temperatures.
[30 °C : ■ **Gr1** ▲ **Gr2**]
[50 °C: □ **Gr1** △ **Gr2** ● **Gr1Cy** ◆ **Gr2Cy**]

Table 7.4 Activation rate constants for **Gr1**, **Gr2**, **Gr1Cy** and **Gr2Cy** during the metathesis of 1-octene

T / °C	Precatalyst	Activation rate / s^{-1}	Half-life / min
30[a]	**Gr1**	3.84×10^{-4}	30
	Gr2	1.17×10^{-4}	99
50	**Gr1Cy**	7.35×10^{-4}	11

[a] Obtained by P van Helden during his Honours mini project[39]

Additionally, the various regions of the ^{1}H NMR spectra of **Gr1**, **Gr2**, **Gr1Cy** and **Gr2Cy**, i.e. aliphatic, aromatic and alkenic regions, were plotted against time (presented in Appendix F) to determine whether any noticeable changes appear. For all systems, the alkenic region changed as a result of 1-octene being converted to 7-tetradecene. The aliphatic regions of **Gr1**, **Gr2** and **Gr1Cy** remained almost unchanged, with only minute changes visible. On the other hand, for **Gr2Cy**, the methyl groups of the H_2IMes ligand disappeared within 40 min from the start of the reaction, together with the signal for the CH_2 group of the NHC-backbone at δ 4.1 ppm changing dramatically (NMR spectra in Appendix F). A similar observation was made for **Gr2** at 50 °C, although the signal at δ 4.1 ppm did not follow a similar pattern. This indicates that the NHC ligand

either participates in the reaction, or the complex decomposes. However, this should be investigated in more detail to get clarity on the participation and/ decomposition of the NHC ligand and complexes.

Although it is generally accepted that the Grubbs carbenes initiate with the dissociation of PCy_3, this is not necessarily the case for the hemilabile complexes, since only one or no PCy_3 is present in the system. Therefore, these systems either initiate through the decoordination of the labile N-atom of the pyridine ring or through dissociation of L. Since hemilabile ligands are known to release a free coordination site "on demand" of competing substrates such as an alkene and occupying it otherwise, the decoordination of the N-atom was considered as a viable route of initiation. However, this brought about the question whether the ruthenium centre becomes coordinatively unsaturated with or without the influence of the incoming alkene. This was not investigated in detail in this study, but preliminary results show that two different mechanisms might be playing a role in the catalytic conversion of 1-octene with **Gr1Cy** and **Gr2Cy**, of which the O,N-ligand in **Gr2Cy** show hemilability. This should, however, be investigated in more detail to determine the influence of the solvent and alkene on the hemilability of the complexes. Monitoring the precatalyst over time in the absence and presence of the alkene with ^{1}H and ^{31}P NMR should be helpful in answering this question. Nevertheless, the modelling results indicated that the decoordination of the labile N-atom of the pyridine ring for both hemilabile systems was more favourable than the dissociation of L. However, for **Gr1Cy** this decoordination is only 3 kcal/mol more favourable compared to 46 kcal/mol for **Gr2Cy**. This indicates that the possibility of PCy_3 dissociation from **Gr1Cy** should not be excluded, since the formation of $O{=}PCy_3$ was experimentally observed for all first generation systems.

The modelling results of the activation steps for **Gr1** and **Gr2** indicated that the formation of the heptylidene is kinetically and thermodynamically more favourable than the formation of the methylidene. This supported the ^{1}H NMR results at 25 °C, but due to insufficient data within the first 20 min of the two reactions, no conclusions could be made with regards to the preference of the one species forming before the other. However, for **Gr1Cy** and **Gr2Cy**, the formation of the methylidene was shown to be thermodynamically favoured, while the kinetically favoured species was predicted to be the heptylidene, regardless of the preferred initiation step. This supported the observed formation of 5 carbene species for **Gr2Cy**, since the benzylidene was converted to the heptylidene within 30 min, which would react with 1-octene to form the Ru-methylidene intermediate and 7-tetradecene. The methylidene remained in the reaction mixture for the duration of the reaction without being depleted. The slow decrease in the signal of the methylidene suggested a possible conversion to the uncoordinated species, since the signal of the uncoordinated system kept increasing as the signal of the coordinated species decreased (**Figure 5.42** and **5.46**). Although modelling results eliminated the possible conversion of the methylidene

to the heptylidene, which would be followed by the formation of the uncoordinated methylidene species, it should not be excluded. This is due to the fact that solvent and temperature effects, which were not taken into consideration with the modelling study, could facilitate these conversions. This indicates that these systems are very complex and all factors should be considered before making any conclusions with regards to the preferred mechanistic route. The modelling results for **Gr1Cy** does not support the experimental results, since only 3 carbene signals were observed in the ^{1}H NMR. This might indicate that the reaction proceeds at such a fast rate that some of the carbene signals are not observed at the time of recording the NMR spectrum. However, this should then have been applicable to **Gr2Cy**, which was shown to initiate faster than **Gr1Cy** at 60 °C (see Chapter 5, **Table 5.5**). Therefore, a different mechanism is involved during the metathesis of 1-octene with **Gr1Cy**. This can either be an associative mechanism, or a combination of the dissociative and associative mechanisms. Since the formation of $O{=}PCy_3$ is observed in the GC analysis, it might be worthwhile to investigate the reaction with ^{31}P-NMR to monitor the disappearance of the **Gr1Cy** phosphorous signal together with the formation of new signals.

It was also noted that coordination of 1-octene parallel to the carbene and perpendicular to the Cl-Ru-Cl line ($C_{\perp}$) was more energetically favoured than coordination parallel to the Cl-Ru-Cl line ($C_{\parallel}$) for **Gr2**, **Gr1Cy** and **Gr2Cy**. Investigation of the various coordination modes of 1-octene to **Gr1** was still ongoing at the time of completion of this study, but this is also expected to be the more favoured route. The observed increase in the energies of the intermediates in the $C_{\parallel}$ mode is due to the fact that the alkene has to turn approximately 90° to align with the benzylidene carbene bond ($C_{\perp}$ mode). Investigation of the catalytic cycle of the hemilabile complexes is necessary to fully understand the mechanism(s) involved during the metathesis of 1-octene and therefore explain the observed experimental results. From investigating the catalytic cycle of **Gr1**, the formation of *trans*-tetradecene was shown to be thermodynamically favoured, which supports the experimental results. This indicates that valuable information can be obtained from theoretical investigations.

It is also evident that Gibbs free energy (ΔG) corrections still need to be made to the electronic energies to include vibrational, translational and rotational energies of the molecules. This would provide important thermodynamic information of the reaction, which could be more accurately correlated to experimental observations. This was ongoing at the time of completion of this study and the results are not included in this study.

7.5 SUMMARY OF RECOMMENDATIONS

During the course of this study, a number of theoretical and experimental research possibilities were identified. They are shortly summarised below.

Experimental:

- Investigate the influence of
  - a range of polar and non polar solvents;
  - temperature;
  - precatalyst concentration;
  - alkene chain length
  - phenol and
  - type of alkene, *inter alia* functionalised alkenes such as fatty acids

  on the activity of the various first and second generation hemilabile complexes.
- Investigate the ROMP and RCM activity of the various first and second generation hemilabile complexes.
- NMR investigation of:
  - thermolytic decomposition of the hemilabile complexes to monitor rate of disappearance of the carbene α-H
  - ^{1}H and ^{31}P NMR investigation of the first generation hemilabile complexes to determine:
    - the influence of the alkene and/or the solvent on creating an open coordination site
    - the possibility of PCy_3 dissociation together with the formation of new complexes
  - Monitor the synthesis of the hemilabile complexes, especially those that were unsuccessfully synthesised, to determine whether any new carbenes form or whether the complex decomposes completely. If carbenes form, the synthesis methods could be adapted to extract the formed complex from the reaction mixture at a certain time period.
  - Investigate the possibility of H exchange between ligands and the carbene moiety with deuterium labelling studies.
- Investigate the isomerisation activity of the hemilabile complexes at temperatures above 80 °C, since the SMP formation of these systems increased exponentially with temperature.
- Investigate the use of silver and sodium salts, rather than lithium or thallium salts, for incorporating carboxylic acids into the Grubbs carbenes.

Theoretical:

- Investigate the influence of the steric and electronic effects of the R groups of the O,N-ligands on the metathesis activity of the hemilabile complexes. As illustrated in **Figure 7.10**, a variety of O,N-ligands should be considered in which the steric and electronic properties of the ligand are varied, even if the ligands are fictitious.
- Investigate the catalytic cycles of the two dissociative mechanisms of **Gr1Cy** and **Gr2Cy** to determine the viability of the proposed mechanism, as well as shed light on the observed experimental results
- Investigate the initiation, activation and catalytic steps of the remaining hemilabile complexes, alongside with the NMR-studies, to elaborate on the observed higher thermal stability and activity of these complexes in comparison to **Gr1** and **Gr2**.
- Study alternative mechanisms for the first generation hemilabile complexes, such as:
    - the associative coordination of the alkene prior to decoordination of the N-atom of the pyridine ring or dissociation of PCy_3,
    - a combined dissociative and associative mechanism:
        - the dissociation of PCy_3 is followed by the coordination of the alkene to form either the heptylidene or methylidene intermediate
        - coordination of PCy_3 to form the methylidene or heptylidene precatalyst
        - decoordination of the N-atom of the pyridine ring prior to, or after coordination of the alkene
- Investigate the possibility of an associative mechanism for the second generation hemilabile complexes
- Investigate different coordination positions of the alkene to the Ru-centre, such as *cis* or *trans* to the carbene instead of *trans* to L.
- Complete the vibrational analysis studies of
    - the already optimised intermediates to make Gibbs free energy corrections to the electronic energies and
    - optimise the various transition states of the activation and catalytic steps

  to be able to more accurately determine the rate determining steps, and therefore elucidate experimental results.

Theoretical investigations should be done in combination with experimental work to help researchers gain insight into the reaction mechanisms, explain observed trends, as well as determine reasons for unsuccessful synthesis and/or catalytic reactions.

7.6 REFERENCES

1. Dinger, M.B. and Mol, J.C., *Adv. Synth. Catal.*, 2002, **366**, 671
2. Maechling, S., Zaja, M., and Blechert, S., *Adv. Synth. Catal.*, 2005, **347**, 1413
3. Lehman, S.E., Jr., Schwendeman, J.E., O'Donnell, P.M., and Wagener, K.B., *Inorg. Chim. Acta.*, 2003, ***345***, 190
4. Huang, J., Schanz, H.-J., Stevens, E.D., and Nolan, S.P., *Organometallics*, 1999, **18**, 5375
5. Weskamp, T., Kohl, F.J., Hieringer, W., Gleich, D., and Herrmann, W.A., *Angew. Chem. Int. Ed.*, 1999, **38**, 2416
6. Huang, J., Stevens, E.D., Nolan, S.P., and Petersen, J.L., *J. Am. Chem. Soc.*, 1999, **121**, 2674
7. Scholl, M., Trnka, T.M., Morgan, J.P., and Grubbs, R.H., *Tetrahedron Lett.*, 1999, **40**, 2247
8. Fürstner, A., Thiel, O.R., Ackermann, L., Schanz, H.-J., and Nolan, S.P., *J. Org. Chem.*, 2000, **65**, 2204
9. Arisawa, M., Terada, Y., Takahashi, K., Nakagawa, M., and Nishida, A., *J. Org. Chem.*, 2006, **71**, 4255
10. Bourgeois, D., Pancrazi, A., Nolan, S.P., and Prunet, J., *J. Organomet. Chem.*, 2002, **643-644**, 247
11. Dharmasena, U.L., Foucault, H.M., Dos Santos, E.N., Fogg, D.E., and Nolan, S.P., *Organometallics*, 2005, **24**, 1056
12. Denk, K., Fridgen, J., and Herrmann, W.A., *Adv. Synth. Catal.*, 2002, **344**, 666
13. Wijkens, P., Jastrzebski, J.T.B.H., Van der Schaaf, P.A., Kolly, R., Hafner, A., and Van Koten, G., *Org. Lett.*, 2000, **2**, 1621
14. Chang, S., Jones II, L., Wang, C., Henling, L.M., and Grubbs, R.H., *Organometallics*, 1998, **17**, 3460
15. Conrad, J.C., Amoroso, D., Czechura, P., Yap, G.P.A., and Fogg, D.E., *Organometallics*, 2003, **22**, 3634
16. De Clercq, B. and Verpoort, F., *Adv. Synth. Catal.*, 2002, **344**, 639
17. De Clercq, B. and Verpoort, F., *Tetrahedron Lett.*, 2001, **42**, 8959
18. Nieczypor, P., Buchowicz, W., Meester, W.J.N., Rutjes, F.P.J.T., and Mol, J.C., *Tetrahedron Lett.*, 2001, **42**, 7103
19. Buchowicz, W., Mol, J.C., Lutz, M., and Spek, A.L., *J. Organomet. Chem.*, 1999, **588**, 205
20. Amoroso, D., Snelgrove, J.L., Conrad, J.C., Drouin, S.D., Yap, G.P.A., and Fogg, D.E., *Adv. Synth. Catal.*, 2002, **344**, 757
21. Coalter III, J.N., Bollinger, J.C., Eisenstein, O., and Caulton, K.G., *New J. Chem.*, 2000, **24**, 925

22. Hahn, F.E., Paas, M., and Frohlich, R., *J. Organomet. Chem.*, 2005, **690**, 5816

23. Monfette, S. and Fogg, D.E., *Organometallics*, 2006, **25**, 1940

24. Sanford, M.S., Ulman, M., and Grubbs, R.H., *J. Am. Chem. Soc.*, 2001, **123**, 749

25. Sanford, M.S., Love, J.A., and Grubbs, R.H., *J. Am. Chem. Soc.*, 2001, **123**, 6543

26. Sanford, M.S. and Love, J.A. *in* ***Handbook of Metathesis***, Grubbs, R.H., Ed., *Mechanism of Ruthenium-Catalysed Olefin Metathesis Reactions*, Vol. 1, Wiley, 2003, p. 112

27. Dinger, M.B. and Mol, J.C., *Organometallics*, 2003, **22**, 1089

28. Herrmann, W.A., Lobmaier, G.M., Priermeier, T., Mattner, M.R., and Scharbert, B., *J. Mol. Catal. A: Chem.*, 1997, **117**, 455

29. Love, J.A., Sanford, M.S., Day, M.W., and Grubbs, R.H., *J. Am. Chem. Soc.*, 2003, **125**, 10103

30. Trnka, T.M., Morgan, J.P., Sanford, M.S., Wilhelm, T.E., Scholl, M., Choi, T.L., Ding, S., Day, M.W., and Grubbs, R.H., *J. Am. Chem. Soc.*, 2003, **125**, 2546

31. McGuinness, D.S., Cavell, K.J., Skeleton, B.W., and White, A.H., *Organometallics*, 1998, **18**, 1596

32. Parr, R.G. and Yang, W., *J. Am. Chem. Soc.*, 1984, **106**, 4049

33. Ulman, M. and Grubbs, R.H., *Organometallics*, 1998, **17**, 2484

34. Adlhart, C. and Chen, P., *J. Am. Chem. Soc.*, 2004, **126**, 3496

35. Adlhart, C., Hinderling, C., Baumann, H., and Chen, P., *J. Am. Chem. Soc.*, 2000, **122**, 8204

36. Janse van Rensburg, W., Steynberg, P.J., Kirk, M.M., Meyer, W.H., and Forman, G.S., *J. Organomet. Chem.*, 2006, **691**, 5312

37. Forman, G.S., McConnell, A.E., Tooze, R.P., Janse van Rensburg, W., Meyer, W.H., Kirk, M.M., Dwyer, C.L., and Serfontein, D.W., *Organometallics*, 2005, **24**, 4528

38. Jordaan, M., Van Helden, P., Van Sittert, C.G.C.E., and Vosloo, H.C.M., *J. Mol. Catal. A: Chem.*, 2006, **254**, 145

39. Van Helden, P. 2004. ***A Computational Study on the Ligand Effects in Alkene Cross-metathesis***, (mini project report written as part of the Honours course at North-West University) PU for CHE, Potchefstroom, 21 p. (unpublished)

Acknowledgements

On completion of this study, I would like to express my sincerest appreciation and gratitude to:

- God Almighty for the opportunity, health, motivation, guidance and love He gave to me during this study.
- My father for his love, encouragement, motivation and for his firm belief in me. My family and friends for their love, support and interest.
- My study leader, prof. H.C.M. Vosloo, for his guidance and countless suggestions, as well as all the times he helped me despite his busy schedule.
- Dr. Johan Jordaan for his motivation, love and support during this study.
- Andre Joubert (North-West University) and Megan Kirk (Sasol Technology R&D) for acquiring the NMR data.
- Drr. Wolfgang H. Meyer (Sasol Technology R&D) and Werner Janse van Rensburg (Sasol Technology R&D) for their valuable discussions.
- Sasol Technology R&D, the THRIP programme (grant # 2789) of the National Research Foundation of South Africa as well as the North-West University (NWU) for their financial contribution towards this study.
- Hendrine Krieg for the language editing of this dissertation.
- Staff and students of the School of Chemistry at the North-West University (Potchefstroom campus) for their friendship and support.

Appendix A

Appendix A (p. 283 – 302) is available on the enclosed CD

Appendix B

Appendix B (p. 303 – 334) is available on the enclosed CD

Appendix C1

^{1}H, ^{13}C and DEPT NMR spectra of the synthesised ligands (L1 – L4):

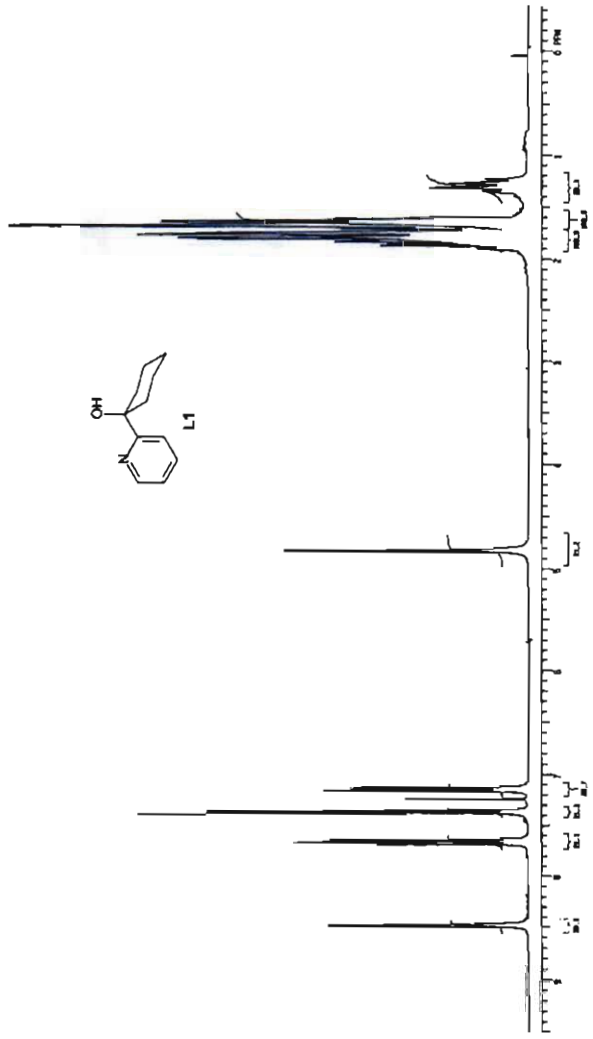

Spectrum C.1 ^{1}H NMR spectrum of 1-(2'-pyridinyl)cyclohexanol.

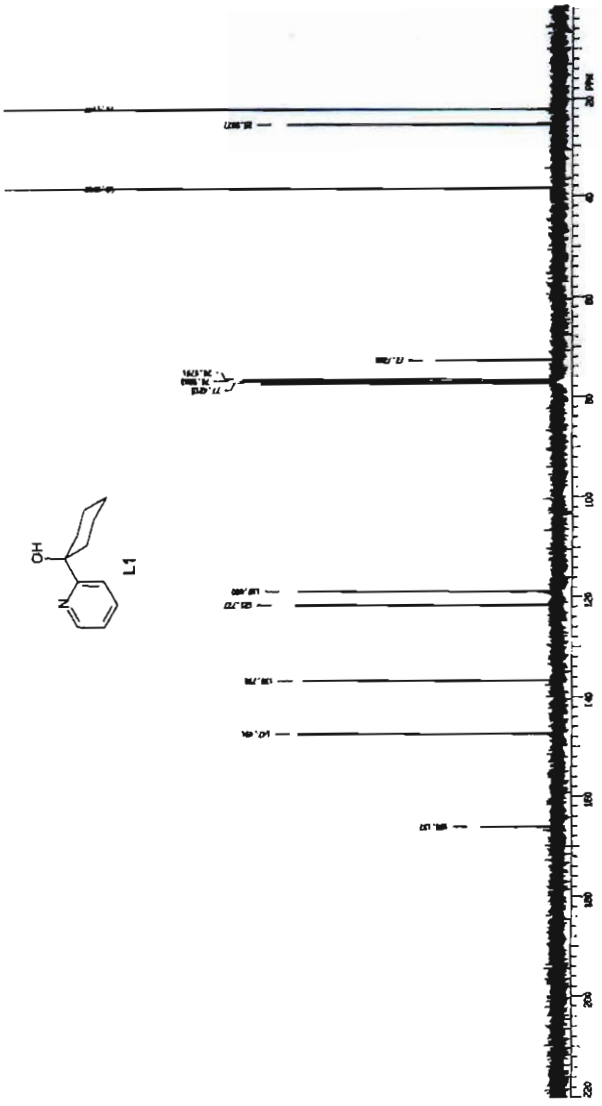

Spectrum C.2 ^{13}C NMR spectrum of 1-(2'-pyridinyl)cyclohexanol.

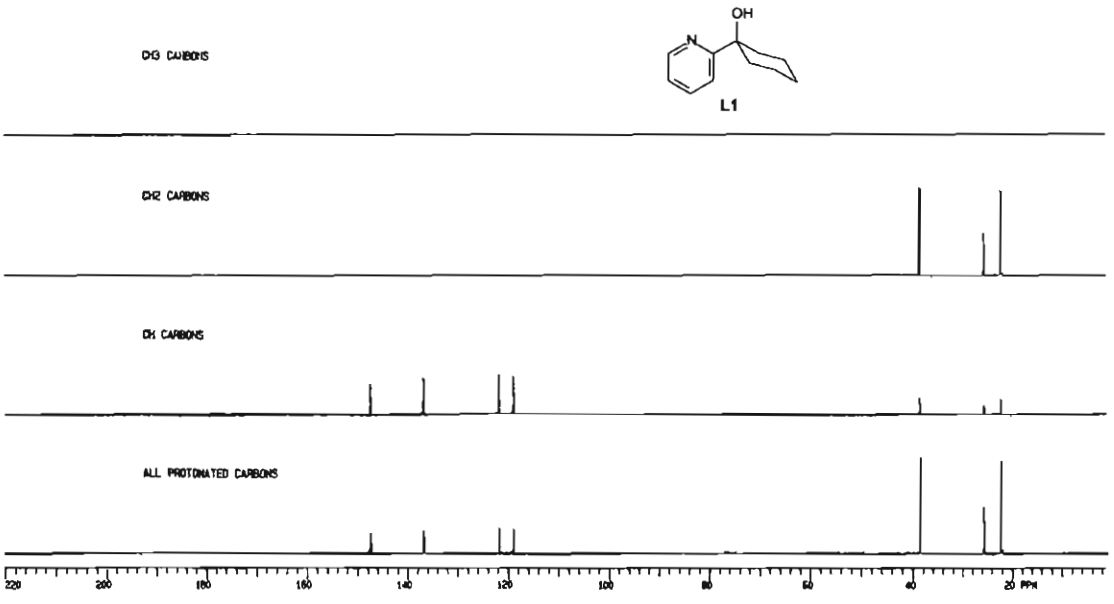

Spectrum C.3 DEPT of 1-(2'-pyridinyl)cyclohexanol.

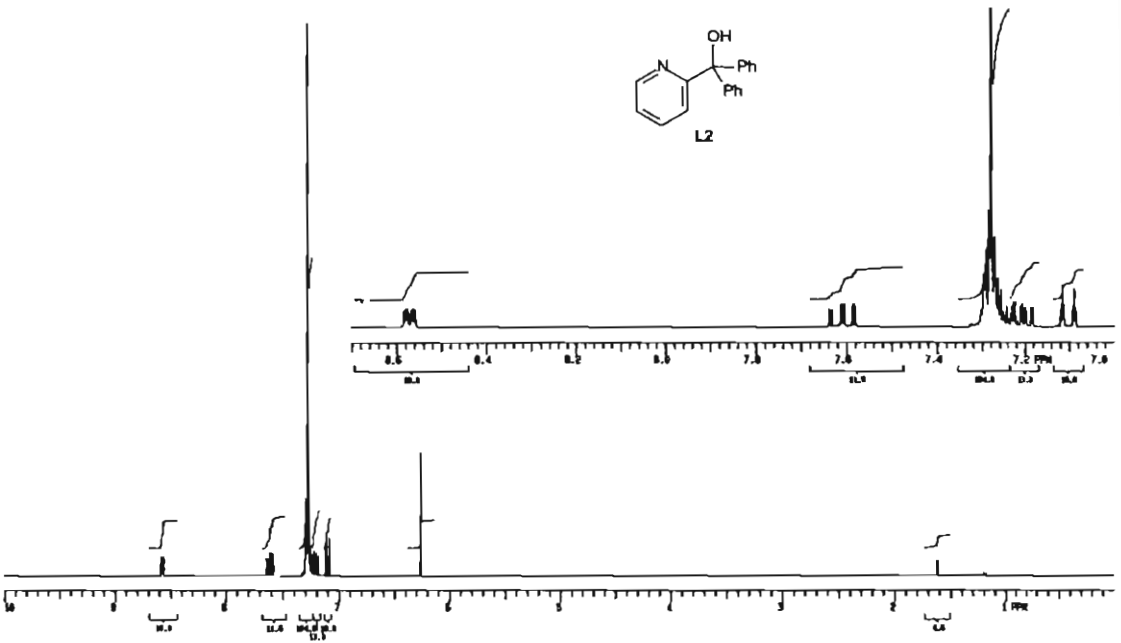

Spectrum C.4 ^{1}H NMR spectrum of 1-(2'-pyridinyl)-2,4-dimethylpentan-3-ol.

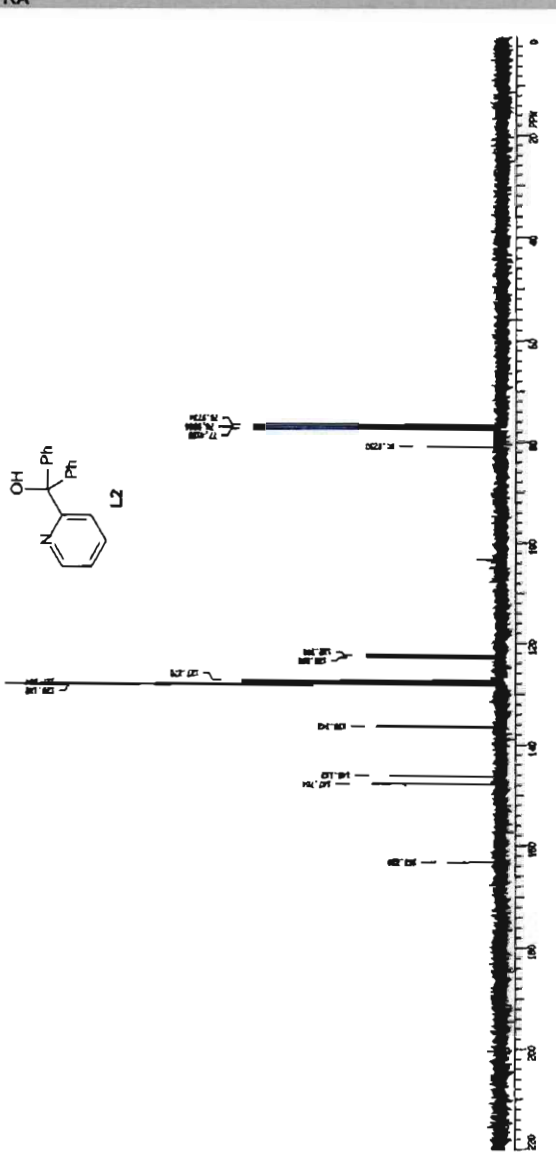

Spectrum C.5 ^{13}C NMR spectrum of 1-(2'-pyridinyl)-2,4-dimethylpentan-3.

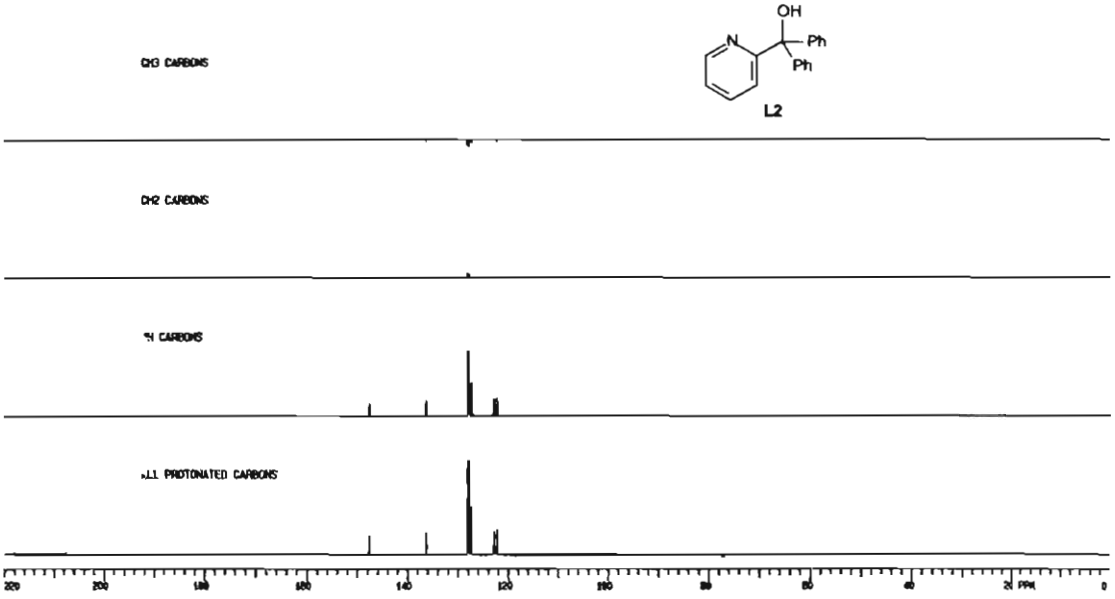

Spectrum C.6 DEPT of 1-(2'-pyridinyl)-2,4-dimethylpentan-3-ol.

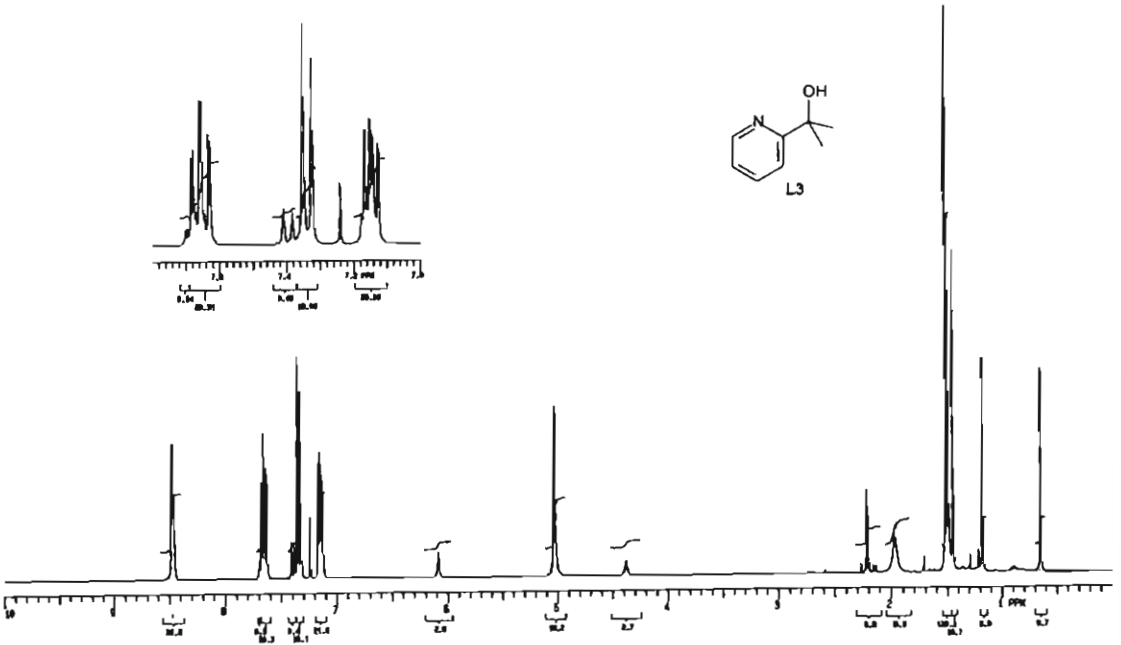

Spectrum C.7 ^{1}H NMR spectrum of 1-(2'-pyridinyl)propan-2-ol.

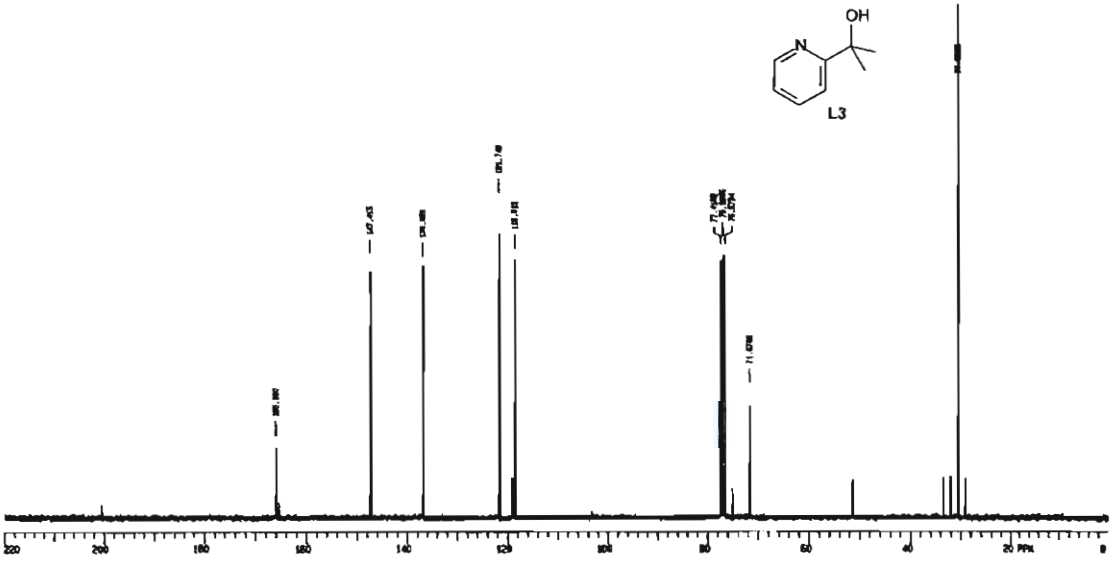

Spectrum C.8 ^{13}C NMR spectrum of 1-(2'-pyridinyl)propan-2-ol.

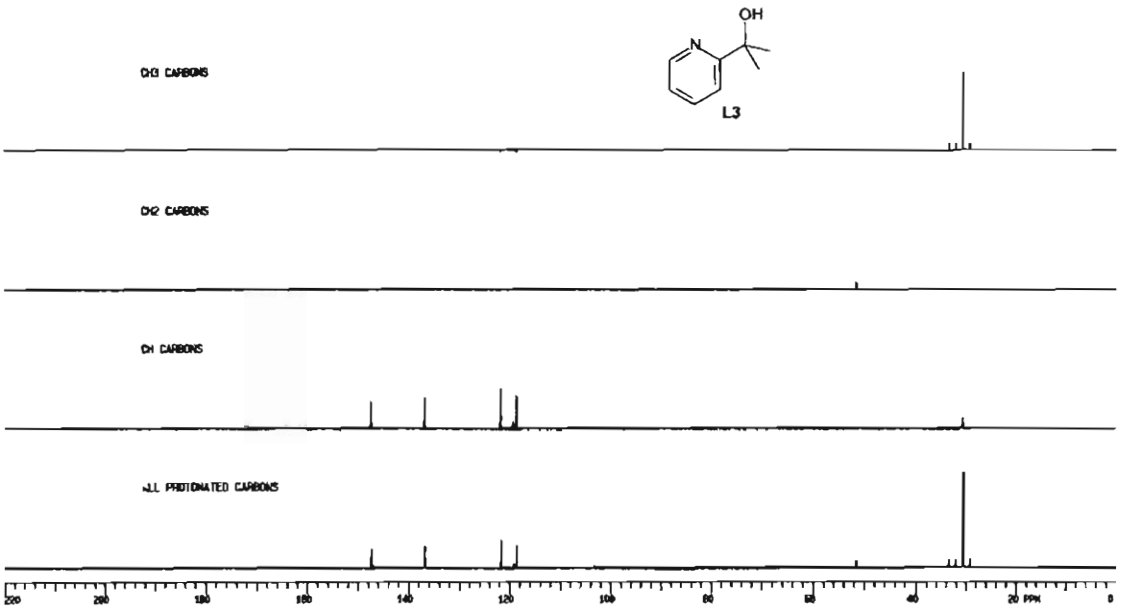

Spectrum C.9 DEPT of 1-(2'-pyridinyl)propan-2-ol.

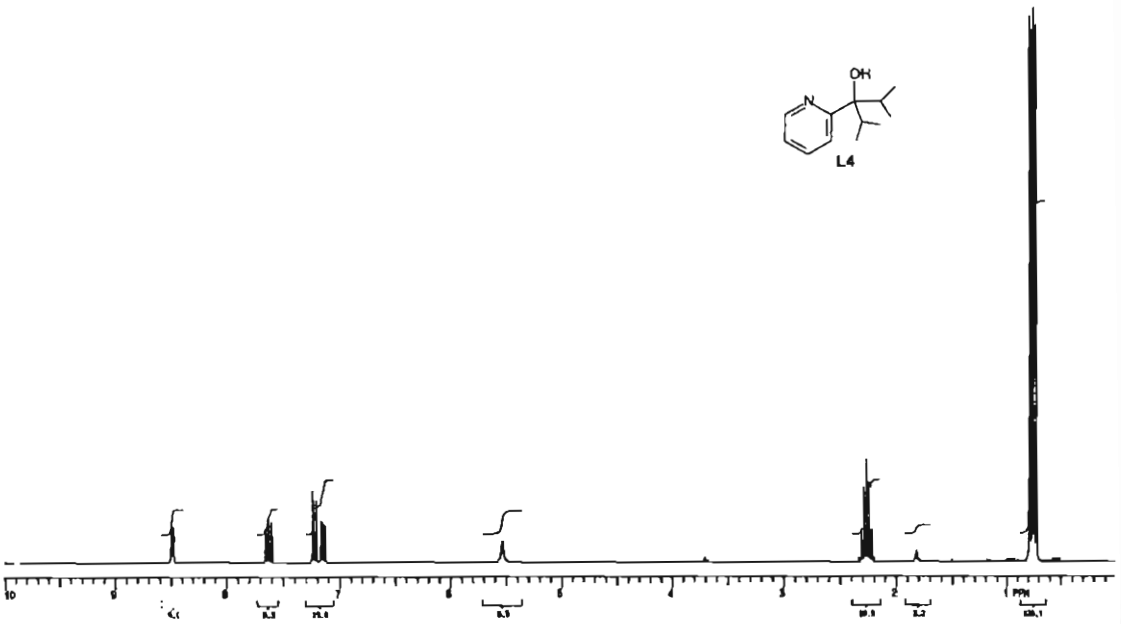

Spectrum C.10 ^{1}H NMR spectrum of 1-(2'-pyridinyl)-2,4-dimethylpentan-3-ol.

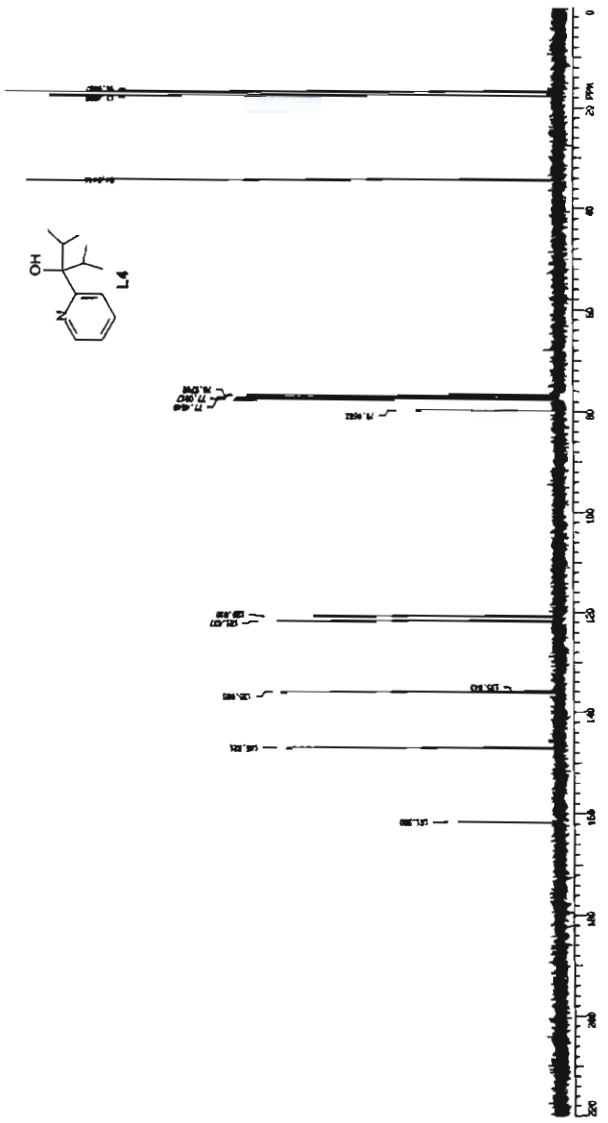

Spectrum C.11 ^{13}C NMR spectrum of 1-(2'-pyridinyl)-2,4-dimethylpentan-3-ol.

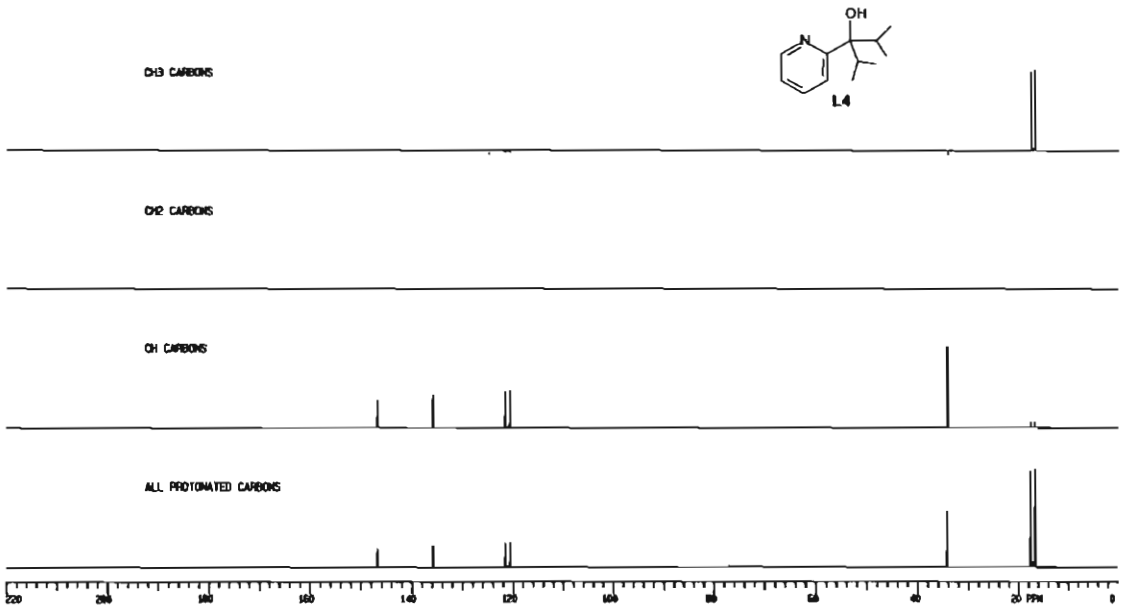

Spectrum C.12 DEPT of 1-(2'-pyridinyl)-2,4-dimethylpentan-3-ol.

NMR spectra of the starting complexes (**Gr1** and **Gr2**) and their pyridine derivatives:

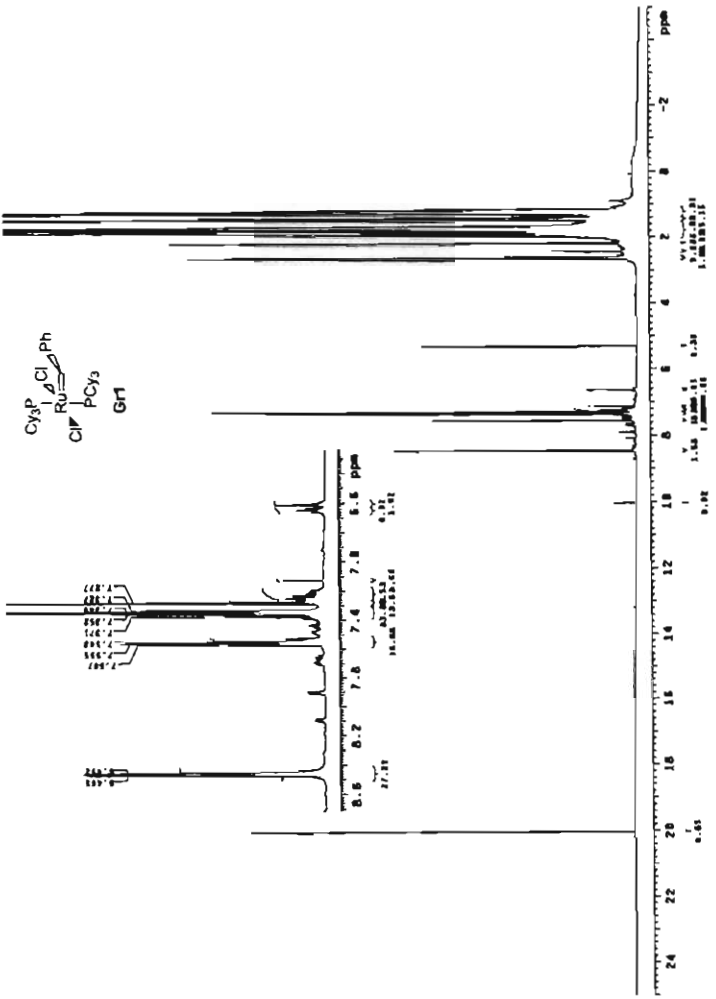

Spectrum C.13 ^{1}H NMR spectrum of benzylidene-dichloro(bis(tricyclohexylphosphine))ruthenium.

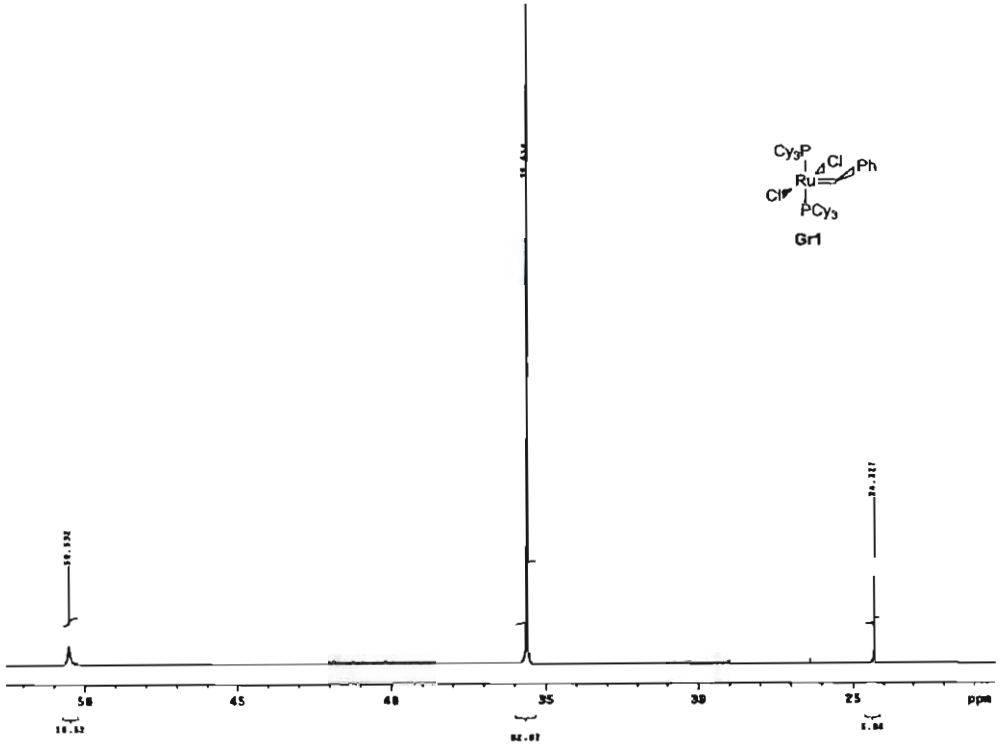

Spectrum C.14 ^{31}P NMR spectrum of benzylidene-dichloro(bis(tricyclohexylphosphine))ruthenium.

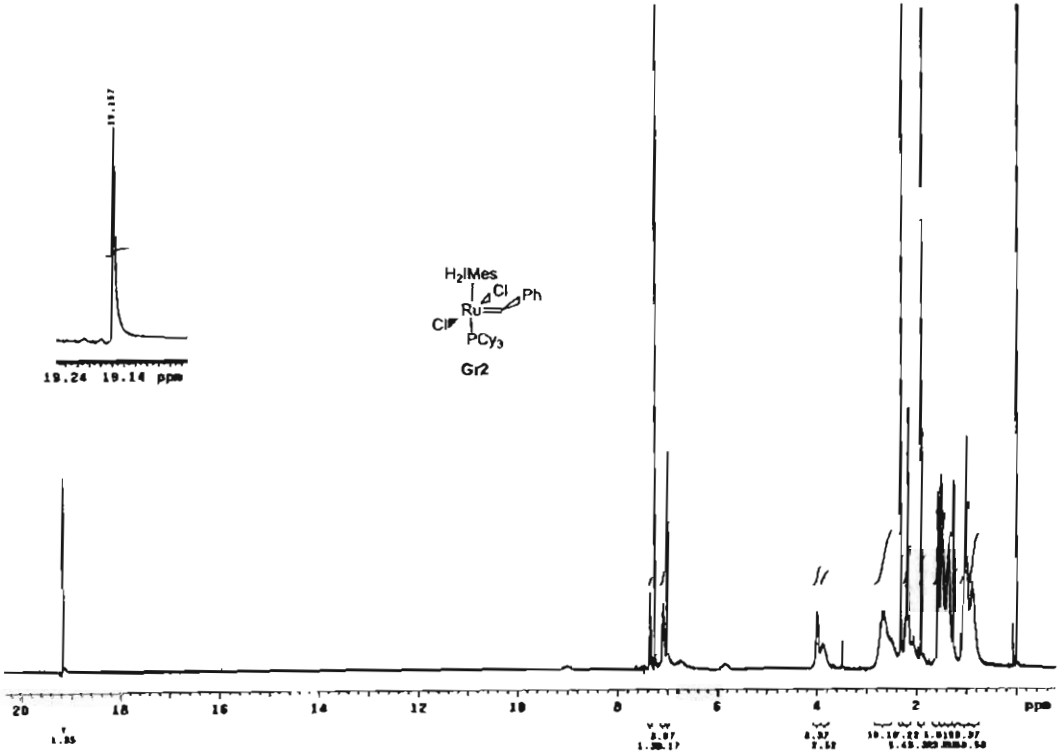

Spectrum C.15 ^{1}H NMR spectrum of benzylidene-dichloro(tricyclohexylphosphine)(1,3-bis-(2,4,6-trimethylphenyl)-2-imadazolidinylidene)-ruthenium.

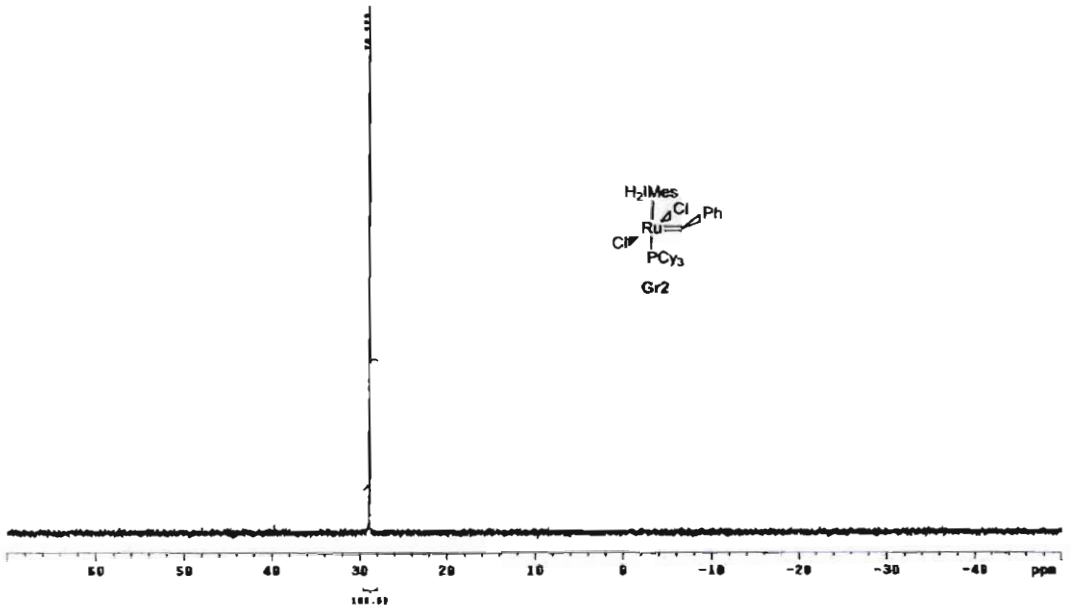

Spectrum C.16 ^{1}H NMR spectrum of benzylidene-dichloro(tricyclohexylphosphine)(1,3-bis-(2,4,6-trimethylphenyl)-2-imadazolidinylidene)-ruthenium.

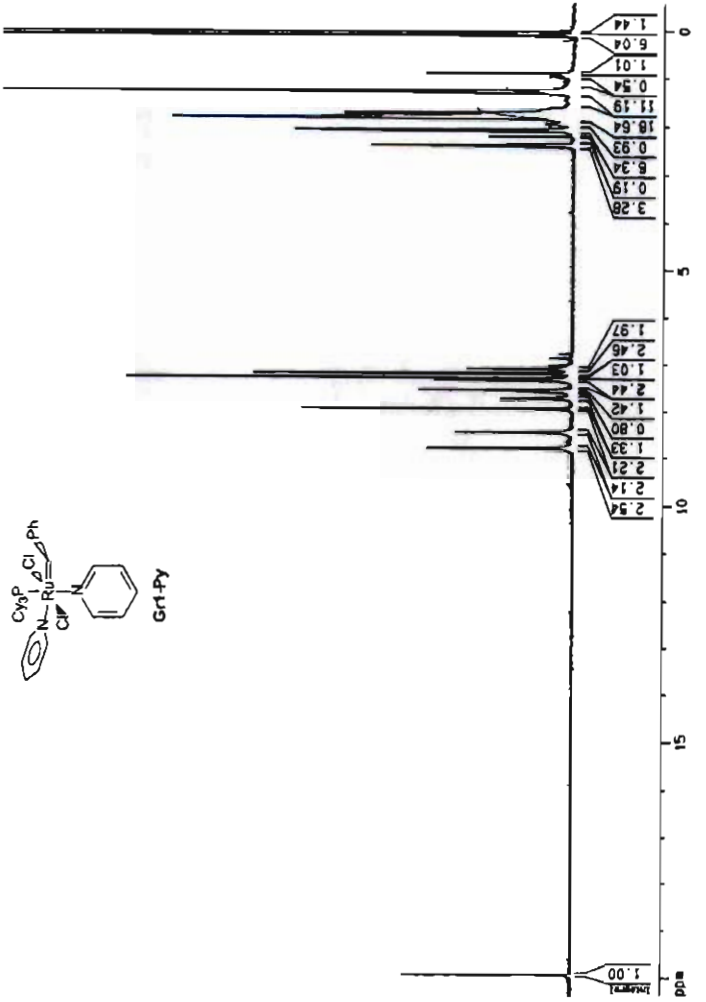

Spectrum C.17 ^{1}H NMR spectrum of benzylidene-dichloro(tricyclohexylphosphine)bis(pyridine)ruthenium.

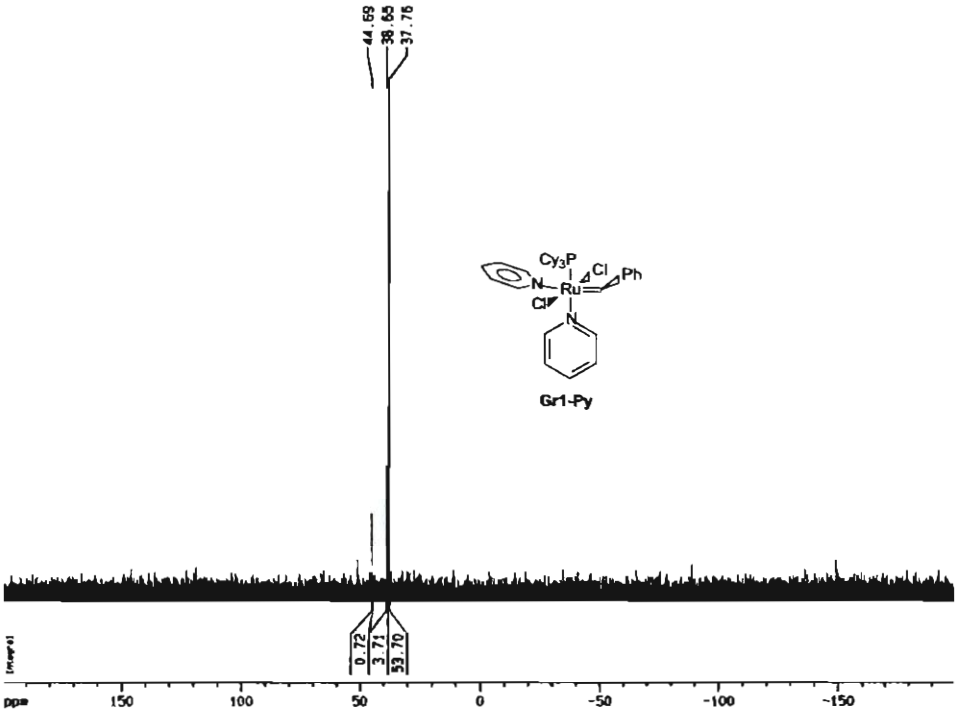

Spectrum C.18 ^{31}P NMR spectrum of benzylidene-dichloro(tricyclohexylphosphine)bis(pyridine)ruthenium.

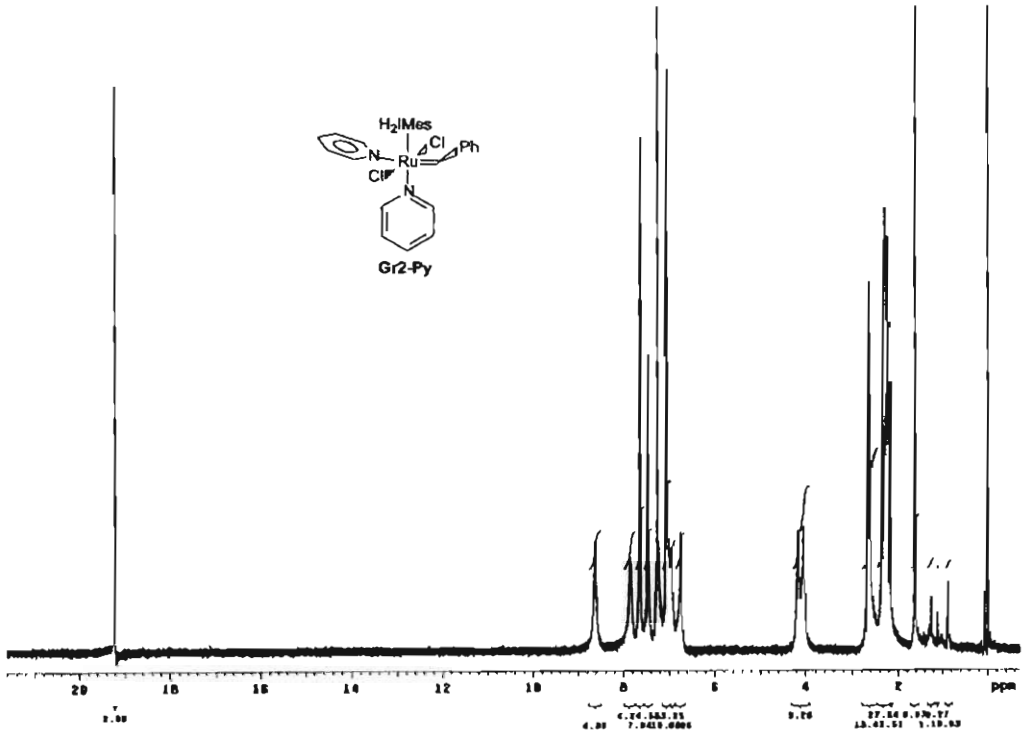

Spectrum C.19 ^{1}H NMR spectrum of benzylidene-dichloro(1,3-bis-(2,4,6-trimethylphenyl)-2-imadazolidinylidene)bis(pyridine)ruthenium.

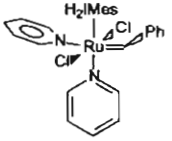

Gr2-Py

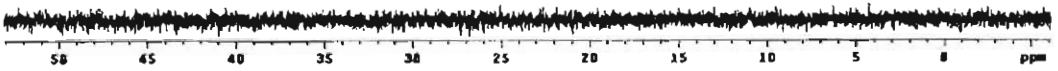

Spectrum C.20 ^{31}P NMR spectrum of benzylidene-dichloro(1,3-bis-(2,4,6-trimethylphenyl)-2-Imadazolidinylidene)bis(pyridine)ruthenium.

^{1}H, ^{31}P and COSY NMR of the successfully synthesised first generation O,N-chelated complexes:

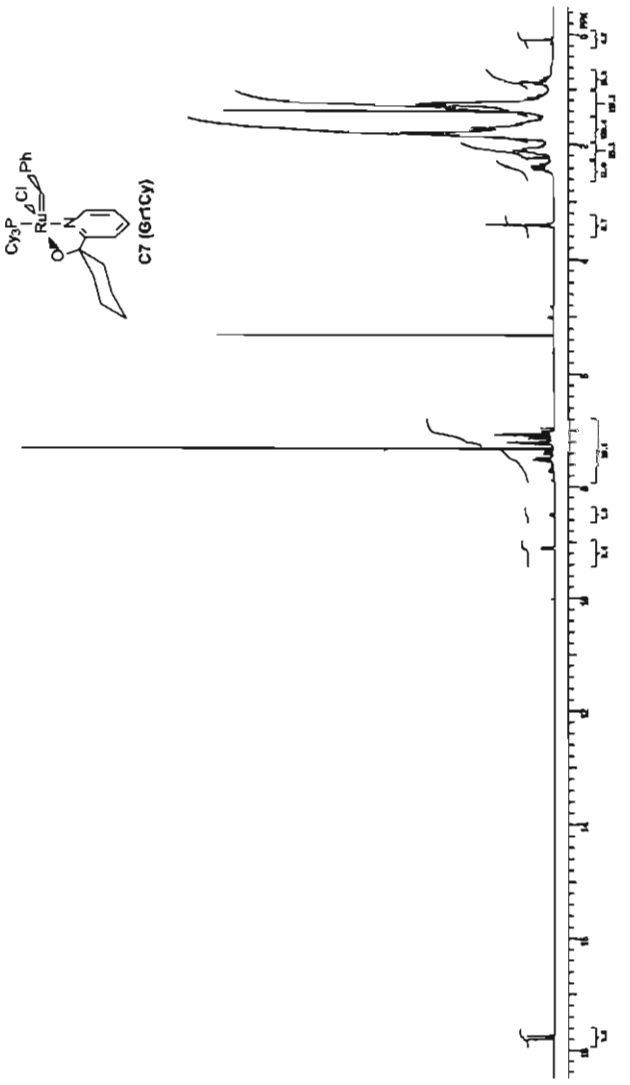

Spectrum C.21 ^{1}H- MR spectra of benzylidene-chloro(tricyclohexylphosphine)-[1-(2'-pyridinyl)cyclohexan-1-olato]ruthenium.

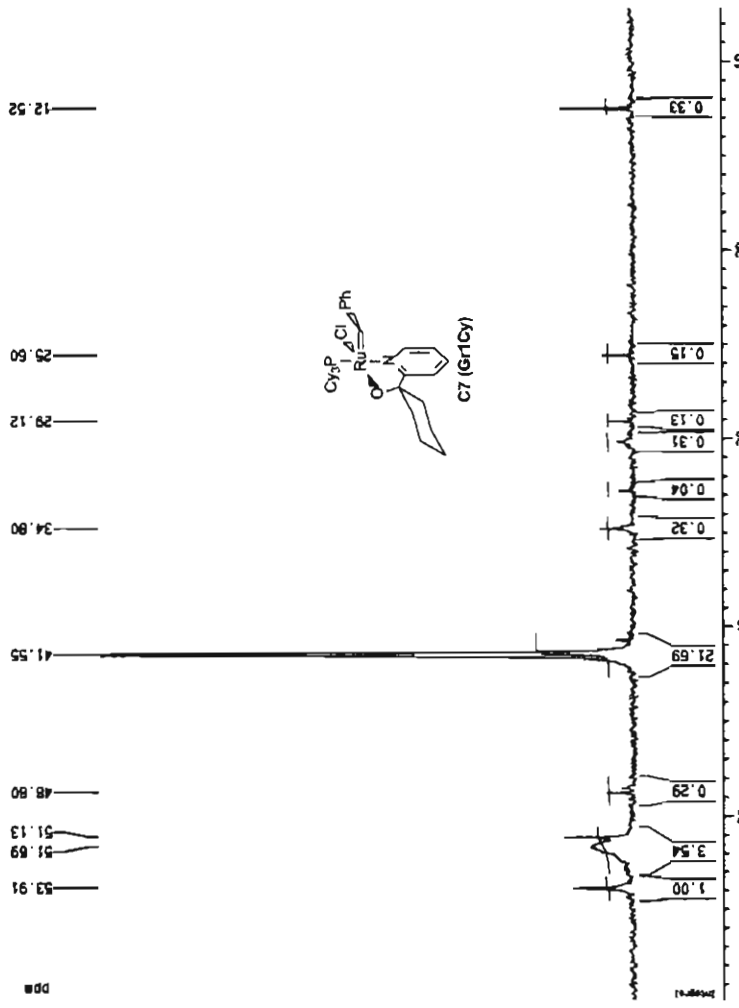

Spectrum C.22 ^{31}P NMR spectrum of benzylidene-chloro(tricyclohexylphosphine)-[1-(2'-pyridinyl)cyclohexan-1-olato]ruthenium.

Spectrum C.23 COSY NMR spectrum of benzylidene-chloro(tricyclo-hexylphosphine)-[1-(2'-pyridinyl)cyclohexan-1-olato]ruthenium.

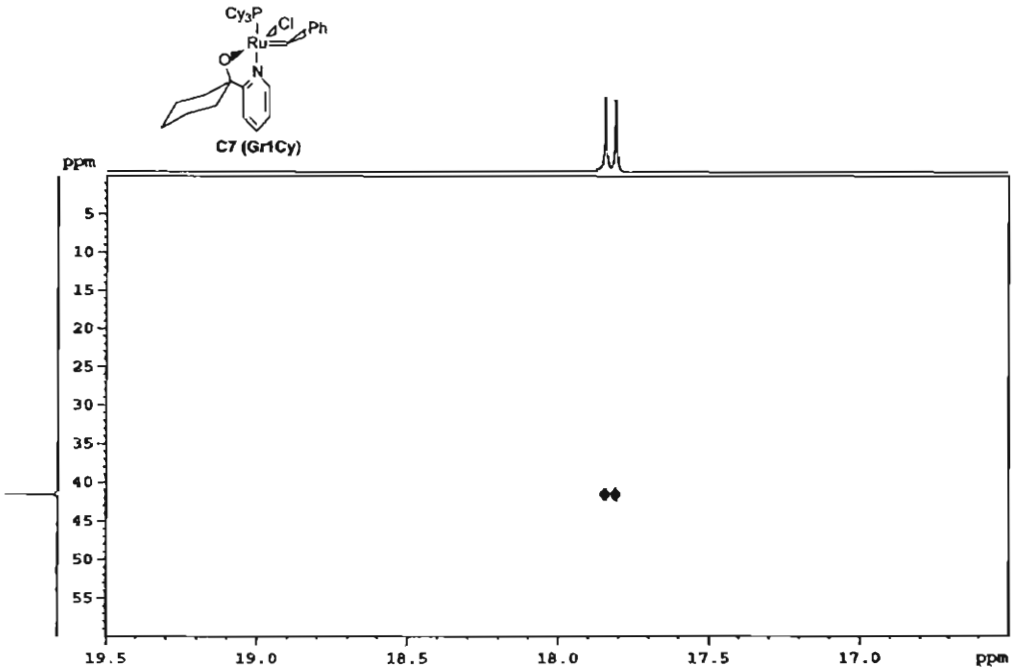

Spectrum C.24 P-H correlation spectrum of benzylidene-chloro(tricyclo-hexylphosphine)-[1-(2'-pyridinyl)cyclohexan-1-olato]ruthenium.

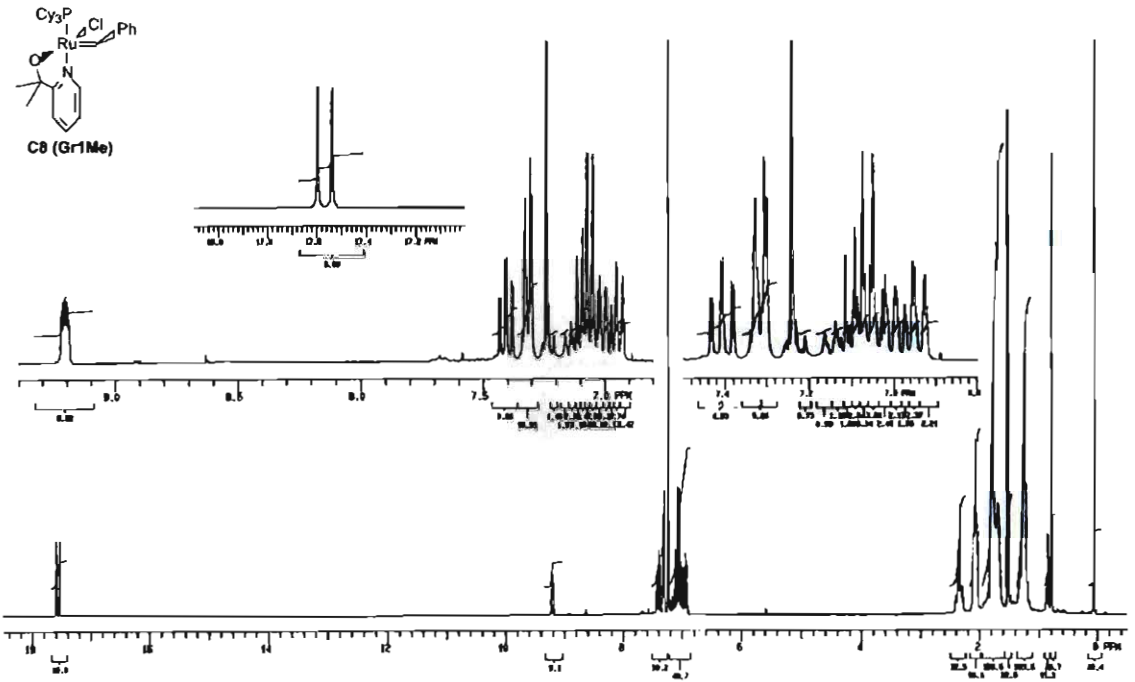

Spectrum C.26 ^{1}H NMR spectrum of benzylidene-chloro(tricyclohexylphosphine)-[1-(2'-pyridinyl)propan-2-olato]ruthenium.

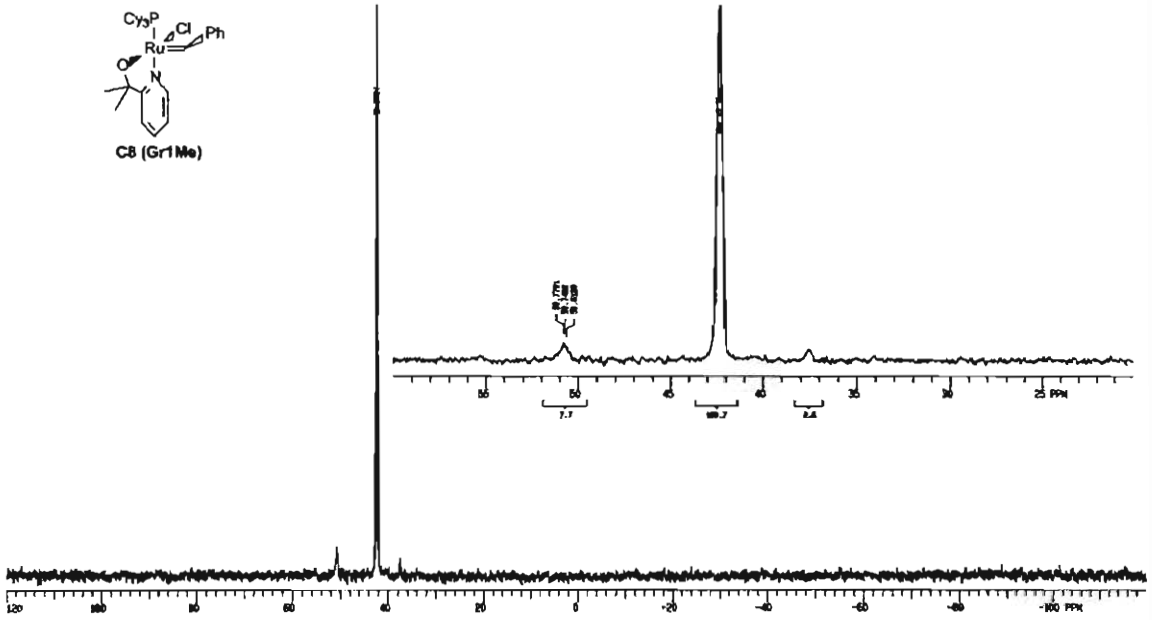

Spectrum C.26 ^{31}P NMR spectrum of benzylidene-chloro(tricyclohexylphosphine)-[1-(2'-pyridinyl)propan-2-olato]ruthenium.

Spectrum C.27 COSY NMR spectrum of benzylidene-chloro(tricyclohexylphosphine)-[1-(2'-pyridinyl)-propan-2-olato]ruthenium.

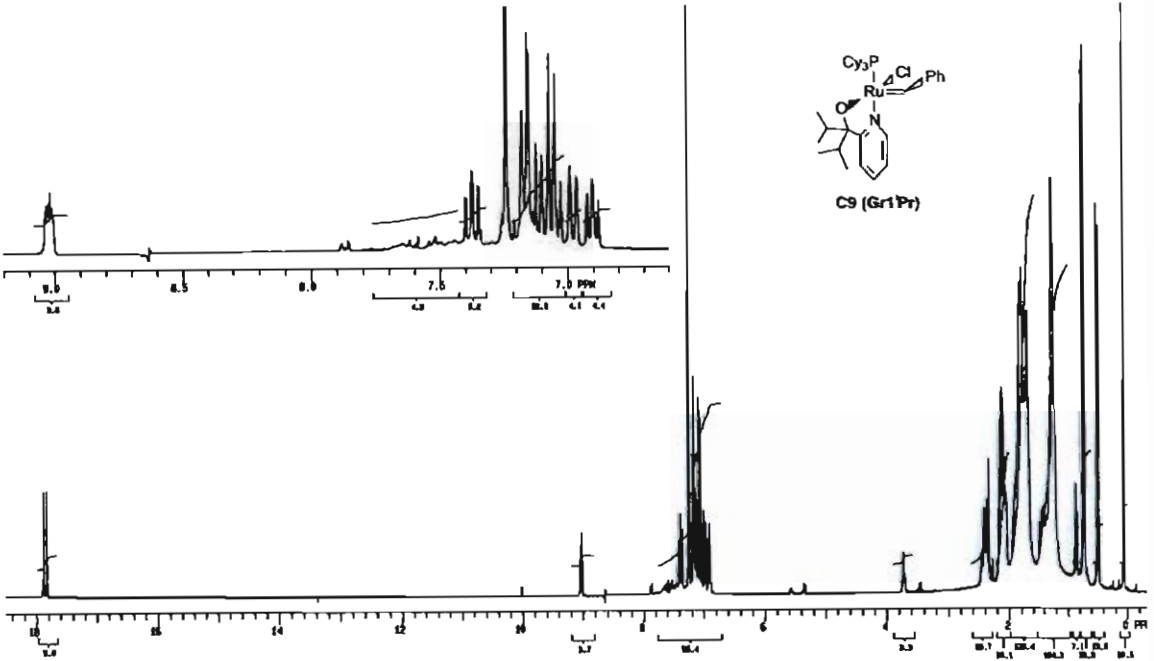

Spectrum C.28 ^{1}H NMR spectrum of benzylidene-chloro(tricyclohexylphosphine)-[1-(2'-pyridinyl)-2,4-dimethylpentan-3-olato]ruthenium.

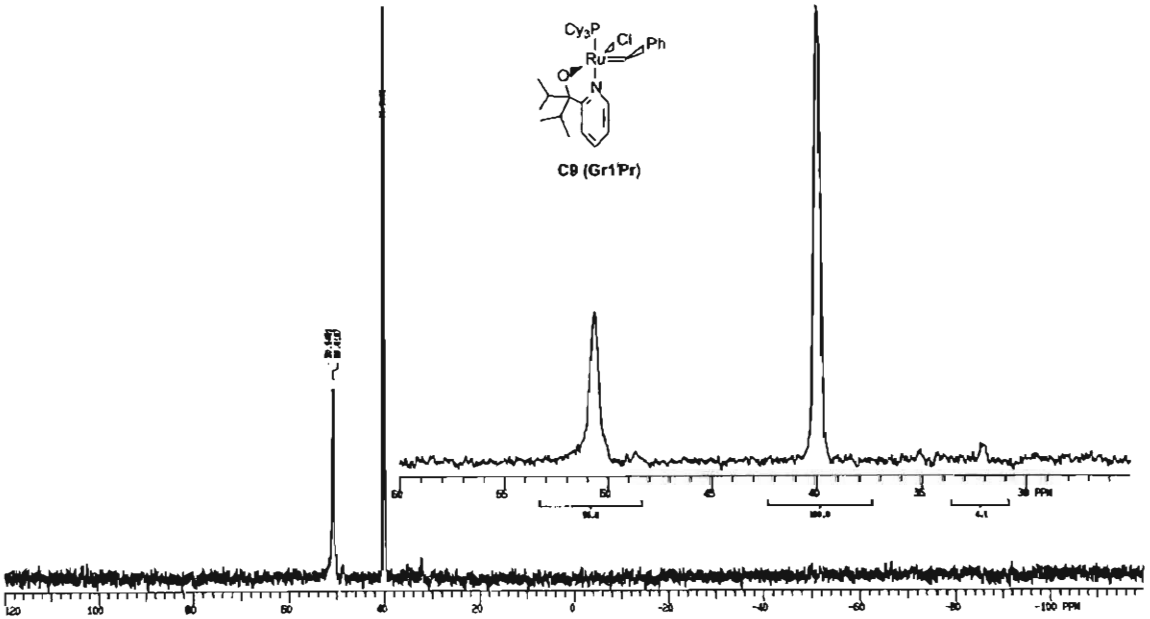

Spectrum C.29 ^{31}P NMR spectrum of benzylidene-chloro(tricyclohexylphosphine)-[1-(2'-pyridinyl)-2,4-dimethylpentan-3-olato}ruthenium.

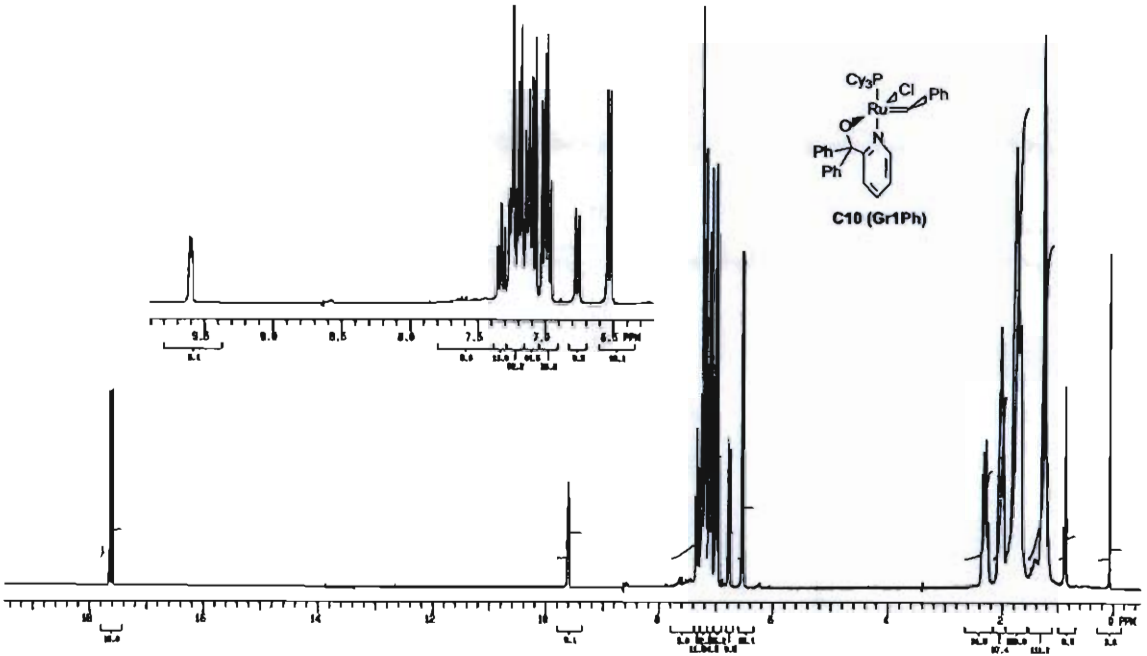

Spectrum C.30 ^{1}H NMR spectrum of benzylidene-chloro(tricyclohexylphosphine)-[1-(2'-pyridinyl)-1,1-diphenyl-methanolato]ruthenium.

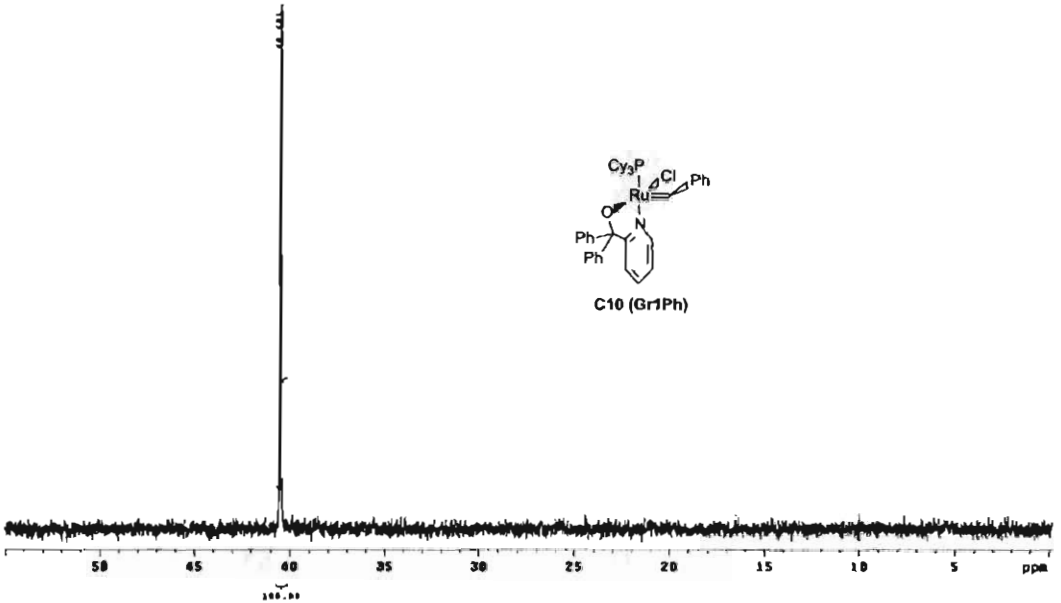

Spectrum C.31 ^{31}P NMR spectrum of benzylidene-chloro(tricyclohexylphosphine)-[1-(2'-pyridinyl)-1,1-diphenyl-methanolato]ruthenium.

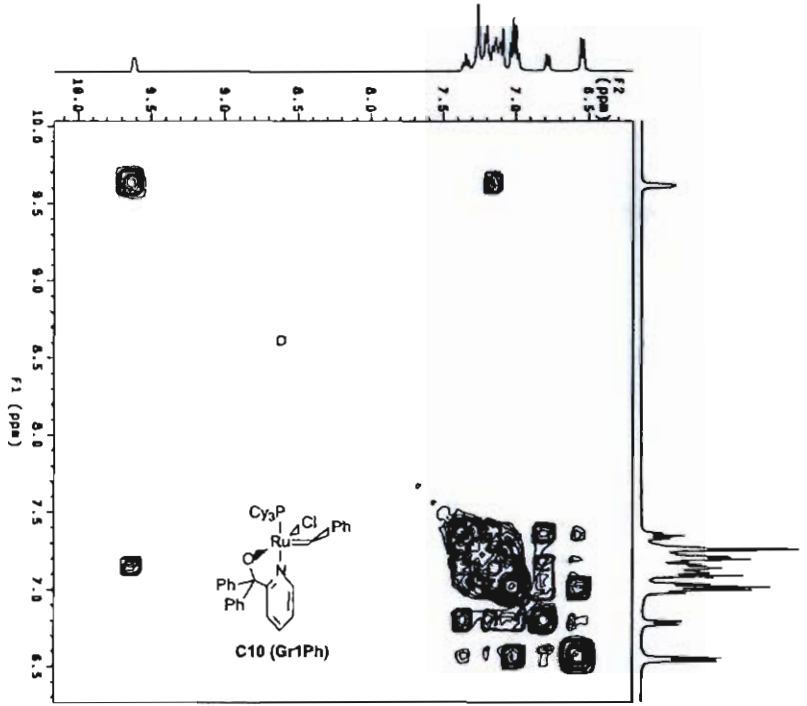

Spectrum C.32 COSY NMR spectrum of benzylidene-chloro(tricyclohexylphosphine)-[1-(2'-pyridinyl)-1,1-diphenyl-methanolato]ruthenium

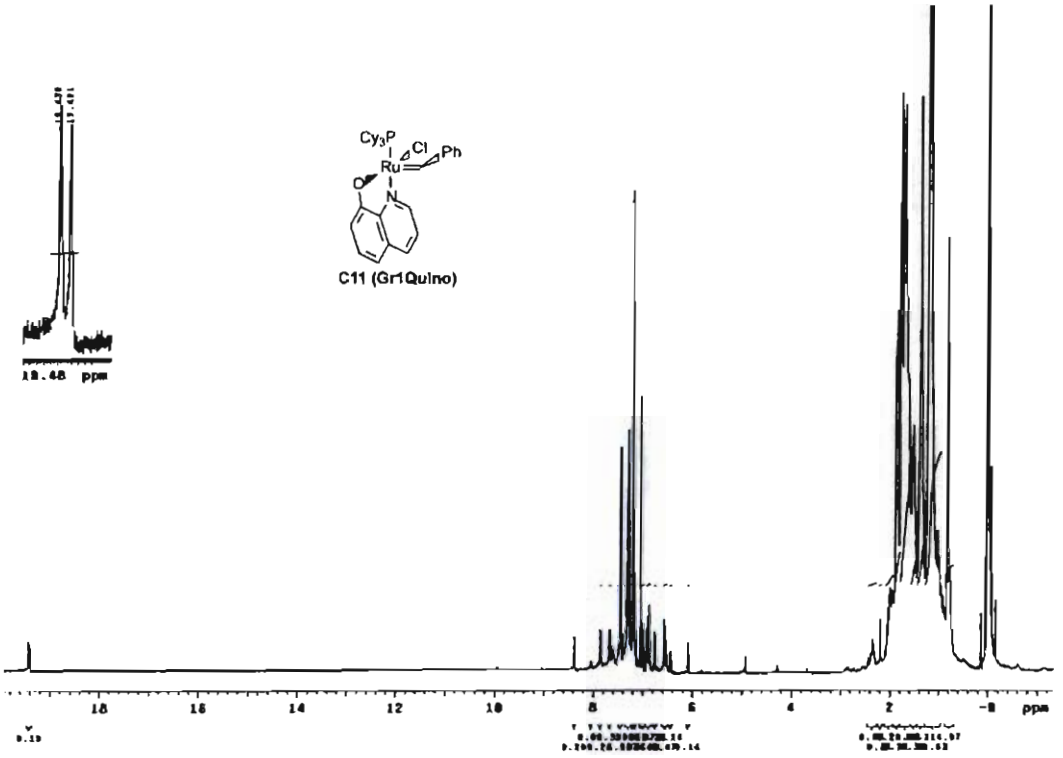

Spectrum C.33 ^{1}H NMR spectrum of benzylidene-chloro(tricyclohexylphosphine)-[8-quinolinolato]ruthenium.

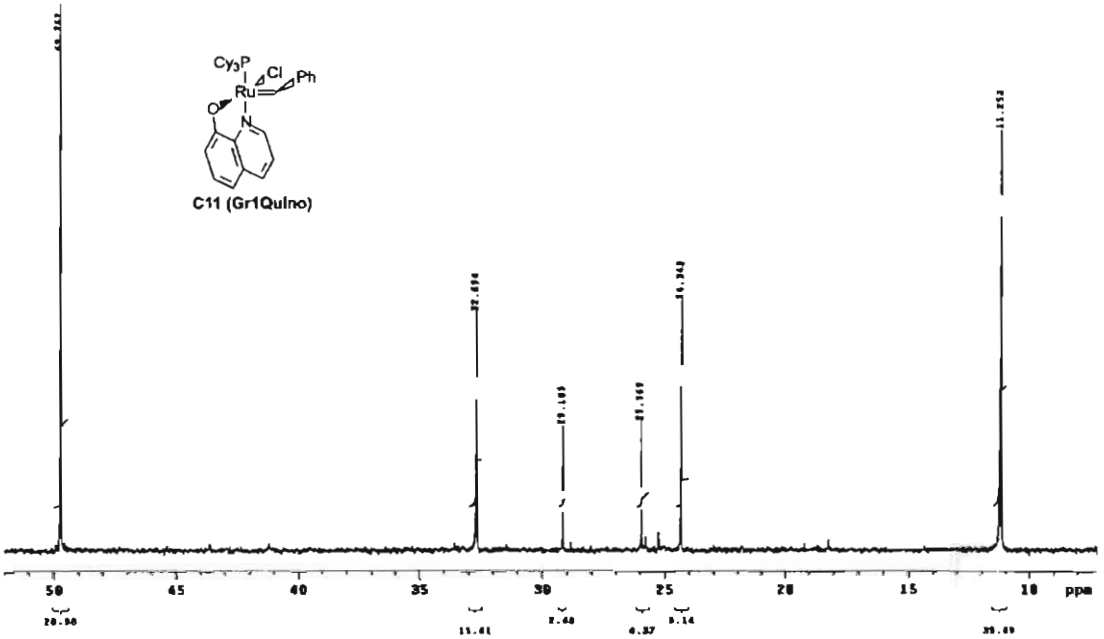

Spectrum C.34 ^{31}P NMR spectrum of benzylidene-chloro(tricyclohexylphosphine)-[8-quinolinolato]ruthenium.

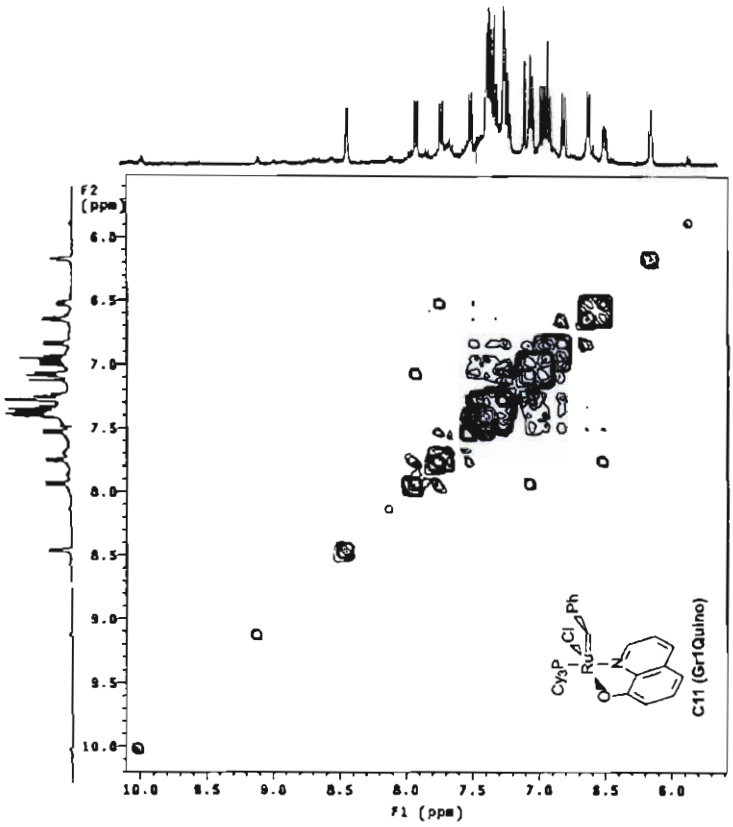

Spectrum C.35 COSY NMR spectrum of benzylidene-chloro(tricyclohexylphosphine)-[8-quinolinolato]ruthenium.

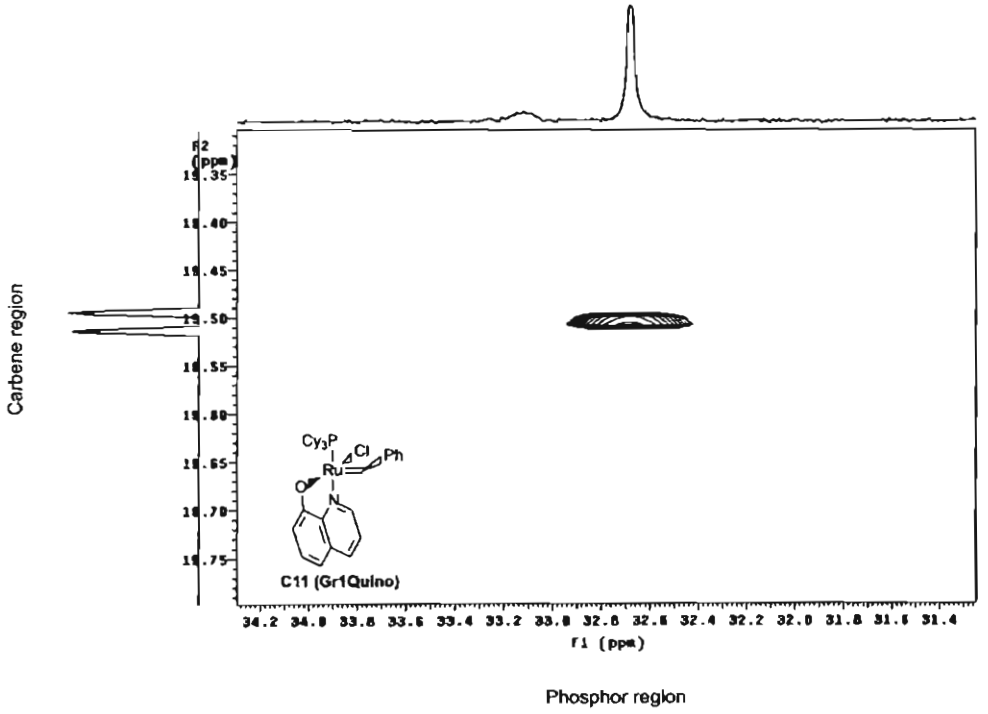

Spectrum C.36 P-H NMR correlation spectrum of benzylidene-chloro(tricyclohexylphosphine)-[8-quinolinolato]ruthenium.

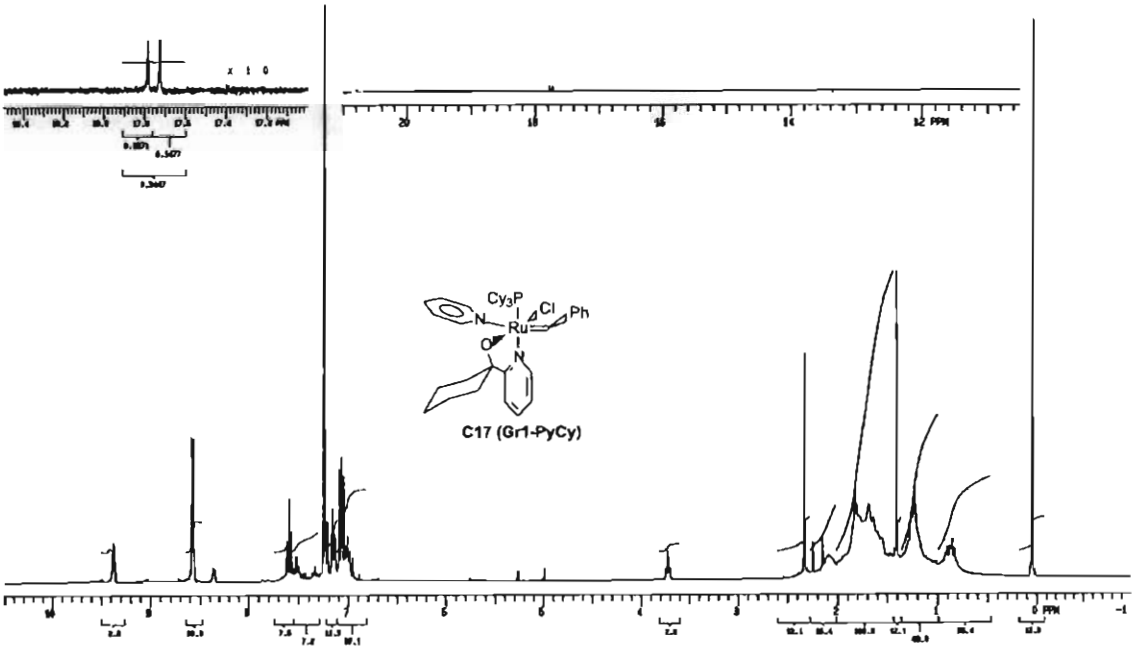

Spectrum C.37 ^{1}H NMR spectrum of benzylidene-chloro(tricyclohexylphosphine)pyridine-[1-(2'-pyridinyl)cyclohexan-1-olato]ruthenium.

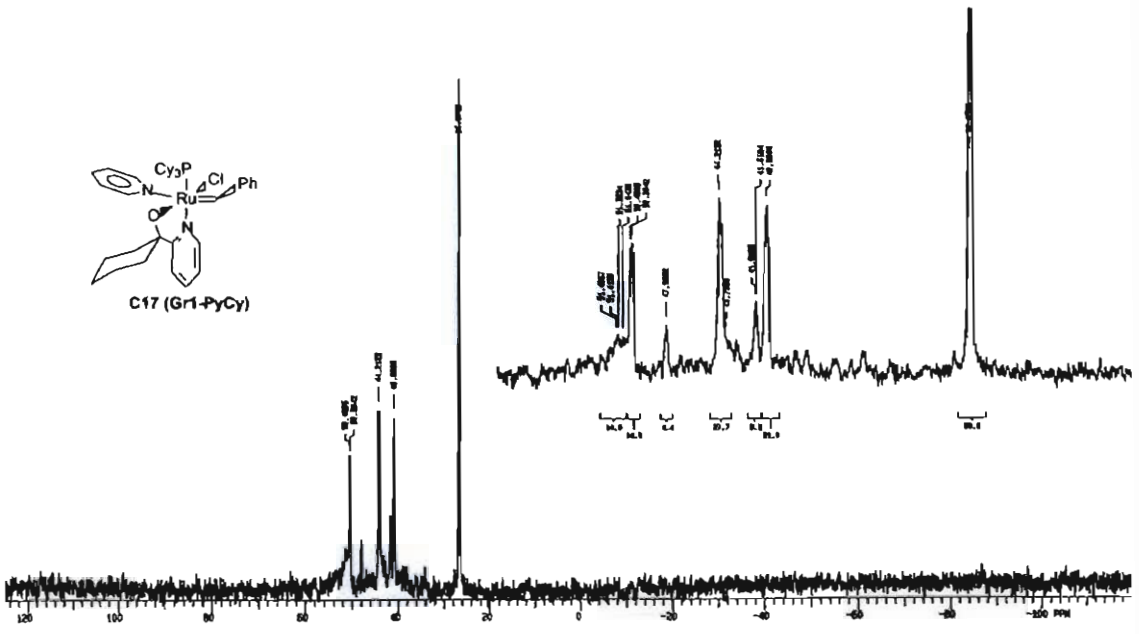

Spectrum C.38 ^{31}P NMR spectrum of benzylidene-chloro(tricyclohexylphosphine)pyridine-[1-(2'-pyridinyl)cyclohexan-1-olato]ruthenium.

^{1}H, ^{31}P and COSY NMR of the successfully synthesised second generation O,N-chelated complexes:

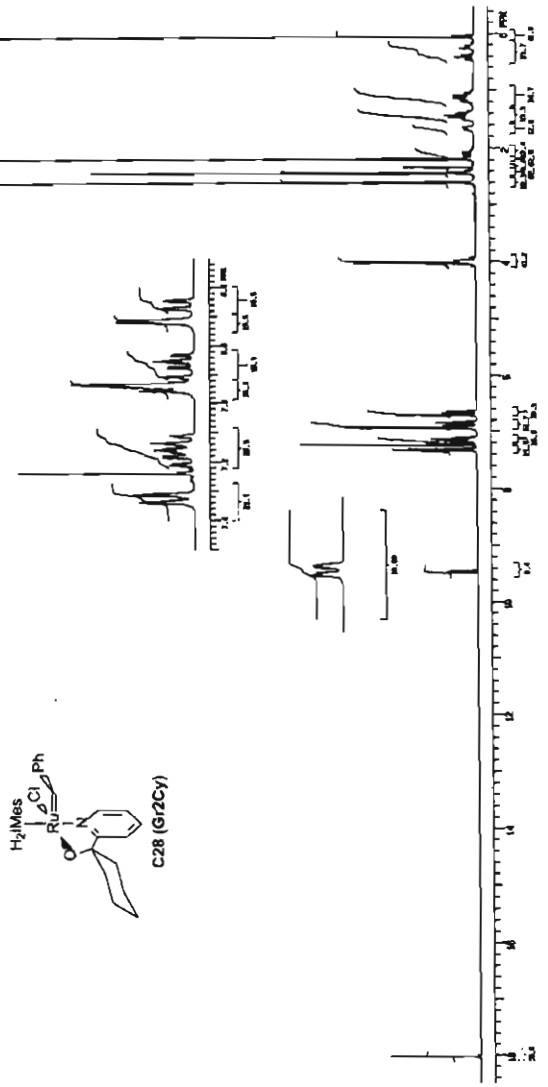

Spectrum C.39 ^{1}H NMR spectrum of benzylidene-chloro(1,3-bis-(2,4,6-trimethylphenyl)-2-imidazolidinylidene)-[1-(2'-pyridinyl)cyclohexan-1-olato]ruthenium.

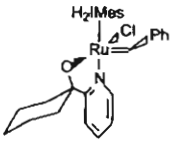

C28 (Gr2Cy)

Spectrum C.40 ^{31}P NMR spectrum of benzylidene-chloro(1,3-bis-(2,4,6-trimethylphenyl)-2-imidazolidinylidene)-[1-(2'-pyridinyl)cyclohexan-1-olato]ruthenium.

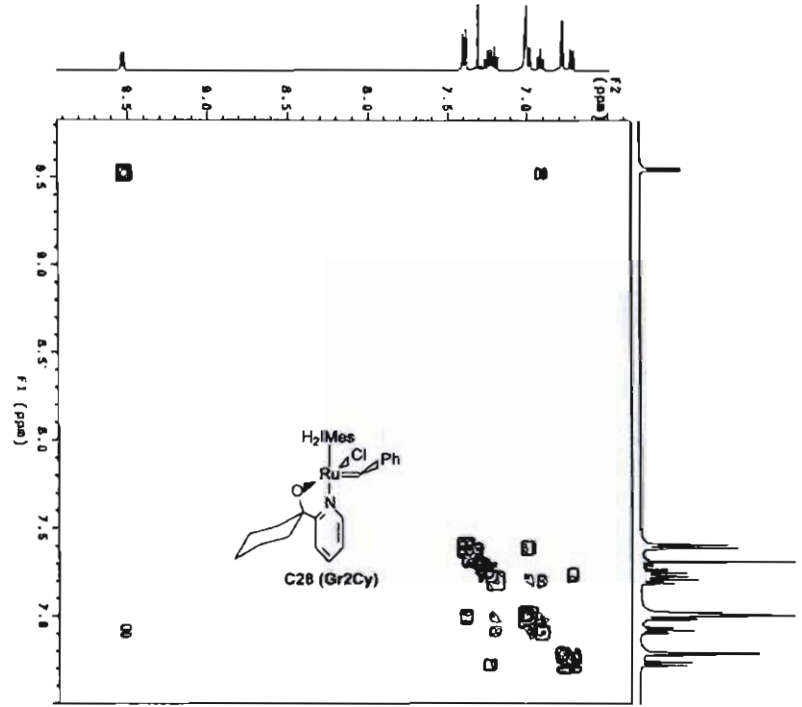

Spectrum C.41 COSY NMR spectrum of benzylidene-chloro(1,3-bis-(2,4,6-trimethylphenyl)-2-imidazolidinylidene)-[1-(2'-pyridinyl)cyclohexan-1-olato]ruthenium.

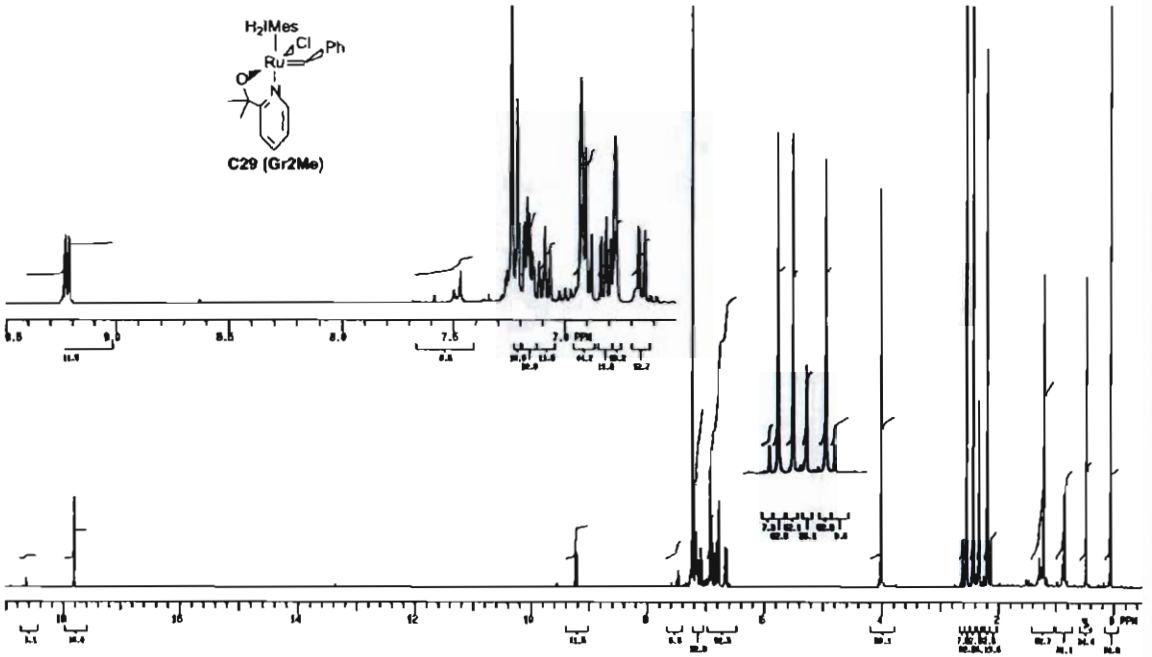

Spectrum C.42 ^{1}H NMR spectrum of benzylidene-chloro(1,3-bis-(2,4,6-trimethylphenyl)-2-imidazolidinylidene)-[1-(2'-pyridinyl)propan-2-olato]ruthenium.

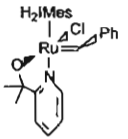

C29 (Gr2Me)

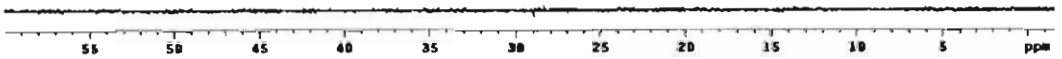

Spectrum C.43 ^{31}P NMR spectrum of benzylidene-chloro(1,3-bis-(2,4,6-trimethylphenyl)-2-imidazolidinylidene)-{1-(2'-pyridinyl)propan-2-olato}ruthenium.

Spectrum C.44 COSY NMR spectrum of benzylidene-chloro(1,3-bis-(2,4,6-trimethylphenyl)-2-imidazolidinylidene)-[1-(2'-pyridinyl)propan-2-olato]ruthenium.

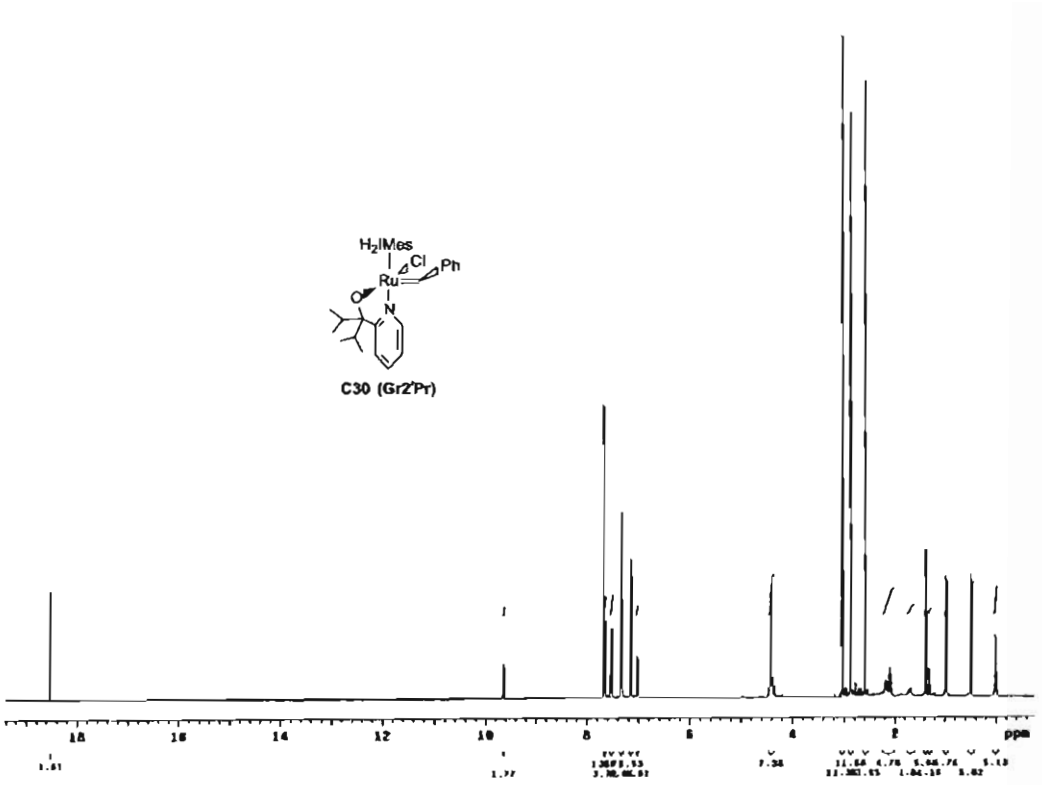

Spectrum C.45 ^{1}H NMR of benzylidene-chloro(1,3-bis-(2,4,6-trimethylphenyl)-2-imidazolidinylidene)-[1-(2'-pyridinyl)-2,4-dimethylpentan-3-olato]ruthenium.

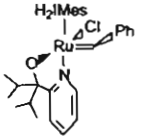

C30 (Gr2ⁱPr)

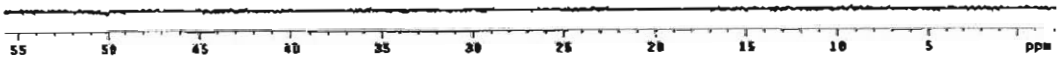

Spectrum C.46 ^{31}P NMR of benzylidene-chloro(1,3-bis-(2,4,6-trimethylphenyl)-2-imidazolidinylidene)-[1-(2'-pyridinyl)-2,4-dimethylpentan-3-olato]ruthenium.

Spectrum C.47 COSY NMR of benzylidene-chloro(1,3-bis-(2,4,6-trimethylphenyl)-2-imidazolidinylidene)-[1-(2'-pyridinyl)-2,4-dimethylpentan-3-olato]ruthenium.

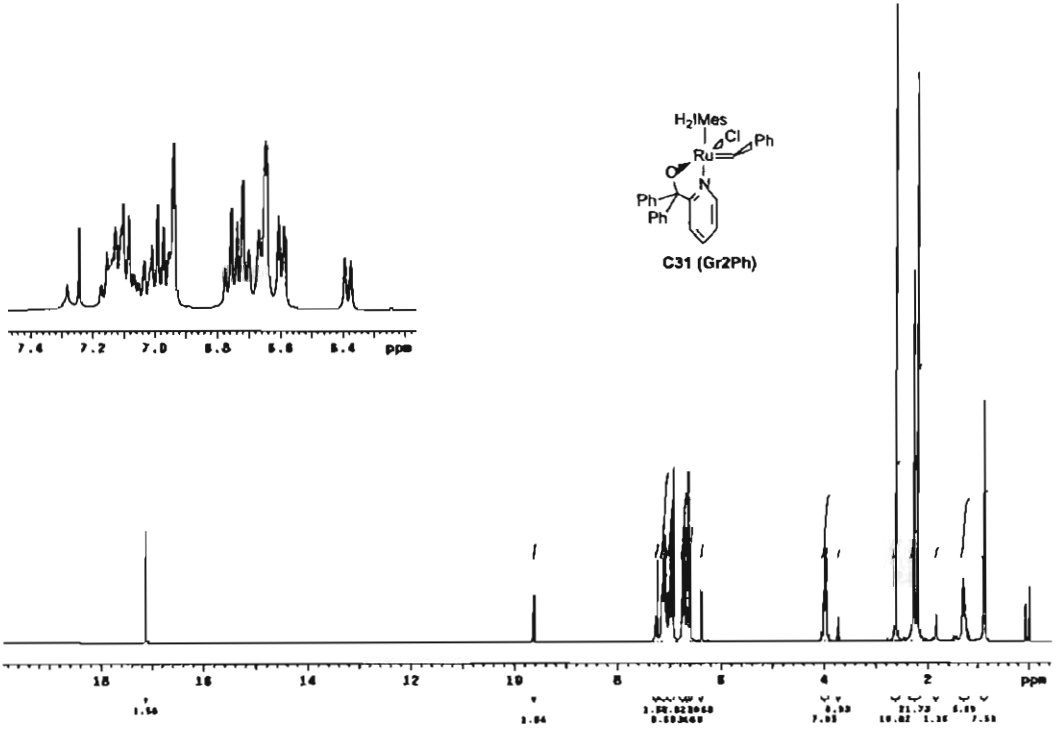

Spectrum C.48 ^{1}H NMR of benzylidene-chloro(1,3-bis-(2,4,6-trimethylphenyl)-2-imidazolidinylidene)-[1-(2'-pyridinyl)-1,1-diphenyl-methanolato]ruthenium.

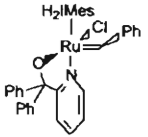

C31 (Gr2Ph)

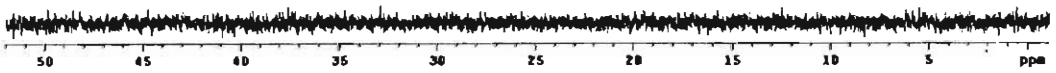

Spectrum C.49 ^{31}P NMR of benzylidene-chloro(1,3-bis-(2,4,6-trimethylphenyl)-2-imidazolidinylidene)-[1-(2'-pyridinyl)-1,1-diphenyl-methanolato]ruthenium.

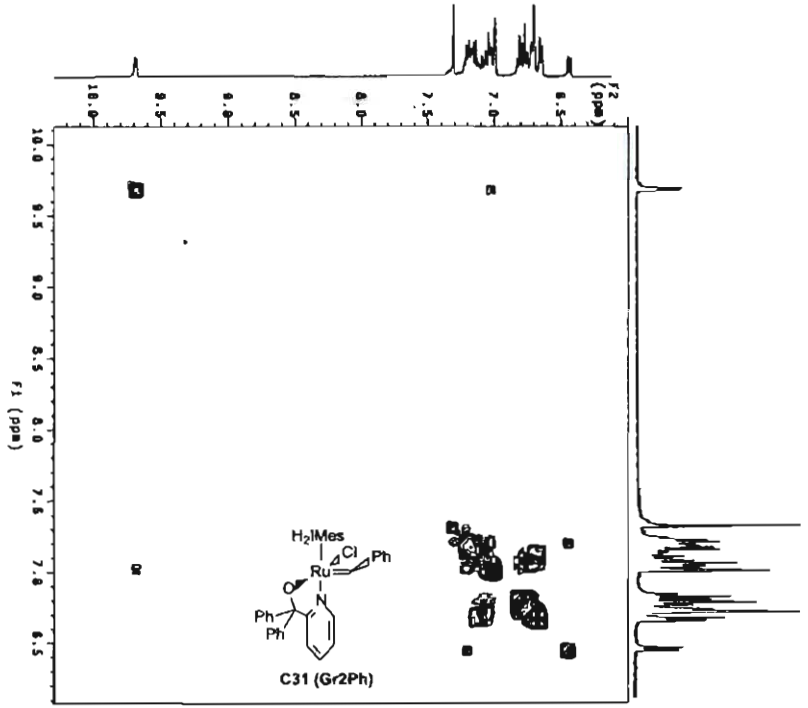

Spectrum C.50 COSY NMR of benzylidene-chloro(1,3-bis-(2,4,6-trimethylphenyl)-2-imidazolidinylidene)-[1-(2'-pyridinyl)-1,1-diphenyl-methanolato]ruthenium.

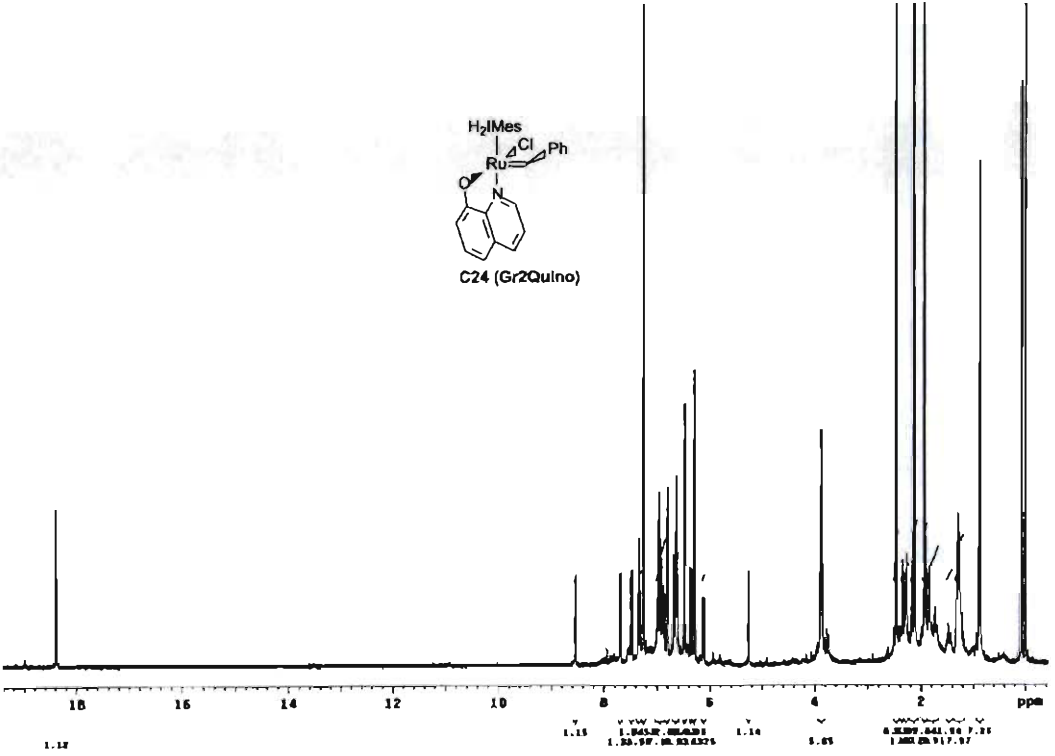

Spectrum C.51 ^{1}H NMR of benzylidene-chloro(1,3-bis-(2,4,6-trimethylphenyl)-2-imidazolidinylidene)-[8-quinolinolate]ruthenium.

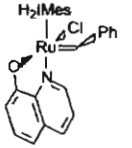

C24 (Gr2Quino)

Spectrum C.52 ^{31}P NMR of benzylidene-chloro(1,3-bis-(2,4,6-trimethylphenyl)-2-imidazolidinylidene)-[8-quinolinolate]ruthenium.

Spectrum C.53 COSY NMR of benzylidene-chloro(1,3-bis-(2,4,6-trimethylphenyl)-2-imidazolidinylidene)-[8-quinolinolate]ruthenium.

^{1}H and ^{31}P NMR-spectra of the reactions of pyca with Gr1, Gr2 and Gr1-Py:

Spectrum C.54 ^{1}H NMR of benzylidene-chloro(tricyclohexylphosphine)pyridine-[pridine-2-carboxylato]ruthenium after reaction of Gr1 with the Tl-salt of pyca.

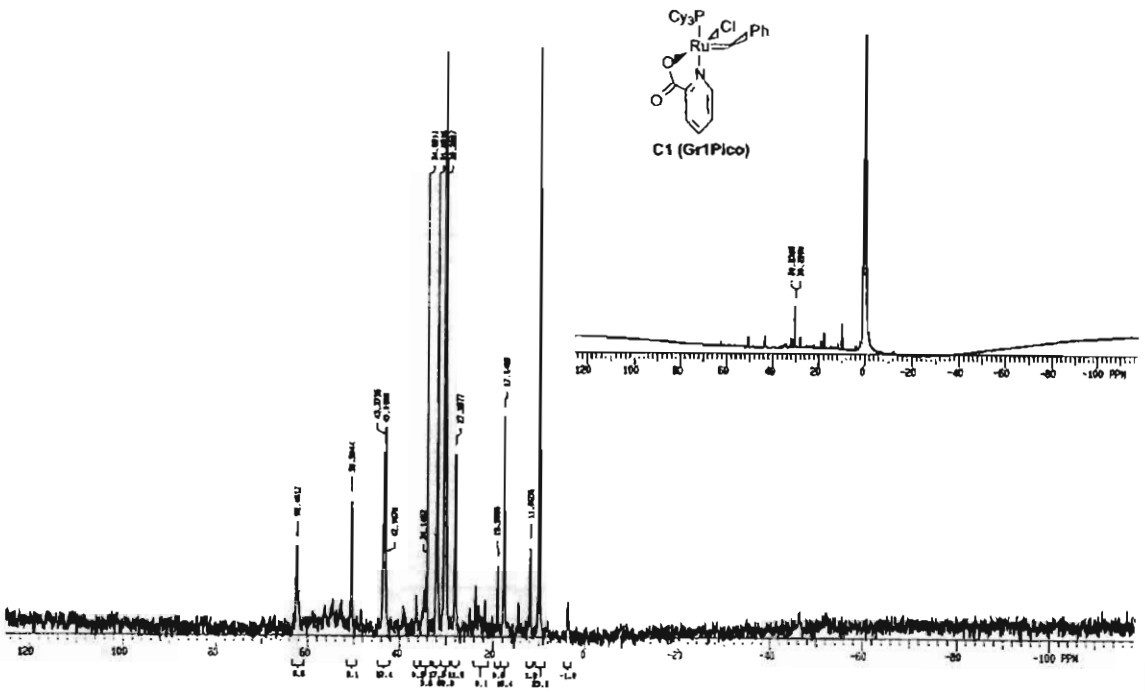

Spectrum C.55 ^{31}P NMR of benzylidene-chloro(tricyclohexylphosphine)pyridine-[pridine-2-carboxylato]ruthenium after reaction of Gr1 with the Tl-salt of pyca.

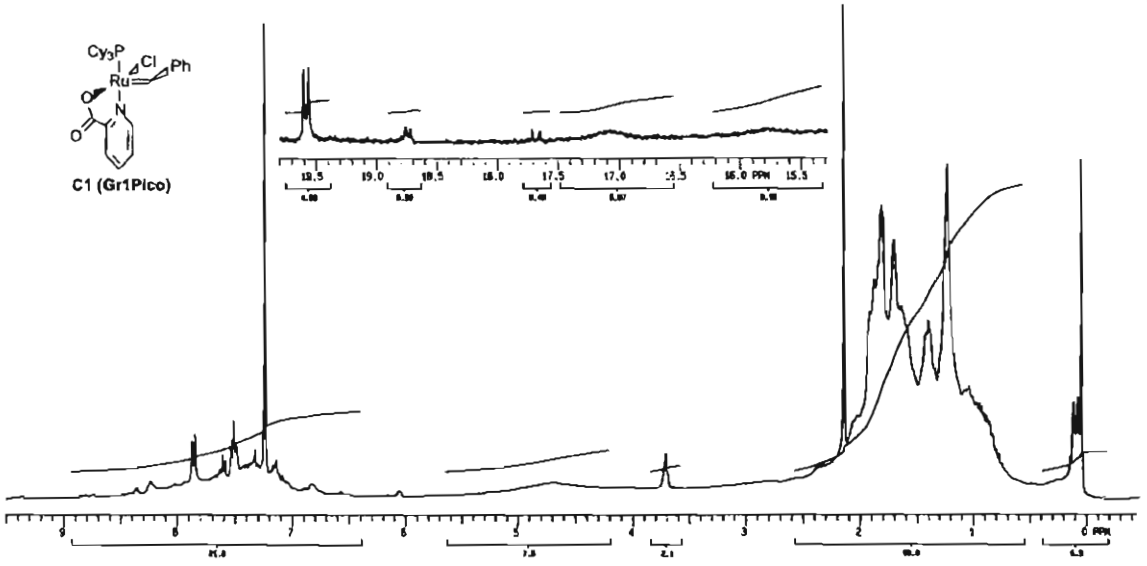

Spectrum C.56 ^{1}H NMR of benzylidene-chloro(tricyclohexylphosphine)pyridine-[pridine-2-carboxylato]ruthenium after reaction of **Gr1** with the Li-salt of pyca.

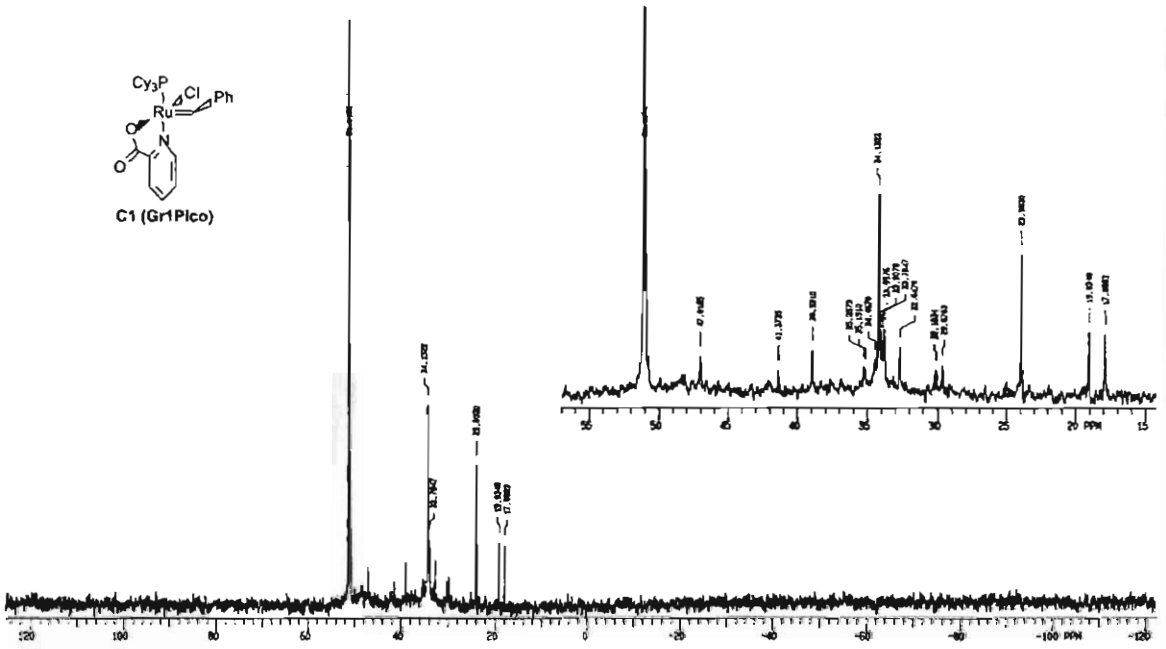

Spectrum C.47 ^{31}P NMR of benzylidene-chloro(tricyclohexylphosphine)pyridine-[pridine-2-carboxylato]ruthenium after reaction of **Gr1** with the Li-salt of pyca.

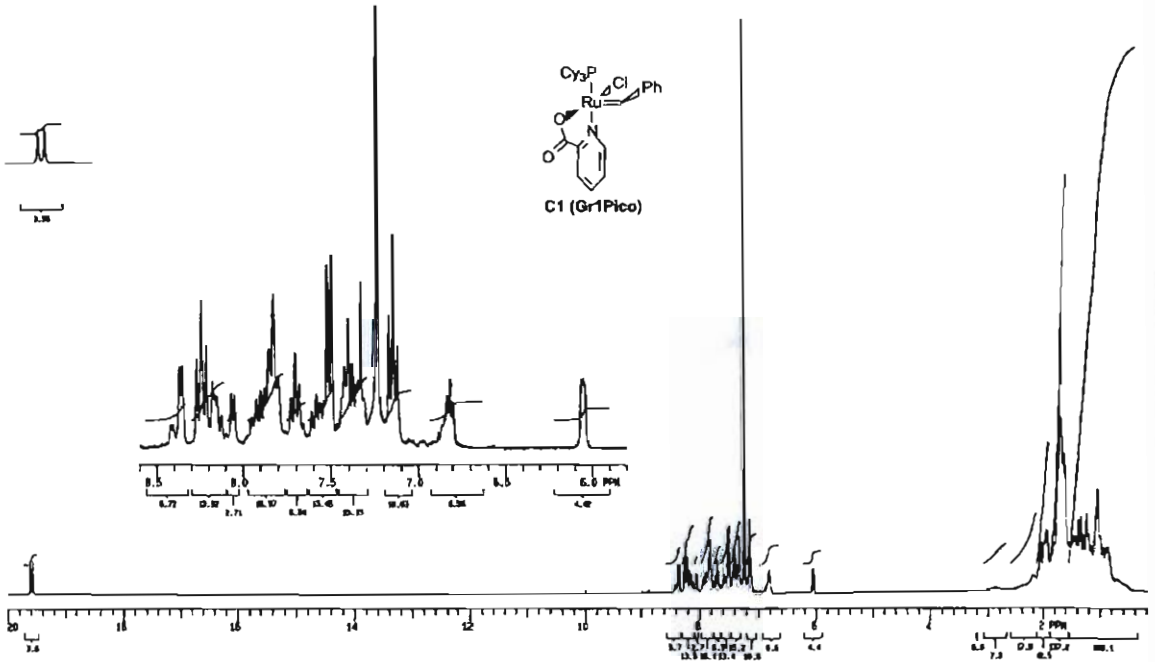

Spectrum C.58 ^{1}H NMR of benzylidene-chloro(tricyclohexylphosphine)pyridine-[pridine-2-carboxylato]ruthenium after reaction of **Gr1** with the Na-salt of pyca.

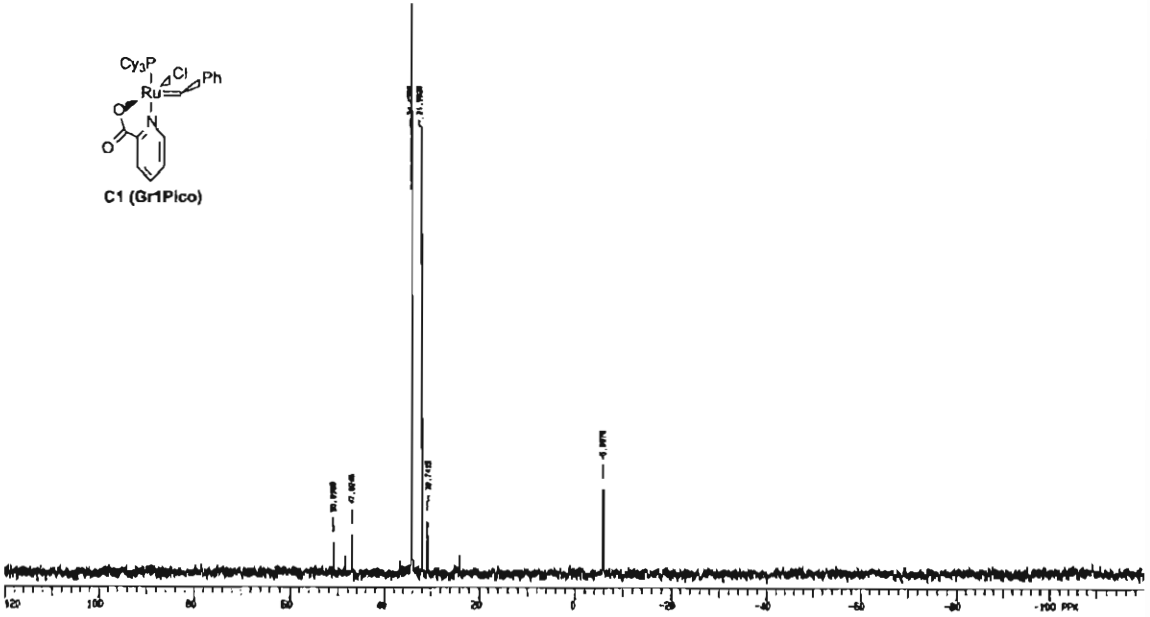

Spectrum C.59 ^{31}P NMR of benzylidene-chloro(tricyclohexylphosphine)pyridine-[pridine-2-carboxylato]ruthenium after reaction of **Gr1** with the Na-salt of pyca.

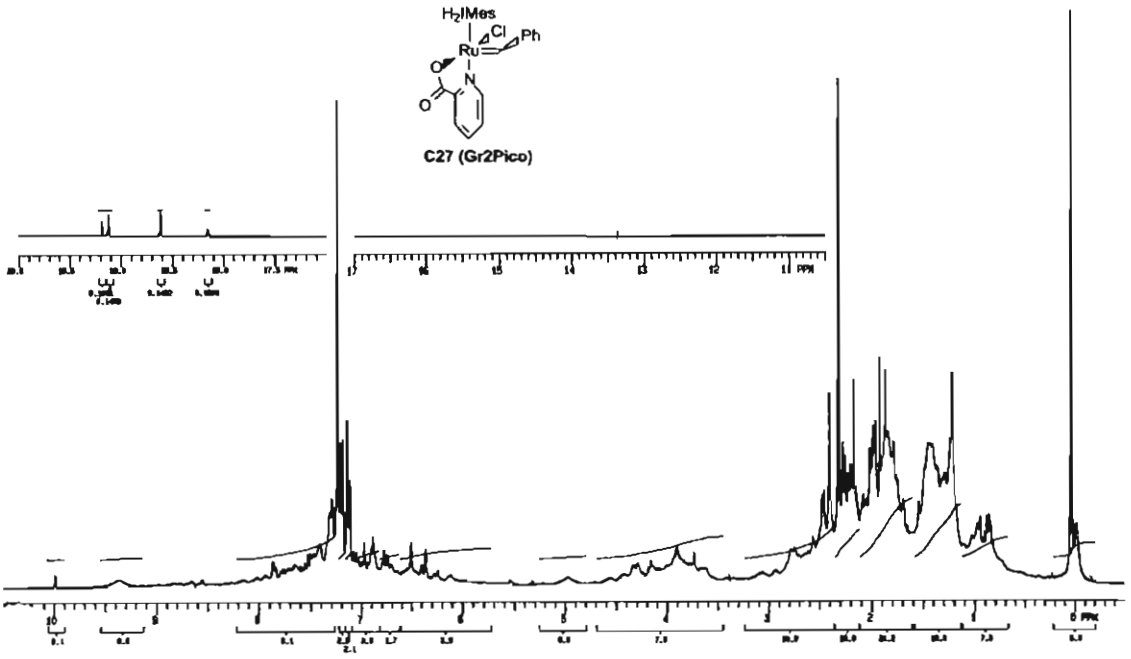

Spectrum C.60 ^{1}H NMR of benzylidene-chloro(1,3-bis-(2,4,6-trimethylphenyl)-2-imidazolidinylidene)-(2-pyridinecarboxy-lato)-ruthenium after reaction of **Gr2** with the Tl-salt of pyca.

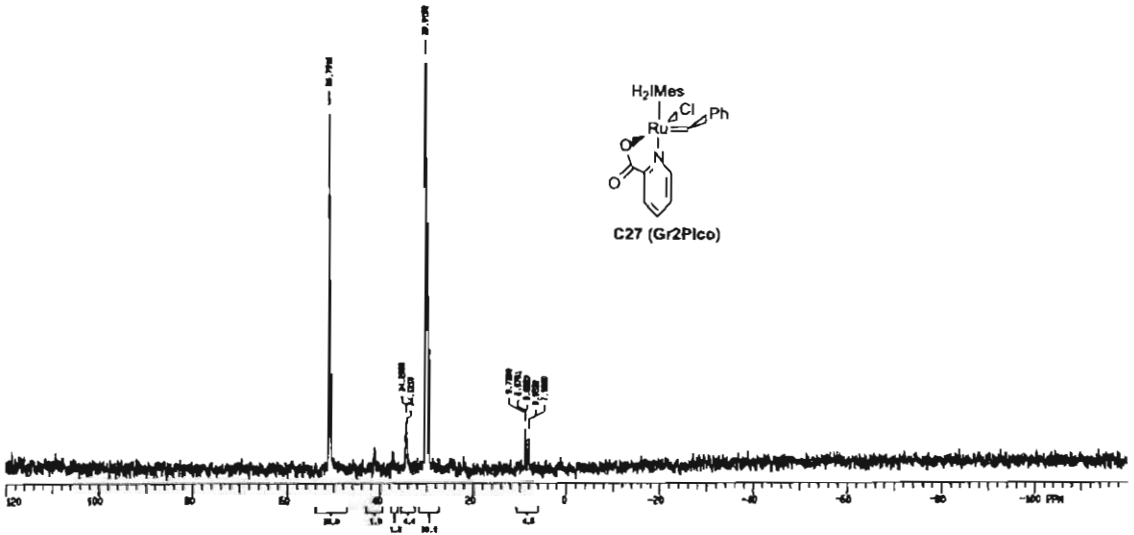

Spectrum C.61 ^{31}P NMR of benzylidene-chloro(1,3-bis-(2,4,6-trimethylphenyl)-2-imidazolidinylidene)-(2-pyridinecarboxy-lato)-ruthenium after reaction of **Gr2** with the Tl-salt of pyca.

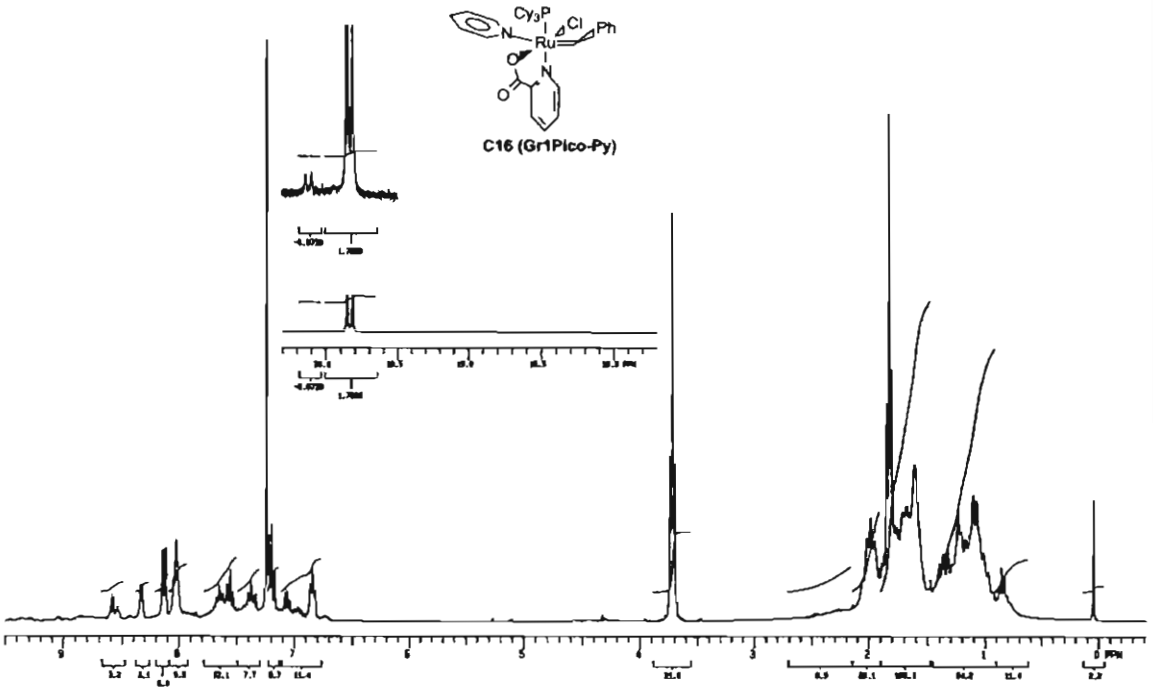

Spectrum C.62 ^{1}H NMR of benzylidene-chloro(tricyclohexylphosphine)pyridine-[pridine-2-carboxylato]ruthenium after reaction of **Gr1-Py** with the Li-salt of pyca.

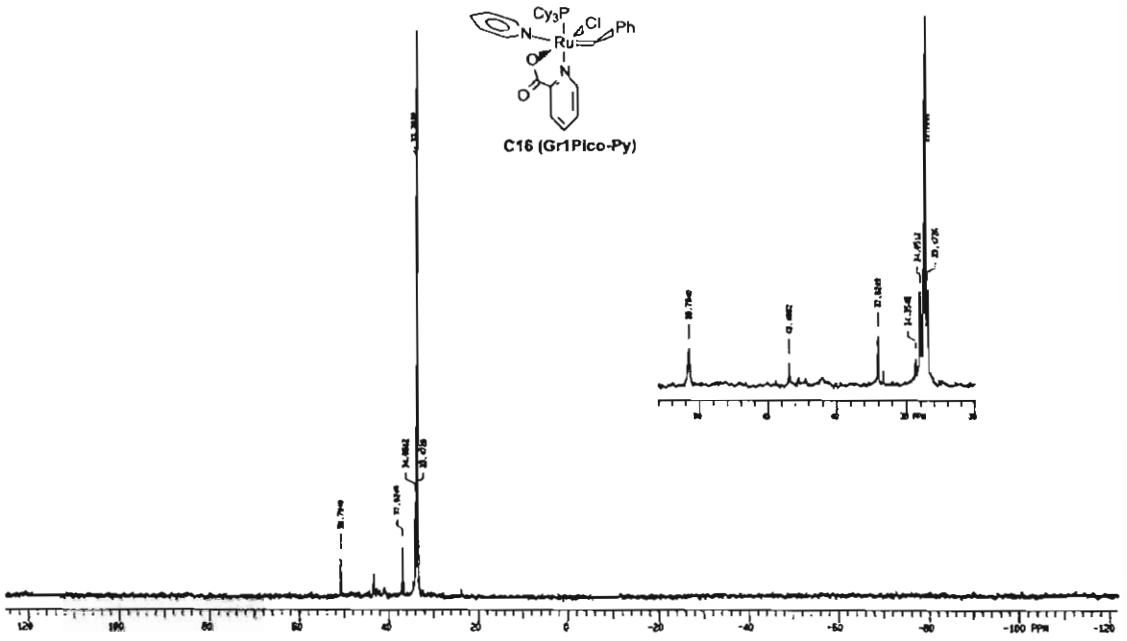

Spectrum C.63 ^{31}P NMR of benzylidene-chloro(tricyclohexylphosphine)pyridine-[pridine-2-carboxylato]ruthenium after reaction of Gr1-Py with the Li-salt of pyca.

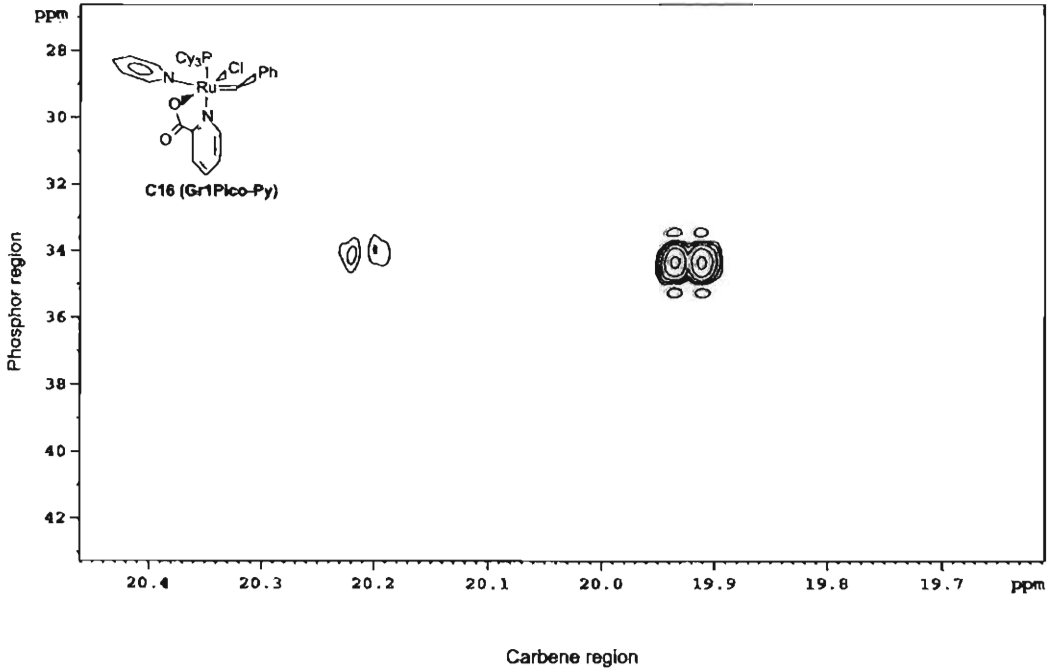

Spectrum C.64 P-H NMR correlation spectrum of benzylidene-chloro(tricyclohexylphosphine)pyridine-[pridine-2-carboxylato]ruthenium after reaction of **Gr1-Py** with the Li-salt of pyca.

Appendix C2

^{1}H and ^{31}P NMR spectra of the unsuccessfully synthesised complexes are displayed below to illustrate that the reaction mixtures either contained unreacted starting materials or decomposition products. Only the known decomposition products of **Gr1** and **Gr2** (**Table C.1**) could be identified with any certainty.

Table C.1 Assignment of ^{31}P NMR signals of known decomposition products of **Gr1** and **Gr2**.[22,23]

^{31}P-signal/ppm	Assignment
50.457	$O=PCy_3$
11.260	Free PCy_3
24 – 26	$[Ru(PCy_3)_2ClPhCO]$
47 – 48	$[Ru(PCy_3)_2ClHCO]$
22 – 23	$[Ru(PCy_3)(H_2IMes)ClPhCO]$
46 – 47	$[Ru(PCy_3)(H_2IMes)ClHCO]$

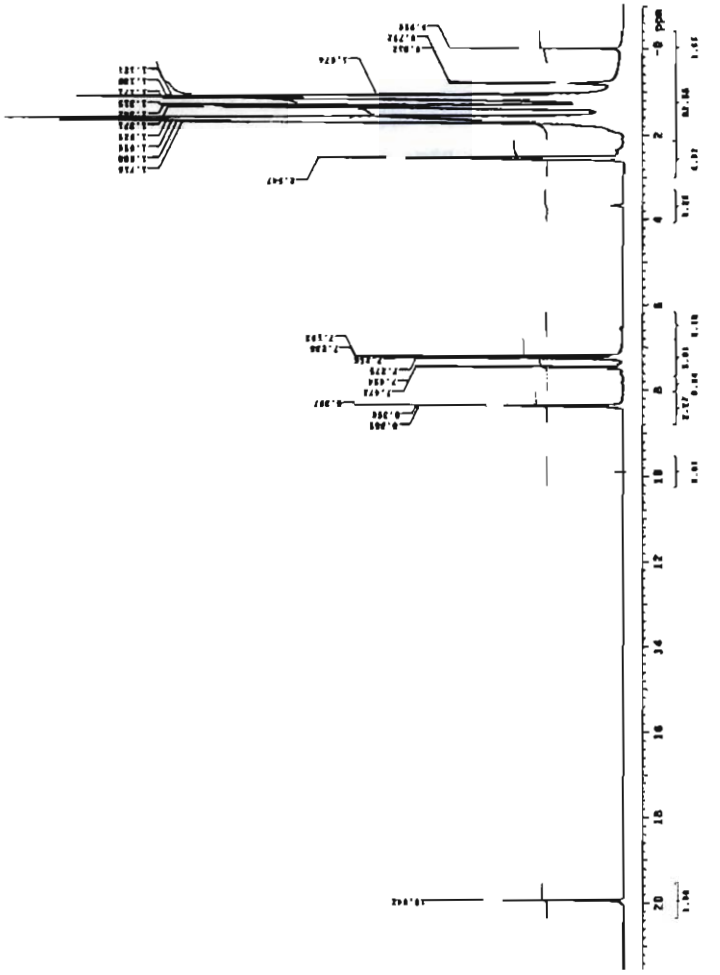

Spectrum C.65 ^{1}H NMR spectrum obtained after reacting **Gr1** with the Li-salt of furoic acid (**L12**) to synthesise **C3**.

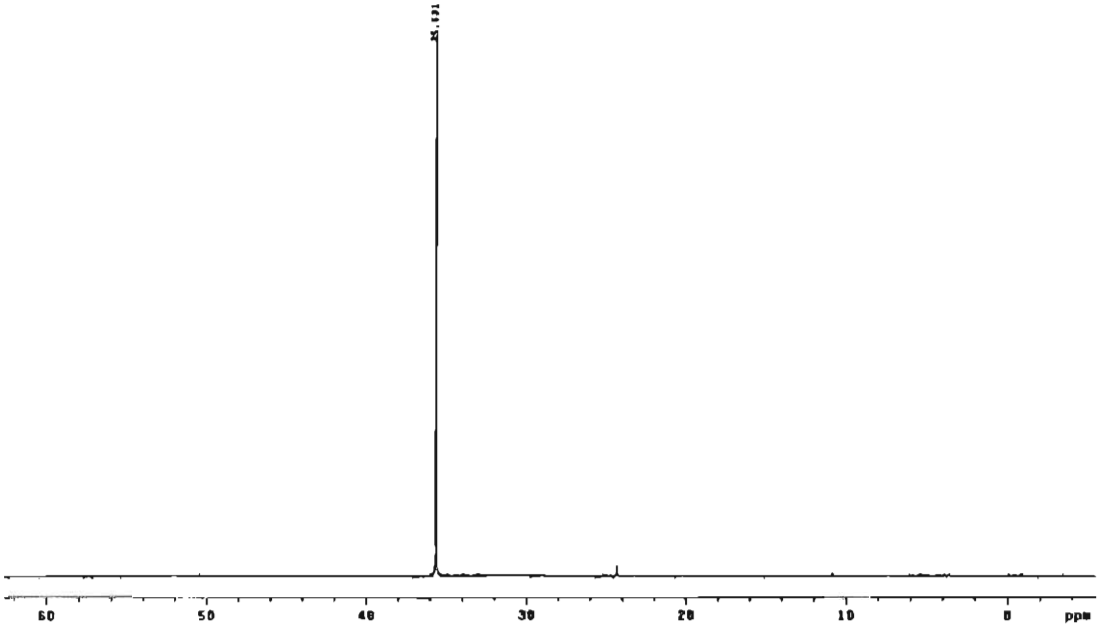

Spectrum C.66 ^{31}P NMR spectrum obtained after reacting Gr1 with the Li-salt of furoic acid (L12) to synthesise C3.

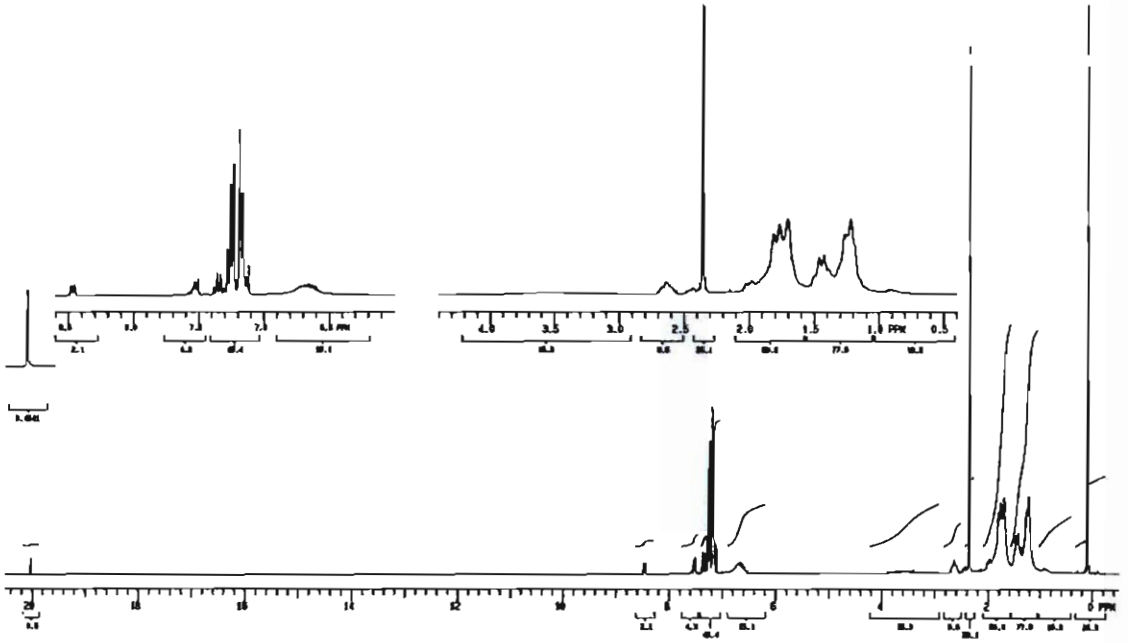

Spectrum C.67 ^{1}H NMR spectrum obtained after reacting **Gr1** with the Li-salt of **L10** to synthesise **C4**.

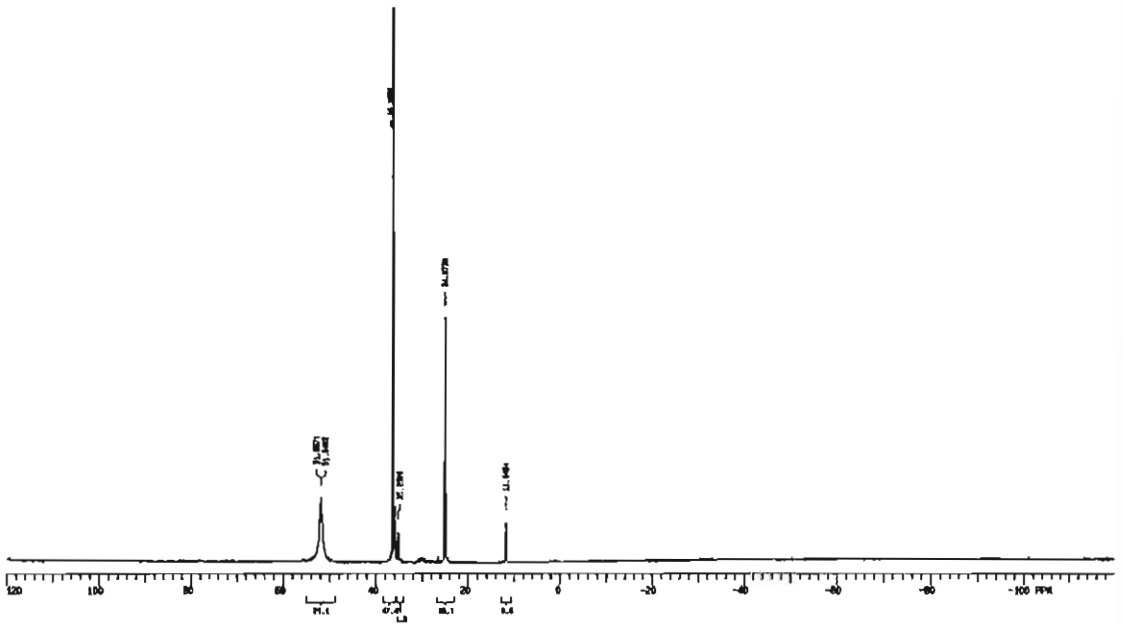

Spectrum C.68 ^{31}P NMR spectrum obtained after reacting **Gr1** with the Li-salt of **L10** to synthesise **C4**.

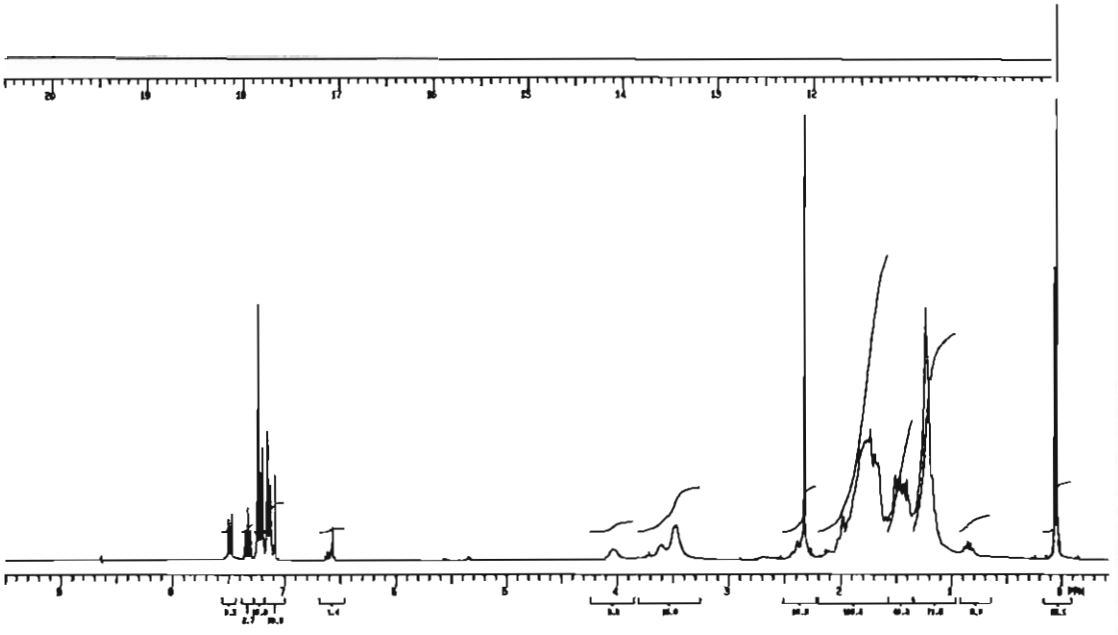

Spectrum C.69 ^{1}H NMR spectrum obtained after reacting **Gr1** with the Li-salt of **L9** to synthesise **C5**.

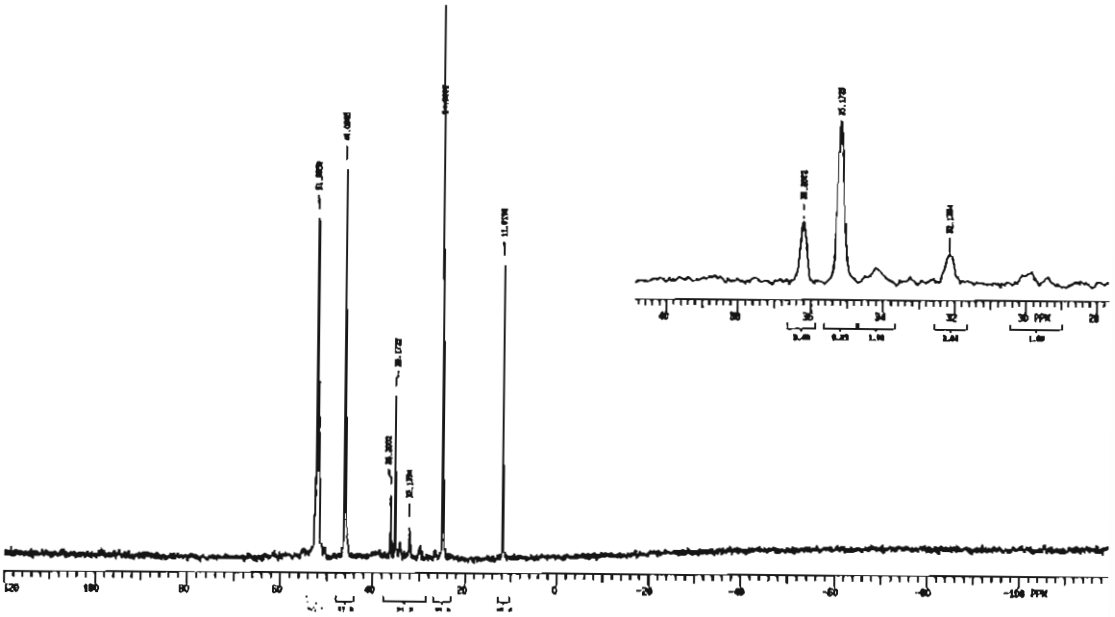

Spectrum C.70 ^{31}P NMR spectrum obtained after reacting **Gr1** with the Li-salt of **L9** to synthesise **C5**.

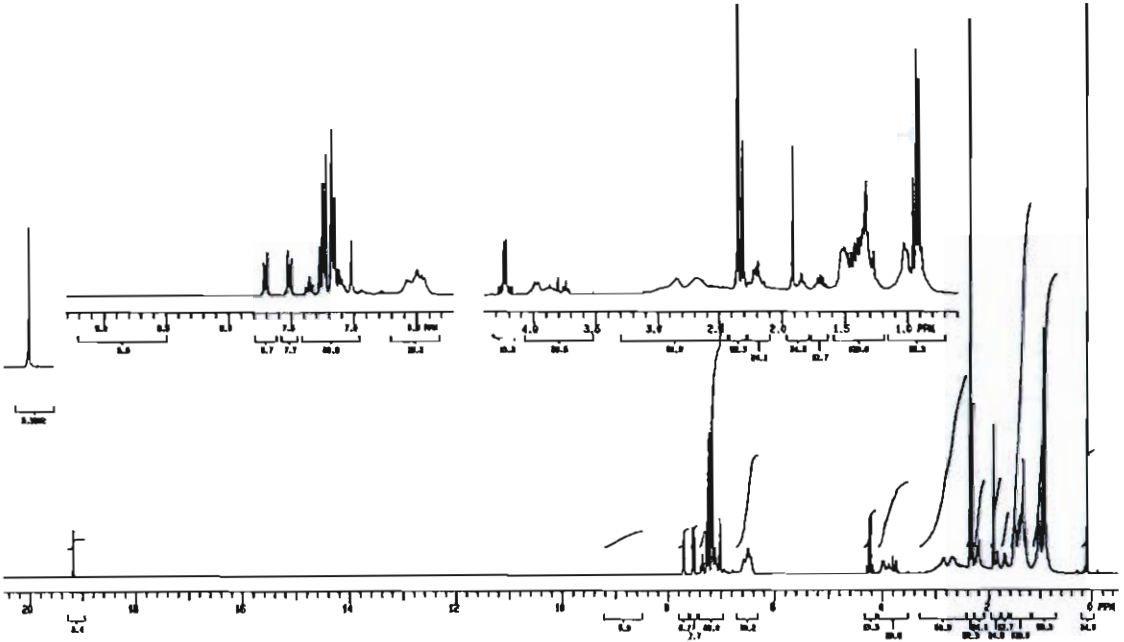

Spectrum C.71 ^{1}H NMR spectrum obtained after reacting **Gr2** with the Li-salt of **L10** to synthesise **C26**.

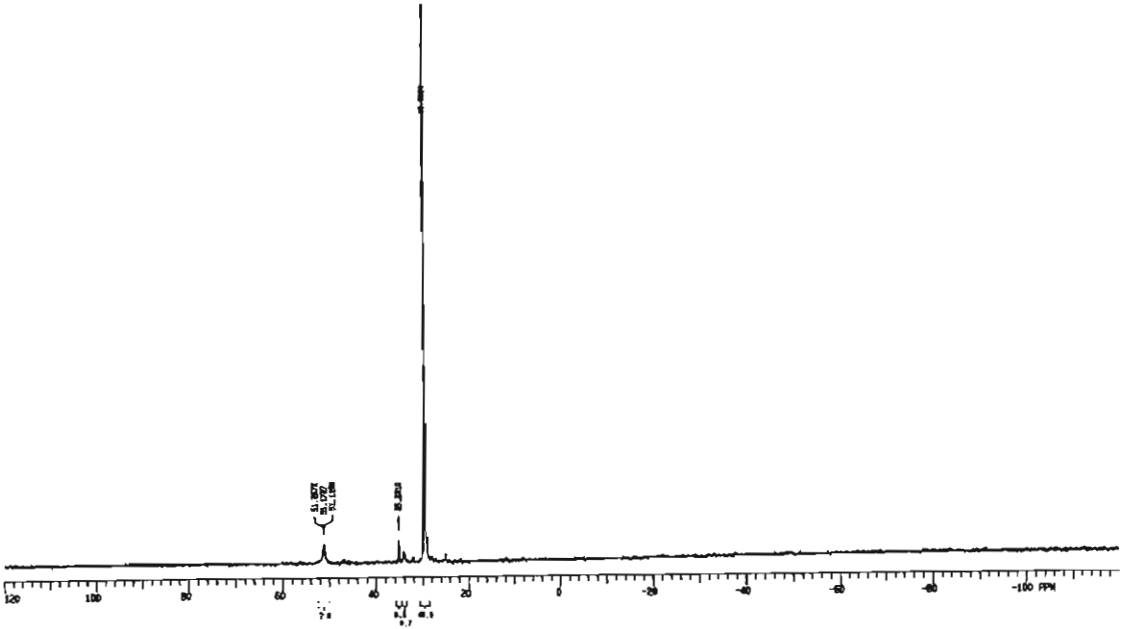

Spectrum C.72 ^{31}P NMR spectrum obtained after reacting **Gr2** with the Li-salt of **L10** to synthesise **C26**.

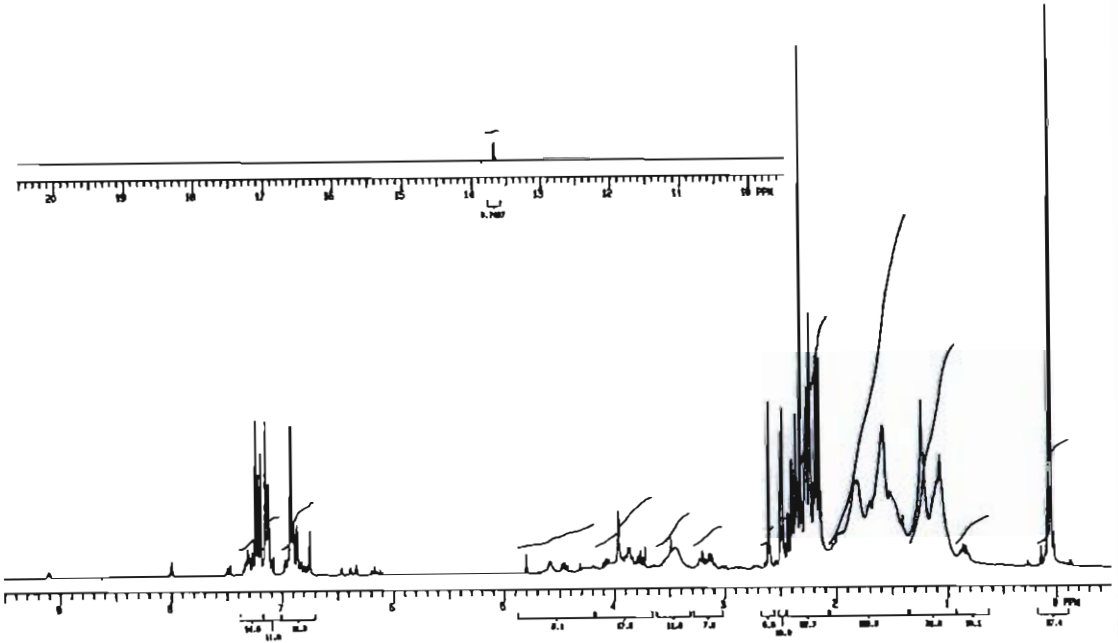

Spectrum C.73 ^{1}H NMR spectrum obtained after reacting **Gr2** with the Li-salt of **L9** to synthesise **C25**.

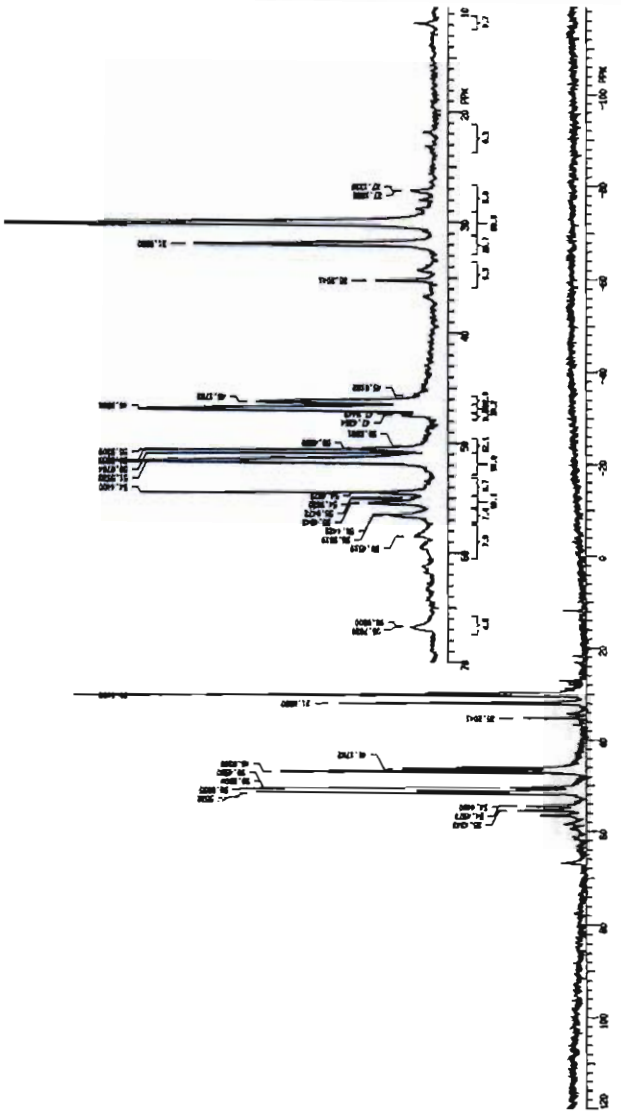

Spectrum C.74 ^{31}P NMR spectrum oblained after reacting **Gr2** with the Li-sall of **L9** to synthesise **C25**.

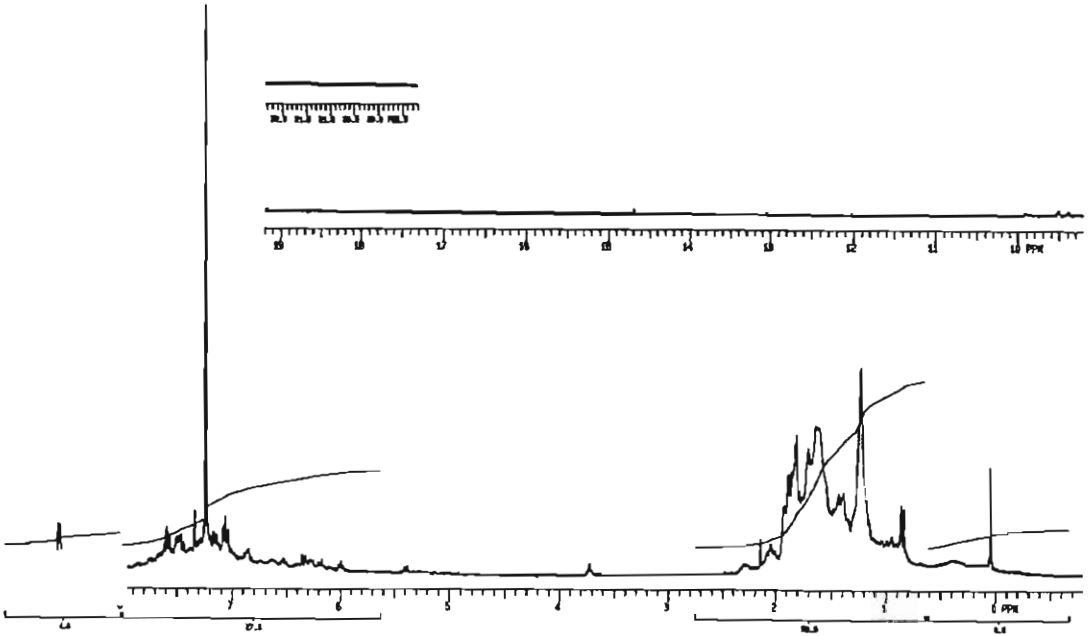

Spectrum C.75 ^{1}H NMR spectrum obtained after reacting **Gr1** with the Tf-salt of **L5** to synthesize **C14**.

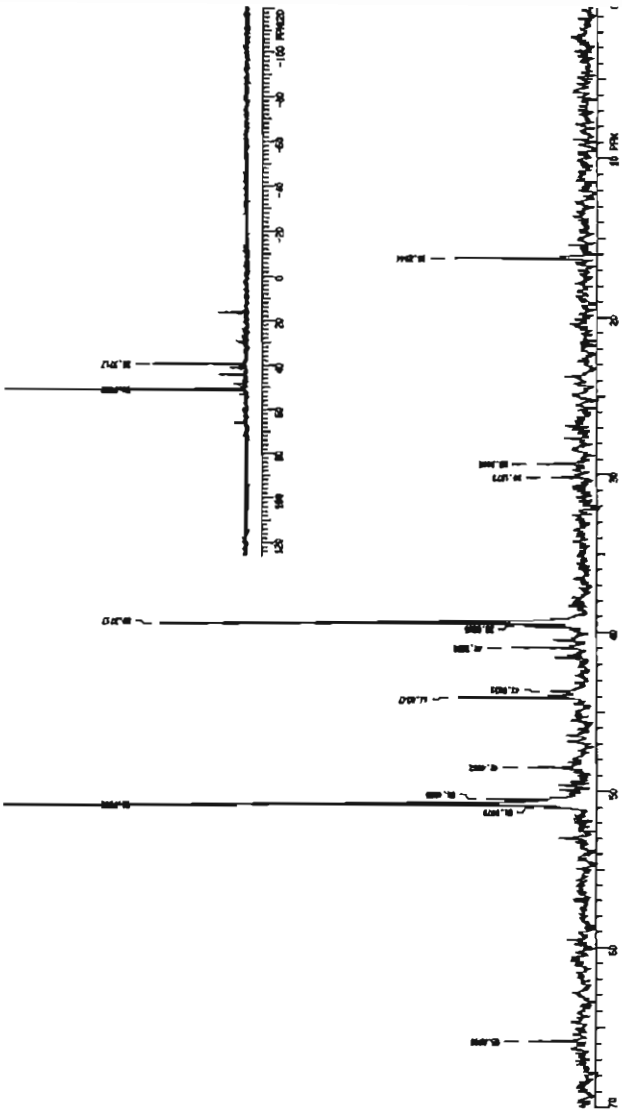

Spectrum C.76 ^{31}P NMR spectrum obtained after reacting **Gr1** with the Tl-salt of **L5** to synthesise **C14**.

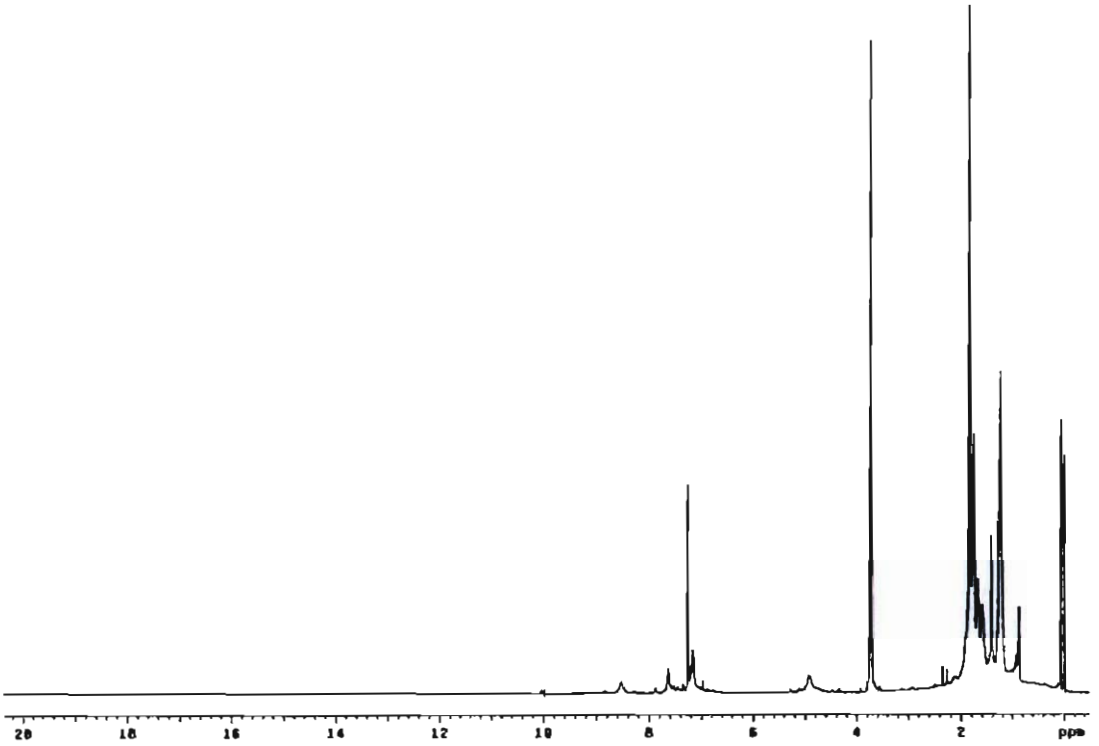

Spectrum C.77 ^{1}H NMR spectrum obtained after reacting **Gr1** with the Li-salt of **L6** to synthesise **C6**.

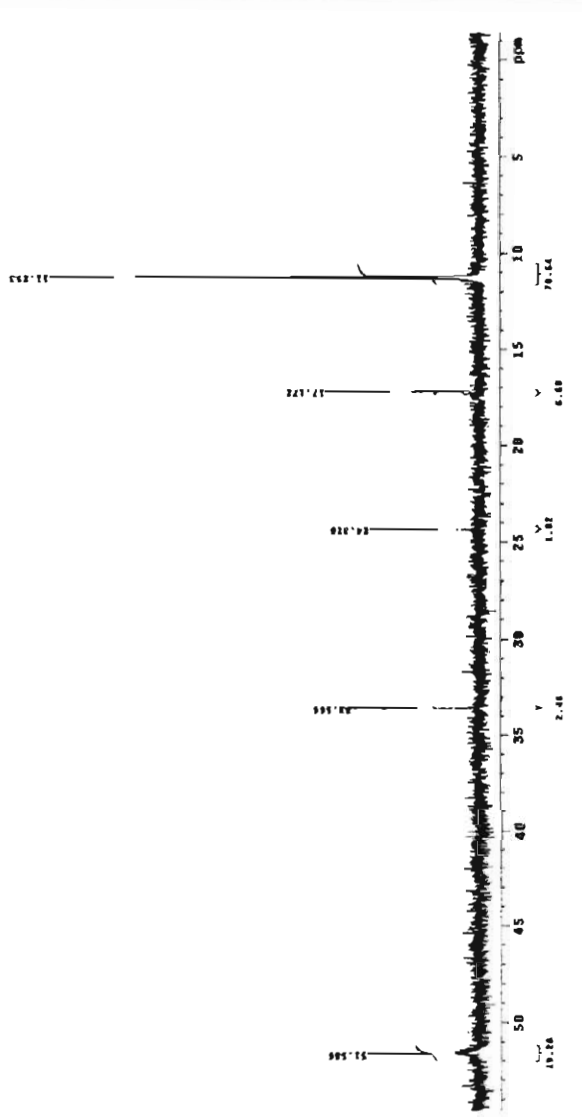

Spectrum C.78 ^{31}P NMR spectrum obtained after reacting **Gr1** with the Tl-salt of **L6** to synthesise **C6**.

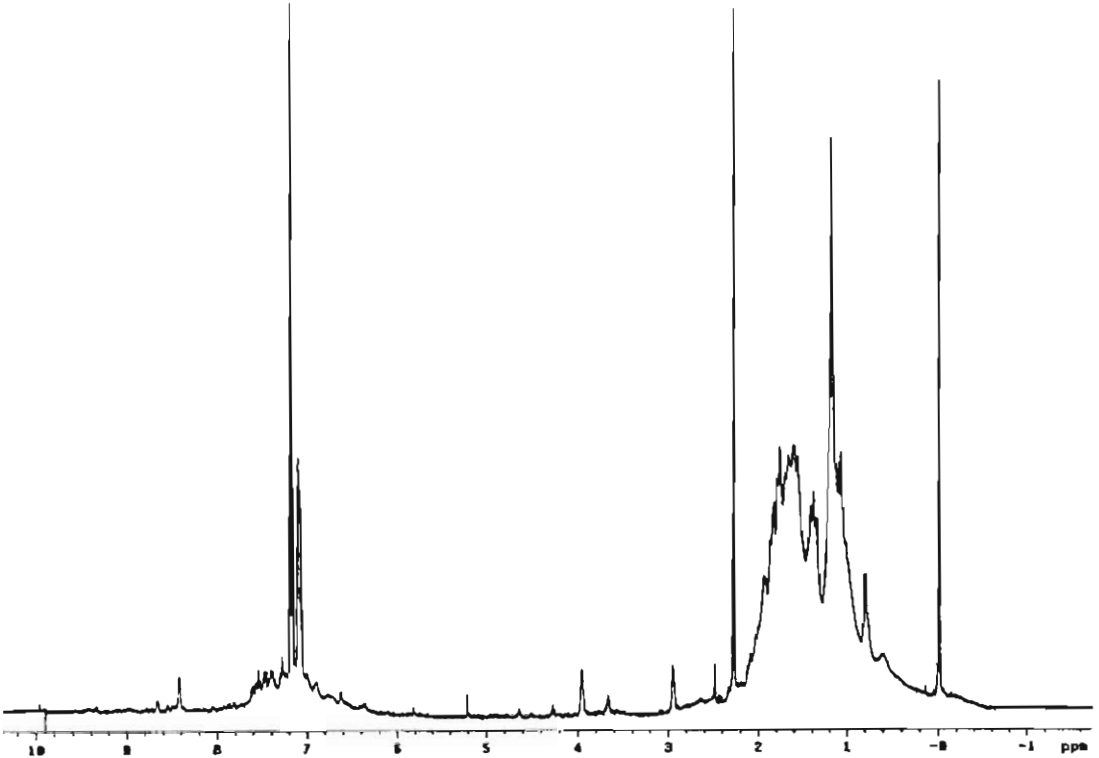

Spectrum C.79 ^{1}H NMR spectrum obtained after reacting **Gr1** with the Tl-salt of L7 to synthesise **C13**.

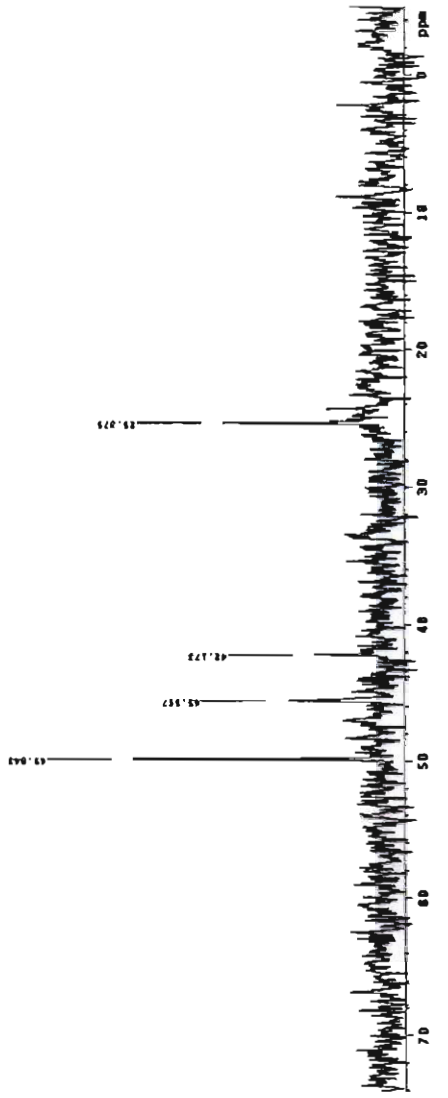

Spectrum C.80 ^{31}P NMR spectrum obtained after reacting **Gr1** with the Tl-salt of **L7** to synthesise **C13**.

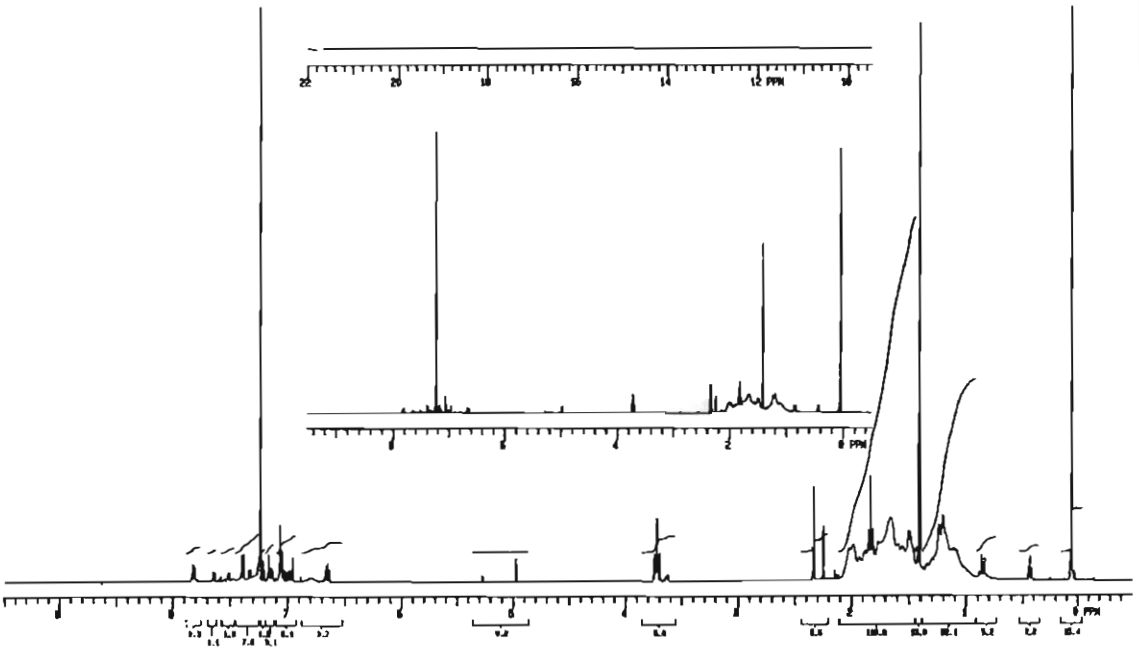

Spectrum C.81 ^{1}H NMR spectrum obtained after reacting **Gr1** with the Tl-salt of **L14** to synthesise **C2**.

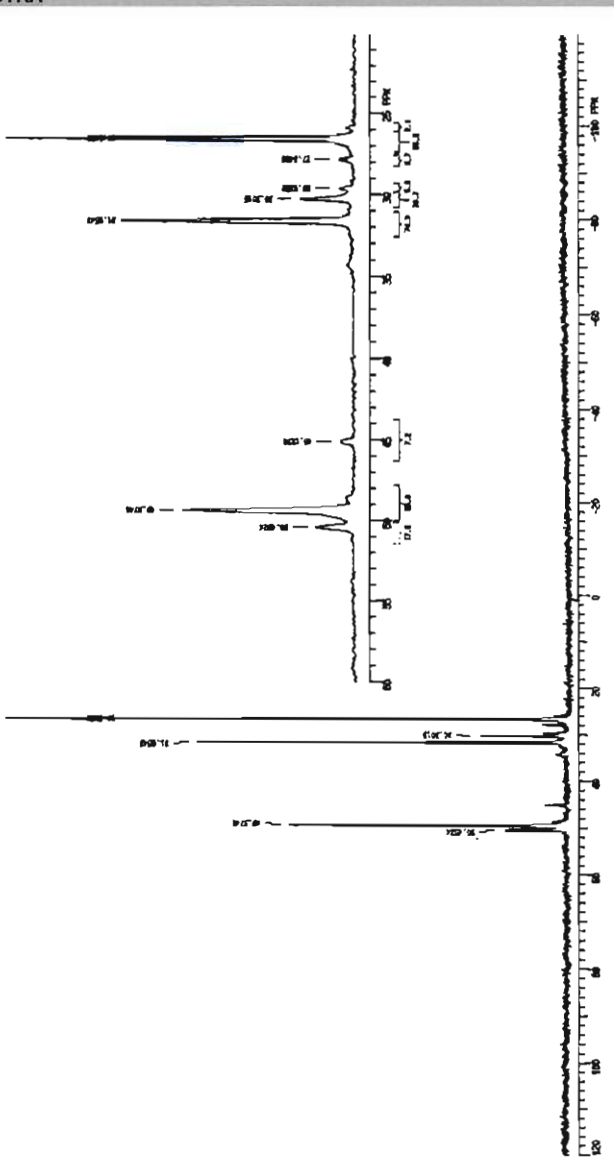

Spectrum C.82 ^{31}P NMR spectrum oblained after reacting Gr1 with the Tl-salt of **L14** to synthesise **C2**.

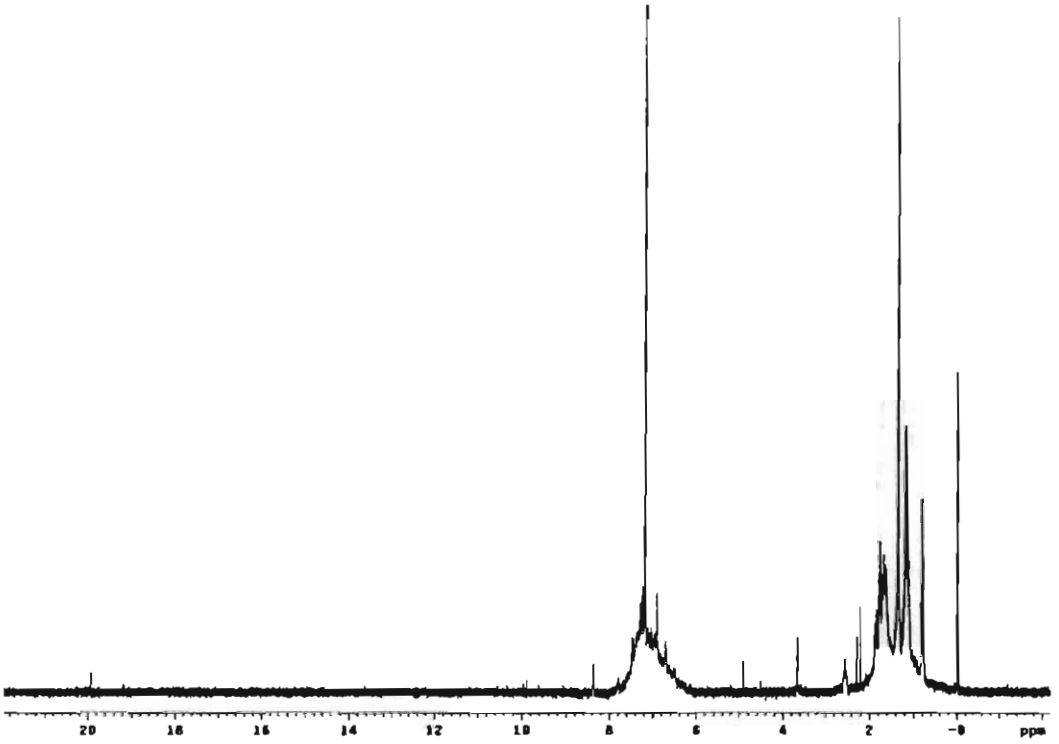

Spectrum C.83 ^{1}H NMR spectrum obtained after reacting **Gr1** with the Tl-salt of **L15** to synthesise **C12**.

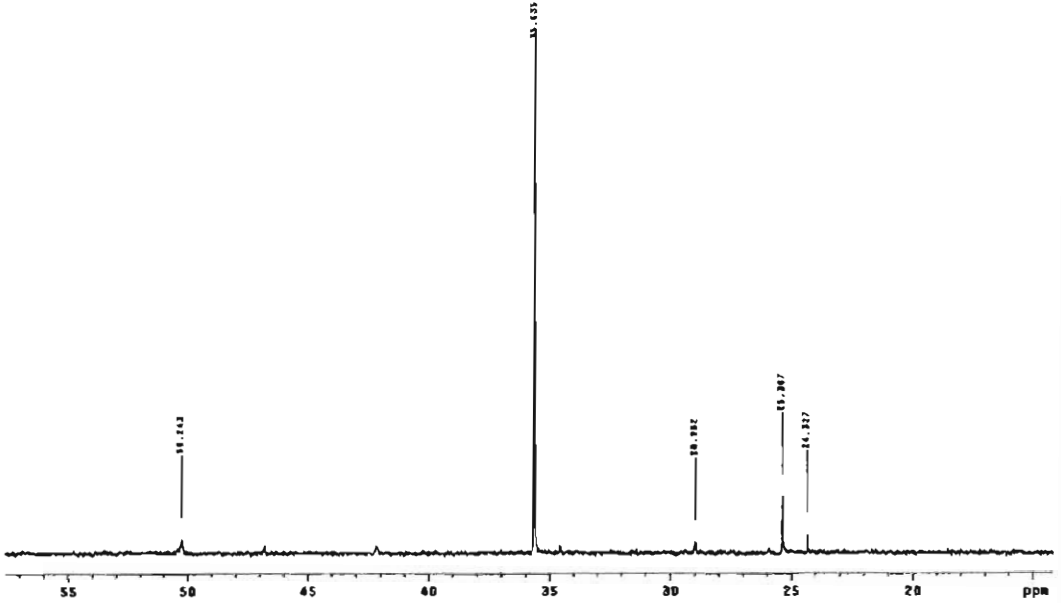

Spectrum C.84 ^{31}P NMR spectrum obtained after reacting **Gr1** with the Tl-salt of **L15** to synthesise **C12**.

Appendix C3

Appendix C3 (p. 421 – 442) is available on the enclosed CD

Appendix D

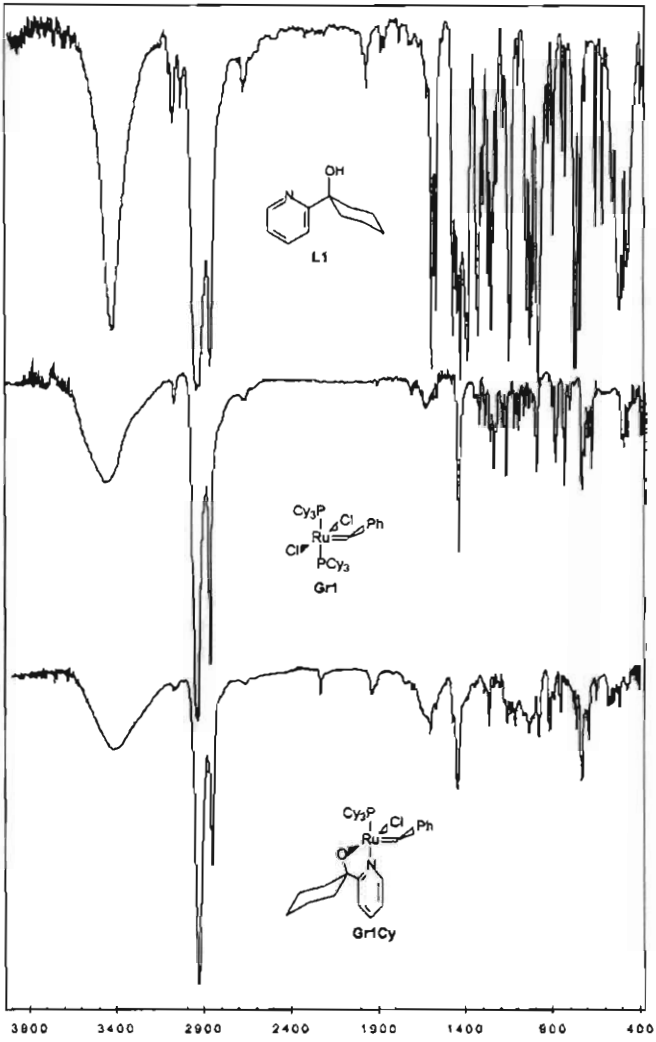

Spectrum D.1 IR-spectrum of **Gr1Cy** compared to **L1** and **Gr1**.

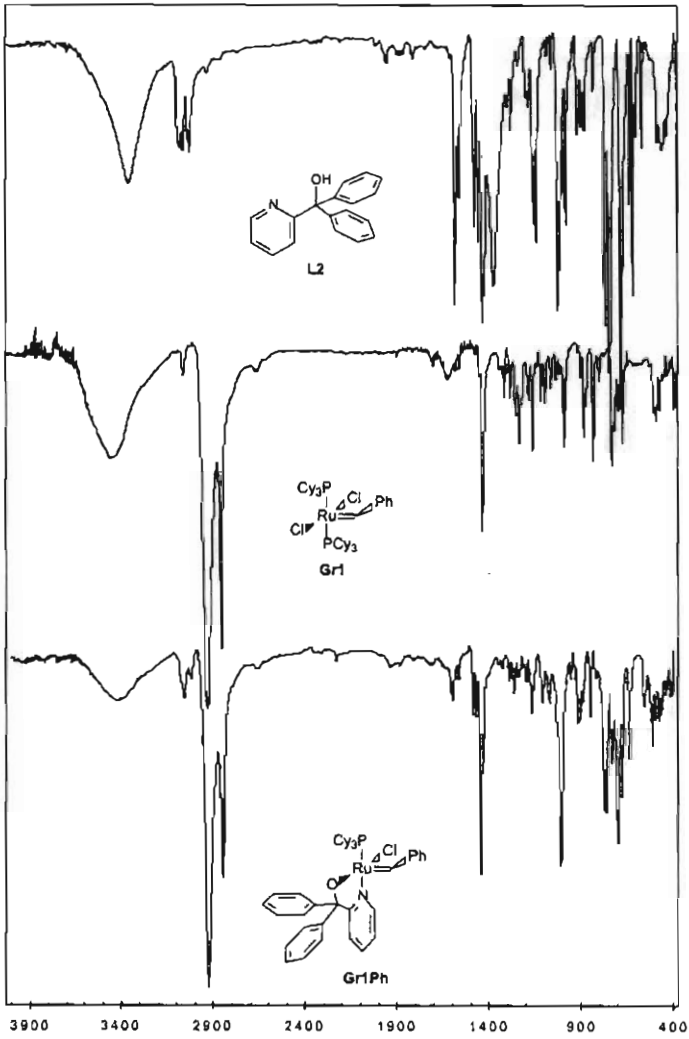

Spectrum D.2 IR-spectrum of Grl Ph compared to L2 and Grl.

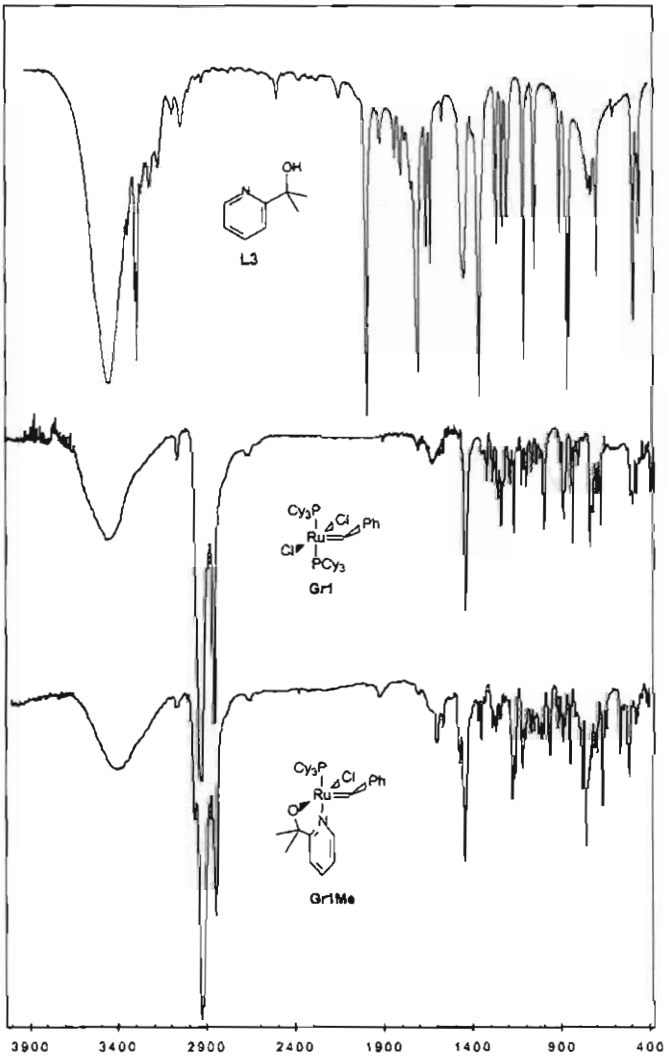

Spectrum D.3 IR-spectrum of **Grl Me** compared to **L3** and **Grl** (spectrum of L3 from literature).

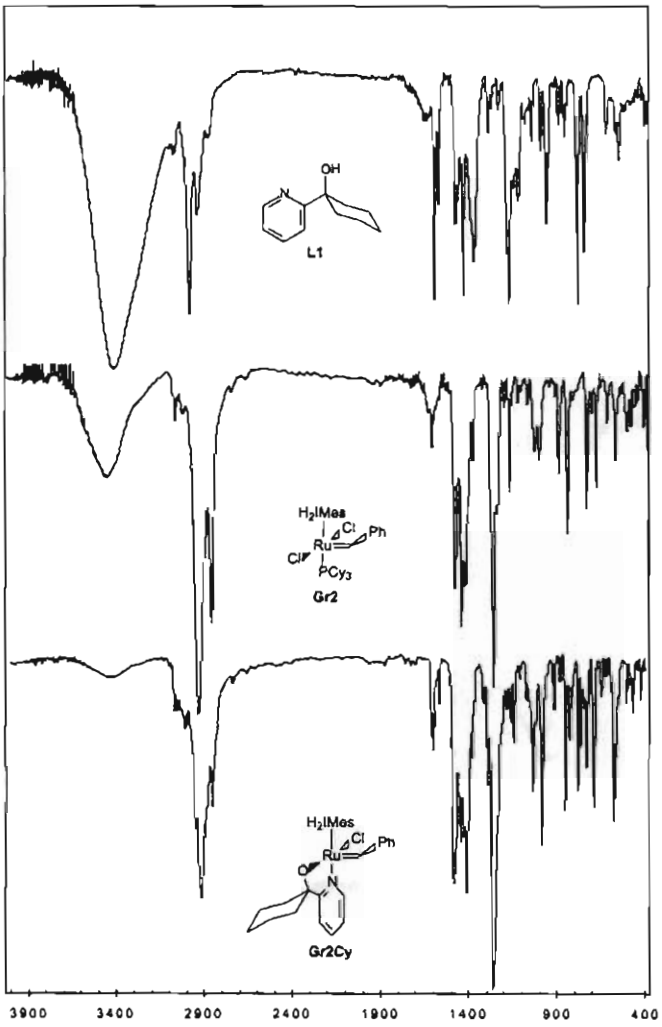

Spectrum D.4 IR-spectrum of **Gr2Cy** compared to **L1** and **Gr2**.

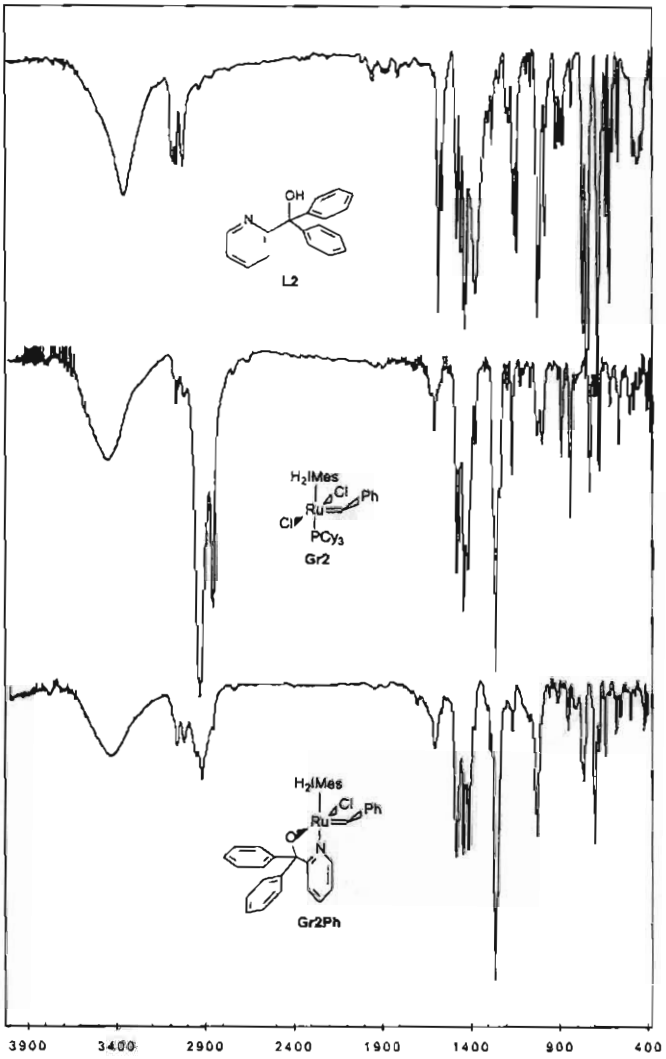

Spectrum D.5 IR-spectrum of **Gr2Ph** compared to **L2** and **Gr2**.

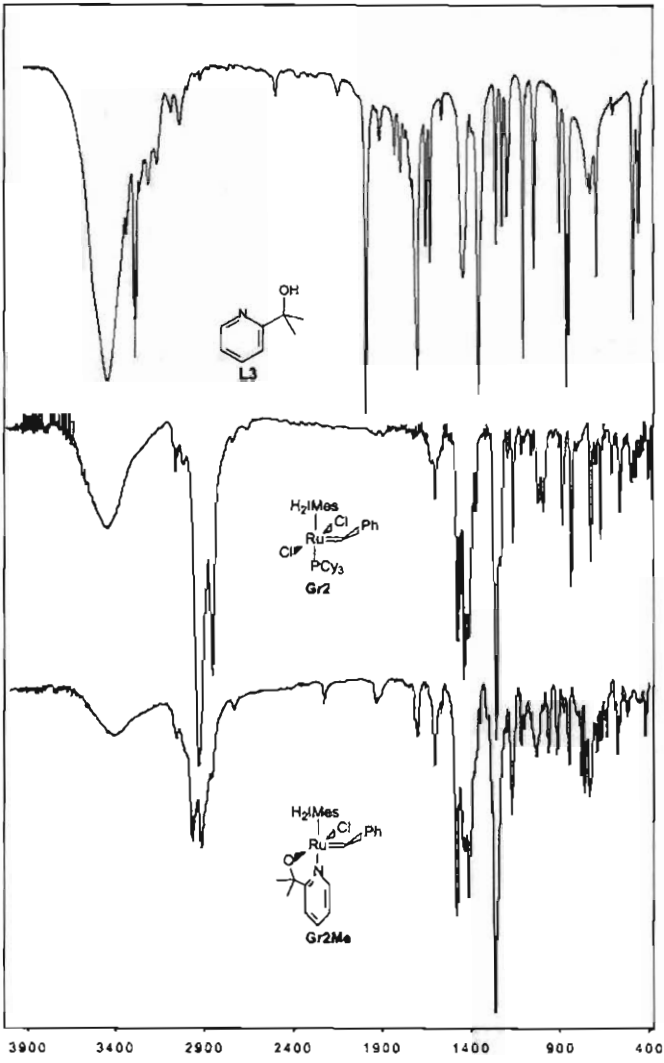

Spectrum D.6 IR-spectrum of **Gr2Me** compared to **L3** and **Gr2** (spectrum of **L3** from literature).

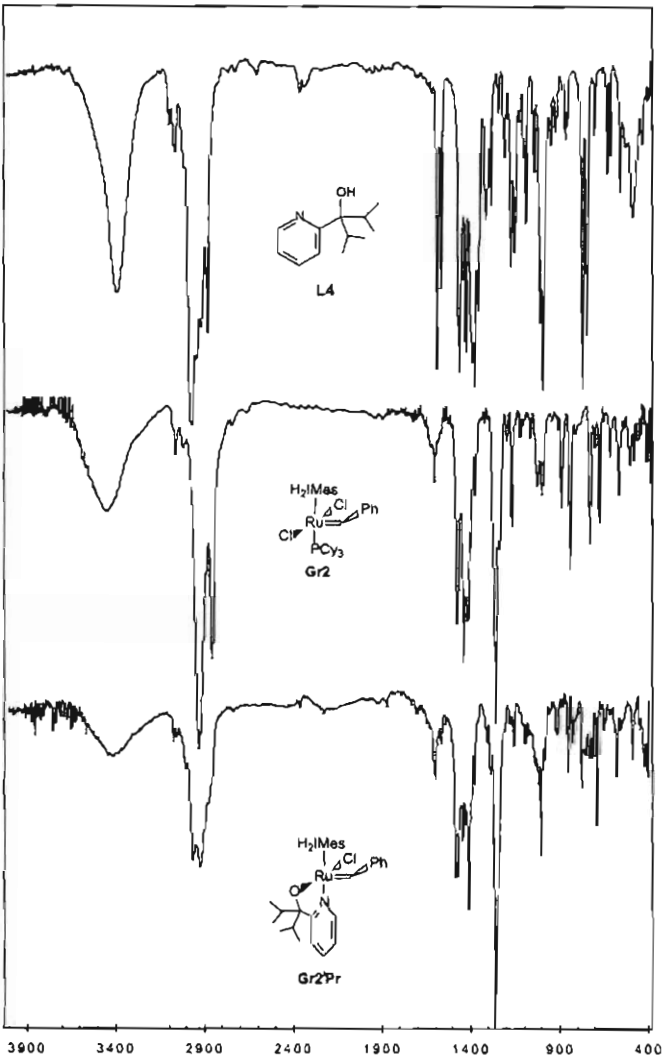

Spectrum D.7 IR-spectrum of Gr2^{i}Pr compared to L4 and Gr2.

Appendix E

The different reactions that can occur during the metathesis of 1-octene are illustrated in the following reaction schemes.[1] It consists of a number of self-metathesis reactions of the formed 1-alkenes as a result of the isomerisation and cross-metathesis reactions. For example, 1-octene can be isomerised to 2-, 3- and 4-octene, whereby cross-metathesis of 1-octene with 2-octene will lead to a range of internal and terminal alkenes. The terminal alkenes can again undergo isomerisation as well as cross-metathesis with other alkenes etc. Therefore, the process can repeat itself to produce a range of C_2 to C_{14} alkenes. Oligomerisation reactions, i.e. di-, tri and tetramerisation reactions can also occur to produce higher alkenes, i.e. C_{15} and longer.[1,2]

Primary self-metathesis 1 :

Isomerisation 1 :

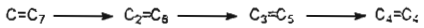

Secondary self-metathesis 1 :

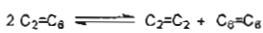

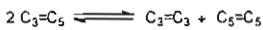

Secondary cross-metathesis 1 :

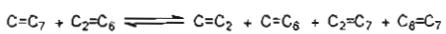

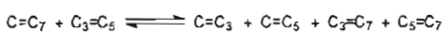

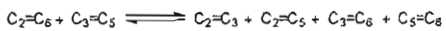

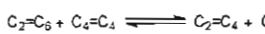

Dimerisation 1 :

Primary self-metathesis 2 :

$$\left\{\begin{array}{l} 2\,C{=}C_4 \rightleftharpoons C{=}C + C_4{=}C_4 \\ 2\,C{=}C_5 \rightleftharpoons C{=}C + C_5{=}C_5 \end{array}\right\}$$

$$2\,C{=}C_6 \rightleftharpoons C{=}C + C_6{=}C_6$$

Isomerisation 2 : $C{=}C_6 \longrightarrow C_2{=}C_5 \longrightarrow C_3{=}C_4$

Secondary cross-metathesis 2 :

$$C{=}C_6 + C_2{=}C_5 \rightleftharpoons C{=}C_2 + C{=}C_5 + C_2{=}C_6 + C_5{=}C_6$$

$$C{=}C_6 + C_3{=}C_4 \rightleftharpoons C{=}C_3 + C{=}C_4 + C_3{=}C_6 + C_4{=}C_6$$

$$C_2{=}C_5 + C_3{=}C_4 \rightleftharpoons C_2{=}C_3 + C_2{=}C_4 + C_3{=}C_5 + C_4{=}C_5$$

Secondary self-metathesis 2 :

$$2\,C_2{=}C_5 \rightleftharpoons C_2{=}C_2 + C_5{=}C_5$$

$$2\,C_3{=}C_4 \rightleftharpoons C_3{=}C_3 + C_4{=}C_4$$

Dimerisation 2 : $2\,C{=}C_6 \longrightarrow C_{14}$

Primary self-metathesis 3 :

$$\left\{\begin{array}{l} 2\,C{=}C_4 \rightleftharpoons C{=}C + C_4{=}C_4 \\ 2\,C{=}C_5 \rightleftharpoons C{=}C + C_5{=}C_5 \end{array}\right\}$$

Isomerisation 3 : $C{=}C_5 \longrightarrow C_2{=}C_4 \longrightarrow C_3{=}C_3$

Secondary self-metathesis 3 : $2\,C_2{=}C_3 \rightleftharpoons C_2{=}C_2 + C_3{=}C_3$

Secondary cross-metathesis 3 :

$$C{=}C_5 + C_2{=}C_4 \rightleftharpoons C{=}C_2 + C{=}C_4 + C_2{=}C_5 + C_4{=}C_5$$

$$C{=}C_5 + C_3{=}C_3 \rightleftharpoons C{=}C_3 + C_3{=}C_5$$

$$C_2{=}C_4 + C_3{=}C_3 \rightleftharpoons C_2{=}C_3 + C_3{=}C_4$$

Dimerisation 3 : $2\,C{=}C_5 \longrightarrow C_{12}$

Trimerisation 3 : $3\,C{=}C_5 \longrightarrow C_{18}$

Primary self-metathesis 4 : $2\,C{=}C_4 \rightleftharpoons C{=}C + C_4{=}C_4$

Isomerisation 4 : $C{=}C_4 \longrightarrow C_2{=}C_3$

Secondary self-metathesis 4 : $2\,C_2{=}C_3 \rightleftharpoons C_2{=}C_2 + C_3{=}C_3$

Secondary cross-metathesis 4 : $C{=}C_4 + C_2{=}C_3 \rightleftharpoons C{=}C_2 + C_3{=}C_3 + C_2{=}C_4 + C_3{=}C_4$

Dimerisation 4 : $2\,C{=}C_4 \longrightarrow C_{10}$

Trimerisation 4 : $3\,C{=}C_4 \longrightarrow C_{15}$

Primary self-metathesis 5 : $2\,C{=}C_3 \rightleftharpoons C{=}C + C_3{=}C_3$

Isomerisation 5 : $C{=}C_3 \longrightarrow C_2{=}C_2$

Secondary self-metathesis 5 : —

Secondary cross-metathesis 5 : $C{=}C_3 + C_2{=}C_2 \rightleftharpoons C{=}C_2 + C_2{=}C_3$

Dimerisation 5 : $2\ C{=}C_3 \longrightarrow C_6$

Trimerisation 5 : $3\ C{=}C_3 \longrightarrow C_{12}$

Tetramerisation 5 : $4\ C{=}C_3 \longrightarrow C_{16}$

Primary self-metathesis 6 : $2\ C{=}C_2 \rightleftharpoons C{=}C + C_2{=}C_2$

Isomerisation 6 : —

Secondary self-metathesis 6 : —

Secondary cross-metathesis 6 : —

Dimerisation 6 : $2\ C{=}C_2 \longrightarrow C_6$

Oligomerisation 6 : $3\ C{=}C_2 \longrightarrow C_9$

$4\ C{=}C_2 \longrightarrow C_{12}$

$5\ C{=}C_2 \longrightarrow C_{15}$

$6\ C{=}C_2 \longrightarrow C_{18}$

References

1. Mtshatsheni, K.N.G., ***Metathesis of Alkenes using Ruthenium Carbene Complexes***, M.Sc dissertation, North-West University (Potchefstroom Campus), 2005

2. Van Schalkwyk, C., ***Die Katalitiese Sintese van Lineêre Alkene via 'n Metatesereaksie***, Ph.D thesis, Potchefstroomse Universiteit vir Christelike Hoër Onderwys, 2001

Appendix F

Appendix F (p. 455 – 472) is available on the enclosed CD

Appendix G

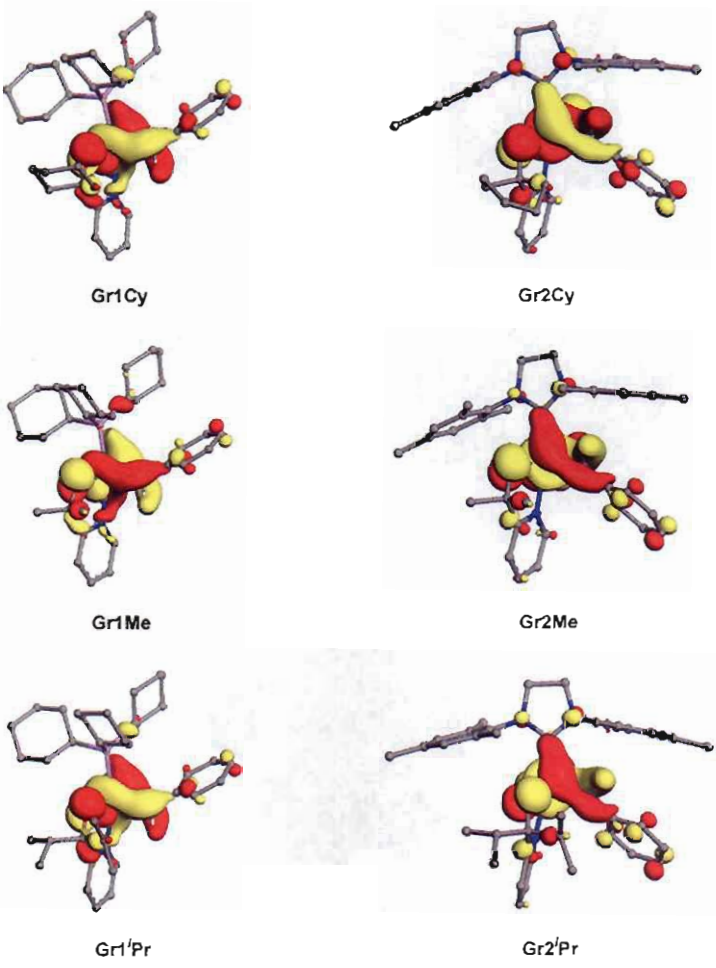

Figure G.1 HOMO orbitals of **Gr1**, **Gr1-B** and a representative of the first and second generation hemilabile Ru=C complexes.

Gr1-*f*+

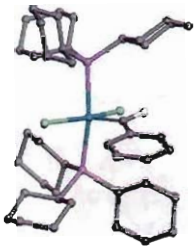

Gr1

Gr2-*f*+

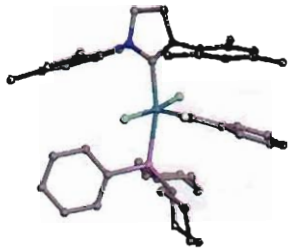

Gr2

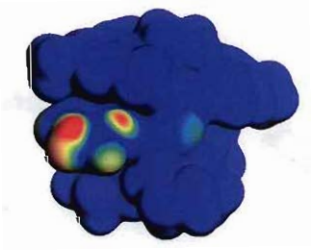

Gr2-180-*f*+
(turned at an 180° angle)

Figure G.2 Optimised geometry of the precatalysts of the first and second generation hemilabile complexes together with maps of the nucleophilic (*f*+) Fukui functions on the electron isodensity surface.

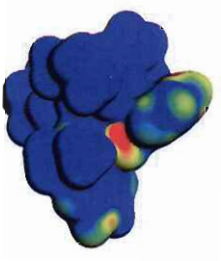

Gr1Me-*f*+

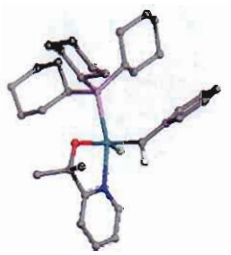

Gr1Me

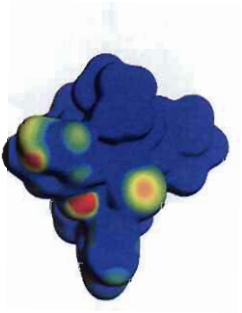

Gr1Me-180-*f*+
(turned at an 180° angle)

Figure G.3 Optimised geometry of **Gr1Me**, together with maps of the nucleophlic (*f*+) Fukui functions on the electron isodensity surface.

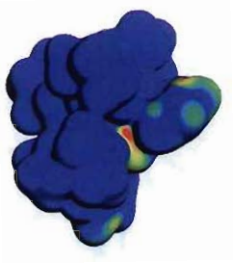

Gr1^{i}Pr-*f*+

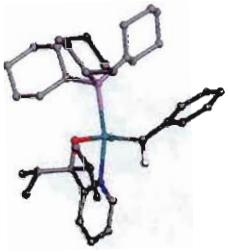

Gr1^{i}Pr

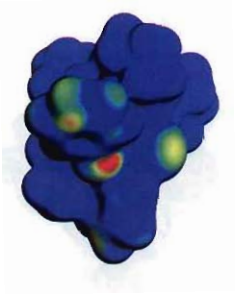

Gr1^{i}Pr -180-*f*+
(turned at an 180° angle)

Figure G.4 Optimised geometry of **Gr1 ^{i}Pr**, together with maps of the nucleophilic (*f*+) Fukui functions on the electron isodensity surface.

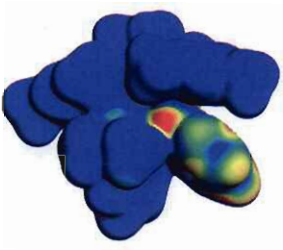

Gr2Me-*f*+

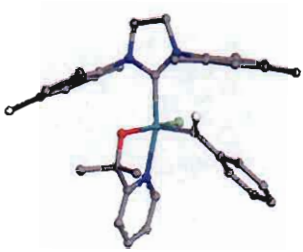

Gr2Me

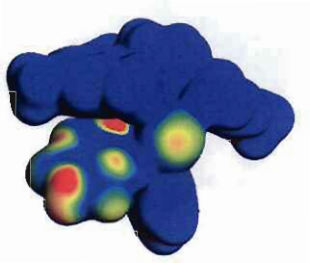

Gr2Me-180-*f*+
(turned at an 180° angle)

Figure G.5 Optimised geometry of **Gr2Me**, together with maps of the nucleophlic (*f*+) Fukui functions on the electron isodensity surface.

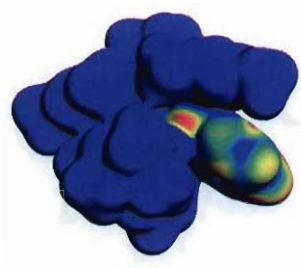

Gr2^{i}Pr-*f*+

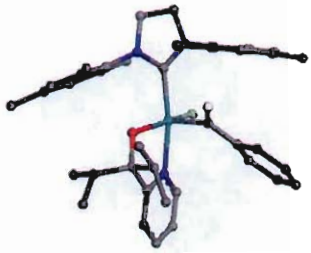

Gr2^{i}Pr

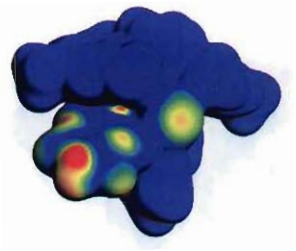

Gr2^{i}Pr-180-*f*+
(turned at an180° angle)

Figure G.6 Optimised geometry of **Gr2^{i}Pr**, together with maps of the nucleophlic (*f*+) Fukui functions on the electron isodensity surface.